General Disclaimer

One or more of the Following Statements may affect this Document

- This document has been reproduced from the best copy furnished by the organizational source. It is being released in the interest of making available as much information as possible.

- This document may contain data, which exceeds the sheet parameters. It was furnished in this condition by the organizational source and is the best copy available.

- This document may contain tone-on-tone or color graphs, charts and/or pictures, which have been reproduced in black and white.

- This document is paginated as submitted by the original source.

- Portions of this document are not fully legible due to the historical nature of some of the material. However, it is the best reproduction available from the original submission.

LARGE-EDDY SIMULATION OF A TURBULENT MIXING LAYER

by

N. N. MANSOUR,
J. H. FERZIGER,
and
W. C. Reynolds

Prepared from work done under Grant
NASA-NgR-05-020-622

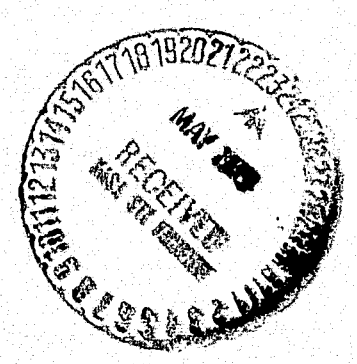

Report No. TF-11

Thermosciences Division
Department of Mechanical Engineering
Stanford University
Stanford, California

April 1978

LARGE-EDDY SIMULATION OF A TURBULENT MIXING LAYER

by

N. N. Mansour, J. H. Ferziger, and W. C. Reynolds

Prepared from work done under Grant
NASA-NgR-05-020-622

Technical Report Number TF-11

Thermosciences Division
Department of Mechanical Engineering
Stanford University
Stanford, California

April 1978

Acknowledgments

The authors gratefully acknowledge the many useful discussions and contributions of Mr. P. Moin. We are indebted to Dr. U. B. Mehta for helping get this work started and familiarizing the senior author with the computation facility at NASA-Ames Research Center. Dr. A. Leonard made numerous suggestions and corrections to the manuscript which the authors gratefully acknowledge.

The senior author is indebted to the National Council for Scientific Research (Lebanon) for its support at the initial stages of his graduate studies.

The diligent efforts and editing of Ms. Ruth Korb resulted in a superb job of preparation of the final copy. This work was supported by NASA-Ames Research Center under Grant NASA-NgR-05-020-622.

Abstract

The three-dimensional, time-dependent (incompressible) vorticity equations have been used to simulate numerically the decay of isotropic box turbulence and time-developing mixing layers. The vorticity equations are spatially filtered to define the large-scale turbulence field, and the subgrid scale turbulence is modeled. A general method has been developed to show numerical conservation of momentum, vorticity, and energy that is much simpler than previous methods and is widely applicable. The terms that arise from filtering the equations have been treated (for both periodic boundary conditions and no-stress boundary conditions) in a fast and accurate way by using fast Fourier transforms. Use of vorticity as the principal variable is shown to produce results equivalent to those obtained by use of the primitive variable equations.

A new subgrid scale model is used in conjunction with the vorticity equations and is shown to produce results that compare well with the experimental results. The new model offers advantages both in computational speed and in storage.

The vortex-pairing mechanism, observed in the spatially developing counterpart of the time-developing mixing layer, has been simulated numerically. It is interesting to note that with simply two vortices pairing, self-similar mean velocity and mean turbulence intensity profiles are obtained. The vortex-pairing mechanism is shown to be persistent even with the presence of large-amplitude, three-dimensional background turbulence. A number of different initial fields have been studied. The presence of large organized structures, in the initial conditions, is shown to be essential in order to predict growth rates of the mixing layers comparable to those observed experimentally. The rate of growth is found to be very dependent on the initial field, a fact also observed experimentally.

Table of Contents

		Page
Acknowledgments		iii
Abstract		iv
List of Tables		vii
List of Figures		viii
Nomenclature		xiii
Chapter		
1	INTRODUCTION	1
	1.1 Background	1
	1.2 Experimental Background	3
	1.3 Motivation and Objectives	5
	1.4 Overview	6
2	THEORETICAL FOUNDATIONS	8
	2.1 Definitions of the Large and Subgrid Scales	8
	2.2 Dynamical Equations in Vorticity Form	9
	2.3 Subgrid Scale Models	10
	2.3.1 Model ω-1	11
	2.3.2 Model ω-2	12
	2.4 Filtering	13
	2.4.1 Sharp Cut-off (SCK) Filter	13
	2.4.2 Gaussian (GS) Filter	14
	2.5 Computing Velocity Field from the Vorticity Field	14
	2.6 Summary	15
3	NUMERICAL METHOD	17
	3.1 Notations	17
	3.2 Numerical Approximation	17
	3.2.1 Fourth-Order Scheme	18
	3.2.2 Pseudo-Spectral Method	20
	3.3 Time Differencing	25
	3.4 Conservation Properties	25
	3.5 Differenced Vorticity Equations	29
	3.6 Poisson Equation	30
	3.7 Numerical Filtering	31
	3.8 Summary	34
4	DECAY OF ISOTROPIC TURBULENCE	36
	4.1 Background	36
	4.2 Initial Conditions	36
	4.3 Selection of C_v	37
	4.4 Results	37
	4.4.1 Fourth-Order Finite Differences	38
	4.4.2 Pseudo-Spectral Method	38
	4.5 Computational Details	39

Chapter Page

5 MIXING LAYER: TWO-DIMENSIONAL COMPUTATIONS 41

5.1 Preview 41
5.2 Some Experimental Results 41
5.3 Boundary Conditions 44
5.4 Initial Conditions 45
5.5 Mesh Size Selection 46
5.6 Selection of β 48
5.7 Mean Velocity Profiles 48
5.8 Mean Turbulence Intensity Profiles 49
5.9 Summary 49

6 MIXING LAYER: THREE-DIMENSIONAL COMPUTATIONS 51

6.1 Preview 51
6.2 Boundary Conditions and Mesh-Size Selection 51
6.3 Initial Conditions 52
6.4 Momentum Thickness 53
6.5 Mean Velocity Profiles 54
6.6 Mean Turbulence Intensity Profiles 54
6.7 Vorticity Contours 56
6.8 Two-Point Correlations 57
6.9 Summary and Conclusions 59

7 CONCLUSIONS AND RECOMMENDATIONS 60

References 63

Appendix

A Subgrid Scale Models for the Vorticity Equations 136
B Fast Discrete Sine Transform (FDST); Fast Discrete Cosine Transform (FDCT) 138
C Effect of a Sinusoidal Vorticity Perturbation on a Uniform Vortex Array 140
1. Initial Conditions 140
2. Results 140
D Interactions Between Streamwise and Spanwise Vorticity . . 142
1. Initial Conditions 142
2. Results 142
E Computer Program Written to Calculate Turbulent Mixing Layers 160

List of Tables

Table		Page
1.1	Experimental Results	67
4.1	Computations of the Decay of Isotropic Turbulence	75
6.1	Three-Dimensional Computations of Turbulent Mixing Layers	103

List of Figures

Figure		Page
1.1	r.m.s. streamwise velocity profiles for different initial conditions (experimental results from Foss, 1977)	69
1.2	Mean velocity profiles for different initial conditions (experimental results from Foss, 1977).	70
2.1	Filtered point vortex with SCK (sharp cut-off in k-space) filter	71
2.2	Filtered point vortex with a GS (Gaussian in real space) filter	72
3.1	Comparison of modified wave number	73
3.2	Filtered top-hat function	74
4.1	Decay of mean square filtered velocity for $16 \times 16 \times 16$ mesh. $< >$ = average over all space	76
4.2	Filtered energy spectra. Fourth-order differencing with 16^3 mesh; model ω-1, $C_v = 0.235$	77
4.3	Filtered energy spectra. Pseudo-spectral computation with 16^3 mesh; model ω-1, $C_v = 0.212$	78
4.4	Filtered energy spectra. Pseudo-spectral computation with 16^3 mesh; model ω-1, $C_v = 0.213$	79
4.5	Filtered energy spectra. Pseudo-spectral computation with 16^3 mesh; model ω-2. $C_v = 0.186$	80
4.6	Filtered energy spectra. Pseudo-spectral computation with 16^3 mesh; model ω-2. $C_v = 0.188$	81
4.7	Filtered energy spectra. Pseudo-spectral computation with 32^3 mesh, 2nd-order differencing for model ω-2. $C_v = 0.188$	82
5.1	Coherent structure in a mixing layer (Roshko, 1976). Dashed box: schematic of a computational box that moves approximately with the mean velocity	83
5.2	Mixing layer. Experimental setup and coordinate system . .	84
5.3	Computational box and coordinate system	85
5.4	Initial conditions setup $\left(\beta = \frac{1}{2} - \frac{(x_1 - x_2)}{L}\right)$	86
5.5	Non-dimensional momentum thickness (θ/θ_{in}) as a function of time for various β. Two-dimensional computations	87

List of Figures (cont.)

Figure		Page
5.6a	Contour plots of the spanwise vorticity ($\bar{\omega}_2$) for β = 6/16, at time T = 0. Constant vorticity lines are plotted at eight levels. Higher numbers on these lines indicate higher levels ($\bar{\omega}_{2,max}$ = .702)	88
5.6b	Contour plots of the spanwise vorticity ($\bar{\omega}_2$) for β = 5/16, at time T = 0. Constant vorticity lines are plotted at eight levels. Higher numbers on these lines indicate higher levels ($\bar{\omega}_{2,max}$ = 0.564)	89
5.6c	Contour plots of the spanwise vorticity ($\bar{\omega}_2$) for β = 4/16, at time T = 0. Constant vorticity lines are plotted at eight levels. Higher numbers on these lines indicate higher levels ($\bar{\omega}_{2,max}$ = 0.444)	90
5.6d	Contour plots of the spanwise vorticity ($\bar{\omega}_2$) for β = 3/16, at time T = 0. Constant vorticity lines are plotted at eight levels. Higher numbers on these lines indicate higher vorticity levels ($\bar{\omega}_{2,max}$ = 0.421)	91
5.6e	Contour plots of the spanwise vorticity ($\bar{\omega}_2$) for β = 2/16, at time T = 0. Constant vorticity lines are plotted at eight levels. Higher numbers on these lines indicate higher levels ($\bar{\omega}_{2,max}$ = 0.416)	92
5.6f	Contour plots of the spanwise vorticity ($\bar{\omega}_2$) for β = 1/16, at time T = 0. Constant vorticity lines are plotted at eight levels. Higher numbers on these lines indicate higher levels ($\bar{\omega}_{2,max}$ = 0.415)	93
5.7a	Contour plots of the spanwise vorticity ($\bar{\omega}_2$) for β = 6/16, at time T = 16.78. Constant vorticity lines are plotted at eight levels. Higher numbers on these lines indicate higher levels ($\bar{\omega}_{2,max}$ = 0.394)	94
5.7b	Contour plots of the spanwise vorticity ($\bar{\omega}_2$) for β = 5/16, at time T = 16.78. Constant vorticity lines are plotted at eight levels. Higher numbers on these lines indicate higher levels ($\bar{\omega}_{2,max}$ = 0.358)	95
3.7c	Contour plots of the spanwise vorticity ($\bar{\omega}_2$) for β = 4/16, at time T = 16.78. Constant vorticity lines are plotted at eight levels. Higher numbers on these lines indicate higher levels ($\bar{\omega}_{2,max}$ = 0.322)	96
5.7d	Contour plots of the spanwise vorticity ($\bar{\omega}_2$) for β = 3/16, at time T = 16.78. Constant vorticity lines are plotted at eight levels. Higher numbers on these lines indicate higher levels ($\bar{\omega}_{2,max}$ = 0.276)	97

List of Figures (cont.)

Figure		Page
5.7e	Contour plots of the spanwise vorticity ($\bar{\omega}_2$) for β = 2/16, at time T = 16.78. Constant vorticity lines are plotted at eight levels. Higher numbers on these lines indicate higher levels ($\bar{\omega}_{2,max}$ = 0.248)	98
5.7f	Contour plots of the spanwise vorticity ($\bar{\omega}_2$) for β = 1/16, at time T = 16.78. Constant vorticity lines are plotted at eight levels. Higher numbers on these lines indicate higher levels ($\bar{\omega}_{2,max}$ = 0.245)	99
5.8	Mean velocity profiles. Two-dimensional computations (β = 3/16)	100
5.9	Mean turbulence intensity profiles. Two-dimensional computations (β = 3/16)	101
6.1	Three-dimensional computation box. Random velocity setup and coordinate system	102
6.2	Non-dimensional momentum thickness (θ/θ_{in}) as a function of time. Three-dimensional computations	103
6.3	Non-dimensional momentum thickness (θ/θ_{in}) as a function of time	104
6.4a	Mean velocity profiles. Three-dimensional computation (case a)	105
6.4b	Mean velocity profiles. Three dimensional computation (case b)	106
6.4c	Mean velocity profiles. Three-dimensional computations (case c)	107
6.5	Integral of the turbulence energy as a function of time .	108
6.6a	Mean turbulence intensity profiles. Three-dimensional computations (case a)	109
6.6b	Mean turbulence intensity profiles. Three-dimensional computations (case b)	110
6.6c	Mean turbulence intensity profiles. Three-dimensional computations (case c)	111
6.7	Mean turbulence intensity profiles. Three-dimensional computation (C_v = 0)	112
6.8	Integral of the turbulence energy as a function of time .	113

List of Figures (cont.)

Figure		Page
6.9a	Contour plots of the spanwise vorticity ($\bar{\omega}_2$) in an x-z plane, at time T = 0. Constant vorticity lines are plotted at eight levels. Higher numbers on these lines indicate higher vorticity levels ($\bar{\omega}_{2,max} = 0.228$)	114
6.9b	Contour plots of the spanwise vorticity ($\bar{\omega}_2$) for different x-z planes, at time T = 0. In each plane, constant vorticity lines are plotted at eight levels. Higher numbers on these lines indicate higher vorticity levels . .	115
6.9c	Contour plots of the spanwise vorticity ($\bar{\omega}_2$) for different x=z planes, at time T = 0. In each plane, constant vorticity lines are plotted at eight levels. H igher numbers on these lines indicate higher vorticity levels . .	119
6.10a	Contour plots of the spanwise vorticity ($\bar{\omega}_2$) in an x-z plane, at time T = 16.78. Constant vorticity lines are plotted at eight levels. Higher numbers on these lines indicate higher vorticity levels ($\bar{\omega}_{2,max} = 0.185$	123
6.10b	Contour plots of the spanwise vorticity ($\bar{\omega}_2$) for different x=z planes, at time T = 16.78. In each plane, constant vorticity lines are plotted at eight levels. Higher numbers on these lines indicate higher levels	124
6.10c	Contour plots of the spanwise vorticity ($\bar{\omega}_2$) for different x-z planes, at time T = 16.78. In each plane, constant vorticity lines are plotted at eight levels. Higher numbers on these lines indicate higher levels	128
6.11a	Two point correlations (z = 17 is the center plane of the mixing layer, $\Delta z/\theta_{in} = 1.023$; case a)	132
6.11b	Two-point correlations (z = 17 is the center plane of the mixing layer, $\Delta z/\theta_{in} = 1.023$; case b)	133
6.11c	Two-point correlations (z = 17 is the center plane of the mixing layer, $\Delta z/\theta_{in} = 1.023$; case c)	134
7.1	Formation of streamwise cellular structures in a mixing layer	135
C.1	Non-dimensional momentum thickness (θ/θ_{in}) as a function of time for various C_2/C_1	145
C.2	Mean velocity profiles ($C_2/C_1 = 0.1$)	146
C.3	Mean turbulence intensity profiles ($C_2/C_1 = 0.1$)	147

List of Figures (cont.)

Figure		Page
D.1	Contour plots of the streamwise vorticity $(\bar{\omega}_1)$ at time T = 0. Constant vorticity lines are plotted at eight levels. Higher numbers on these lines indicate higher vorticity levels	148
D.2	Non-dimensional momentum thickness (θ/θ_{in}) as a function of time	149
D.3a	Mean velocity profiles (case a)	150
D.3b	Mean velocity profiles (case b)	151
D.4a	Mean turbulence intensity profiles (case a)	152
D.4b	Mean turbulence intensity profiles (case b)	153
D.5a	Contour plots of the spanwise vorticity $(\bar{\omega}_2)$ in an x-z plane $(y/\theta_{in} = 4.09)$, at time T = 16.78. Constant vorticity lines are plotted at eight levels. Higher numbers on these lines indicate higher levels (case a)	154
D.5b	Contour plots of the spanwise vorticity $(\bar{\omega}_2)$ in an x-z plane $(y/\theta_{in} = 4.09)$, at time T = 16.78. Constant vorticity lines are plotted at eight levels. Higher numbers on these lines indicate higher levels (case b)	155
D.6a	Contour plots of the streamwise vorticity $(\bar{\omega}_1)$ in an x-z plane $(y/\theta_{in} = 4.09)$, at time T = 16.78. Constant vorticity lines are plotted at eight levels. Higher numbers on these lines indicate higher vorticity levels (case a)	156
D.6b	Contour plots of the streamwise vorticity $(\bar{\omega}_1)$ in an x-z plane $(y/\theta_{in} = 4.09)$, at time T = 16.78. Constant vorticity lines are plotted at eight levels. Higher numbers on these lines indicate higher levels (case b)	157
D.7	Projection of the vorticity vector in an x-z plane $(y/\theta_{in} = 4.09)$ at time T = 16.78	158
D.8	Contour plots of the spanwise vorticity $(\bar{\omega}_2)$ in a y-z plane $(x/\theta_{in} = 9.55)$, at time T = 16.78. Constant vorticity lines are plotted at eight levels. Higher numbers on these lines indicate higher vorticity levels $(\bar{\omega}_{2,max} = 0.714)$	159

Nomenclature

A		Integral of the Gaussian filter
A_i		Integral of the Gaussian filter in the i-direction
C_v		Subgrid scale constant
$\overline{E}(k)$		Filtered energy spectrum
f, g		Flow variables
$\overline{f}$, $\overline{g}$		Filtered (large-scale) components of flow variables
f', g'		Subgrid scale components of flow variables
$G(x)$		Filter function
$\hat{G}(k)$		Fourier transform of the filter function
$G_D(x)$		Discretized filter in real space
$\hat{G}_D(k)$		Discretized filter in k-space.
h		Mesh size in any given direction
h_i		Mesh size in the i-direction
k		Wave number
k_i		Wave number in the i-direction
k_i'		Modified wave number in the i-direction
k_c		Cut-off wave number
$\mathscr{L}$		Length scale of large eddies
L		Length of computational box in any given direction
L_i		Length of computational box in the i-direction
M		Size of the experimental turbulence-generating grid
N		Number of mesh points in any given direction
N_i		Number of mesh points in the i-direction
q		r.m.s. velocity
r	$\equiv$	u_2/u_1 velocity ratio

R_T = $q\ell/\nu$, Reynolds number based on large eddy length

R_λ = $q\lambda/\nu$, Reynolds number based on Taylor micro-scale

S Scalar

$S_{ij} \equiv \frac{1}{2}\frac{\partial}{\partial x_j}\overline{u}_i + \frac{\partial}{\partial x_i}\overline{u}_j$, strain rate tensor

T = Non-dimensional time

$\equiv \frac{U_o t}{M}$, decay of isotropic turbulenc-

$\equiv \frac{\Delta u t}{\theta_{in}}$, mixing layer

t Real time

u_i Velocity in the i-direction

$\overline{u}_i$ Filtered velocity in the i-direction

u_i' Subgrid scale velocity in the i-direction

u_1 Velocity of high-speed side

u_2 Velocity of low-speed side

V General vector

V_i Component of a general vector in the i-direction

W_{ij} Curl of subgrid scale stress

x Streamwise coordinate

x_o Virtual origin of a mixing layer

y spanwise coordinate

z Cross-flow coordinate

Greek letters

Δ Filter width (= 2h) in any direction

Δ_i Filter width in the i-direction

$\Delta u = u_1 - u_2$ velocity difference

ε Total energy dissipation

ε_{ijk} The completely anti-symmetric tensor of rank 3

η $z/(x-x_o)$ self-similarity coordinate

γ Constant (= 6) in Gaussian filter

λ Taylor microscale

ν_T Eddy viscosity

$\omega_i \equiv \varepsilon_{ipq} \frac{\partial}{\partial x_p} u_q$, vorticity component in the i-direction

$\bar{\omega}_i$ Filtered vorticity component in the i-direction

ω_i' Subgrid scale vorticity component in the i-direction

ψ_i Component of vector potential in the i-direction

ρ Density

$\tau_{ij} \equiv \overline{u_i'u_j'} + \overline{u_j'\bar{u}_i} + \overline{u_i'\bar{u}_j} - \frac{1}{3}(\overline{u_k'u_k'} + 2\overline{u_k'\bar{u}_k})\,\delta_{ij}$

σ Spread parameter

σ_o Spread parameter for r = o

θ Momentum thickness

$< >_{xy}$ Horizontal planar average

Arguments

(i,j,k) Computational mesh index for (x,y,z)

Superscripts

(n) Time step

Chapter 1

INTRODUCTION

1.1 Background

Turbulent flows have been the subject of experimental and theoretical investigations since the last century. Despite the formidable amount of effort invested in this field, our ability to predict flows of technical importance remains severely limited. The major difficulty encountered by the theoretical investigations arises from the nonlinear character of the equations of motion. Statistical averages of the equations of motion give rise to the so-called Reynolds stresses. The equations for the Reynolds stresses in turn give rise to higher-order statistical quantities, and so on. The usual approach to computing turbulent flows is to model the terms that arise from the nonlinear character of the equations of motion. This approach usually requires a great deal of experimental information.

We know the underlying physical principles of most fluid flows, and the quantities of interest are completely determined by known equations. With the introduction of large computers, three-dimensional, time-dependent computation of turbulent flows has become possible. However, in order to resolve all the scales of motion even in the simplest turbulent flow, namely, the isotropic homogeneous case, Kwak et al. (1975) estimated the number of mesh points needed in any given direction to be

$$N = R_T^{3/4} \tag{1.1}$$

where

R_T = $(q\ell/\nu)$,
ν = kinematic viscosity,
ℓ = length scale of large eddies, and
q = r.m.s. velocity.

Equation (1.1) shows that one can do a full simulation only at very low Reynolds number. Indeed, Clark et al. (1977), using a $64 \times 64 \times 64$ mesh system, were able to solve the isotropic homogeneous turbulence

problem for $R_\lambda = q\lambda/\nu = 38.1$, where λ is the Taylor microscale. Their predicted results compared well with the experimental results. However, turbulent flows of technical importance have much higher Reynolds numbers, and all the scales of motion cannot be resolved for these flows.

One of the more promising approaches to solving turbulence problems is "large-eddy simulation". In large-eddy simulation, one calculates the large-scale turbulent motions with a relatively coarse time-dependent, three-dimensional computation that uses some sort of model (the "subgrid scale model") for the small scales. The basic motivations for this approach are twofold. First, experimental observations of turbulent flows show that the large turbulent structures differ markedly from one flow type to another (e.g., jet vs. boundary layer), but the small-scale turbulent structures are quite similar. Thus, while there is little hope of concocting a "universal" model for the large structures, it may be possible to do so for the small-scale motions. Second, as computer capabilities grow, our capability of resolving smaller scales will grow and the effects of the subgrid scale model will diminish. Thus, while we are limited to simple flows with the present computer capabilities, large-eddy simulation is a tool that may be used on future generation computers.

Kwak et al. (1975) and Shaanan et al. (1975) have shown that homogeneous turbulent flows can be simulated reasonably well with a relatively small number of mesh points ($16 \times 16 \times 16$). Orszag and Pao (1974), using a $32 \times 32 \times 32$ mesh system, predicted the momentumless wake of a self-propelled body. Deardorff (1970) and Schuman (1973) computed the central region of a plane channel flow using the large-eddy simulation approach. While Deardorff and Schumann did not handle the wall (no slip) problem, Moin et al. (1978) have solved the channel flow problem, including the laminar sublayer. In this work we shall study the time-developing, two-stream mixing layer.

Previous works on prediction of the two-stream mixing layer have concentrated on the initial stages (roll-up) of the development of the layer. Patnaik et al. (1976), starting with an initial distribution that is an unstable eigensolution of the Taylor-Goldstein equation, predicted the two-dimensional roll-up of a stably stratified horizontal mixing layer. Another method that has been used to compute the mixing layer in two

dimensions is the vortex-tracing method used by Ashurst (1977). This method suffers from high computational costs and ad-hoc assumptions concerning the effects of viscosity. The high computational cost of the vortex-tracing method can be reduced by using the vortex-in-cell method (Wang, 1977). These works have treated two-dimensional cases, but the mixing layer exhibits three-dimensionality. This is apparent from the shadowgraph pictures of Brown and Roshko (1974) and the spanwise velocity fluctuation measurements of Spencer and Jones (1971).

1.2 Experimental Background

The two-dimensional turbulent mixing layer plays an essential role in many technological problems. For example, the initial regions of planar jets can be approximated as two independent, two-dimensional mixing layers. Flow over a backward-facing step (with a large step height) is another example of the two-dimensional mixing layer. Many other flow situations can be identified with the mixing layer. In combustion processes, fluid mechanics plays a major role in mixing the reactants, and better understanding of turbulent mixing is needed. The mixing layer is perhaps the simplest situation in which two flows come into contact; obviously the ability to analyze simple problems is necessary before one can analyze more complicated ones.

In 1947, Liepmann and Laufer studied the mixing layer and established the general features of the flow. However, the fundamental understanding of the structure of the flow is still far from complete, and many controversial questions need to be answered. We shall address some of these questions. The reader is referred to Murthy (1975) for an extensive review and interpretation of the available literature on the mixing layer. With the advancement of the techniques of hot-wire anemometry, Wygnanski and Fiedler (1970) attempted to reproduce Liepmann and Laufer data and extend it to include other measurements. However, differences in intensity levels and rate of growth of the layer emerged. These differences were attributed to the presence of a trip wire in the Wygnansky and Fiedler experiment that was not used by Liepmann and Laufer. Batt (1975) studied both configurations and showed that the differences are due to the tripping of the layer. Foss (1977) investigated the effects of the

laminar/turbulent boundary layer states on the development of a plane mixing layer. He found that the development of the layer is dependent on the initial conditions (the status of the boundary layers before the two streams merge). Figs. 1.1 and 1.2 show r.m.s. fluctuations of the streamwise velocity and the mean velocity profiles obtained by Foss. These figures show that different self-similar stages are obtained for different initial conditions. Foss argues that this is due to the sensitivity of choosing the virtual origin of the mixing layer (x_o) and that the character of the (initial) disturbance, not its amplitude, is responsible for the substantial effect on the virtual origin. More recently, Oster et al. (1977) showed that by oscillating the initial conditions of the mixing layer they can more than double the growth rate of the layer. The effect depends on the frequency and amplitude of the oscillations introduced. These experimental results show that the "universality" of the self-similar stage of the mixing layer is in doubt, at least up to $Re = 1.5 \times 10^6$. Fiedler and Thies (1977) showed that the two-dimensional shear layer only slowly reaches a self-similar state and that every disturbance is of long influence. Table 1.1 shows tabulated results extracted from the Fiedler and Thies paper, and it can be clearly seen that different experiments predict different growth rate of the layer.

Winant and Browand (1974), using dye visualization in a mixing layer, observed that initially the fluid rolls up into discrete, two-dimensional vortical structures. These structures then interact by rolling around each other to form a single larger structure. This pairing process controls the growth of their mixing layer. Brown and Roshko (1974) also observed the amalgamation process at Reynolds number 2.5×10^5. Chandrsuda and Bradshaw (1975) argue that the two-dimensional, large-eddy structure observed by Brown and Roshko is unlikely to survive indefinitely if the ambient entrained fluid is weakly turbulent. They advance the argument: "It is probable that if the Brown and Roshko type of orderly structure is once formed it can last for a large number of characteristic wavelengths -- that is, up to high Reynolds numbers based on streamwise distance -- but <u>not</u> indefinitely. The question can be settled only by measurements in a two-stream mixing layer at a much higher Reynolds number than was used by Brown and Roshko." Dimotakis and Brown (1976) showed the existence of

large structures at Reynolds number = 3×10^6 and attributed the growth of the mixing layer to both pairing and "tearing". Tearing is described in their paper as an event where "a large structure will occasionally find itself in the vicinity of another, or in between two others, in whose straining field it disintegrates." The tearing process was first advanced by Moore and Saffman (1975) on the basis of exact solutions for uniform vortices in straining fields.

1.3 Motivation and Objectives

In many flows of practical interest there are interactions between irrotational regions and turbulent regions. Examples of such flows are the shear layer, turbulent jets, and turbulent boundary layers with irrotational free stream flow. In such flows, the regions are separated by a very thin superlayer across which there is normally a jump in the vorticity components parallel to the layer. The dynamical equations for the vorticity seem to be suited to simulate such flows, since the vorticity is identically zero in the irrotational region. However, previous workers used the dynamical equations in the primitive variables (velocity, pressure) and there has been doubt (Orszag and Israeli, 1974) that the vorticity equations could be used to solve turbulent flow problems. Our objectives were therefore as follows:

- To explore the feasibility of using the vorticity equation to simulate turbulent flows.
- To find a subgrid scale model appropriate to the vorticity equations and to determine any constants in this model.
- To simulate a turbulent flow with interactions between turbulent regions and non-turbulent irrotational regions; we chose the mixing layer.

In order to use the three-dimensional, time-dependent vorticity equations, we need to develop a numerical approximation based on these equations that conserves mass, momentum, vorticity, and energy. We also need to assess numerical finite-difference methods and, in particular, the fourth-order and pseudo-spectral methods.

1.4 Overview

The equations of motion of the large eddies are derived by averaging (filtering) the vorticity equations in space. In Chapter 2, we describe the approach to solving turbulent flow problems that is called large-eddy simulation. We show that the use of a filter that is smooth in the real space is required to handle rotational-irrotational regions. We present a new subgrid scale model to be used in conjunction with the vorticity equations that is much simpler and faster than the one that would be obtained from the more commonly used Smagorinsky model.

In Chapter 3, we describe the numerical methods used in this work, briefly discussing the fourth-order and pseudo-spectral approximations and numerical filtering. We develop a numerical approximation to the vorticity equation that conserves mass, momentum, vorticity, and energy, and a method of deriving conservation properties that is much simpler than previous methods and is widely applicable. We present a new treatment of the filtered convective and stretching terms that is more accurate and faster than previously used methods.

In Chapter 4, the isotropic homogeneous turbulence problem is solved using both fourth-order differencing and the pseudo-spectral approximation. The numerical approximations to the partial derivatives of the subgrid scale model are discussed. We show that the use of the vorticity equation to solve turbulent flow problems is feasible and that the new model produces results equivalent to those produced by previously established models.

In Chapter 5, we discuss the two-dimensional computation of a mixing layer. An array of vortices is perturbed, and the momentum thickness growth rate is discussed as a function of the perturbation. It is interesting to note that self-similar, mean velocity and turbulence intensity profiles are obtained with vortex pairing.

In Chapter 6 a three-dimensional computation of a turbulent mixing layer is studied. It is found that the presence of large structures in the initial conditions is essential for the successful prediction of turbulent mixing layers. Our studies of different initial conditions produce different growth rates of the layer -- a fact supported experimentally. Self-similar, mean-velocity profiles are obtained with different flow structures. However, turbulence intensity profiles show a rapid decay when

large turbulent structures are not present. We show that our subgrid scale model inhibits the production of turbulent fluctuations when we start with random turbulent fluctuations added to a mean velocity profile, i.e., the model is incapable of handling transitional flows, with present computational limitations.

Chapter 2

THEORETICAL FOUNDATIONS

2.1 Definitions of the Large and Subgrid Scales

In the previous chapter it was shown that, due to computer limitations, one cannot do a full simulation of the dynamical equations of turbulent fluid motion except at extremely low Reynolds numbers. We pointed out that the large-scale turbulent structures differ markedly from one flow to another (e.g., jet vs. boundary layer), while the small-scale turbulent structures are quite similar, and that large-eddy simulation is a promising approach.

In the large-eddy simulation approach, the first and most fundamental step is defining the large-scale field. A general approach that recognizes the continuous nature of the flow variables is the "filter function" approach of Leonard (1973). If f is some flow variable, we can decompose it as follows:

$$f = \overline{f} + f' \tag{2.1}$$

where $\overline{f}$ is the large-scale (filtered) component and f' is the residual field. Leonard defined the filtered field by:

$$\overline{f} = \int_{\mathcal{D}} G(\underline{x}-\underline{x}')\, f(\underline{x}')\, d\underline{x}' \tag{2.2}$$

where $G(\underline{x}-\underline{x}')$ is the filter function, and the integral is extended over the whole flow field. One can think of $\overline{f}$ as a <u>local</u> spatial-averaged field.

It can be shown that if G is piecewise continuously differentiable and $G(\underline{r})$ goes to zero as $r \to \infty$ and is integrable over an infinite domain, then

$$\overline{\frac{\partial f}{\partial x}} = \frac{\partial \overline{f}}{\partial x} \tag{2.3a}$$

However, in general,

$$\overline{\bar{f}\bar{g}} \neq \bar{f}\bar{g} \tag{2.3b}$$

Properties (2.3a) and (2.3b) will be used in deriving the dynamical equations of the large scales motion.

2.2 Dynamical Equations in Vorticity Form

In Chapter 1, we pointed out that in many flows of practical interest there are interactions between irrotational regions and rotational turbulent regions. Examples of such flows are shear layers, turbulent jets, and turbulent boundary layers with irrotational free streams. In such flows the regions are separated by a very thin superlayer across which there is normally a jump in the vorticity parallel to the layer. These flows are a challenge to the experimentalist; the difficulties arise from the fact that it is hard to determine the region of the flow in which the measurements are made. One faces a similar problem in trying to simulate such flows numerically. The difficulty arises from the fact discussed earlier, that it is impossible to capture all of the scales of motion in the turbulent region. The best we can do is to filter the dynamical equations to obtain equations that describe the behavior of the large eddies, and to model the small scales. Since in the irrotational region the vorticity is identically zero, the dynamical equations for the vorticity seem to be suited to simulate such flows.

Now let us derive the dynamical equations for the large-scale vorticity field. For an incompressible fluid with constant viscosity, the equations of motion for the primitive variables may be written:

$$\frac{\partial u_i}{\partial t} - \varepsilon_{ijk} u_j \omega_k = -\frac{\partial}{\partial x_i}\left(\frac{P}{\rho} - \frac{1}{2} u_i u_i\right) - \nu \varepsilon_{ijk} \frac{\partial}{\partial x_j} \omega_k \tag{2.4}$$

$$\frac{\partial u_i}{\partial x_i} = 0 \tag{2.5}$$

The vorticity equation is obtained by taking the curl of Eqn. (2.4). Operating on it with $\varepsilon_{pqi}\, \partial/\partial x_q$ gives:

$$\frac{\partial}{\partial t}\omega_i + \frac{\partial}{\partial x_j}(u_j\omega_i - u_i\omega_j) = \nu\frac{\partial^2\omega_i}{\partial x_j x_j} \tag{2.6}$$

Multiplying Eqn. (2.6) by a filtering function $G(\underline{x}-\underline{x}')$ and integrating over the whole flow field, we obtain:

$$\frac{\partial}{\partial t}\bar{\omega}_i + \frac{\partial}{\partial x_j}\overline{(u_j\omega_i - u_i\omega_j)} = \nu\frac{\partial^2\bar{\omega}_i}{\partial x_j\partial x_j} \tag{2.7}$$

The fact that a finite-difference approximation of Eqn. (2.7) would involve approximating higher derivatives of the velocity than would be the case with the primitive equations (Orszag and Israeli, 1974) need not worry us in this case. Since the equations are filtered, we shall be dealing with smooth functions.

As can be expected, when averaging nonlinear equations, we run into the closure problem; i.e., we need to express the quantities $\overline{u_j\omega_i}$ and $\overline{u_i\omega_j}$ in terms of $\bar{u}$ and $\bar{\omega}$. Expanding u and ω as in Eqn. (2.1), one obtains

$$\overline{u_j\omega_i - u_i\omega_j} = \overline{\bar{u}_j\bar{\omega}_i - \bar{u}_i\bar{\omega}_j} + W_{ij} \tag{2.8}$$

where

$$W_{ij} = \overline{\bar{u}_j\omega_i' + u_j'\bar{\omega}_i - \bar{u}_i\omega_j' - u_i'\bar{\omega}_j + u_j'\omega_i' - u_i'\omega_j'} \tag{2.9}$$

We note that W_{ij} contains subgrid scale quantities and hence must be modeled.

2.3 Subgrid Scale Models

We first note that the model of W_{ij} should satisfy the following necessary conditions:

1. Antisymmetry, since W_{ij} is an antisymmetric tensor and therefore

$$\frac{\partial}{\partial x_i}\frac{\partial}{\partial x_j}W_{ij} = 0 \tag{2.10}$$

It is important to preserve the antisymmetry property of W_{ij} in order to assure $\partial\omega_i/\partial x_i = 0$, since the dynamical equations for the

vorticity do not contain a pressure-like term which could be used to adjust the divergence of the vorticity.

2. It should vanish in an irrotational region, since W_{ij} vanishes in such regions.

3. It should be an energy sink, since it represents subgrid-scale effects.

2.3.1 Model ω - 1

Previous workers (Kwak et al., 1975; Shaanan et al., 1975), working with the filtered dynamical equations in the primitive variables, used an eddy-viscosity model for their subgrid-scale model. They modeled the term:

$$\tau_{ij} = \overline{u_i'u_j'} + \overline{u_j'\bar{u}_i} + \overline{u_i'\bar{u}_j} - \frac{1}{3}\left(\overline{u_k'u_k'} + 2\overline{u_k'\bar{u}_k}\right)\delta_{ij}$$

by setting

$$\tau_{ij} = -2\nu_T\bar{S}_{ij} \tag{2.11}$$

where

$$\bar{S}_{ij} = \frac{1}{2}\left(\frac{\partial}{\partial x_i}\bar{u}_j + \frac{\partial}{\partial x_j}\bar{u}_i\right) \tag{2.12}$$

is the strain rate tensor of the filtered field and ν_T is an eddy viscosity associated with the subgrid scale motions.

Smagorinsky (1963) suggested a model for ν_T

$$\nu_T = (C_s\Delta)^2\,(2\bar{S}_{ij}\bar{S}_{ij})^{1/2} \tag{2.13}$$

where C_s is a constant and Δ is the filter width. We note that in a non-turbulent region this model of ν_T may have a non-zero value, and hence it may give rise to residual stresses. Since our main objective is to handle interactions between a turbulent region and a non-turbulent region, this model was rejected for the present work.

One way to avoid this difficulty is to relate ν_T directly to vorticity. Previous workers (Kwak et al., 1975; Donaldson, 1972) used

$$\nu_T = (C_v\Delta)^2\,(\bar{\omega}_i\bar{\omega}_i)^{1/2} \tag{2.14}$$

where C_v is a constant. Clark et al. (1977) have shown that this model is as accurate as Smagorinsky's for homogeneous isotropic turbulence.

The dynamical equations for large-scale vorticity field could have been derived by taking the curl of the filtered dynamical equations for the primitive variables. Hence the curl of Eqn. (2.11) could be used to model W_{ij}; this would give

$$W_{ij} = - \varepsilon_{ijk} \frac{\partial}{\partial x_\ell} (2\nu_T \bar{S}_{k\ell}) \tag{2.15}$$

where $\bar{S}_{k\ell}$ and ν_T are defined by Eqns. (2.12) and (2.14), respectively. We shall refer to this as Model ω-1.

2.3.2 Model ω-2

We note that the model given by Eqn. (2.15) involves computing the strain-rate tensor $\bar{S}_{k\ell}$, which is an expensive process. It also uses the velocity field and hence requires storage space for the velocity fields even after the convective and stretching terms have been computed. Much computational saving could be obtained with a model that involves only the vorticity field; one such model is

$$W_{ij} = - \frac{\partial}{\partial x_j} (\nu_T \bar{\omega}_i) + \frac{\partial}{\partial x_i} (\nu_T \bar{\omega}_j) \tag{2.16}$$

where ν_T is defined by Eqn. (2.14). We shall refer to this as model ω-2.

Both models ω-1 and ω-2 can be shown to satisfy all three properties mentioned previously (see Appendix A). Model ω-2 offers computational as well as storage advantages over model ω-1 and will be tested in Chapter 4 (along with model ω-1), for the case of isotropic homogeneous turbulence.

2.4 Filtering

2.4.1 Sharp Cut-off (SCK) Filter

Analytically, a filter that divides the large scales and the subgrid scales into two distinct regions in the Fourier sense would be convenient. Then $\overline{f}$ would contain all scales larger than a cut-off scale, and the subgrid scales (f') would contain all scales smaller than this cut-off scale. A one-dimensional version of such a filter is

$$G(x-x') = \frac{\sin[k_c(x-x')]}{\pi(x-x')} \tag{2.17}$$

and its Fourier transform is

$$H(k) = \begin{cases} 0 & \text{if } |k| > k_c \\ 1 & \text{otherwise} \end{cases} \tag{2.18}$$

We shall refer to this as the SCK (Sharp cut-off in k-space) filter.

In inhomogeneous flows with turbulent rotational regions and irrotational regions, the two regions are separated by a sharp vorticity jump. In order to evaluate the ability of the SCK filter to smooth out jumps in the vorticity field, we apply it to a point vortex situated at the origin:

$$\omega(x,y) = \delta(x)\,\delta(y) \tag{2.19}$$

and

$$\bar{\omega}(x,y) = \frac{\sin[k_c x]}{\pi x}\,\frac{\sin[k_c y]}{\pi y} \tag{2.20}$$

$\bar{\omega}$ is plotted in Fig. 2.1.

First we note that this filter creates oscillations and negative vorticity, which are undesirable from a physical point of view. Second, those oscillations decay slowly (they go as x^{-1}), so the spreading into the irrotational region is excessive.

2.4.2 Gaussian (GS) Filter

Another filter that has been used by previous workers (Kwak et al., 1975) is the Gaussian spatial (GS) filter:

$$G(x-x') = \sqrt{\frac{\gamma}{\pi}} \frac{1}{\Delta} \exp\{-\gamma(x-x')^2/\Delta^2\} \tag{2.21}$$

where γ is a constant and Δ is the filter width.

Applying this filter to a point vortex situated at the origin, we get

$$\bar{\omega}(x,y) = \frac{\gamma}{\pi} \frac{1}{\Delta^2} \exp\{-\frac{\gamma}{\Delta^2}(x^2+y^2)\} \tag{2.22}$$

$\bar{\omega}$ is plotted in Fig. 2.2.

We note that in this case we have created neither oscillations nor negative vorticity. By filtering the point vortex (Eqn. (2.19)), we have created another vortex with a Gaussian core of width Δ.

We conclude that a Gaussian filter smoothes out jumps better than the sharp cut-off filter. Therefore, the GS filter was used in the cases investigated in this work.

2.5 Computing Velocity Field from the Vorticity Field

When the vorticity equation is used, the velocity becomes a diagnostic variable; i.e., the time variation of the velocity is not given explicitly by the equations but can be deduced once the vorticity is known. To do so, we shall define a vector potential ψ_k (see Lamb, 1932) such that:

$$\bar{u}_i = \varepsilon_{ijk} \frac{\partial}{\partial x_j} \psi_k \tag{2.23}$$

ψ_k can be chosen to be solenoidal; i.e.,

$$\frac{\partial}{\partial x_k} \psi_k = 0 \tag{2.24}$$

Taking the curl of (2.23) and using (2.24), we get

$$\frac{\partial^2}{\partial x_j \partial x_j} \psi_i = -\bar{\omega}_i \tag{2.25}$$

Solving the Poisson equation (2.25) and using (2.23), we get the velocity field from the vorticity field.

Note that the velocity field could have been deduced in another fashion by setting

$$\bar{\omega}_i = \varepsilon_{ijk} \frac{\partial}{\partial x_j} \bar{u}_k \tag{2.26}$$

then taking the curl $\varepsilon_{pqi}\, \partial/\partial x_q$ of Eqn. (2.26) to get:

$$\frac{\partial^2}{\partial x_j \partial x_j} \bar{u}_i = - \varepsilon_{ijk} \frac{\partial}{\partial x_j} \bar{\omega}_k \tag{2.27}$$

and finally, solving the Poisson equation (2.27), we get the velocity field. This approach involves differentiation of the vorticity field, followed by a double integration, whereas the first approach of (2.25) involves double integration followed by differentiation (2.23). Numerically, the first approach is usually more desirable; but in our case the two approaches are equivalent. Eqns. (2.23)-(2.25) will be used in this study.

2.6 Summary

Neglecting the molecular viscosity, the filtered dynamical equations in vorticity form become

$$\frac{\partial \bar{\omega}_i}{\partial t} + \frac{\partial}{\partial x_j} \overline{(\bar{u}_j \bar{\omega}_i - \bar{u}_i \bar{\omega}_j)} = - \frac{\partial}{\partial x_j} W_{ij} \tag{2.28}$$

$$\frac{\partial^2 \psi_i}{\partial x_j \partial x_j} = - \bar{\omega}_i \tag{2.25}$$

$$\bar{u}_i = \varepsilon_{ijk} \frac{\partial}{\partial x_j} \psi_k \tag{2.23}$$

where W_{ij} is modeled as

$$W_{ij} = - \varepsilon_{ijk} \frac{\partial}{\partial x_\ell} (2\nu_T \bar{S}_{k\ell}) \tag{2.15}$$

or

or

$$W_{ij} = -\frac{\partial}{\partial x_j}(\nu_T \bar{\omega}_i) + \frac{\partial}{\partial x_i}(\nu_T \bar{\omega}_j) \tag{2.16}$$

where

$$\nu_T = (C_v \Delta)^2 (\bar{\omega}_i \bar{\omega}_i)^{\frac{1}{2}} \tag{2.14}$$

and

$$\bar{S}_{ij} = \frac{1}{2}\left(\frac{\partial}{\partial x_j}\bar{u}_i + \frac{\partial}{\partial x_i}\bar{u}_j\right) \tag{2.12}$$

with

$$G(\underline{x}-\underline{x}') = \sqrt{\left(\frac{\gamma}{\pi}\right)^3}\frac{1}{\Delta_1\Delta_2\Delta_3}\exp\left\{-\gamma\left[\frac{(x_1-x_1')^2}{\Delta_1^2}+\frac{(x_2-x_2')^2}{\Delta_2^2}+\frac{(x_3-x_3')^2}{\Delta_3^3}\right]\right\} \tag{2.29}$$

and

$$\Delta = (\Delta_1\Delta_2\Delta_3)^{1/3}$$

It is in this form that the problem will be solved numerically.

Chapter 3

NUMERICAL METHOD

Analytical solutions of the governing equations discussed in the previous chapter can be found for only very special cases, none representing turbulence. Therefore, we propose using large computing machines to solve these equations for particular cases of interest. Numerical approximations of the governing equations require special care. In this chapter we discuss these approximations and present the methods we use to solve the difference approximation to the governing differential equations.

3.1 Notations

A region of continuous space is divided into a uniform rectangular mesh; h_i $(i=1,2,3)$ represents the mesh width in the i^{th} direction. The mesh width need not be the same as the averaging width introduced in the previous chapters; we have used $\Delta_i = 2h_i$ and $\gamma = 6$. For details on the effects of the filter width on the computational results see Kwak et al. (1975).

We then write the ℓ-component of the filtered flow quantity f_ℓ at the n^{th} time step as

$$f_\ell^{(n)}(i,j,k) \quad , \qquad \ell = 1,2,3 \tag{3.1}$$

where (i,j,k) are the mesh point index for (x,y,z).

We define the operator notation $\delta/\delta\xi$ to be the numerical approximation to the continuous derivatives $(\partial/\partial\xi)$.

3.2 Numerical Approximation

Once space is discretized into mesh points, it remains to approximate the partial derivatives in terms of the values of the functions at those points. We have used two different approximation schemes: a fourth-order scheme and a pseudo-spectral method.

3.2.1 Fourth-Order Scheme

Using Taylor series expansions one can easily show that the approximation to the partial derivatives,

$$\frac{\delta \bar{u}}{\delta x_1} = \frac{1}{12h_1} \{\bar{u}(i-2) - 8\bar{u}(i-1) + 8\bar{u}(i+1) - \bar{u}(i+2)\} \qquad (3.2)$$

is fourth-order accurate, i.e., the error in this approximation is of $O(h^4)$. (For simplicity, the arguments j and k are not shown.)

If periodic boundary conditions are to be used, $\bar{u}$ can be represented by a discrete Fourier expansion (see next section).

$$\bar{u} = \sum_{\underline{n}} \hat{\bar{u}}(k)\, e^{i\underline{k}\cdot\underline{x}} \qquad (3.3)$$

where, for i = 1,2,3,

$$k_i = \frac{2\pi}{N_i h_i} n_i = \text{wave number in the } x_i \text{ direction}$$

$$n_i = -\frac{N_i}{2}, \ldots, 0, \ldots, \frac{N_i}{2} - 1$$

$$N_i = \text{number of mesh points in } x_i \text{ direction}$$

$\hat{\bar{u}}(k)$ is the discrete Fourier transform of $\bar{u}$. Taking the discrete Fourier transform of (3.2), we get

$$\frac{\delta \hat{\bar{u}}}{\delta x_1} = \frac{1}{12h_1} \left\{ e^{-i2h_1k_1} - 8e^{-ih_1k_1} + 8e^{ih_1k_1} - e^{i2h_1k_1} \right\} \hat{\bar{u}}$$

$$= \frac{i}{6h_1} \{8 \sin(h_1k_1) - \sin(2h_1k_1)\} \hat{\bar{u}}$$

$$= ik_1' \hat{\bar{u}}$$

where

$$k_1' = \frac{1}{6h_1} \{8 \sin(h_1k_1) - \sin(2h_1k_1)\} \qquad (3.4)$$

is called the modified wave number.

Representation (3.4) allows us to evaluate the numerical approximation (3.2) for the range of wave numbers up to π/h_1, the highest wave number that can be represented on a grid of size h_1. The Fourier transform of the exact derivative is $ik_1\hat{\bar{u}}$, so that, by comparing the modified wave number k_1' with k_1, we see how well the approximation works (see Fig. 3.1).

A more important consequence of representation (3.4) is that it allows us to integrate numerically in a manner consistent with our difference approximation. In order to make this point clear, suppose we know the value, f, of the numerical approximation of the differential equation

$$\frac{\delta\bar{u}}{\delta x_1} = f \tag{3.5}$$

and we would like to find $\bar{u}$, which when fourth-order finite differenced, gives us f exactly (to machine round-off). One way to do this is to write

$$A\bar{u}(i) = f(i) \tag{3.6}$$

where

$$A = \frac{1}{12h_1}\begin{bmatrix} 0 & 8 & -1 & 0 & & & 0 & 1 & -8 \\ -8 & 0 & 8 & -1 & & & 0 & 0 & 1 \\ 1 & -8 & 0 & 8 & -1 & & & & \\ \cdot & & & & & & & & \\ \cdot & & & & & & & & \\ \cdot & & & & & & & & \\ -1 & 0 & 0 & & & & & & \\ 8 & -1 & 0 & . & . & . & 1 & -8 & 0 \end{bmatrix}$$

for the case of periodic boundary conditions. This system of equations can then be solved in some standard way.

Another way to handle this problem is by taking the discrete Fourier transform of (3.5) to get

$$ik_1'\hat{\bar{u}} = \hat{f} \tag{3.7}$$

Then, by solving for $\hat{\underline{u}}$,

$$\hat{\underline{u}} = \frac{\hat{f}}{ik_1'} \tag{3.8}$$

multiplying (3.8) by $e^{i\underline{k}\cdot\underline{x}}$, and summing over all $\underline{k}$, we obtain $\bar{u}$. In this case only the one-dimensional transform is needed. This method, which is much more powerful than the previous one when integration in more than one direction is needed, will be used extensively for the solution of the Poisson equations (2.21).

3.2.2 Pseudo-Spectral Method

Periodic boundary conditions

Suppose $f(x_1)$ is periodic in the x_1 direction with period L (in the following we shall consider the one-dimensional case) and satisfies the "Dirichlet condition", i.e.,

- $f(x_1)$ is defined at every point of the interval $0 \leq x_1 \leq L$,
- $f(x_1)$ is everywhere single-valued, finite, and sectionally continuous,
- $f(x_1)$ is of "bounded variation", i.e., $f(x_1)$ does not have an infinite number of maxima and minima.

It can be shown (Lanczos, 1956) that a function of this type can be expanded in a convergent Fourier series.

$$f(x_1) = \sum_{n_1=-\infty}^{\infty} \hat{f}(k_1)\, e^{ik_1x_1} \tag{3.9}$$

where

$$k_1 = \frac{2\pi}{L} n_1 \qquad n_1 = -\infty, \ldots, 0, 1, \ldots, \infty$$

and

$$\hat{f}(k_1) = \frac{1}{L}\int_0^L f(x_1)\, e^{-ik_1x_1}\, dx_1 \tag{3.10}$$

Since computers cannot handle infinite series, we have to truncate (3.9). This is justifiable if $f(k_1)$ falls off rapidly for large $|k_1|$; this is the case of interest, since we filter the flow variables. Also, as mentioned before, we need to discretize in space. If N_1 mesh points are used in the x_1 direction, the discrete analogs of Eqns. (3.9) and (3.10) become:

$$f(x_1) = \sum_{n_1=-N_1/2}^{N_1/2-1} \hat{f}(k_1)\, e^{ik_1x_1} \tag{3.11}$$

where

$$k_1 = \frac{2\pi}{N_1 h_1} n_1 \qquad n_1 = -\frac{N_1}{2}, \ldots, 0, \ldots, \frac{N_1}{2} - 1$$

$$x_1 = jh_1 \qquad j = 0, \ldots, N_1 - 1$$

$$h_1 = L/N_1$$

$$\hat{f}(k_1) = \frac{1}{N_1} \sum_{j=o}^{N_1-1} f(x_1)\, e^{-ik_1x_1} \tag{3.12}$$

Fast algorithms (for $N_1 = 2^n$; $n = 1,2,\ldots$) have been developed (Fast Fourier Transform -- FFT) by various workers (Cooley and Tukey, 1965; Singleton, 1967) to evaluate the series (3.11) and (3.12) for the inverse-transform and the forward-transform, respectively. These will not be described in this work (we used a routine developed by Singleton, 1967).

If we regard the expansion (3.11) as an interpolating formula, so that we treat x_1 as a continuous variable, and differentiate the entire equation, we obtain

$$\frac{\delta f}{\delta x_1} = \sum_{n_1} \hat{f}(k_1)\, ik_1\, e^{ik_1x_1} \tag{3.13}$$

The expansion (3.13) can be considered an approximation to the partial derivatives. Thus, to compute the partial derivatives of $\bar{u}$, for the case of periodic boundary conditions, we proceed as follows: we find the discrete Fourier transform of the function in the direction in which the partial derivative is needed, i.e., we compute $\hat{f}(k_1)$ from $f(x_1)$.

Multiplying $f(k_1)$ by $ik_1 e^{ik_1 x_1}$ and summing over all k_1, we obtain $\delta f/\delta x_1$. This is called the "pseudo-spectral" approach. This method has been analyzed by Lanczos (1956) and, with the development of techniques to compute the summations (3.11) rapidly, it has been proposed by Kreiss and Oliger (1973) as an approximation method and advocated by Orszag (1973) and Fox and Orszag (1973).

For the range of wave numbers that can be captured with a given spacing and number of grid points and for periodic boundary conditions, the pseudo-spectral method yields extremely accurate values of the partial derivatives (see Fig. 3.1).

The above method is limited to the case of periodic boundary conditions. However, the idea can be applied to other types of boundary conditions by using a set of orthogonal functions appropriate to the given boundary conditions.

f = 0 boundary conditions

If $f(x_1)$ is required to vanish at the boundary, i.e., $f(x_1) = 0$ for $x_1 = 0$ and $x_1 = L$, and is twice differentiable (a physically reasonable assumption), the Hilbert-Schmidt theory shows that its Fourier sine series

$$f(x_1) = \sum_{n_1=o}^{\infty} \hat{f}^s_{n_1} \sin\left[\frac{n_1 \pi}{L} x_1\right] \tag{3.14}$$

where

$$\hat{f}^s_{n_1} = \frac{2}{L}\int_o^L f(x_1) \sin\left[\frac{n_1 \pi}{L} x_1\right] dx_1 \tag{3.15}$$

is absolutely and uniformly convergent. As in the previous section, we shall use the discrete analogs to (3.14) and (3.15), i.e.,

$$f(x_1) = \sum_{n_1=o}^{N_1-1} \hat{f}^s(n_1) \sin\left[\frac{n_1 \pi}{(N_1-1)h_1} x_1\right] \tag{3.16}$$

$$\hat{f}^s(n_1) = \frac{2}{(N_1-1)} \sum_{j=o}^{N_1-1} f(x_1) \sin\left[\frac{n_1 \pi}{(N_1-1)h_1} x_1\right] \tag{3.17}$$

where

$$n_1 = 0, \ldots, N_1 - 1$$

$$h_1 = L/(N_1 - 1)$$

$$x_1 = jh_1 \quad , \quad j = 0, \ldots, N_1 - 1$$

and $\hat{f}^s(n_1)$ is the Fourier sine transform of $f(x_1)$. By using the FFT routine, a technique to compute the summation in Eqns. (3.16) and (3.17) can be rapidly developed. A detailed development of the Fast Discrete Sine Transform (FDST) is given in Appendix B. Generally, the FDST requires twice as much computation (for a given number of mesh points) as does the FFT.

If we regard the expansion (3.16) as an interpolating formula, treating x_1 as a continuous variable, and differentiate, one obtains:

$$\frac{\delta f}{\delta x_1} = \sum_{n_1=o}^{N_1-1} \hat{f}^s(n_1)\, k_1 \cos\left[\frac{n_1\pi}{(N_1-1)h_1}\, x_1\right] \tag{3.18}$$

where $k_1 = n_1\pi/(N_1-1)h_1$. In order to be able to use (3.18) as an approximation formula for the partial derivatives, we need an FDST to find $\hat{f}^s(n_1)$; we also need a Fast Discrete Cosine Transform (FDCT). The discrete Fourier cosine series is defined in analogy to (3.16):

$$f(x_1) = \sum_{n_1=o}^{N_1-1} \hat{f'}^c(n_1) \cos\left[\frac{n_1\pi}{(N_1-1)h_1}\, x_1\right] \tag{3.19}$$

and

$$\hat{f}^c(n_1) = \frac{2}{(N_1-1)} \sum_{j=o}^{N_1-1} f'(x_1) \cos\left[\frac{n_1\pi}{(N_1-1)h_1}\, x_1\right] \tag{3.20}$$

with

$$\hat{f'}^c(n_1) = \begin{cases} \frac{1}{2}\hat{f}^c(n_1) & n_1 = 0, N_1 - 1 \\ \hat{f}^c(n_1) & n_1 \neq 0, N_1 - 1 \end{cases}$$

$$f'(x_1) = \begin{cases} \frac{1}{2} f(x_1) & x_1 = 0, L \\ f(x_1) & x_1 \neq 0, L \end{cases}$$

where $\hat{f}^{c}(n_1)$ is the Fourier cosine transform of $f(x_1)$.

Note that in (3.18) $\hat{f}^{s}(0) = \hat{f}^{s}(N_1 - 1) = 0$, making (3.18) exactly a discrete cosine transform of $k_1 \hat{f}^{s}(n_1)$.

By using the FFT routine, a technique of computing the summations in Eqn. (3.19) and (3.20) can be rapidly developed. A detailed development of the Fast Discrete Cosine Transform (FDCT) is given in Appendix B.

Thus, to compute the partial derivatives of a function which is zero at the boundary, we find its discrete sine transform $\hat{f}^{s}(n_1)$, multiply it by $n_1\pi/[(N_1 - 1)h_1]$ and inverse transform using an FDCT routine. This method yields an extremely accurate approximation of the partial derivative when the function vanishes at the boundary, but its use is restricted to cases with a uniform mesh.

$\partial f/\partial x = 0$ boundary conditions

If $f(x_1)$ is our function whose partial derivative $\partial f/\partial x_1$ vanishes at the boundary, i.e., $\partial f/\partial x_1 = 0$ for $x_1 = 0$ and $x_1 = L$, then, by using arguments similar to those used before, it can be shown that its Fourier cosine series,

$$f(x_1) = \sum_{n_1=0}^{\infty} \hat{f}'^{c}_{n_1} \cos\left[\frac{n_1\pi}{L} x_1\right] \tag{3.21}$$

where

$$\hat{f}^{c}_{n_1} = \frac{2}{L}\int_0^L f(x_1) \cos\left[\frac{n_1\pi}{L} x_1\right] dx_1 \tag{3.22}$$

$$\hat{f}'^{c}_{n_1} = \begin{cases} \hat{f}^{c}_{n_1}, & n_1 \neq 0 \\ \frac{1}{2}\hat{f}^{c}_{n_1}, & n_1 = 0 \end{cases}$$

is uniformly and absolutely convergent.

Equations (3.19) and (3.20) are the discrete equivalents of the above equations. If we regard expansion (3.19) as an interpolating formula treating x_1 as a continuous variable, then differentiate, we obtain:

$$\frac{\delta f}{\delta x_1} = \sum_{n_1=0}^{N_1-1} - \hat{f}^{c}(n_1)\, k_1 \sin\left[\frac{n_1\pi}{(N_1-1)h_1} x_1\right] \tag{3.23}$$

Obviously (3.23) satisfies the conditions $\partial f/\partial x_1 = 0$ at $x_1 = 0$ and $x_1 = L$, and (3.23) is the discrete sine expansion of the partial derivative.

Thus, to compute the partial derivative of a function for which $\partial f/\partial x_1 = 0$ at the boundary, we find its discrete cosine transform $\hat{f}^c(n_1)$, multiply it by $-k_1$, and take the inverse transform using an FDST routine.

The three methods described in this section will be used extensively as our approximation tools.

3.3 Time Differencing

To advance in time, a second-order Adams-Bashforth method was used. This method has been used by previous workers (Kwak et al., 1975; Shaanan et al., 1975), and use of a higher-order method was not felt necessary.

If $\partial\bar{\omega}_i/\partial t = M_i$, the Adams-Bashforth formula for $\bar{\omega}_i$ at time-step $n + 1$ is

$$\bar{\omega}_i^{n+1} = \bar{\omega}_i^n + \Delta t \left(\frac{3}{2} M_i^{(n)} - \frac{1}{2} M_i^{(n-1)} \right) \tag{3.24}$$

In our case,

$$M_i = - \frac{\partial}{\partial x_j} \overline{(\bar{u}_j \bar{\omega}_i - \bar{u}_i \bar{\omega}_j)} - \frac{\partial}{\partial x_j} W_{ij}$$

Note that this is a two-step explicit method. It is started with the Euler method:

$$\omega_i^1 = \omega_i^0 + \Delta t \, M_i^{(0)} \tag{3.25}$$

3.4 Conservation Properties

As was pointed out by Phillips (1959), numerical integration of the finite-difference analog of the Navier-Stokes equations may introduce nonlinear instabilities if proper care is not taken. Arakawa (1966), working with the two-dimensional vorticity equation, showed that by properly conserving vorticity, energy, and enstrophy $(\omega_i \omega_i)$, these instabilities disappear. Lilly (1965), working with the primitive variables, developed a spatial-differencing scheme that conserves momentum and energy. By

conservation we mean that, in the absence of external forces and viscous dissipation, the only way that the momentum and kinetic energy in a control volume can change is by flow through the surface. This property must be retained by the numerical approximation. In the simple case of periodic boundary conditions, we have

$$\frac{d}{dt}\int_D \bar{u}_i dv = 0 \quad \text{(i.e., momentum conservation)} \tag{3.26}$$

$$\frac{d}{dt}\int_D \frac{1}{2}\bar{u}_i\bar{u}_i dv = 0 \quad \text{(i.e., energy conservation)} \tag{3.27}$$

It is usually easy to devise a numerical approximation to the dynamical equations in primitive form that conserves momentum, i.e., summation over the flow volume of the approximate equations would give the discrete equivalent of Eqn. (3.26). However, the difficulties arise when trying to show energy conservation, since in general the identity

$$u_i \frac{\partial}{\partial x_j} u_i = \frac{\partial}{\partial x_j} \frac{1}{2} u_i u_i \tag{3.28}$$

does not hold in finite-difference form.

Writing the equations of motion in the following form (Tennekes and Lumley, 1972):

$$\frac{\partial}{\partial t} u_i + u_j\left(\frac{\partial u_i}{\partial x_j} - \frac{\partial u_j}{\partial x_i}\right) = -\frac{\partial}{\partial x_i}\left(\frac{P}{\rho} + \frac{1}{2} u_j u_j\right) \tag{3.29}$$

$$\frac{\partial}{\partial x_i} u_i = 0 \tag{3.30}$$

and integrating over the flow volume, we get

$$\frac{\partial}{\partial t}\int_s u_i dv + \int_s u_j\left(\frac{\partial u_i}{\partial x_j} - \frac{\partial u_j}{\partial x_i}\right) dv = -\int_s \frac{\partial}{\partial x_i}\left(\frac{P}{\rho} + \frac{1}{2} u_j u_j\right) dv \tag{3.31}$$

For periodic boundary conditions, integration by parts yields:

$$\int_s u_j \frac{\partial}{\partial x_j} u_i \, dv = -\int_s u_i \frac{\partial}{\partial x_j} u_j \, dv = 0 \quad \text{(using (3.30))}$$

$$\int_s u_j \frac{\partial}{\partial x_i} u_j \, dv = -\int_s u_j \frac{\partial}{\partial x_i} u_j \, dv = 0$$

and

$$\int_{\mathcal{D}} \frac{\partial}{\partial x_i}\left(\frac{P}{\rho} + \frac{1}{2}\, u_j u_j\right) dv \;=\; 0$$

Hence Eqn. (3.31) reduces to Eqn. (3.26) and we have momentum conservation.

Now, multiplying Eqn. (3.29) by u_i, we get:

$$\frac{\partial}{\partial t}\,\frac{1}{2}\, u_i u_i \;=\; -\, u_i\, \frac{\partial}{\partial x_i}\left(\frac{P}{\rho} + \frac{1}{2}\, u_j u_j\right) \tag{3.32}$$

where the convective terms sum to zero by symmetry.

Integrating (3.32) over the entire domain yields:

$$\frac{\partial}{\partial t}\int_{\mathcal{D}} \frac{1}{2}\, u_i u_i \, dv \;=\; -\int_{\mathcal{D}} u_i\, \frac{\partial}{\partial x_i}\left(\frac{P}{\rho} + \frac{1}{2}\, u_j u_j\right) dv \tag{3.33}$$

For periodic boundary conditions, integration by parts yields:

$$\int_{\mathcal{D}} u_i\, \frac{\partial}{\partial x_i}\left(\frac{P}{\rho} + \frac{1}{2}\, u_j u_j\right) dv \;=\; -\int \left(\frac{P}{\rho} + \frac{1}{2}\, u_j u_j\right) \frac{\partial}{\partial x_i}\, u_i \, dv$$

$$= \; 0 \qquad \text{(using (3.30))}$$

Hence Eqn. (3.33) reduces to Eqn. (3.27) and we have energy conservation.

We notice that, with the equations written in the form Eqn. (3.29), we did not need the identity (3.28) to show energy conservation from the dynamical equations in primitive form. The conservation properties were obtained by making use of only integration by parts and the continuity equation.

Consider the numerical approximation of Eqns. (3.29) and (3.30):

$$\frac{\partial}{\partial t}\, u_i + u_j \left(\frac{\delta u_i}{\delta x_j} - \frac{\delta u_j}{\delta x_i}\right) \;=\; -\,\frac{\delta}{\delta x_i}\left(\frac{P}{\rho} + \frac{1}{2}\, u_j u_j\right) \tag{3.34}$$

$$\frac{\delta}{\delta x_i}\, u_i \;=\; 0 \tag{3.35}$$

where we are using $\delta/\delta x_i$ to denote the numerical approximations to the partial derivatives $\partial/\partial x_i$, and the same approximations are used in both equations (3.34, 3.35) for any given independent variable. In order to

have long-term integration stability, Eqn. (3.34) should numerically conserve momentum and energy.

If we follow the steps used in deriving the conservation properties from Eqns. (3.29) and (3.30), we realize that the conservation properties will follow if we can establish numerical summation by parts. Consider the one-dimensional case, where we have, for periodic boundary conditions,

$$\int u(x) \frac{\partial}{\partial x} f(x)\, dx = -\int f(x) \frac{\partial}{\partial x} u(x)\, dx$$

The numerical analog of the above equation is:

$$\sum_{j=o}^{N-1} u(j) \frac{\delta}{\delta x} f(j) = -\sum_{j=o}^{N-1} f(j) \frac{\delta}{\delta x} u(j) \qquad (3.36)$$

Expanding $u(j)$ in Fourier series, we get:

$$u(j) = \sum_{n=-N/2}^{N/2-1} \hat{u}(n) \exp(2\pi ijn/N) \quad ; \quad j = 0,1,\ldots,N-1$$

where the $\hat{u}(n)$ are given by the inverse transform:

$$\hat{u}(n) = \frac{1}{N} \sum_{j=o}^{N-1} u(j) \exp(-2\pi ijn/N) \quad ; \quad n = -\frac{N}{2}, \ldots, \frac{N}{2}-1$$

Also,

$$\frac{\delta}{\delta x} f(j) = \sum_{n=-N/2}^{N/2-1} ik'(n) \left\{ \frac{1}{N} \sum_{j'=o}^{N-1} f(j') \exp(-2\pi ij'n/N) \right\} \exp(2\pi ijn/N) \qquad (3.37)$$

where $k'(n)$ is the modified wave number. The modified wave numbers for the numerical methods we are using are

- $ik' = ik$ for pseudo-spectral, (3.38)
- $ik' = i \frac{1}{6h} [8 \sin(kh) - \sin(2kh)]$ (fourth-order approximation.

Substituting Eqn. (3.37) into the left-hand side of Eqn. (3.36) yields

$$\sum_{j=o}^{N-1} u(j) \frac{\delta}{\delta x} f(j) = \frac{1}{N} \sum_{j=o}^{N-1} \sum_{j'=o}^{N-1} \sum_{n=-N/2}^{N/2-1} ik'(n)\, u(j)\, f(j') \cdot \exp(-2\pi ij'n/N) \exp(2\pi ijn/N)$$

Now, changing the summation index in the last sum from n to $-n$, we see that this expression will agree with the right-hand side of Eqn. (3.36), provided that:

$$k'(n) = -k'(-n) \tag{3.39}$$

$$k'\left(-\frac{N}{2}\right) = 0 \tag{3.40}$$

Condition (3.39) is satisfied by all the methods under consideration, and $k'(-N/2) = 0$ is true for the finite-difference method. The pseudo-spectral method cannot differentiate between $f = \exp(ij\pi)$ and $f = \exp(-ij\pi)$, and, due to this confusion at $n = -N/2$, $k'(-N/2)$ is set equal to zero for the pseudo-spectral method. Hence, summation by parts is obtained when (3.39) and (3.40) hold. Summing Equation (3.34) over all mesh points, using the generalization of (3.36) to three dimensions and using Eqn. (3.35) yields the numerical equivalent of (3.26). Multiplying Eqn. (3.34) by u_i, the nonlinear term in the left-hand side of (3.34) will sum to zero by symmetry; then, using as before the three-dimensional generalization of (3.36) and (3.35), summing over all mesh points will yield the numerical equivalent of Eqn. (3.27).

3.5 Differenced Vorticity Equations

In order to insure that the numerical approximation to the vorticity equations are equivalent to the numerical primitive equations, we must take the numerical curl of Eqn. (3.34). Before doing so, we note that, numerically,

$$\nabla \cdot \nabla \times \underline{V} = \varepsilon_{ijk} \frac{\delta}{\delta x_i} \frac{\delta}{\delta x_j} V_k \tag{3.41}$$

$$\nabla \times \nabla S = \varepsilon_{ijk} \frac{\delta}{\delta x_j} \frac{\delta}{\delta x_k} S \tag{3.42}$$

where $\underline{V}$ and S are any vector or scale, respectively, the above expressions are identically zero, if for each direction the same approximation is used for all operators.

The numerical curl of (3.34) is

$$\frac{\partial}{\partial t}\omega_i + \frac{\delta}{\delta x_j}(u_j\omega_i - u_i\omega_j) = 0 \qquad (3.43)$$

Equation (3.43) conserves vorticity, i.e., summing it over all space the total vorticity in any control volume (subject to periodic boundary conditions) does not change with time. Hence in the form (3.34), the primitive equations also conserve vorticity.

The numerical divergence of (3.43) is

$$\frac{\partial}{\partial t}\frac{\delta}{\delta x_i}\omega_i = 0$$

Therefore, an $\underline{\omega}$ field solenoidal at time t will remain solenoidal at time $t + \Delta t$.

3.6 Poisson Equation

Having the vorticity field ω_i at time step n, we have to find the velocity field in order to be able to advance in time. To do so, we shall define a vector potential (also called the vector stream function) ψ_k, such that

$$\bar{u}_i = \varepsilon_{ijk}\frac{\delta}{\delta x_j}\psi_k \qquad (3.44)$$

ψ_i can be chosen to be solenoidal; i.e.,

$$\frac{\delta}{\delta x_i}\psi_i = 0 \qquad (3.45)$$

Taking the curl of Eqn. (3.44) and using Eqn. (3.45), we get

$$\frac{\delta}{\delta x_j}\frac{\delta}{\delta x_j}\psi_i = -\bar{\omega}_i \qquad (3.46)$$

The Poisson equations (3.46) will be integrated using the approach introduced in Section 3.2. For the case of periodic boundary condition, the discrete Fourier transform of Eqn. (3.46) is

$$-k_j'k_j'\hat{\psi}_i = -\hat{\bar{\omega}}_i \qquad (3.47)$$

where k'_i is the modified wave vector introduced in Section 3.2. Solving for $\hat{\psi}_i$, we have

$$\hat{\psi}_i = \frac{\hat{\bar{\omega}}_i}{k'_j k'_j} \tag{3.48}$$

and by inverting the transform we obtain the stream vector consistent with our numerical differencing. It satisfies two conditions. First, the velocity field obtained using (3.44) will be solenoidal. We have in Fourier space:

$$k'_i \hat{\bar{u}}_i = \varepsilon_{ijk} k'_i k'_j \hat{\psi}_k = 0 \tag{3.49}$$

Second, taking the curl of (3.44), we have in Fourier space:

$$\begin{aligned} \hat{\bar{\omega}}_i &= \varepsilon_{ijk}\, ik'_j\, \hat{\bar{u}}_k = -\varepsilon_{ijk}\, \varepsilon_{kpq}\, k'_j k'_p\, \hat{\psi}_q \\ &= -k'_j k'_j \hat{\psi}_i + k'_i k'_j\, \hat{\psi}_j \end{aligned} \tag{3.50}$$

Since $k'_j \hat{\psi}_j = 0$, (3.50) is exactly the Poisson equation (3.47).

3.7 Numerical Filtering

Examination of Eqn. (3.24) reveals that the only numerical problem left is the numerical evaluation of the $\overline{\bar{u}_j \bar{\omega}_i} - \bar{u}_i \bar{\omega}_j$ term. Since $\bar{u}_j \bar{\omega}_i - \bar{u}_i \bar{\omega}_j$ can be computed easily, the problem is that of numerical filtering. Filtering is the evaluation of a convolution integral

$$\overline{\bar{u}_j \bar{\omega}_i} = \int_{-\infty}^{+\infty} \bar{u}_j \bar{\omega}_i\, G(x-x')\, dx' \tag{3.51}$$

If this integral is evaluated using conventional integration routines, the computation cost is prohibitive. Previous workers (Leonard, 1973; Kwak et al., 1975; Shaanan et al., 1975) argued that the filtered terms $\bar{u}_j(x')$ and $\bar{\omega}_i(x')$ are smooth, and they expanded those terms in a Taylor series about x. Using a Gaussian for $G(x)$, they obtained:

$$\overline{\bar{u}_j \bar{\omega}_i} = \bar{u}_j \bar{\omega}_i + \frac{\Delta^2}{4\gamma} \nabla^2 (\bar{u}_j \bar{\omega}_i) + O(\Delta^4) \tag{3.52}$$

and the $O(\Delta^2)$ term was called the Leonard term. The above approximation will require the use of a fourth-order, finite-differencing method (Kwak et al, 1975) or a modified second-order method (Shaanan et al., 1975) that yields the Leonard term as its truncation error. However, when higher-order methods are used the expansion (3.52) needs to be extended to higher orders, and the computational expense becomes prohibitive. When periodic boundary conditions are used, we can take the Fourier transform of Eqn. (3.51) to get:

$$\widehat{\overline{\overline{u}_j\overline{\omega}_i}} = (\widehat{\overline{u}_j\overline{\omega}_i})\,\hat{G} \tag{3.53}$$

Thus, given $\overline{u}_i$ and $\overline{\omega}_i$, one can compute the term $(\widehat{\overline{u}_j\overline{\omega}_i})$, multiply it by $\hat{G}$, then simply invert the transform to obtain $\overline{\overline{u}_j\overline{\omega}_i}$.

When $\overline{u}_j\overline{\omega}_i$ vanishes at the boundaries, i.e., $\overline{u}_j\overline{\omega}_i = 0$ at $x = 0$ and $x = L$, we can expand it in a Fourier sine series. Taking the one-dimensional case, for simplicity, we set

$$\overline{u}_j\overline{\omega}_i = \sum_{n=0}^{\infty} (\widehat{\overline{u}_j\overline{\omega}_i})^s \sin\left(\frac{n\pi}{L}x\right) \tag{3.54}$$

Substituting (3.54) in (3.51), we get

$$\overline{\overline{u}_j\overline{\omega}_i} = \int_{-\infty}^{+\infty} \sum_{n=0}^{\infty} (\widehat{\overline{u}_j\overline{\omega}_i})^s \sin\left(\frac{n\pi}{L}(x-x')\right) G(x')\,dx'$$

Since the series (3.54) is absolutely and uniformly convergent, we can take the summation outside the integration to obtain

$$\overline{\overline{u}_j\overline{\omega}_i} = \sum_{n=0}^{\infty} (\widehat{\overline{u}_j\overline{\omega}_i})^s \left\{ \int_{-\infty}^{+\infty} \sin\left(\frac{n\pi}{L}x\right) \cos\left(\frac{n\pi}{L}x'\right) G(x')\,dx' + \int_{-\infty}^{+\infty} \cos\left(\frac{n\pi}{L}x\right) \sin\left(\frac{n\pi}{L}x'\right) G(x')\,dx' \right\}$$

If $G(x)$ is an even function, which is the case when (2.21) is used, the second term in the bracket vanishes and one obtains

$$\begin{aligned} \overline{\overline{u}_j\overline{\omega}_i} &= \sum_{n=0}^{\infty} (\widehat{\overline{u}_j\overline{\omega}_i})^s \left\{ \int_{-\infty}^{+\infty} G(x') \cos\left(\frac{n\pi}{L}x'\right) dx' \right\} \sin\left(\frac{n\pi}{L}x\right) \\ &= \sum_{n=0}^{\infty} (\widehat{\overline{u}_j\overline{\omega}_i})^s \hat{G}^c \sin\left(\frac{n\pi}{L}x\right) \end{aligned} \tag{3.55}$$

where

$$\hat{G}^c = \int_{-\infty}^{+\infty} G(x') \cos\left(\frac{n\pi}{L} x'\right) dx'$$

is the Fourier cosine transform of the Gaussian filter.

What Eqn. (3.55) tells us is that, for the case in which $\bar{u}_j\bar{\omega}_i = 0$ for $x = 0$ and $x = L$, $\overline{\bar{u}_j\bar{\omega}_i}$ can be computed by the following procedure: we first compute the Fourier sine transform $(\bar{u}_j\bar{\omega}_i)^{\hat{}s}$ of $\bar{u}_j\bar{\omega}_i$, and then multiply it by the Fourier cosine transform $\hat{G}^c$ of the filter, to obtain the Fourier sine transform $\overline{(\bar{u}_j\bar{\omega}_i)}^{\hat{}s}$ of $\overline{\bar{u}_j\bar{\omega}_i}$. Finally, inverting the sine transform, we obtain $\overline{\bar{u}_j\bar{\omega}_i}$.

Similarly, it can be shown that, for the case in which $\frac{\partial}{\partial x}\bar{u}_j\bar{\omega}_i = 0$ at $x = 0$ and $x = L$, we have

$$\overline{\bar{u}_j\bar{\omega}_i} = \sum_{n=0}^{\infty} (\bar{u}_j\bar{\omega}_i)^{\hat{}c}\, \hat{G}^c \cos\left(\frac{n\pi}{L} x\right) \qquad (3.56)$$

or

$$\overline{(\bar{u}_j\bar{\omega}_i)^{\hat{}c}} = (\bar{u}_j\bar{\omega}_i)^{\hat{}c}\, \hat{G}^c$$

By the use of the FFT, FDST, and FDCT, "exact" filtering can be obtained for all boundary conditions of interest with acceptable computational speed.

An important property required of a filter is that the filtered value of a constant must be the same constant. Numerically, it is desirable to preserve this property, which is equivalent to requiring the integral of the filter function be unity or $\hat{G}(0) = 1$. The exact continuous Fourier transform of (2.21) is

$$\hat{G}(k) = \exp\left(-\frac{\Delta^2}{4\gamma} k^2\right) \qquad (3.57)$$

When $\hat{G}(k)$ is discretized, we get

$$\hat{G}_D(k) = \exp\left(-\frac{\Delta^2}{4\gamma}\left(\frac{2\pi}{L} n\right)^2\right), \quad n = 0, \pm1, \pm2, \ldots \qquad (3.58)$$

Hence $\hat{G}_D(0) = 1$.

Another property required of a filter is that it smooth out jumps (see Section 2.4) without introducing oscillations. We have modeled the situation with a top-hat function:

$$f(x) = \begin{cases} 1 & x_1 \leq x \leq x_2 \\ 0 & \text{otherwise} \end{cases} \tag{3.59}$$

Analytically, we have

$$\bar{f}(x) = \frac{1}{2}\left(\text{erf}(x_1 - x) - \text{erf}(x_2 - x)\right)$$

which is a smooth function with no oscillations.

When (3.59) is discretized and filtered numerically using $\hat{G}_D(k)$, the top-hat function, Eqn. (3.59), is smoothed out (see Fig. 3.2). However, small oscillations are introduced. This is due to the fact that the discrete inverse transform of (3.58) is not smooth. For this reason we have used a discrete Gaussian in x-space,

$$G_D(x) = \frac{1}{A}\exp\left(-\gamma\frac{(nh)^2}{\Delta^2}\right) \tag{3.60}$$

where

where

$$A = \sum_{n}^{x = hn} \exp\left(-\gamma\frac{(nh)^2}{\Delta^2}\right) \tag{3.61}$$

as our filter function. The oscillations in the x-space (see Fig. 3.2) do not appear when this filter is used.

3.8 Summary

The dynamical equations in vorticity form will be solved as follows:

$$\omega_i^{n+1} = \omega_i^n + \Delta t\left(\frac{3}{2}M_i^n - \frac{1}{2}M_i^{n-1}\right) \tag{3.24}$$

where

$$M_i = -\frac{\delta}{\delta x_j}\left(\overline{\bar{u}_j\bar{\omega}_i - \bar{u}_i\bar{\omega}_j}\right) - \frac{\delta}{\delta x_j}W_{ij}$$

$$W_{ij} = -\varepsilon_{ijk} \frac{\delta'}{\delta x_\ell} (2\nu_T \bar{S}_{k\ell}) \tag{3.25}$$

or

$$W_{ij} = -\frac{\delta'}{\delta x_j} (\nu_T \bar{\omega}_i) + \frac{\delta'}{\delta x_i} (\nu_T \bar{\omega}_j) \tag{3.26}$$

$$\nu_T = (C_v \Delta)^2 (\bar{\omega}_i \bar{\omega}_i)^{\frac{1}{2}} \tag{3.27}$$

and

$$\bar{S}_{ij} = \frac{1}{2}\left(\frac{\delta' \bar{u}_i}{\delta x_j} + \frac{\delta' \bar{u}_j}{\delta x_i}\right) \tag{3.28}$$

The numerical differencing $\frac{\delta'}{\delta x}$ used to compute the terms in the model (W_{ij}) need not be of the same order as the numerical differencing $\frac{\delta}{\delta x}$ used to compute the terms in the momentum equation. Filtering of the terms $\overline{\bar{u}_j \bar{\omega}_i - \bar{u}_i \bar{\omega}_j}$ is achieved using the method described in Section 3.7.

Chapter 4

DECAY OF ISOTROPIC TURBULENCE

4.1 Background

In order to assess the feasibility of using the vorticity equations as the governing equations for turbulent flows, we applied the computational methods described in Chapter 3 to the simplest problem in turbulence, namely, the decay of homogeneous isotropic turbulence. This flow was also used to determine the value of the subgrid scale model constant for use in subsequent calculations of other flows.

The grid turbulence experiment of Comte-Bellot and Corrsin (1971) was used as the "target" for our numerical predictions. When viewed in a coordinate frame moving with the mean velocity, this experiment approximates homogeneous isotropic turbulence.

This study was presented in an earlier report (P. Moin et al., 1978) and is rediscussed in this work to support the argument that model ω-2 used in conjunction with the vorticity equations produces similar results to those obtained using the more commonly used model ω-1. The contributions of Mr. P. Moin are gratefully acknowledged.

4.2 Initial Conditions

We started with an initial field that is divergence-free and has a spectrum obtained by filtering the experimental spectrum at the non-dimensional experimental time $T = U_o t/M = 42$. $U_o = 10$ cm/sec is the experimental free-stream air speed, $M = 5.08$ cm is the size of the experimental turbulence-generating grid, and t is the real time in seconds. The initial field was otherwise random. The generation of such a field is discussed in detail by Kwak et al. (1975) and will be briefly outlined herein. The filtered field is generated in k-space by setting:

$$\hat{u}_i(\underline{k}) = \left(\frac{2\pi}{L}\right)^3 \left(\frac{\overline{E}(k)}{2\pi k^2}\right)^{\frac{1}{2}} (aA_i + ibB_i) \qquad (4.1)$$

where

$\overline{E}(k)$ = filtered experimental energy spectrum at time $T = U_o t/M = 42$,

$a = \cos(\theta)$

$b = \sin(\theta)$

where θ is a random angle, A_i and B_i are unit vectors picked such that $A_i k_i' = B_i k_i' = 0$, otherwise random.

To insure that (4.1) is the Fourier transform of a real field, we must have

$$\hat{\overline{u}}_i(\underline{k}) = \hat{\overline{u}}_i^*(-\underline{k}) \tag{4.2}$$

where * indicates complex conjugate. Now, by inverse transforming $\hat{\overline{u}}_i$, $\overline{u}_i$ is obtained.

Using the above initial field, we shall use the methods of Chapters 2 and 3 to predict the spectrum at $T = 98$. The predicted spectrum will be compared with the filtered experimental spectrum at $T = 98$.

4.3 Selection of C_V

The model constant was obtained by matching the computational rate of filtered energy decay to that of the experiment (Fig. 4.1). The values of the constants obtained using different numerical schemes and different models were in most cases within ten percent of each other ($C_V = 0.2 \pm 0.02$, see Table 4.1).

4.4 Results

Under the assumption that the computational box size is large compared to the scale of the energy-containing motions, we can use periodic boundary conditions in all three directions. A uniform cubic mesh system was used with N, the mesh number in each direction, and h, the mesh spacing, chosen such that the computation captures as much of the turbulence energy as possible (Kwak et al., 1975). We used the sets

$$N = 16 \ , \ h = 1.5 \text{ cm} \ , \ t = 6.25 \times 10^{-3} \text{ sec}$$

and

$$N = 32 \ , \ h = 1.0 \text{ cm} \ , \ t = 6.25 \times 10^{-3} \text{ sec}$$

When periodic boundary conditions are used, it was shown in Chapter 3 that the pseudo-spectral method is more powerful than any finite-difference method. However, when the periodic pseudo-spectral methods cannot be used, we may have to use finite-difference methods. Since one of our objectives is to determine the model constant for the vorticity equations, both the fourth-order finite differencing and the pseudo-spectral methods were applied to the case of isotropic homogeneous turbulence.

4.4.1 Fourth-Order Finite Differences

Figure 4.2 shows the energy spectrum obtained by fourth-order finite-differencing the vorticity equation, using model $\omega-1$ (Eqn. (2.1)) for the subgrid-scale model, on a 16^3 mesh. Our results compare well with the experimental results up to wave number 2.5, after which the inaccuracy of fourth-order differencing begins to show. Fourth-order differencing the primitive equations (Kwak et al., 1975; Moin et al., 1978) produced good agreement with the filtered experimental results using the primitive variable version of this model. This shows that the vorticity approach is equivalent to the primitive variable method. Thus the use of the vorticity equations is definitely feasible in turbulent flow computations.

4.4.2 Pseudo-Spectral Method

Figures 4.3-4.6 show the energy spectra obtained using the pseudo-spectral method, with 16^3 mesh. Fig. 4.3 shows the results obtained using model $\omega-1$ (Eqn. (2.15)). We note that for $k \geq 1$ the computed results are considerably lower than the experimental values. This indicates that the subgrid-scale model is draining too much energy from the small structures, and, since our total energy is equal to that of the filtered experimental value, too little energy is taken out from the large structures. In this case, we used the pseudo-spectral approximation to calculate the subgrid scale terms as well as the other terms.

Figure 4.4 shows the energy spectrum obtained using second-order central differencing to approximate the derivatives appearing in the subgrid-scale model (see Section 3.8):

$$\frac{\delta'}{\delta x} f = \frac{f(i+1) - f(i-1)}{2h}$$

We note a considerable improvement in the spectrum, except for a small accumulation of energy at the extreme (high wave number) end of the spectrum, which was present to a lesser extent in Fig. 4.2.

Figures 4.5 and 4.6 are the results from a 16^3 computation using the pseudo-spectral method and model $\omega - 2$ (Eqn. (2.16)) for the subgrid-scale model. We note the same behavior in Fig. 4.5 as in Fig. 4.3; the computed spectrum falls below the experimental spectrum, indicating that using the pseudo-spectral method to compute the spatial derivatives in the subgrid-scale model damps too much energy in the wave number range $k \geq 1$. Using second-order finite differencing to compute the partial derivatives in the model $\omega - 2$ (Eqn. (2.16)), we obtain a significant improvement in the computed spectrum (Fig. 4.6). These results are similar to the results obtained using model $\omega - 1$, indicating that the two models are equally good.

Figure 4.7 shows the energy spectrum obtained from a 32^3 pseudo-spectral calculation, using second-order finite differencing to compute the partial derivatives in model $\omega - 2$. The results are similar to those of the 16^3 computation.

It can be concluded from these results that the vorticity equations provide a satisfactory basis for the simulation of homogeneous isotropic turbulence. Both models $\omega - 1$ and $\omega - 2$ produce similar results. Model $\omega - 2$, given by Eqn. (2.16), will be used in the following computations, due to the computational advantages it offers over model $\omega - 1$ (see Section 2.3). Finally, a relatively coarse 16^3 mesh is sufficient to capture interesting features of the homogeneous isotropic turbulence, and no significant improvement in the energy spectrum was obtained by using a 32^3 mesh system.

4.5 Computational Details

The calculations described above were executed on the CDC-7600 at NASA-Ames Research Center, using programs written in Fortran. The total storage requirements (octal) were as follows:

16^3 Calculation

Large Core Memory:	Fourth-order	310,360
	Pseudo-spectral	230,000
Small Core Memory:	Fourth-order	104,465
	Pseudo-spectral	61,334

32^3 Calculation

Large Core Memory:	Pseudo-spectral	1,110,000
Small Core Memory:		126,605

The computing time per computational time step was approximately as follows:

16^3 Calculation

Fourth order = 2.5 sec CPU time

Pseudo-spectral = 4.0 sec CPU time.

32^3 Calculation

Pseudo-spectral = 34 sec CPU time.

Chapter 5

MIXING LAYER: TWO-DIMENSIONAL COMPUTATION

5.1 Preview

It is well documented (Winant and Browand (W&B), 1974; Brown and Roshko (B&R), 1974; Konrad, 1976; Dimotakis and Brown (D&B), 1976) that in some cases the spatially developing mixing layer contains coherent structures (in the terminology of B&R) or discrete vortices (in the terminology of W&B). In these experiments, the mixing layer grows via the interaction of neighboring vortex-like structures that rotate around and combine with each other to form a similar but larger structure (see Fig. 5.1). This mechanism is called vortex pairing. In this chapter we study the vortex-pairing mechanism by perturbing an infinite array of vortices. The effect of the initial perturbation on the roll-up is discussed. All cases treated in this chapter are completely two-dimensional; three-dimensional cases are discussed in the next chapter.

5.2 Some Experimental Results

The mixing layer is generated in a laboratory by bringing together two streams of fluid of different streamwise velocity (see Fig. 5.2). The measured mean velocity profiles, at different streamwise positions, are self-similar and can be fitted by an error-function (Spencer and Jones (S&J), 1971):

$$\frac{u}{u_1} = r + \frac{(1-r)}{2}\left(1 - \mathrm{erf}\left(\sigma(\eta-\eta_o)\right)\right) \qquad (5.1)$$

where

$r = u_2/u_1$,
u_1 = velocity of the high-speed side,
u_2 = velocity of the low-speed side,
$\eta = z/(x-x_o)$
σ = spread parameter
z = cross-flow coordinate,

x = streamwise coordinate, and

x_o = virtual origin of the layer.

Rearranging (3.1) and normalizing the velocity on $\Delta u = u_1 - u_2$, we get

$$\frac{u - U}{\Delta u} = 0.5 \, \mathrm{erf}\left(\sigma(\eta - \eta_o)\right) \tag{5.2}$$

where $U = (u_1 + u_2)/2$ is the mean velocity. The spread parameter σ is a function of r, and the spread data can be fitted by the expression:

$$\frac{\sigma}{\sigma_o} = \frac{1 + r}{1 - r} \tag{5.3}$$

where σ_o is the spread parameter for $r = 0$. S&J report $\sigma_o = 11$ for other values of σ_o; see Table 1.1.

Defining the momentum thickness, θ, to be

$$\begin{aligned} \theta &= \frac{1}{(\Delta u)^2} \int_{-\infty}^{+\infty} (u - u_2)(u_1 - u) \, dz \\ &= \int_{-\infty}^{+\infty} \left(\frac{1}{4} - \frac{(u - U)^2}{(\Delta u)^2} \right) dz \end{aligned} \tag{5.4}$$

and substituting (5.2) in (5.4), we get

$$\theta = \frac{x - x_o}{\sigma \sqrt{2\pi}} = \frac{x - x_o}{\sigma_o 2 \sqrt{2\pi}} \frac{\Delta u}{U} \tag{5.5}$$

$$\sigma = \frac{x - x_o}{\theta \sqrt{2\pi}} \tag{5.6}$$

Since σ is constant, Eqn. (5.5) shows that the momentum thickness grows linearly with x.

Substituting (5.6) in (5.2), we get:

$$\frac{u - U}{\Delta u} = 0.5 \, \mathrm{erf}\left(\frac{(z - z_o)}{\theta \sqrt{2\pi}} \right) \tag{5.7}$$

Due to computer limitations, one cannot set up a uniform grid that covers the length of the experimental set-up (1.8 m for the W&B case) and

at the same time resolves the large-eddy scale ($\sim$1-4 cm). We propose to use a uniform grid that moves with the mean speed U. The size of the computational domain is chosen so that two vortices are captured in the initial field; i.e., we can imagine that we are following the fluid in the dashed box in Fig. 5.1 as it moves downstream.

In our frame the layer will develop in time rather than space. We shall in fact be studying a portion of a time-developing mixing layer. This layer can be thought of as being created by having two infinite countermoving streams of velocity $\pm \Delta u/2$ brought in contact suddenly at $T = 0$. For this flow, the mean quantities will be horizontal planar-averaged quantities; for example, the mean velocity profile will be defined as

$$< \bar{u} >_{xy} = \frac{1}{A} \int_A \int \bar{u}(x,y,z,t)\, dx\, dy \tag{5.8}$$

The momentum thickness, defined as

$$\theta(t) = \int \left[\frac{1}{4} - \left(\frac{< \bar{u} >_{xy}}{\Delta u} \right)^2 \right] dz \tag{5.9}$$

will be a function of time instead of space. According to the Taylor hypothesis, the state of the flow at the experimental streamwise distance x is the same as that of the computed layer at the computational time variable t. The variables x and t are related by the expression:

$$x = Ut \tag{5.10}$$

Substituting (5.10) in (5.5), we get an expression for the expected momentum thickness of the time-developing layer:

$$\theta(t) = \frac{t - t_o}{\sigma_o 2 \sqrt{2\pi}} \Delta u \tag{5.11}$$

Equation (5.11) shows that $\theta(t)$ should grow linearly with time, with

$$\frac{d\theta}{\Delta u dt} = \frac{1}{\sigma_o 2 \sqrt{2\pi}} \tag{5.12}$$

5.3 Boundary Conditions

The coordinate system used is shown in Fig. 5.3, where the x-direction is the streamwise direction, the y-direction is the spanwise direction, and the z-direction is the cross-flow direction. We shall use periodic boundary conditions in the x- and y-directions; this is allowed if the size of the computational box is sufficiently greater than the integral scale in a given direction. At a large enough z location the flow is essentially horizontal and uniform. We can use no stress boundary conditions in the z-direction (i.e., $\partial u/\partial z = \partial v/\partial z = w = 0$ at $z = 0$ and $z = L$) if the boundaries of our box in this direction are sufficiently far from the center of the layer. This will allow us to expand the velocity fields as follows:

$$\bar{u} = \sum_n \sum_{k_2} \sum_{k_1} \hat{\bar{u}}(k_1,k_2,n)\, e^{i(k_1x+k_2y)} \cos\left(\frac{n\pi z}{L_3}\right) \qquad (5.13)$$

$$\bar{v} = \sum_n \sum_{k_2} \sum_{k_1} \hat{\bar{v}}(k_1,k_2,n)\, e^{i(k_1x+k_2y)} \cos\left(\frac{n\pi z}{L_3}\right) \qquad (5.14)$$

$$\bar{w} = \sum_n \sum_{k_2} \sum_{k_1} \hat{\bar{w}}(k_1,k_2,n)\, e^{i(k_1x+k_2y)} \sin\left(\frac{n\pi z}{L_3}\right) \qquad (5.15)$$

and the vorticity fields as follows:

$$\bar{\omega}_1 = \sum_n \sum_{k_2} \sum_{k_1} \hat{\bar{\omega}}_1(k_1,k_2,n)\, e^{i(k_1x+k_2y)} \sin\left(\frac{n\pi z}{L_3}\right) \qquad (5.16)$$

$$\bar{\omega}_2 = \sum_n \sum_{k_2} \sum_{k_1} \hat{\bar{\omega}}_2(k_1,k_2,n)\, e^{i(k_1x+k_2y)} \sin\left(\frac{n\pi z}{L_3}\right) \qquad (5.17)$$

$$\bar{\omega}_3 = \sum_n \sum_{k_2} \sum_{k_1} \hat{\bar{\omega}}_3(k_1,k_2,n)\, e^{i(k_1x+k_2y)} \cos\left(\frac{n\pi z}{L_3}\right) \qquad (5.18)$$

The pseudo-spectral method will be used to approximate the partial derivatives. The numerical technique was discussed in Chapter 3.

5.4 Initial Conditions

We want to prescribe an initial profile that corresponds to a pair of vortices. It has been shown in Chapter 2 that filtering a line vortex produces a vortex with a Gaussian distribution of vorticity in the core. We shall use this fact to generate our initial conditions.

The initial conditions are generated by starting with two line vortices in the spanwise direction at $(x = x_1,\ z = L_3/2)$ and $(x = x_2,\ z = L_3/2)$ (see Fig. 5.4), and filtering in the x-z plane with the relatively wide Gaussian filter:

$$G(x,z) = \frac{1}{A_1 A_3} \exp\left(-\frac{x^2}{6h_1^2} - \frac{z^2}{6h_3^2}\right) \tag{5.19}$$

where h_i is the mesh size in the i-th direction $(i = 1,3)$ and A_i $(i = 1,2)$ is defined by Eqn. (3.61). This will produce the vorticity field:

$$\bar{\omega}_2 = C_1 \frac{1}{A_1 A_3} \left\{ \exp\left(-\frac{(x-x_1)^2}{6h_1^2}\right) + \exp\left(-\frac{(x-x_2)^2}{6h_2^2}\right) \right\} \exp\left(-\frac{(z-L_3/2)^2}{6h_3^2}\right)$$

$$0 \le x < L_1 \quad , \quad 0 \le z < L_3 \tag{5.20}$$

$$\bar{\omega}_1 = \bar{\omega}_3 = 0$$

$$\bar{\omega}_2(x_1,z) = \bar{\omega}_2(x + nL_1, z) \qquad n = \pm 1, \pm 2, \ldots \text{(periodicity)}$$

where C_1 is an arbitrary constant that adjusts the strength of the vortices. Note that these vortices can be elliptical; they are h_1/h_3 times as long in the streamwise direction as in the cross flow direction.

Equations (5.20) correspond to a perturbed infinite array of vortices with a perturbation parameter β equal to:

$$\beta = \frac{1}{2} - \frac{|x_1 - x_2|}{L_1} \tag{5.21}$$

$\beta = 0$ corresponds to a uniform (unperturbed) vortex array, and we need to deal only with the case $\beta > 0$.

Figures 5.6a-f show constant vorticity contours for $\beta = 6/16$, $5/16$, $4/16$, $3/16$, $2/16$, and $1/16$. Note that for large β the vorticity contours look like those for a single distorted vortex.

5.5 Mesh Size Selection

We have shown in Chapter 4 that a $16 \times 16 \times 16$ mesh system can resolve isotropic homogeneous turbulence with acceptable accuracy. For the cases considered in this chapter there are no variations in the spanwise direction. We dropped the number of meshes in the spanwise direction to $N_2 = 4$, the minimum number of meshes that our three-dimensional code was designed to handle. In the cross-flow direction the mesh number was increased to $N_3 = 33$ in order to allow the layer to grow in this direction. This gives a total number of mesh points of $N_1 \times N_2 \times N_3 = 16 \times 4 \times 33 = 2112$.

The spanwise vorticity is defined by

$$\bar{\omega}_2 = \frac{\partial}{\partial z}\bar{u} - \frac{\partial}{\partial x}\bar{v} \tag{5.22}$$

Averaging (5.22) over x-y planes and using periodic boundary conditions, we get

$$\langle \bar{\omega}_2 \rangle_{xy} = \frac{d}{dz}\langle \bar{u} \rangle_{xy} \tag{5.23}$$

If we substitute in (5.23) the vorticity distribution given by Eqn. (5.20), we get:

$$\frac{d}{dz}\langle \bar{u} \rangle_{xy} = C_1 \frac{2}{L_1 A_3} \exp\left(-\frac{(z-L_3/2)^2}{6h_3^2}\right) \tag{5.24}$$

This ordinary differential equation can be solved together with the boundary condition:

$$\langle \bar{u} \rangle_{xy} = 0 \quad \text{at} \quad z = L_3/2 \tag{5.25}$$

The solution is obtained by simple integration:

$$< \bar{u} >_{xy} = \frac{C_1}{L_1} \operatorname{erf}\left(\frac{z-L_3/2}{\sqrt{6}\, h_3}\right) \tag{5.26}$$

Non-dimensionalizing the velocity Δu, we get:

$$< \bar{u} >_{xy} = 0.5 \operatorname{erf}\left(\frac{z-L_3/2}{\sqrt{6}\, h_3}\right) \tag{5.27}$$

Equating Eqns. (5.26) and (5.27) and solving for C_1, we get:

$$C_1 = 0.5\, L_1 \tag{5.28}$$

The length scales are non-dimensionalized on the momentum thickness. The mesh size was chosen such that the initial momentum thickness is equal to unity. Substituting (5.27) in Eqn. (5.9), we get:

$$\theta_{in} = \frac{\sqrt{6}}{\sqrt{2\pi}}\, h_3 = 1$$

and solving for h_3, we obtain

$$h_3 = \sqrt{\frac{2\pi}{6}} = 1.023 \tag{5.29}$$

The mesh size in the streamwise direction was set equal to:

$$h_1 = \frac{4}{3}\, h_3 = 1.364 \tag{5.30}$$

The non-dimensional time step was picked up to be equal to:

$$\Delta T = \frac{\Delta u \Delta t}{\theta_{in}} = 0.0799 \tag{5.31}$$

which yields a Courant number such that:

$$N_c = U_\infty \frac{\Delta t}{h_1} \leq 0.03$$

which is well within the stability criterion and assures that the error caused by the time advancement will be acceptably small.

The mesh size in the spanwise direction is irrelevant for the cases considered in this chapter. We have set $h_2 = h_3$.

5.6 Selection of β

We have shown in Section 5.2 that, to accord with the experimental observations, the momentum thickness $\theta(t)$ must grow linearly with time; and, using $\sigma_o = 11$ (S&J), we expect:

$$\frac{d\theta}{\Delta u dt} = \frac{1}{\sigma_o 2\sqrt{2\pi}} = 0.018 \qquad (5.32)$$

We have run a series of calculations for different values of β. Fig. 5.5 shows the momentum thickness θ/θ_{in} plotted vs. T for the cases run. For the highly perturbed cases, $\beta \geq 4/16$, the momentum thickness $\theta(t)$ does not grow linearly in time. However, for $\beta = 3/16$, $2/16$, and $1/16$, $\theta(t)$ does grow linearly in time, with $d\theta/\Delta u dt = 0.020$, 0.015, and 0.009, respectively.

Figures 5.6 and 5.7 show constant vorticity (contour) plots for the various cases at times $T = 0$ and $T = 16.78$, respectively. Figs. 5.6a-c and 5.7a-c show that for large β we have essentially one elliptical vortex which grows "fatter" in time, to become more or less circular at time $T = 16.78$. Figs. 5.6d-f show that for small β, we have initially two distinct vortices; these vortices draw closer and rotate around each other (Figs. 5.7d-f). For the case $\beta = 3/16$, the two vortices merge to form one vortex at time $T = 16.78$ (Fig. 5.7d).

The above observations indicate that case $\beta = 3/16$ gives results comparable to the experimental observations. The spread parameter σ_o obtained for $\beta = 3/16$ is equal to

$$\sigma_o = \frac{1}{\frac{d\theta}{\Delta u dt} 2\sqrt{2\pi}} = 9.97$$

which is within 10% of the experimental results of S&J.

5.7 Mean Velocity Profiles

The mean velocity profile $\langle \bar{u} \rangle_{xy}$ defined by Eqn. (5.8) is a function of z and T. Fig. 5.8 shows $2\langle \bar{u} \rangle_{xy}/\Delta u$ plotted vs. z/θ at $\Delta T = 2.4$ intervals, for $\beta = 3/16$. The profiles collapse into one, indicating self-similarity of the mean velocity profiles.

Self-similarity is also observed in the experimental data. Thus, as far as the mean profile is concerned, the data can be fit by pairing vortices with $\beta = 3/16$.

5.8 Mean Turbulent Intensity Profiles

In our computational box, the non-dimensional mean turbulence intensity is defined as

$$\frac{q^2}{2(\Delta u)^2} = \frac{1}{2(\Delta u)^2} < (\bar{u} - <\bar{u}>_{xy})^2 + (\bar{v} - <\bar{v}>_{xy})^2 + (\bar{w} - <\bar{w}>_{xy})^2 >_{xy} \tag{5.33}$$

where $< >_{xy}$ are planar averages defined by Eqn. (5.8).

Figure 5.9 shows the mean turbulence intensity plotted vs. z/θ, for the case $\beta = 3/16$, at $\Delta T = 2.4$ intervals. We note that the turbulence intensity decays slightly at the early stages of the pairing and then reaches a self-similar situation.

Compared with the experimental results, our peak intensity $q^2/2(\Delta u)^2\Big|_{max} = 2.06 \times 10^{-2}$ is substantially lower than the experimental value reported by S&J (3.5×10^{-2}). The low value of the maximum turbulence intensity is due to the fact that we did not take into account the subgrid scale contributions, and that our field is strictly two-dimensional, whereas in reality spanwise fluctuations are present in the experiment of S&J.

5.9 Summary

It is interesting to note that vortex pairing is capable of producing self-similar mean velocity and turbulence intensity profiles, and a linear growth of the momentum thickness that compare with experimental results (for $\beta = 3/16$). We note that, due to periodic boundary conditions, once the vortices have paired we get a uniform vortex array ($\beta = 0$) and the pairing and layer growth stop. If we want the pairing to continue, we would have to perturb the array by displacing the vortices in the streamwise direction. We have not done this because in the actual flow successive pairings are not clearly separated and are random.

A uniform array of vortices can be perturbed in several different ways; for example, by adding a cosine distribution of vorticity to a uniform array, we can enhance the pairing (see Appendix C) and get results similar to the

results presented in this chapter. One could also make the vortices of different strengths or use any combinations of these perturbations.

The perturbation $\beta = 3/16$ (vs. $\beta = 0$ for the unperturbed layer) needed to achieve the observed experimental growth rate of the shear layer may, at first, seem excessive. In the experiments, the downstream vortices exert a significant influence on those in the initial portions of the layer (D&B); recall that the influence of a distant vortical structure on a given point decreases inversely with distance. The cumulative effect of the downstream vortices can be considerable, and, since they tend to be highly turbulent, they may strongly perturb the vortices in the initial section of the mixing layer. Therefore, the value $\beta = 3/16$ may in fact be quite reasonable.

Chapter 6

MIXING LAYER: THREE-DIMENSIONAL COMPUTATIONS

6.1 Preview

In Chapter 5 we started with a two-dimensional initial field, and the numerical simulation of the governing equations stayed two-dimensional. However, actual flows are rarely two-dimensional, and truly turbulent flows are always three-dimensional. (Two-dimensional turbulence is approximated by certain atmospheric structures and in highly stratified fluids.) In this chapter we evaluate the importance of large structures in the development of the mixing layer, which is two-dimensional in the conventional mean sense but contains the three-dimensional structures.

6.2 Boundary Conditions and Mesh-Size Selection

The boundary conditions and coordinate system of Chapter 5 will be used. Periodic boundary conditions will be used in the streamwise (x_1) and spanwise (x_2) directions, and no-stress boundary conditions in the cross-flow (x_3) direction.

The number of meshes used for the cases discussed in this chapter is $16 \times 16 \times 33 = 8448$. The mesh sizes and time step are the same as in the previous chapter. After non-dimensionalizing all coordinates on the initial momentum thickness and the velocity on Δu, the mesh size in the cross-flow (x_3) direction is:

$$h_3 = 1.023$$

In a mixing layer the eddies are suspected of being elongated in the streamwise direction, so we have set:

$$h_1 = \frac{4}{3} h_3$$

and

$$h_2 = h_3$$

We note that if the mixing layer is completely coherent in the spanwise direction the size of the mesh in this direction (h_2) is not critical.

The non-dimensional time step was set equal to

$$\Delta T = \frac{\Delta u \Delta t}{\theta_{in}} = 0.0799$$

6.3 Initial Conditions

We begin by taking the view that the mixing layer is a superposition of a random velocity ($\tilde{u}$) and a mean velocity profile ($u/\Delta u$). We want the initial random profile to be solenoidal (i.e., $\nabla \cdot \tilde{u} = 0$), random in a region of space (see Fig. 6.1), and to decay to zero outside this region.

In Chapter 3 we showed how to generate an isotropic random velocity field u_I on a 16^3 grid. To generate the random part of the initial field that we need here, we start with the field of Chapter 3 and form:

$$\psi(I,J,L) = u_I(I,J,L-9) \qquad L = 14,\ldots,20 \qquad (6.1)$$

$$\psi(I,J,L) = 0 \qquad \text{otherwise}$$

(where I, J, L are the mesh point indices); i.e., a random field over the middle of the shear layer that drops abruptly to zero outside. In order to smooth out the jump between the two regions, ψ is filtered in the z-direction with a Gaussian filter. We get:

$$\bar{\psi} = \int \psi(z')\, G(z-z')\, dz' \qquad (6.2)$$

where

$$G(z) = \frac{1}{A_3} \exp\left(-\frac{z^2}{6h_3^2}\right)$$

The random portion of the initial field is generated by setting

$$\tilde{u} = \nabla \times \bar{\psi} \qquad (6.3)$$

The initial conditions were completed by adding to $\tilde{u}$ an error function mean velocity:

$$\frac{u}{\Delta u} = 0.5 \text{ erf} \frac{(z-L_3/2)}{\sqrt{6}\, h_3} \tag{6.4}$$

Two cases were run:

Case a: $$\frac{|\tilde{u}_i|_{max}}{\Delta u} = 0.01 \qquad (i = 1,2,3)$$

Case b: $$\frac{|\tilde{u}_i|_{max}}{\Delta u} = 0.30 \qquad (i = 1,2,3)$$

In these two cases the large (grid) structures are assumed to be random fluctuations.

The two-dimensional cases studied in Chapter 5 could be considered as unsteady laminar flows, since there is no randomness. We emphasize that there are at least two kinds of randomness:

i) Randomness of the pairing in which the vortices vary in shape, separation distance, strength, number, etc., in a random way. In Chapter 5 we computed realizations using spacing as the perturbation.

ii) Randomness meaning noisy (random) fluctuations.

The calculations described above are designed to look into the second type of randomness. To see what the combined effect would be, we ran still another case in which the initial field contained a vortex pair (with $\beta = 3/16$) and a superimposed random field. For the latter, we took the random field of case (b) described above. This case will be called (c).

Table 6.1 summarizes the cases studied in this chapter. In Appendix D we investigate the interaction between streamwise cellular structures and spanwise vortex pairing.

6.4 Momentum Thickness

In order to study the development of the mixing layer, we would need a measure of the effects of the turbulent rotational region on the non-turbulent irrotational region; the momentum thickness $\theta(t)$ is one such measure. We note that $\theta(t)$, as defined by Eqn. (5.4), is a measure of the momentum defect of the irrotational region. The momentum defect is due to the spreading of vorticity into the irrotational region. Since, in our computation, we have dropped the viscous terms, the growth of the momentum

thickness measures the inviscid mixing or the entrainment of irrotational fluid.

Figure 6.2 shows the non-dimensional momentum thickness θ/θ_{in} (θ_{in} is the initial momentum thickness) plotted vs. T for the three cases considered. We note that in all three cases θ grows linearly with time. The growth rates ($d\theta/\Delta udt$) for cases (a) and (b) are not very different, despite the large differences in turbulence levels. The values of 0.008 and 0.011, respectively, are also substantially lower than the growth rate (0.018) reported experimentally by S&J; they are, in fact, lower than any of the values in Table 1.1. The rate of growth of the momentum thickness is only slightly dependent on the intensity of the turbulent fluctuations in cases (a) and (b), and a higher turbulence intensity produces a higher growth rate. Furthermore, when large organized structures are present (case (c)), the momentum thickness growth rate, $d\theta/\Delta udt$ = 0.02 is equal to what it was in the absence of random fluctuations. Fig. 6.3 shows the non-dimensional momentum thickness θ/θ_{in} plotted vs. T, for case (c) and the two-dimensional case with $\beta = 3/16$. Only at the early stages of the development of the layer do the random fluctuations affect the growth of the momentum thickness.

6.5 Mean Velocity Profiles

An important characteristic of the experimental turbulent mixing layer is the self-similarity of the mean velocity profiles. In our computation, the mean velocity $\langle \bar{u} \rangle_{xy}$ is defined by Eqn. (5.8).

Figures 6.4a, b, and c show $2 \langle \bar{u} \rangle_{xy}/\Delta u$ plotted vs. z/θ at $\Delta T = 2.4$ intervals, for cases (a), (b), and (c), respectively. We obtain self-similar profiles in all cases. This means that self-similarity may be obtained from a wide variety of different flow structures, and does not provide much information about which initial conditions best represent physical reality.

6.6 Mean Turbulence Intensity Profiles

Experimental observations show that the mean turbulence intensity profiles are very nearly self-preserving (Townsend, 1956). This means that:

$$\frac{q^2}{2(\Delta u)^2} = f\left(\frac{z}{\theta}\right) \tag{6.5}$$

Defining the integral of the turbulent energy I_T at a given downstream distance to be

$$I_T = \int_{-\infty}^{+\infty} \frac{q^2}{2(\Delta u)^2}\, dz \tag{6.6}$$

and substituting (6.5) in (6.6), we get

$$I_T = \theta \int_{-\infty}^{+\infty} f\left(\frac{z}{\theta}\right) d\left(\frac{z}{\theta}\right) = C\theta \tag{6.7}$$

where

$$C = \int_{-\infty}^{+\infty} f(\eta)\, d(\eta)$$

Non-dimensionalizing on the initial integral of the turbulent energy, $I_{T,in}$, we get

$$\frac{I_T}{T_{T,in}} = \frac{\theta}{\theta_{in}} = \frac{t-t_o}{t_{in}-t_o} \tag{6.8}$$

Equation (6.8) shows that I_T grows linearly with time if the profiles of $q^2/2(\Delta u)^2$ are self-similar. To compute I_T, the mean turbulent energy defined by Eqn. (5.33) was integrated numerically in the z-direction.

Figure 6.5 shows $I_T/I_{T,in}$ plotted vs. T, for the three cases. We note that for all three cases $I_T/I_{T,in}$ decays with time. However, only for case (c), in which large structures are present, did the decay level off.

Figures 6.6a, b, and c show $q^2/2(\Delta u)^2$ plotted vs. z/θ, at ΔT = 2.4 intervals, for cases (a), (b), and (c), respectively. Consistent with the integral of the turbulence energy results, the turbulence intensity decays in time. The most significant drop of the maximum turbulence intensity occurs in the early stages of the development of the layer.

The fact that the integral of the turbulence energy decays, instead of growing linearly with time, is a clear indication that the term (Eqn. (2.16)) used in our equations (2.28) to model the subgrid scale motions,

has too much of an inhibiting effect on the growth of the turbulent fluctuations.

In order to support the above argument, we ran a case in which we started with the same initial conditions as in case (b), but set $C_v = 0$. Fig. 6.7 shows $q^2/2(\Delta u)^2$ plotted vs. z/θ, and Fig. 6.8 shows $I_T/I_{T,in}$ plotted vs. T, for this case. It is clear that the turbulence intensity grows with time, indicating that in case (b) the subgrid scale model is inhibiting the growth of the turbulence energy.

Recall that when the initial conditions contain nothing but large structures we obtain self-similar turbulent intensity profiles (see Section 5.8), even with $C_v = 0.188$. The decay of the total turbulence energy (Fig. 6.5) might suggest that the subgrid scale constant determined for the decay of the isotropic turbulence case might be too high for the mixing layer case. However, the growth rate of the momentum thickness for case (b) is much lower than the growth rate reported experimentally. With $C_v = 0$, the case (b) layer did not grow, i.e., $d\theta/\Delta u dt = 0$, at least up to $T = 9.6$, which indicates that lowering the subgrid scale constant will not give us a momentum growth comparable to the experiments. We thus surmise that it is essential that large structures be included in the initial conditions if the numerical results are to reproduce significant features of the experimental mixing layer. In principle, we could begin with a laminar shear layer and some small perturbations. The Kelvin-Helmholtz instability would then produce large vortical structures and would eventually produce a velocity field with the experimentally observed features. A computation of this type would require at least an order of magnitude more computing time. As we have noted earlier, the subgrid scale model would inhibit the growth of the perturbations and is not adequate for a computation of transitional flow. We shall need to modify the model if transitional flows are to be computed. An alternative approach would be to increase the amplitude of the perturbations and lower the constant of the subgrid scale model, or use a finer mesh.

6.7 Vorticity Contours

In order to investigate the eddy structures and their dynamics, vorticity contours in x-z planes have been plotted in Figs. 6.9 and 6.10, for the three cases considered, at times $T = 0$ and $T = 16.78$.

Figure 6.9a shows the spanwise vorticity contours for case (a), at time $T = 0$. The combination of a weak random velocity field and a smooth mean velocity distribution yields vorticity contours that are almost unaffected by the random fluctuations. The development at $T = 16.78$, shown in Fig. 6.10a, does not indicate any significant effect of the random fluctuations on the mean. The mean field simply masks the weak fluctuations in both the initial conditions and at $T = 16.78$.

Figures 6.9b show the spanwise vorticity contours for case (b), at different spanwise (x-z) planes. The combination of a strong random velocity field and a mean velocity yields vorticity contours that look spotty. At time $T = 16.78$, Figs. 6.10b show that the spots appear much more elongated. At some planes (e.g., plane 5), there are two vortex tubes that appear as if they might pair, while other planes show only one vortex tube. This indicates that the initially strong random fluctuations are being organized by the mean field, and that the layer is developing through a combination of diffusion (due to the subgrid scale model) and vortex pairing.

Figures 6.9c show the spanwise vorticity contours for case (c) at different spanwise (x-z) planes. Adding random fluctuations to the two spanwise vorticities causes the contour lines of the spanwise vorticity to become irregular. At time $T = 16.78$, the vortices have merged in some planes (e.g., planes 1-4) in Figs. 6.10a, whereas in other planes (e.g., planes 5-6) the vortices are still in the process of merging. This indicates that strong random fluctuations can affect the dynamics of vortex pairing.

6.8 Two-Point Correlations

In order to investigate whether or not the mixing layer shows a tendency to increased or decreased spanwise coherence, the spanwise correlation of the streamwise velocity fluctuations ($R_{uu}(r,z)$) was computed. R_{uu} is defined as

$$R_{uu}(r,z) = \frac{\int_x \int_y u''(x,y,z)\ u''(x,y+r,z)\ dxdy}{\int_x \int_y u''(x,y,z)\ u''(x,y,z)\ dx\ dy} \qquad (6.9)$$

where

$$u'' = \bar{u} - \langle \bar{u} \rangle_{xy}$$

Numerically, this quantity is computed as follows. We first calculate u'', then take its discrete Fourier transform in the y-direction to yield $\hat{u}''(x,k_2,z)$. $\hat{R}(x,k_2,z)$ is then defined to be equal to

$$\hat{R}(x,k_2,z) = \hat{u}''(x,k_2,z)\ \hat{u}''^{*}(x,k_2,z) \qquad (6.10)$$

where $\hat{u}''^{*}$ is the complex conjugate of $\hat{u}''$. Inverse transforming (6.10) yields the discrete equivalent of

$$R(x,r,z) = \int_y u''(x,y,z)\ u''(x,y+r,z)\ dy \qquad (6.11)$$

Finally, line-averaging (6.11) in the x-direction and normalizing yields the discrete equivalent to (6.9).

Figures 6.11 show R_{uu} at $T = 0$ and $T = 16.78$, plotted vs. r at various z locations. We shall define the correlation length to be the abscissa of the point where R_{uu} first crosses the r-axis.

For case (a), Figs. 6.11a show no significant changes in the correlation length between time $T = 0$ and $T = 16.78$. In some parts of the flow the correlation length seems to increase, whereas in other parts the correlation length seems to decrease. These variations are not significant.

Figures 6.11b show that when we start with a large random initial fluctuation superimposed on a mean profile (case (b)), the correlation length increases with time. This indicates that the layer is becoming more organized in the spanwise direction and is consistent with the result stated earlier that the vorticity tends to clump. Apparently there is a tendency toward the formation of two-dimensional vortices.

Figures 6.11c show that when we add a random field to coherent structures (case (c)), the correlation length decreases slightly with time. The only increase in the correlation length occurs at the center of the layer (plane 17 in our case).

If the spanwise correlation length of the streamwise velocity is taken as a measure of the coherence of the layer, our results tend to indicate that a layer that begins with a random field becomes more coherent, and one that starts with two-dimensional vortical structures loses coherence when the random fluctuations are strong.

6.9 Summary and Conclusions

We have shown that the development of the mixing layer is highly dependent on the initial conditions. This dependence is partly physical and partly numerical. Experimentally, the importance of the initial conditions on the development of the two-dimensional mixing layer has been pointed out by several workers (Bradshaw, 1966; Batt, 1975). Analytically, the subgrid scale models have been developed under the assumption that all the energy transferred by the large resolvable scales to the subgrid scales is dissipated. The decay of the turbulence intensity in cases (a) and (b) indicates that it is doubtful that we can compute transition with the present subgrid scale models. The presence of large structures in the initial conditions is essential to the computation of inhomogeneous turbulent flows.

From the above observations we can conclude that in order to predict the initial development of a shear layer one would need a subgrid scale model that allows the energy of the small scale field to build up and eventually reach equilibrium with the large eddies. However, the later development of a shear layer can be predicted with the present subgrid scale models, provided the large structures are explicitly included in the initial conditions. For other flows, it would appear that inclusion of large structures that at least approximate those of the physical flow is essential to obtain reasonable results. Bass and Orszag (1976) attempted to study the evolution of a passive scalar field in a sheared turbulent velocity field, but were unable to obtain physically realistic results. This may have been due to the omission of the large structures in their initial conditions.

Chapter 7

CONCLUSIONS AND RECOMMENDATIONS

In this work we have developed an approach to three-dimensional, time-dependent computations of flows using the vorticity equations. A general method of deriving conservation properties that is applicable to any numerical method in incompressible fluid mechanics was given; its use simplifies the analysis of numerical schemes.

The use of a filter which is smooth in real space has been shown to be essential for the treatment of rotational-irrotational region interactions. The use of Fourier transform methods allows accurate and fast treatment of the term $\overline{u_j \omega_i} - \overline{u_i \omega_j}$, which arises as a consequence of filtering. This is a definite improvement over the expansion in Taylor series (Leonard, 1973) used in previous studies (Kwak et al., 1975), which we believe should be used only when the use of transform methods is not justifiable.

The vorticity equations have been shown to provide a satisfactory basis for the simulation of homogeneous isotropic turbulence. Comparison of our results with results obtained using the primitive variable equations (Mansour et al., 1977; Moin et al., 1978) shows no significant differences.

A new subgrid scale model has been developed and shown to give results comparable to those obtained using the vorticity model (Kwak et al., 1975). The new model offers advantages both in computational speed and in storage. We found that, for the calculation of isotropic homogeneous turbulence, the subgrid scale constant depends only slightly on the numerical method used. The variation is about ten percent and is not likely to have a significant effect on the computed results in shear flows. The use of Fourier spatial differencing has allowed us to look more carefully at the subgrid scale model, and it has been found that replacing exact derivatives with second-order differences (roughly equivalent to averaging the model spatially (Love and Leslie, 1977)) produces improved behavior of the spectrum.

No-stress boundary conditions in one direction and periodic boundary conditions in the other two directions have been incorporated in a three-dimensional, time-dependent code. Flows in which these boundary conditions

can be justified (e.g., two-dimensional wakes, planar jets, mixing layer) can be investigated using this code. We chose the mixing layer.

Two-dimensional computations of the turbulent mixing layer have shown that pairing vortices produce self-similar mean velocity and turbulence intensity profiles. The growth rate of the layer is strongly dependent on the initial conditions, a fact also observed experimentally.

Three-dimensional computations have shown that the presence of large, organized (i.e., not random) structures is essential if the simulation is to reproduce the essential features observed in the experiments. These computations suggest that in order to simulate the initial development of a shear layer one would need a subgrid scale model that allows the energy of the small scale field to build up with time and eventually reach equilibrium with the large eddies. However, the later development of a shear layer can be predicted with the present subgrid scale models, provided the large structures are explicitly included in the initial conditions.

Our results using different initial conditions indicate that self-similarity of the mean velocity profiles can be obtained more easily than self-similarity of the turbulence intensities. The addition of strong random fluctuations to a flow containing pairing vortices disturbs the pairing in a way that causes the vortex tubes to exhibit spanwise variations, and whether or not the merging is completed depends on the spanwise locations. This may explain the onset of three-dimensionality seen in experiments. Fig. 7.1 is a conjecture of what we think might happen. The section of the vortex tube that did not merge could interact with the vortex structure just ahead (or just behind) to form a horseshoe vortex. This horseshoe vortex may get stretched over several rollers, giving the appearance of cellular structures (B&R, Konrad).

In Appendix D we study the interaction between streamwise and spanwise vorticity. Again, the detailed results depend strongly on the initial conditions. Each free shear flow is unique, and the universality that is sought exists only at large downstream distances. This may mean that the computational "prediction" of free shear flows is feasible only to moderate accuracy; the precise behavior of an individual free shear flow may depend on physical details that are not easily controlled. This means that some experimentation will always be necessary.

Work remains to be done on the development of a subgrid scale model that incorporates flow-regime dependence. Ideally, one would like a model that can handle both transition and developed turbulence. With such a model, problems associated with the initial conditions can be studied more carefully, since the linear stability theory is well understood and the initial conditions can be chosen to be solutions of the Orr-Sommerfeld equations. This kind of computation will help understand the effect of the initial conditions on the development of the mixing layer, but will not reproduce experiments exactly.

In the case of the mixing layer, the use of periodic boundary conditions is justifiable only if we move with the mean speed of the flow. However, the size of the eddies grows linearly with the streamwise distance (in our frame linearly in time), and we reach a point at which the size of the box must be increased. In a stationary frame this problem can be avoided, but inflow-outflow boundary conditions must be used. We suggest that future work should concentrate on developing a method of treating the inflow-outflow boundary conditions.

Eventually, it may be possible to treat practical flows such as airfoils, combustion chambers, etc., by these methods. Before that can be done, much more effort should first be devoted to developing subgrid scale models, treatment of boundary conditions, mesh layout and/or mapping, numerical methods, filters, etc., which are the important building blocks of large-eddy simulation.

References

1. Arakawa, A. (1966), "Computational Design for Long-Term Numerical Integration of the Equations of Fluid Motion: Two-Dimensional Incompressible Flow. Part I," Jour. of Computational Physics, 1, No. 1, 119-143.

2. Ashurt, W. T. (1977), "Numerical Simulation of Turbulent Mixing Layers via Vortex Dynamics," Proceedings of Symposium on Turbulent Shear Flows, Penn. State Univ.

3. Bass, A., and Orszag, S. A. (1976), "Spectral Modeling of Atmospheric Flows and Turbulent Diffusion," EPA-600/4-76-007.

4. Batt, R. G. (1975), "Some Measurements on the Effect of Tripping the Two-Dimensional Shear Layer," AIAA J., 13, No. 2, Tech. Notes, 245-247.

5. Brown, G. L., and Roshko, A. (1974), "On Density Effects and Large Structures in Turbulent Mixing Layers," J. Fluid Mech., 64, 775-816.

6. Champagne, F. H., Pao, Y. H., and Wygnanski, I. J. (1976), "On the Two-Dimensional Mixing Regions," J. Fluid Mech., 74, Part 2, 209-250.

7. Chandrsuda, C., and Bradshaw, P. (1975), "An Assessment of the Evidence for Orderly Structure in Turbulent Mixing Layers," I.C. Aero Report 75-03.

8. Clark, R. A., Ferziger, J. H., and Reynolds, W. C. (1977), "Evaluation of Subgrid-Scale Turbulence Models Using a Fully Simulated Turbulent Flow," Report TF-9, Mechanical Engrg. Dept., Stanford University.

9. Comte-Bellot, G., and Corrsin, S. (1971), "Simple Eulerian Time Correlation of Full and Narrow-Band Signals in Grid-Generated Isotropic Turbulence," J. Fluid Mech., 48, Part 2, 273-337.

10. Cooley, J. W., and Tukey, J. W. (1965), "An Algorithm for the Machine Calculation of Complex Fourier Series," Math. Comput., 19, 90, 297-301.

11. Deardorff, J. W. (1970), "A Numerical Study of Three-Dimensional Turbulent Channel Flow at Large Reynolds Numbers," J. Fluid Mech., 41, Part 2, 453-480.

12. Dimotakis, P. E., and Brown, G. L. (1976), "The Mixing Layer at High Reynolds Number: Large-Structure Dynamics and Entrainment," J. Fluid Mech., 78, Part 3, 535-560.

13. Donaldson, C. duP. (1972), "Calculation of Turbulent Shear Flows for Atmospheric and Vortex Motions, AIAA J., 10, No. 1, 4-12.

14. Fiedler, H., and Thies, H. J. (1977), "Some Observations in a Large, Two-Dimensional Shear Layer," Proceedings of Symposium on Turbulence, Berlin; Springer.

15. Foss, J. F. (1977), "The Effects of the Laminar/Turbulent Boundary Layer States on the Development of a Plane Mixing Layer," Proceedings of Symposium on Turbulent Shear Flows, Penn. State Univ., 11.33-11.42.

16. Fox, O. G., and Orszag, S. A. (1973), "Pseudo-spectral Approximation to Two-Dimensional Turbulence," J. of Comp. Physics, 11, No. 4, 612-619.

17. Konrad, J. H. (1976), "An Experiemntal Investigation of Mixing in Two-Dimensional Turbulent Shear Flows with Applications to Diffusion-Limited Chemical Reactions," Project SQUID, Tech. Rept. CIT-8-PU.

18. Kreiss, H. O., and Oliger, S. (1973), Methods for the Approximate Solution of Time-Dependent Problems, GARP Publications, Series No. 10, WMO, Geneva.

19. Kwak, D., Reynolds, W. C., and Ferziger, J. H. (1975), "Three-Dimensional, Time-Dependent Computation of Turbulent Flow," Report No. TF-5, Mech. Engrg. Dept., Stanford University.

20. Lamb, H. (1932), Hydrodynamics, Dover Pub., N. Y.

21. Lanczos, C. (1956), Applied Analysis, Prentice-Hall Pub. Co., Englewood, N. J.

22. Leonard, A. (1974), "On the Energy Cascade in Large-Eddy Simulations of Turbulent Fluid Flows," Adv. in Geophysics, 18A, 237.

23. Liepmann, H. W., and Laufer, J. (1947), "Investigations of Free Turbulent Mixing," NACA Tech. Note No. 1257.

24. Lilly, D. K. (1965), "On the Computational Stability of Numerical Solutions of Time-Dependent, Nonlinear Geophysical, Fluid Dynamic Problems," Monthly Weather Review, 93, No. 1, 11-26.

25. Love, M. D., and Leslie, D. C. (1977), "Studies of Subgrid Modeling with Classical Closures and Bergers' Equation," Proc. of Symposium on Turbulent Shear Flows, Penn. State Univ.

26. Mansour, N. N., Moin, P., Reynolds, W. C., and Ferziger, J. H. (1977), "Improved Methods for Large-Eddy Simulations of Turbulence," Proc. of Symposium on Turbulent Shear Flows, Penn. State Univ.

27. Moin, P., Mansour, N. N., Mehta, U. B., Ferziger, J. H., and Reynolds, W. C. (1978), "Improvements in Large-Eddy Simulation Technique: Special Methods and High -Order Statistics," Report TF-10, Mech. Engrg. Dept., Stanford University.

28. Moin, P., Reynolds, W. C., and Ferziger, J. H. (1978), "Large-Eddy Simulation of an Incompressible Turbulent Channel Flow," Rept. TF-12, Mech. Engrg. Dept., Stanford University.

29. Moore, D. W., and Saffman, P. G. (1975), "The Density of Organized Vortices in a Turbulent Mixing Layer," J. Fluid Mech., 69, Part 3, 465-473.

30. Murthy, J. N. B. (1975), "Turbulent Mixing in Non-Reactive and Reactive Flows - a Review," Proceedings of SQUID Workshop on Turbulent Mixing in Non-Reactive and Reactive Flows, Purdue Univ.

31. Orszag, S. A. (1973), "Comparison of Pseudo-Spectral and Spectral Approximation," Studies in Applied Mathematics, LI, No. 3, 253-259.

32. Orszag, S. A., and Israeli, M. (1974), "Numerical Simulation of Viscous Incompressible Flows," Annual Review of Fluid Mechanics, 6, 281-318.

33. Orszag, S. A., and Pao, Y. H. (1974), "Numerical Computation of Turbulent Shear Flows," Advances in Geophysics, 18A, Academic Press, Inc., N. Y. C., 225-236.

34. Oster, D., Wygnanski, I. J., and Fiedler, H. (1976), "Some Preliminary Observations on the Effect of Initial Conditions on the Structure of the Two-Dimensional Turbulent Mixing Layer," Proc. of SQUID Conference, Plenum Press.

35. Oster, D., Dziomba, B., Wygnanski, I., and Fiedler, H. (1977), "On the Effect of Initial Conditions on he Two-Dimensional Turbulent Mixing Layer," Proceedings of Symposium on Turbulence, Berlin; Springer.

36. Patel, R. P. (1973), "An Experimental Study of a Plane Mixing Layer," AIAA J, 11, 1, 67-71.

37. Patnaik, P. G., Sherman, F. S., and Corcos, G. H. (1976), "A Numerical Simulation of Kelvin-Helmholtz Waves of Finite Amplitude," J. Fluid Mech., 73, Part 2, 215-240.

38. Phillips, N. A. (1959), "An Example of Nonlinear Computational Instability," The Atmosphere and Sea in Motion, Rockefeller Inst. Press, N. Y., 501-504.

39. Roshko, A. (1976), "Structure of Turbulent Shear Flows: A New Look," AIAA J., 14, No. 10, 1349-1357.

40. Schumann, U. (1973), "A Procedure for the Direct Numerical Simulation of Turbulence Flows in Plate and Annular Channels and Its Application in the Development of Turbulence Models," Dissertation, Univ. of Karlsruhe, NASA Tech. Translation NASA TT T 15, 391.

41. Shanaan, S., Ferziger, J. H., and Reynolds, W. C. (1975), "Numerical Simulation of Turbulence in the Presence of Shear," Report TF-6, Mech. Engrg. Dept., Stanford University.

42. Singleton, R. C. (1967), "On Computing the Fast Fourier Transforms," Communications of the ACM, 10, No. 10, 647-654.

43. Smagorinsky, J. (1963), "General Circulation Experiments with the Primitive Equations. I. The Basic Experiment," Monthly Weather Review, 91, No. 3, 99-165.

44. Spencer, B. W., and Jones, B. G. (1971), "Statistical Investigation of Pressure and Velocity Fields in the Turbulent Two-Stream Mixing Layer," AIAA Paper #71-613.

45. Tennekes, H., and Lumley, J. L. (1974), A First Course in Turbulence, MIT Press, Cambridge, Mass.

46. Thies, H. J. (1977), "Experimentelle Untersuchung der freien Scherschicht mit gestörten Angangsbedingungen," Diplomarbeit Tu - Berlin, FB 9.

47. Townsend, A. A., The Structure of Turbulent Shear Flow, Cambridge Univ. Press, Cambridge, England.

48. Wang, S. S. (1977), "A Study of the Kelvin-Helmholtz Instability by Grid-Insensitive Vortex Tracing," Ph.D. thesis, Stanford University, Institute of Plasma Research Report No. 710.

49. Winant, C. D., and Browand, F. K. (1974), "Vortex Pairing: the Mechanism of Turbulent Mixing-Layer Growth at Moderate Reynolds Number," J. Fluid Mech., 63, Part 2, 237-255.

50. Wygnanski, I., and Fiedler, H. E. (1970), "The Two-Dimensional Mixing Region," J. Fluid Mech., 41, Part 2, 327-361.

51. Yule, A. J. (1971), "Spreading of Turbulent Mixing Layers," AIAA J., 10, No. 5, Tech. Notes, 686-687.

Table 1.1

EXPERIMENTAL RESULTS

(Table from Fiedler and Thies, 1977)

Author(s)	u_2/u_1	Re_L^*	L^* (mm)	σ_o	$\frac{d\theta}{\Delta u dt}$	Remarks
Liepmann & Laufer (1947)	0	$9 \cdot 10^5$	900	11.76	0.016	No trip
Wygnanski & Fiedler (1970)	0	$5 \cdot 10^5$	600	8.70	0.022	Trip
Batt (1975)	0	$7 \cdot 10^5$	640	8.89	0.022	Trip
	0	$7 \cdot 10^5$	640	11.76	0.016	No trip
Spencer & Jones (1971)	0	$1 \cdot 10^6$	560	10.52	0.018	No trip
Champagne, Pao & Wygnanski (1976)	0	$4 \cdot 10^5$	600	9.62	0.020	Trip (B.L. not turb.)
Patel (1973)	0	$2 \cdot 10^6$	1020	10.53	0.018	No trip
Oster, Wygnanski & Fiedler (1976)	0	$1.1 \cdot 10^6$	1100	9.21	0.021	Trip
	0	$1.1 \cdot 10^6$	1100	11.29	0.017	No trip
Foss (1977)	0	$6.7 \cdot 10^5$	510	9.00	0.021	Turb. B.L.
	0	$6.7 \cdot 10^5$	510	12.12	0.016	Lam. B.L.
Dimotakis & Brown (1976)	0.2	$3 \cdot 10^5$	600	9.87	0.020	No trip
Oster, Wygnanski & Fiedler (1976)	0.4	$2.8 \cdot 10^5$	470	12.12	0.016	Trip
	0.4	$2.8 \cdot 10^5$	470	10.81	0.018	No trip
Spencer & Jones (1971)	0.3	$1 \cdot 10^6$	680	12.31	0.016	No trip
	0.6	$2.8 \cdot 10^5$	320	13.14	0.015	No trip
Yule (1971)	0.3	$5 \cdot 10^5$	650	9.44	0.020	No trip
	0.61	$1.4 \cdot 10^5$	290	9.23	0.021	No trip
						No B.L.- suction
Thies (1977)	0	$2.4 \cdot 10^6$	3600	10.05	0.019	
		$3.8 \cdot 10^6$		9.52	0.020	No trip
		$5.1 \cdot 10^6$		9.09	0.021	
		$2.4 \cdot 10^6$		10.31	0.019	
		$4.2 \cdot 10^6$		9.37	0.021	2 mm trip
		$2.4 \cdot 10^6$		10.24	0.019	
		$3.7 \cdot 10^6$		9.57	0.020	4 mm trip
		$5.1 \cdot 10^6$		9.15	0.021	
		$2.4 \cdot 10^6$		10.23	0.019	Zig-zag trip

Table 1.1 (cont.)

Author(s)	u_2/u_1	Re_L^*	L^* (mm)	σ_o	$\frac{d\theta}{\Delta u dt}$	Remarks
						B.L.-suction
Thies (1977) (cont.)	0	$8.0 \cdot 10^6$	3600	9.17	0.021	No trip
		$2.5 \cdot 10^6$		10.10	0.019	("near" region)
		$0.8 \cdot 10^6$		13.13	0.015	
		$2.4 \cdot 10^6$		9.80	0.020	2 mm trip
		$0.8 \cdot 10^6$		9.43	0.020	("near region)
		$8.0 \cdot 10^6$		8.95	0.022	4 mm trip
		$2.0 \cdot 10^6$		9.6	0.020	8 mm trip
		$8.0 \cdot 10^6$		9.0	0.021	
		$2.4 \cdot 10^6$		10.21	0.019	Zig-zag trip

The following assumptions were used to reduce the data:

$$\sigma_o = \sigma \frac{\Delta u}{\Sigma u}$$

$$L^* = L \frac{\Delta u}{\Sigma u}$$

$$Re_L^* = \frac{\Delta u \, L^*}{\nu} ,$$

$$L = x_{max}$$

$$\sigma = \frac{2}{\eta_{0.1} - \eta_{0.95}}$$

$$\Delta u = u_1 - u_2$$

$$\Sigma u = u_1 + u_2$$

$$\frac{d\theta}{\Delta u dt} = \frac{1}{2.07 \, \sigma_o \sqrt{2\pi}}$$

——— Boundary layer turbulent at the splitter plate

- - - - - Boundary layer laminar at the splitter plate

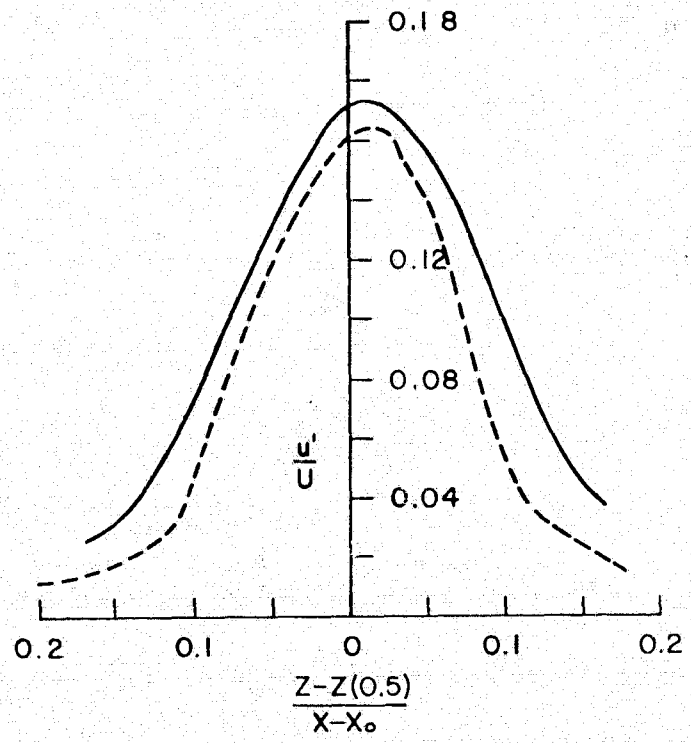

Fig. 1.1. r.m.s. streamwise velocity profiles for different initial conditions (experimental results from Foss, 1977).

——— Boundary layer turbulent at the splitter plate

----- Boundary layer laminar at the splitter plate

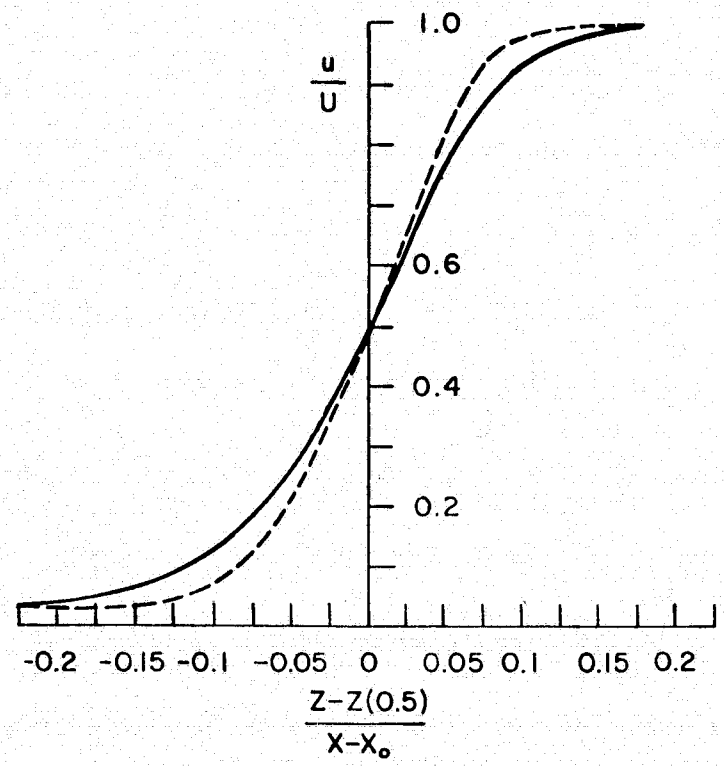

Fig. 1.2. Mean velocity profiles for different initial conditions (experimental results from Foss, 1977).

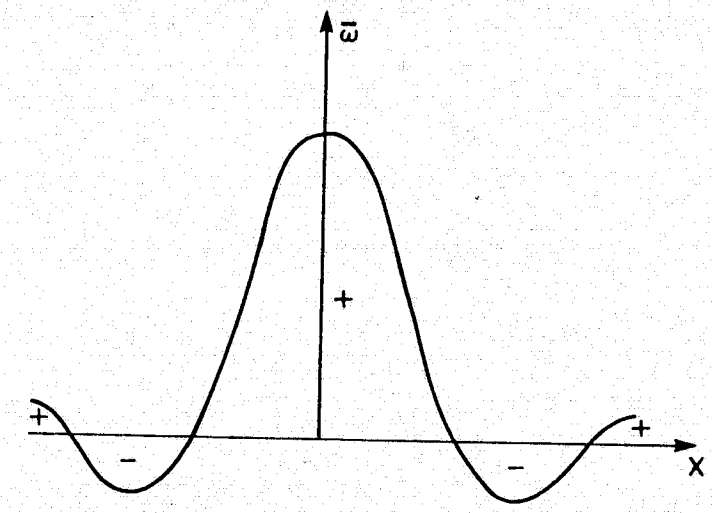

Fig. 2.1. Filtered point vortex with an SCK (sharp cut-off in k-space) filter, $y = 0$.

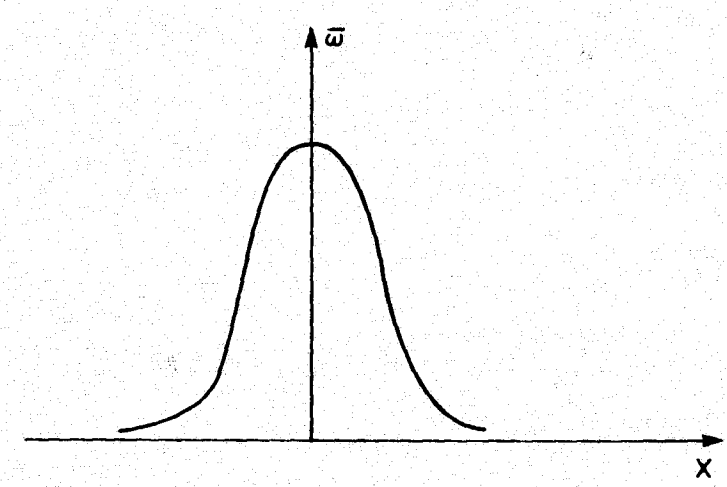

Fig. 2.2. Filtered point vortex with a GS (Gaussian in real space) filter, $y = 0$.

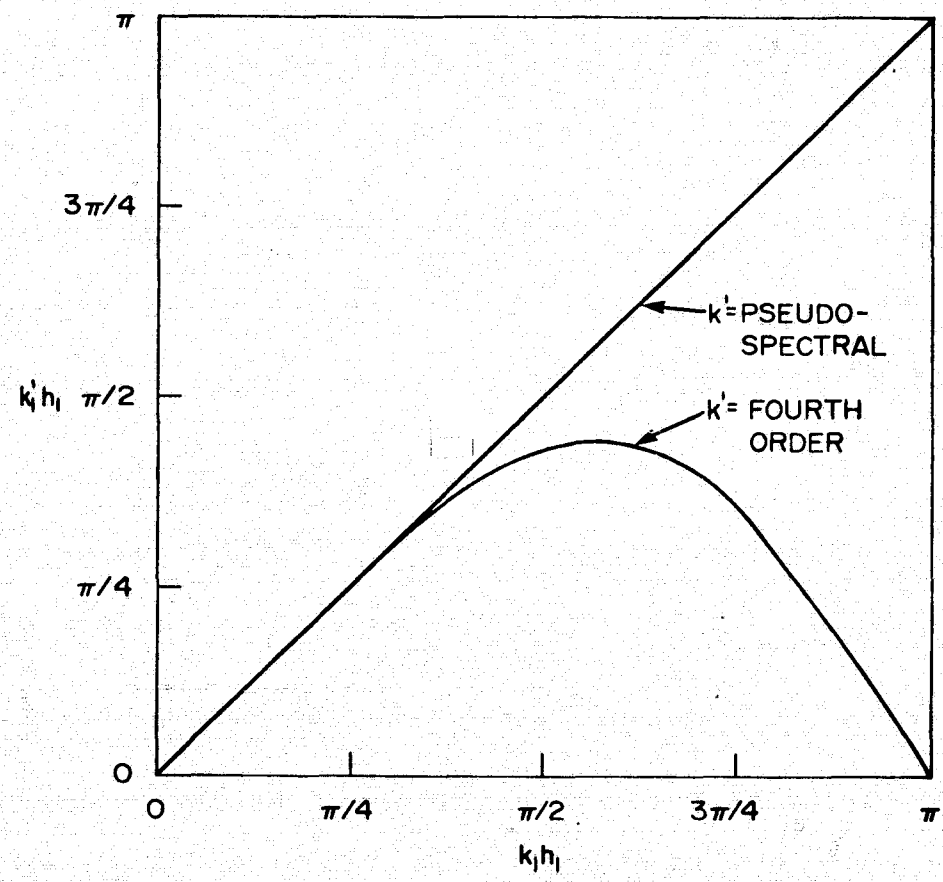

Fig. 3.1. Comparison of modified wave numbers.

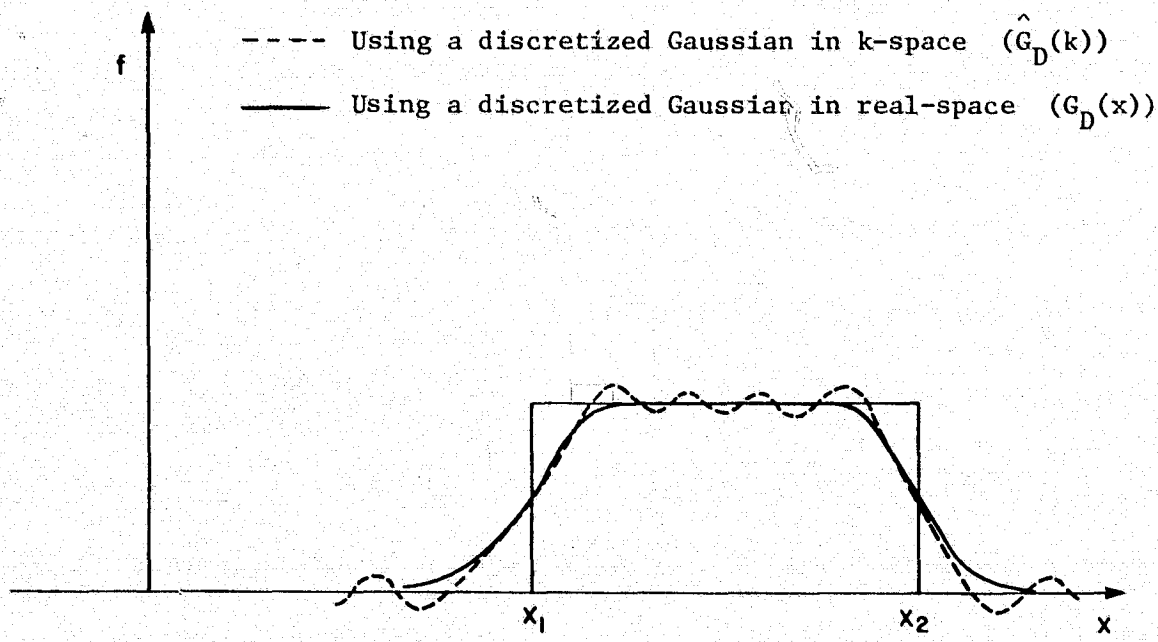

Fig. 3.2. Filtered top-hat function.

Table 4.1

Computations of the Decay of Isotropic Turbulence

No. of Mesh Points	Subgrid Scale Model	Numerical Scheme	Numerical Scheme for the Subgrid Scale Model	Model Constant	Figure
$16 \times 16 \times 16$	Model ω-1	Fourth-order diff.	Second-order diff.	$C_v = 0.235$	4.2
$16 \times 16 \times 16$	Model ω-1	Pseudo-spectral	Pseudo-spectral	$C_v = 0.212$	4.3
$16 \times 16 \times 16$	Model ω-1	Pseudo-spectral	Second-order diff.	$C_v = 0.213$	4.4
$16 \times 16 \times 16$	Model ω-2	Pseudo-spectral	Pseudo-spectral	$C_v = 0.186$	4.5
$16 \times 16 \times 16$	Model ω-2	Pseudo-spectral	Second-order diff.	$C_v = 0.188$	4.6
$32 \times 32 \times 32$	Model ω-2	Pseudo-spectral	Second-order diff.	$C_v = 0.188$	4.7

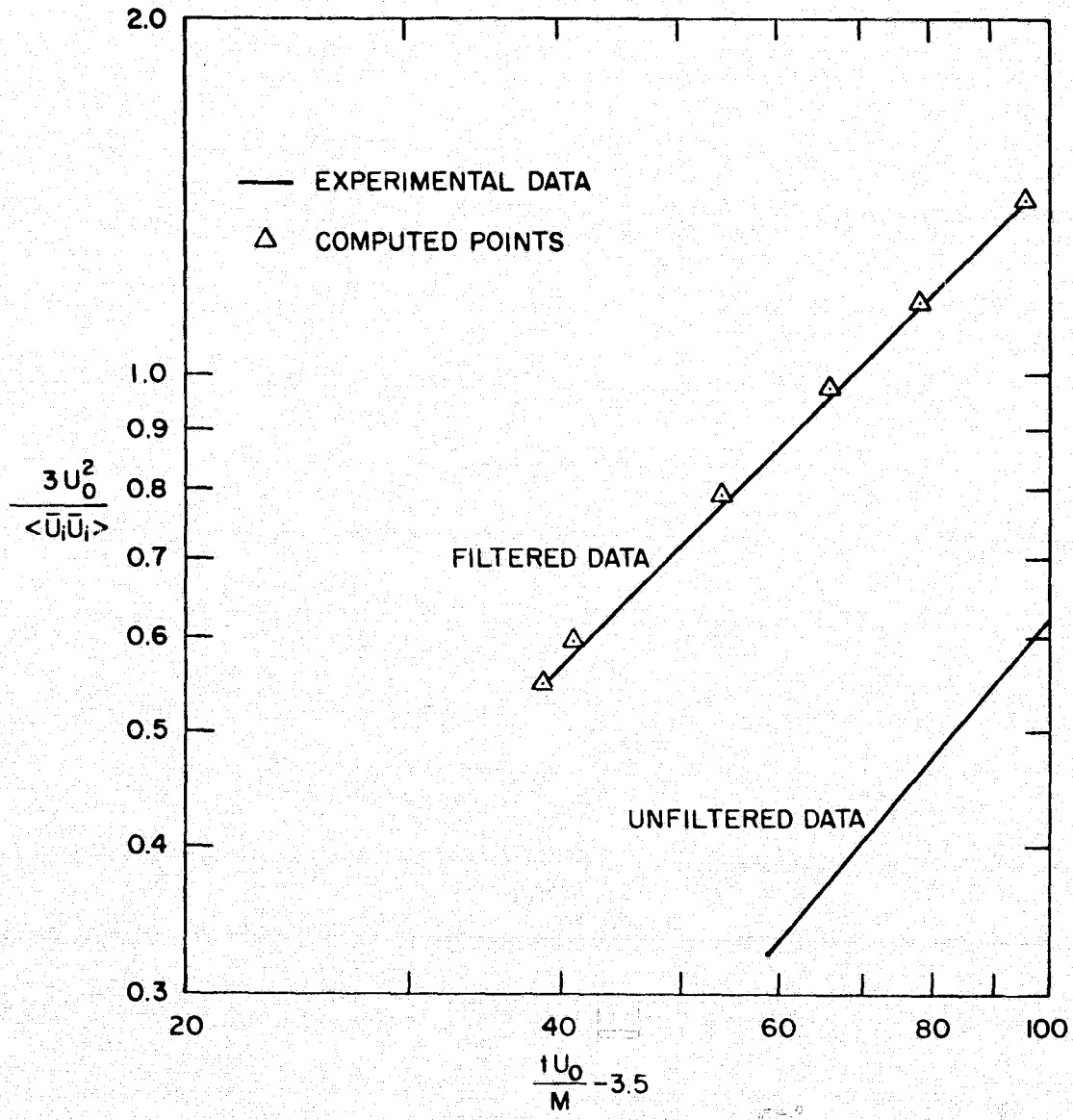

Fig. 4.1. Decay of mean square filtered velocity for $16 \times 16 \times 16$ mesh. $\langle\ \rangle$ = average over all space.

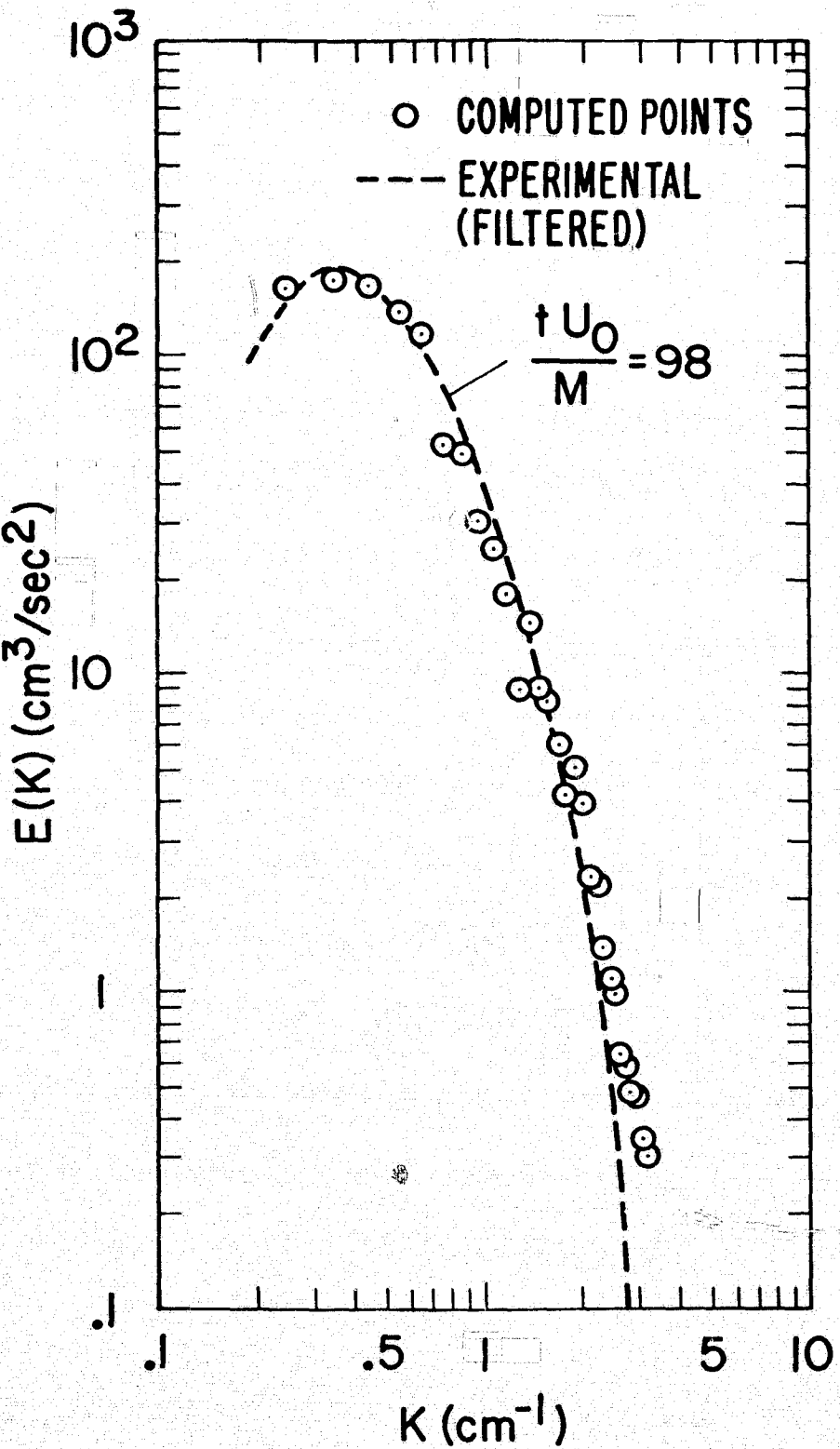

Fig. 4.2. Filtered energy spectra. Fourth-order differencing with 16^3 mesh; model ω-1, $C_v = 0.235$.

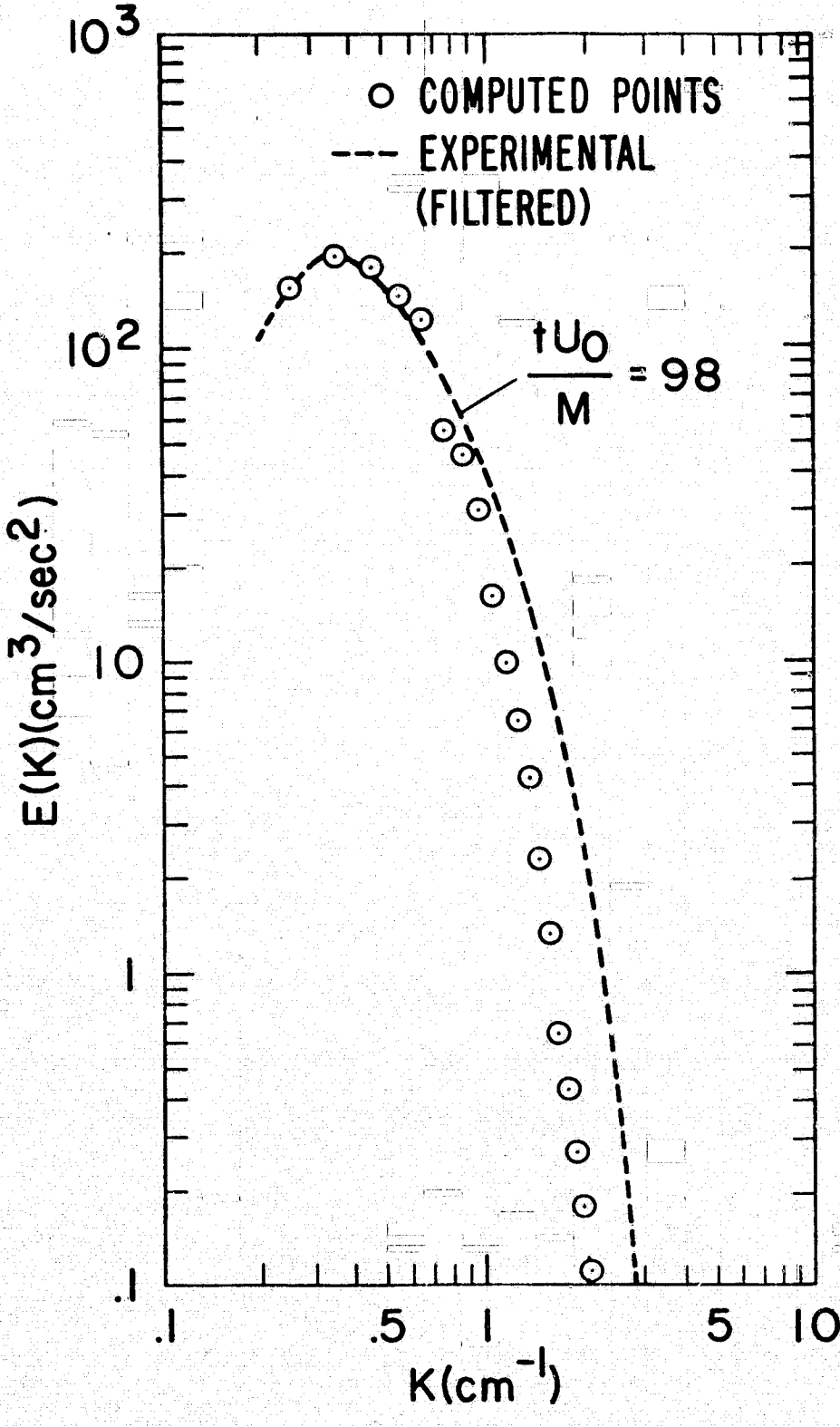

Fig. 4.3. Filtered energy spectra. Pseudo-spectral computation with 16^3 mesh; model ω-1. $C_v = 0.212$.

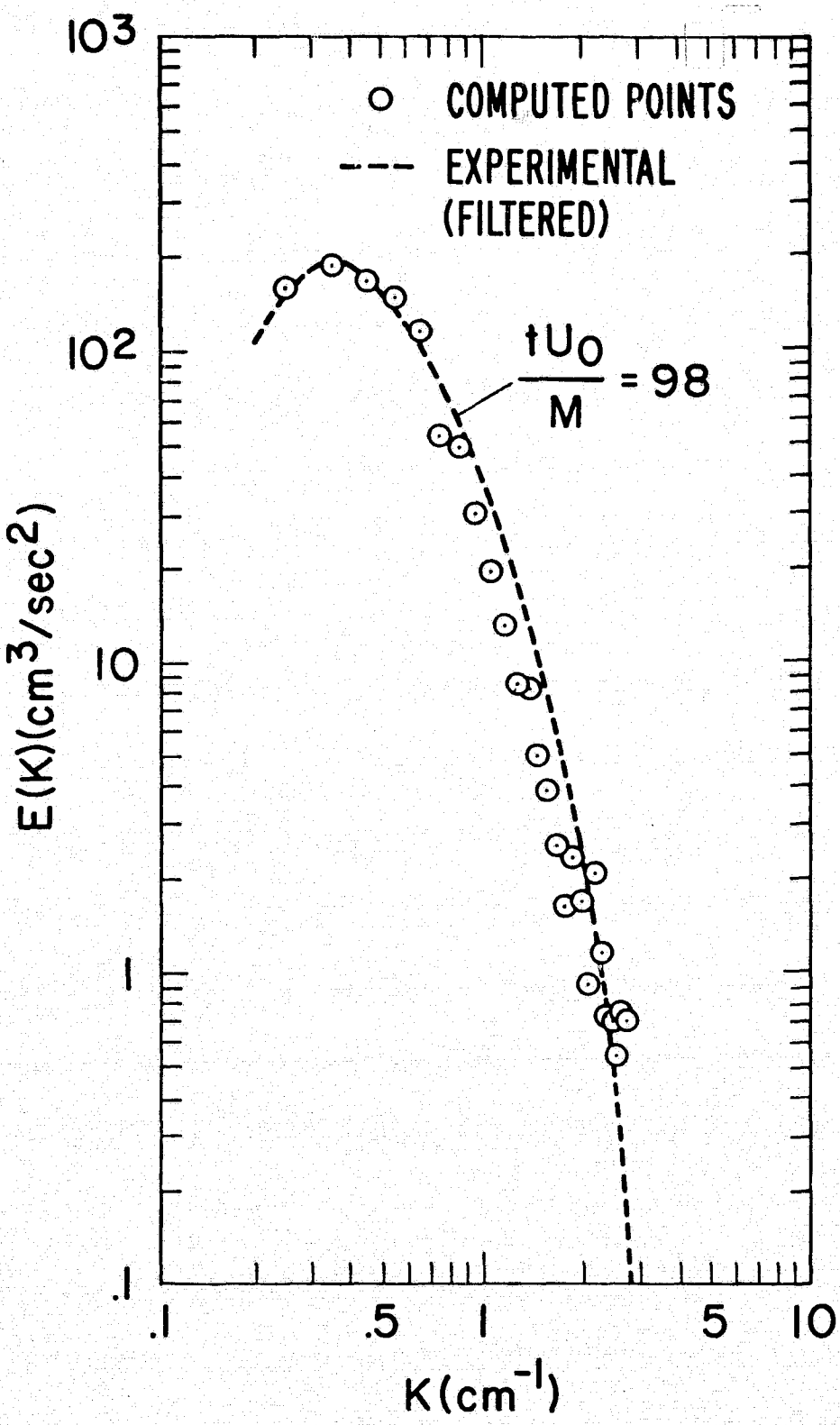

Fig. 4.4. Filtered energy spectra. Pseudo-spectral computation with 16^3 mesh; 2nd-order differencing for model ω-1. $C_v = 0.213$.

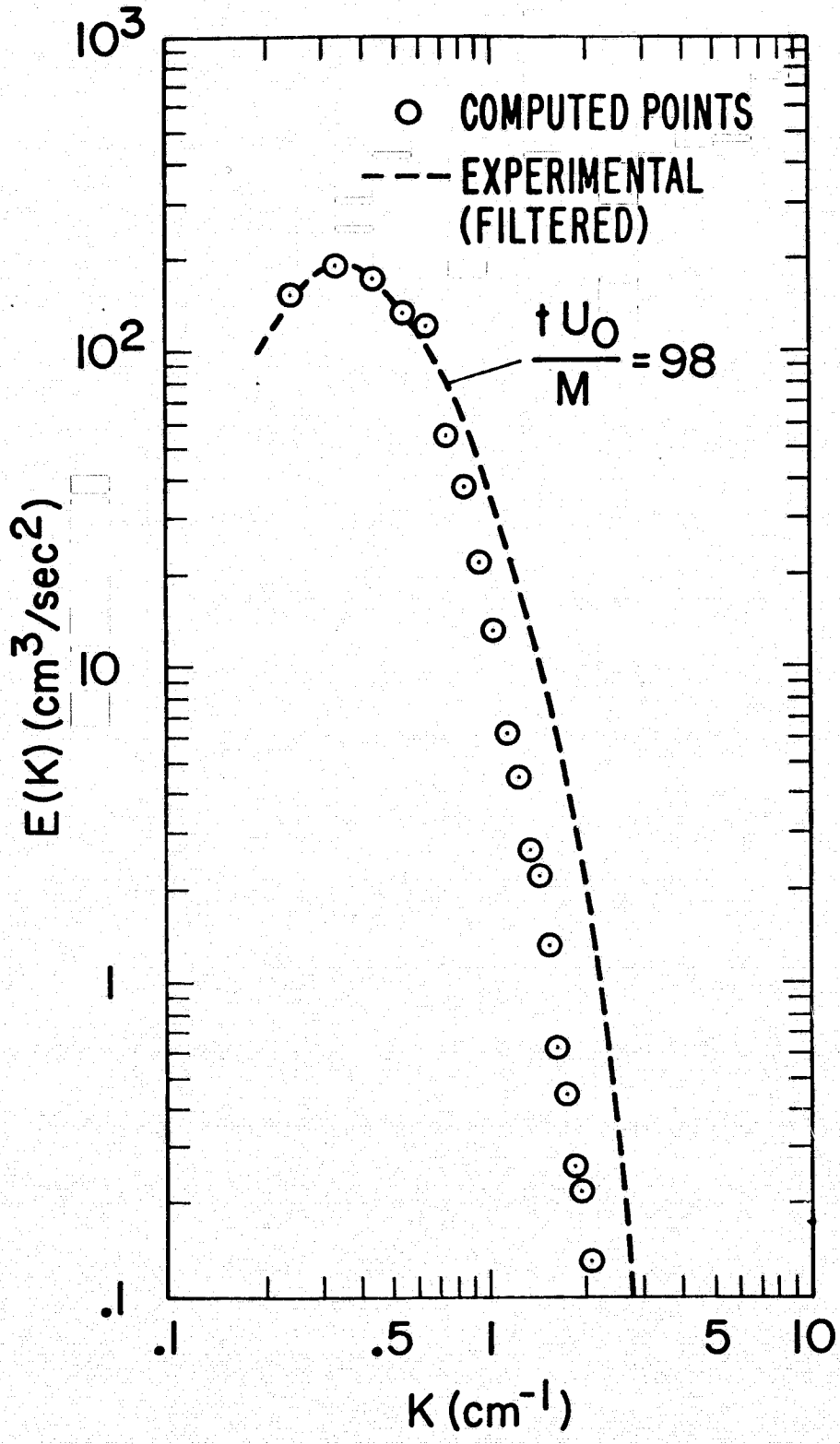

Fig. 4.5. Filtered energy spectra. Pseudo-spectral computation with 16^3 mesh; model ω-2. $C_v = 0.186$.

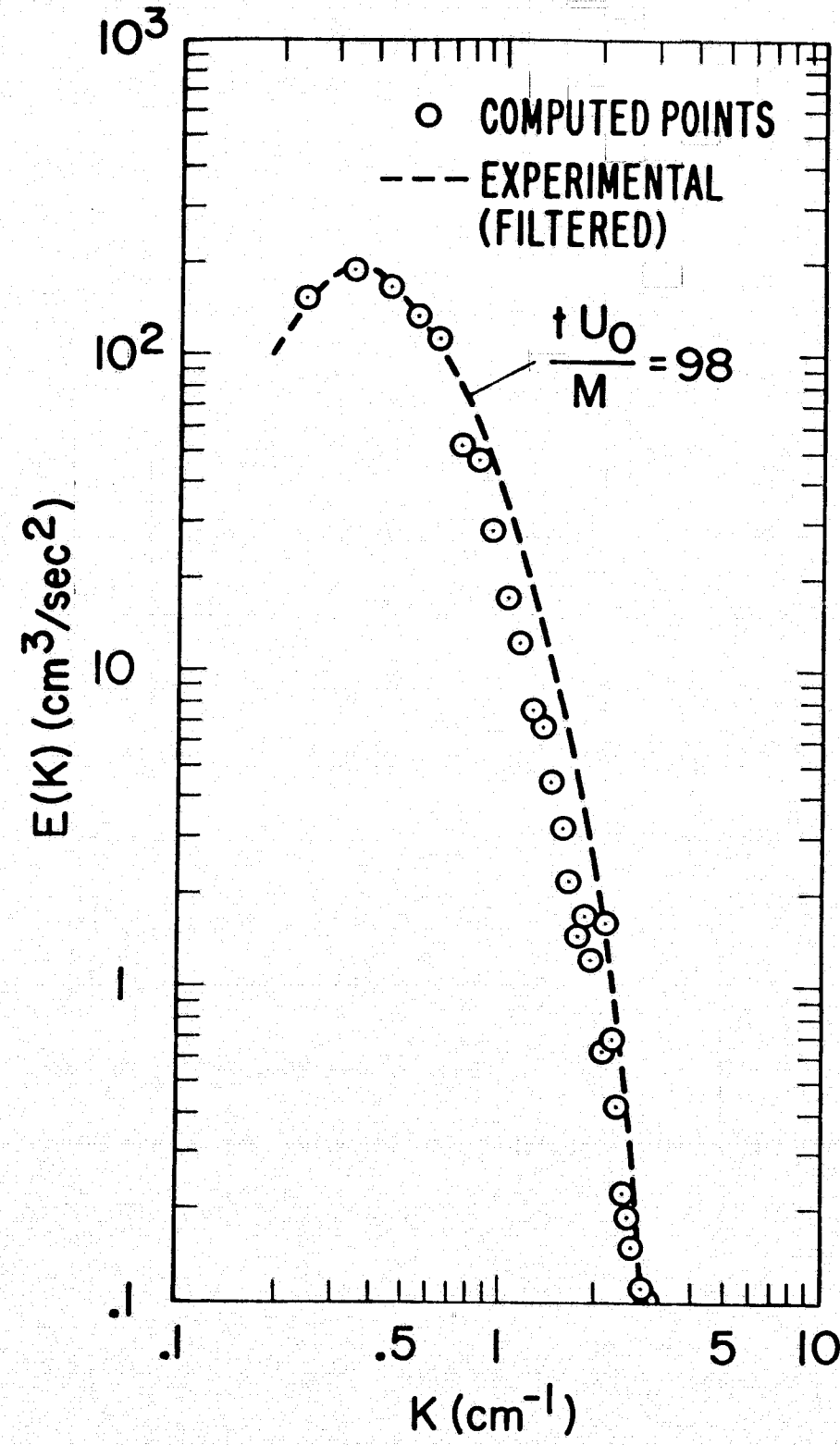

Fig. 4.6. Filtered energy spectra. Pseudo-spectral computation with 16^3 mesh; 2nd-order differencing for model ω-2. $C_v = 0.188$.

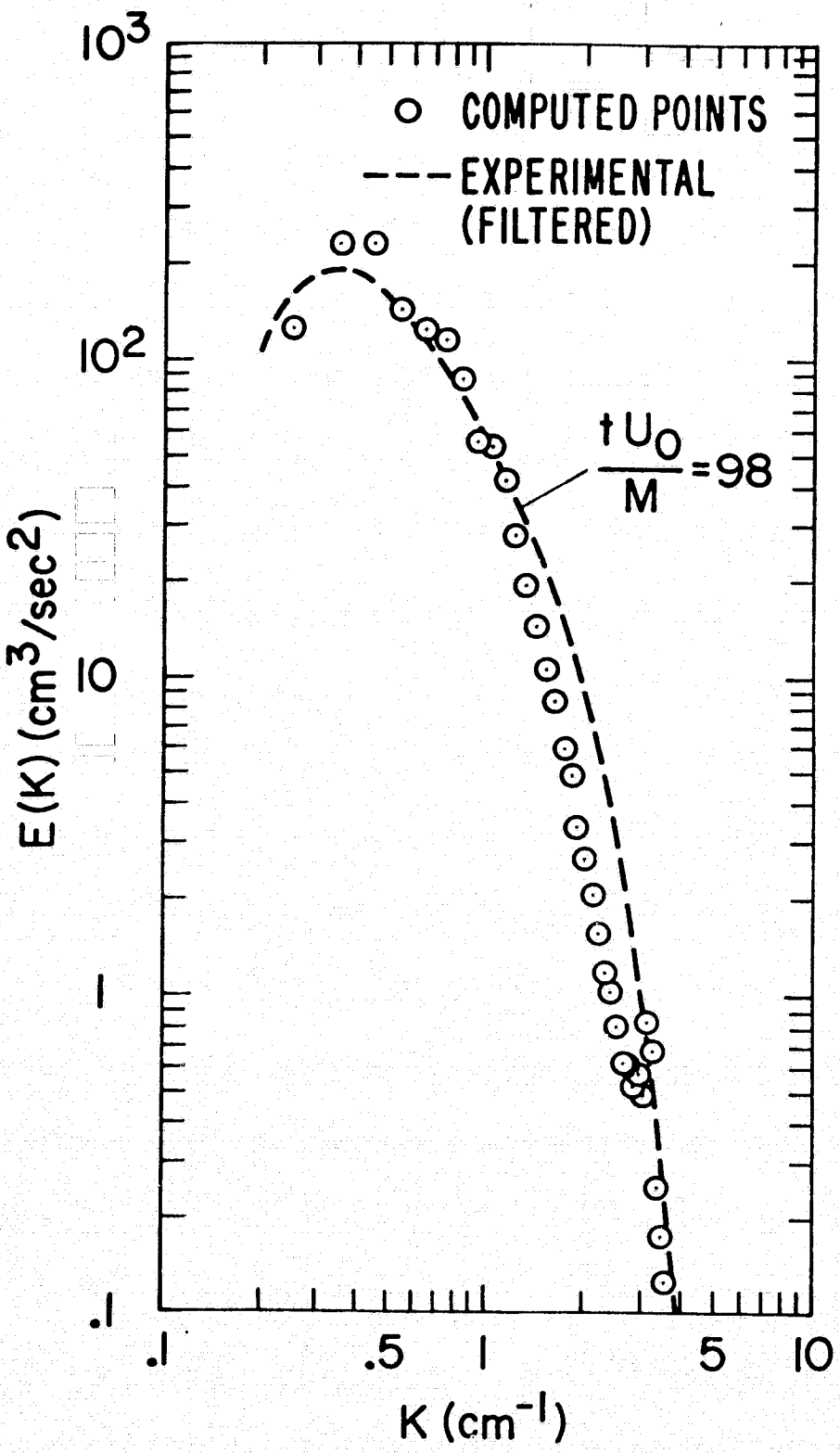

Fig. 4.7. Filtered energy spectra. Pseudo-spectral computation with 32^3 mesh; 2nd-order differencing model ω-2. $C_v = 0.188$.

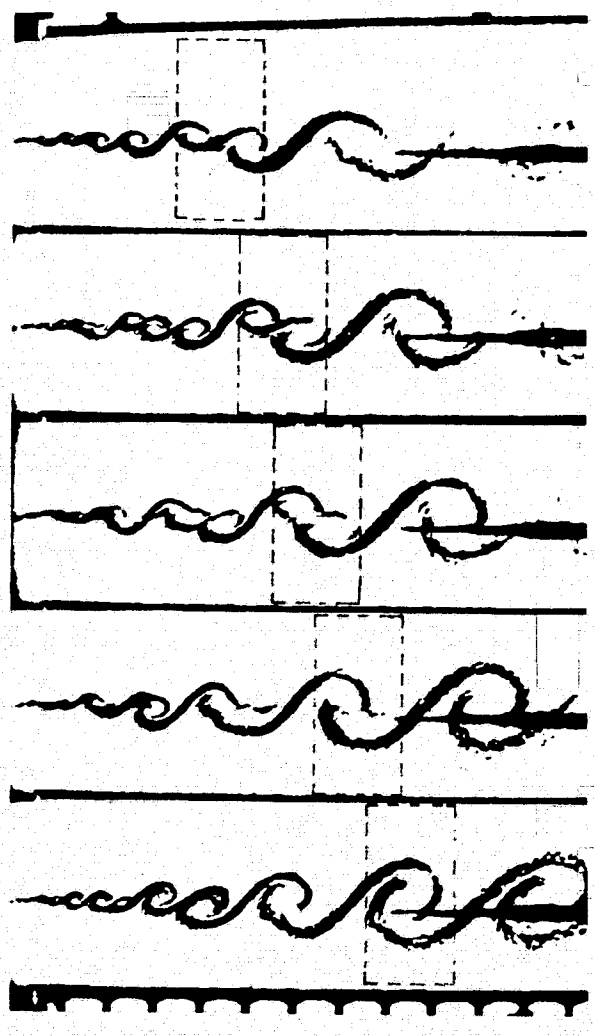

Fig. 5.1. Coherent structure in a mixing layer (Roshko, 1976). Dashed box: schematic of a computational box that moves approximately with the mean velocity.

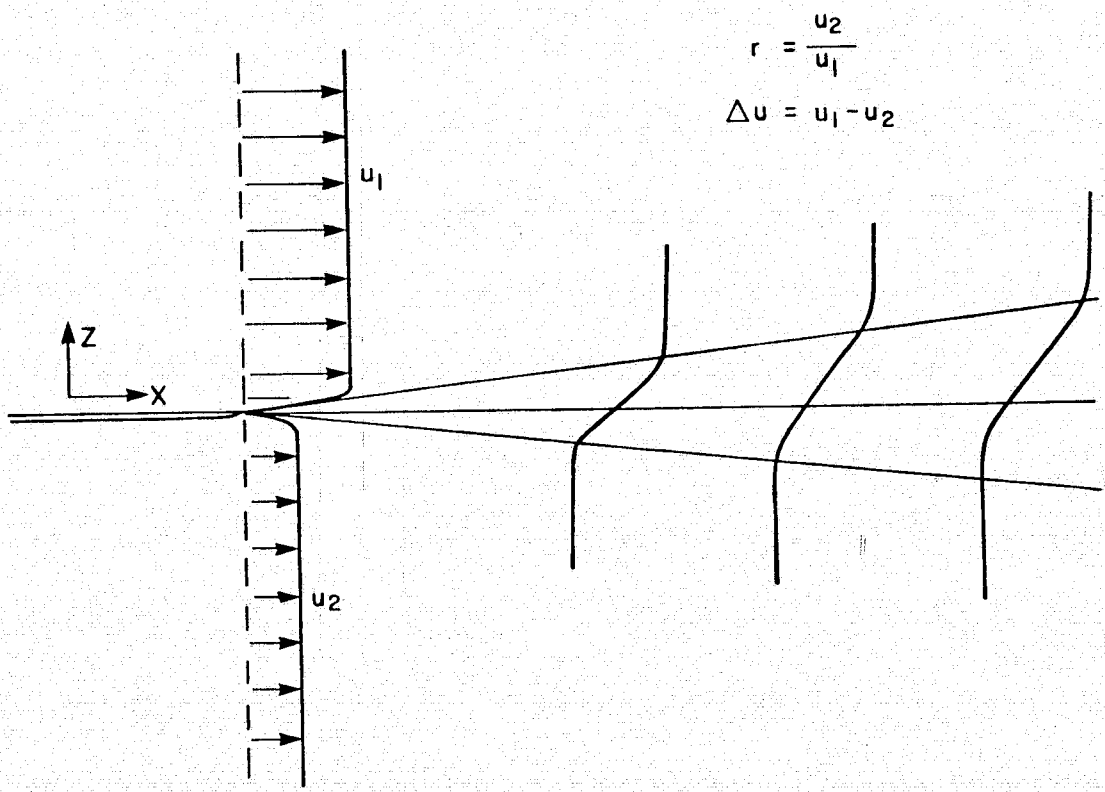

Fig. 5.2. Mixing layer. Experimental setup and coordinate system.

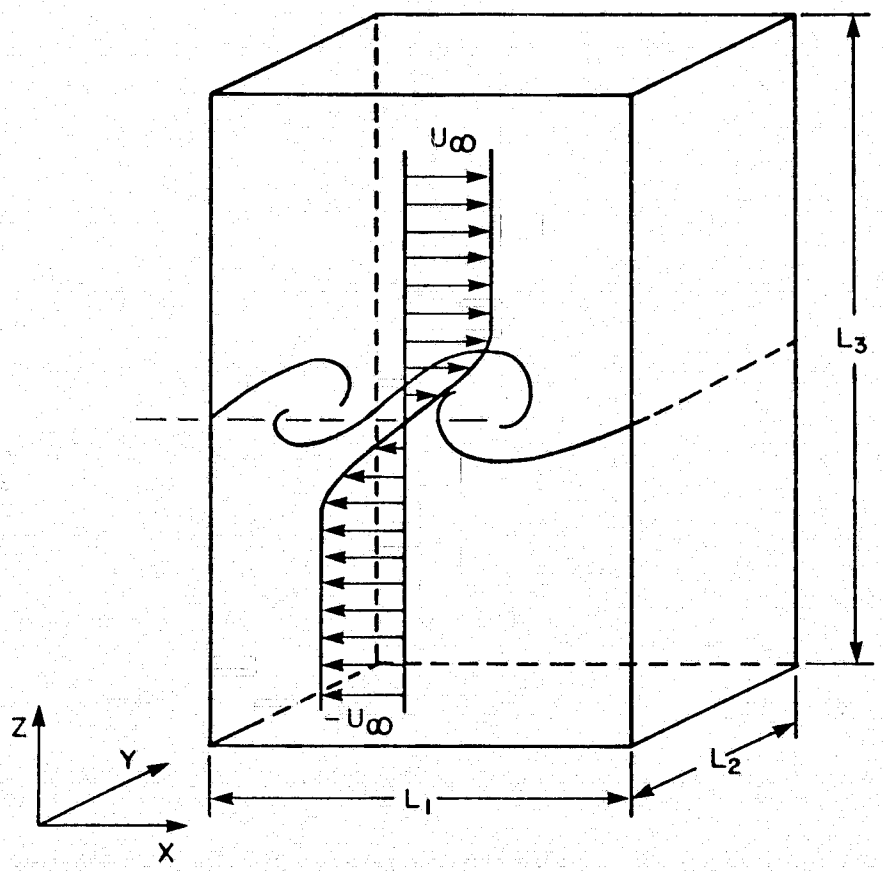

Fig. 5.3. Computational box and coordinate system.

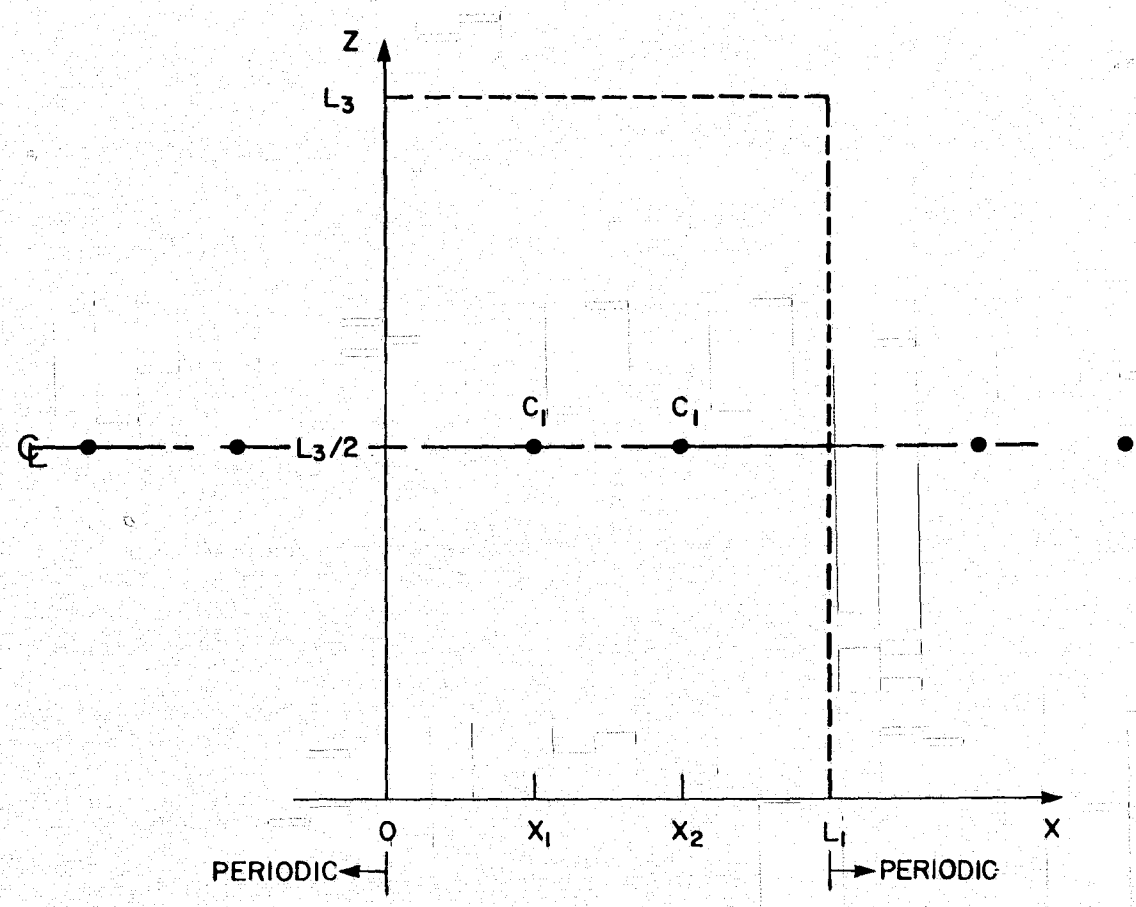

Fig. 5.4. Initial conditions setup $\left(\beta = \frac{1}{2} - \frac{|x_1 - x_2|}{L}\right)$

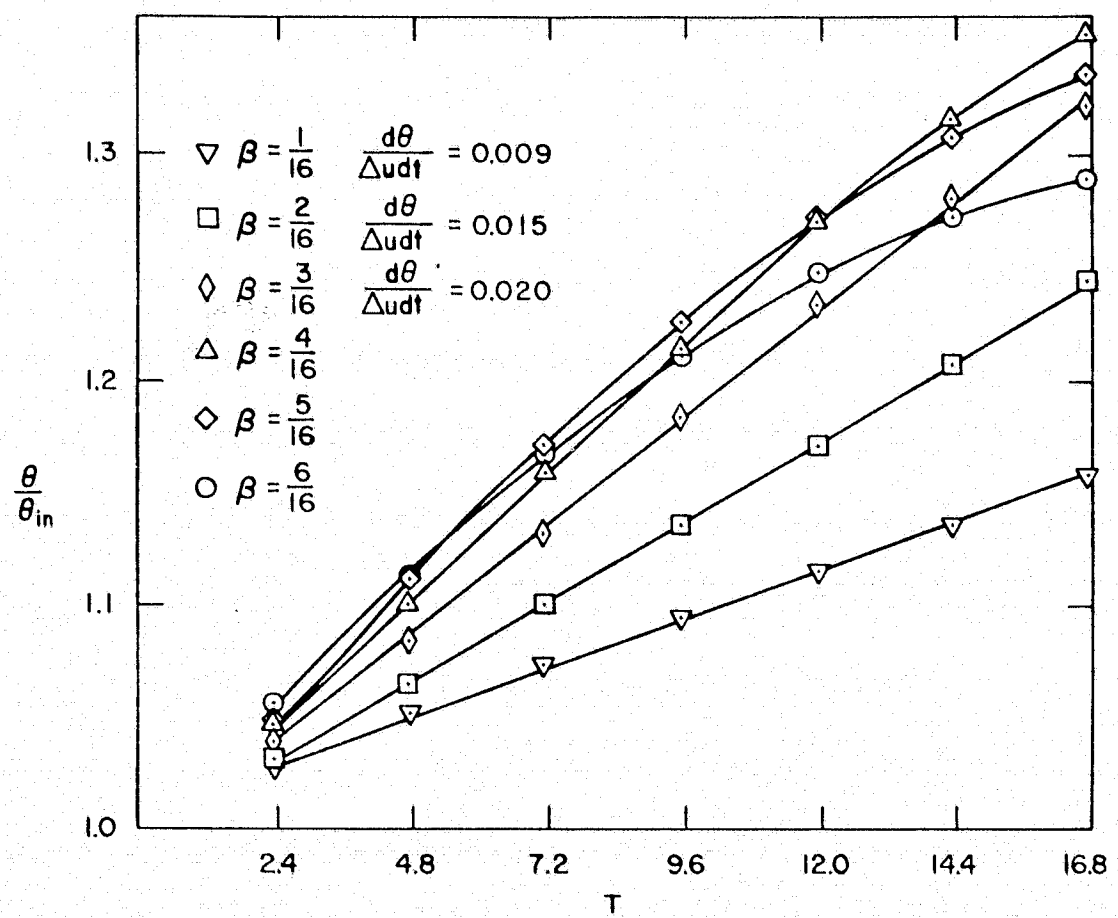

Fig. 5.5. Non-dimensional momentum thickness (θ/θ_{in}) as a function of time for various β. Two-dimensional computations.

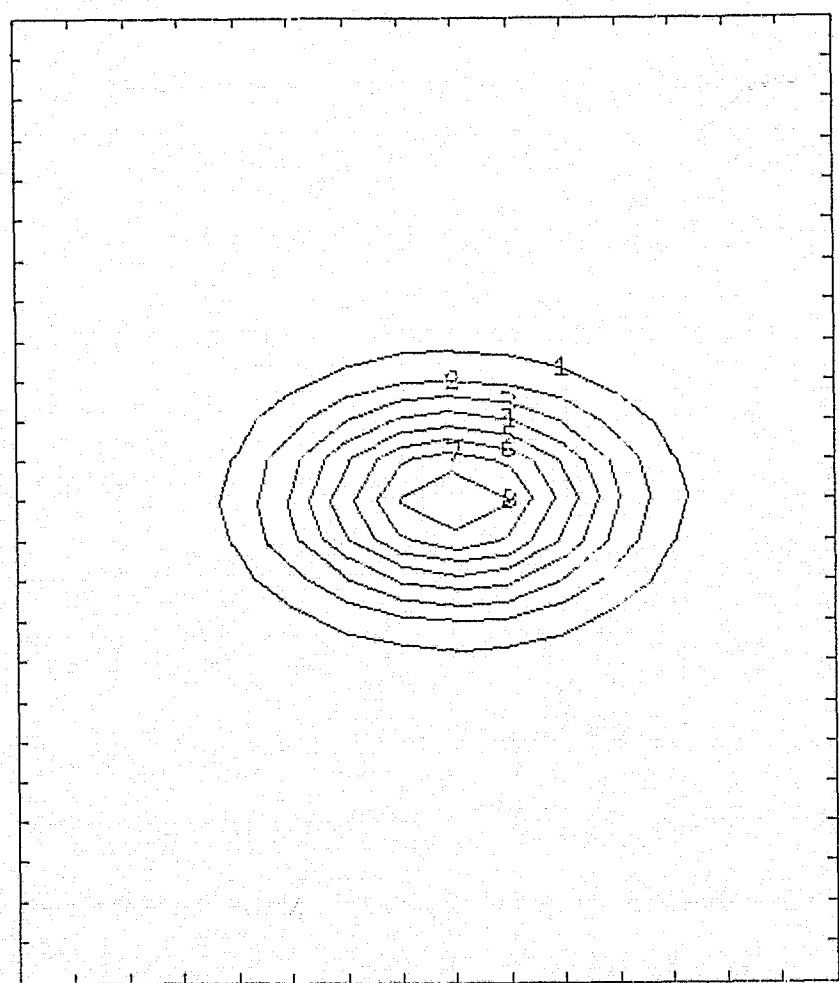

Fig. 5.6a. Contour plots of the spanwise vorticity $(\bar{\omega}_2)$ for $\beta = 6/16$, at time $T = 0$. Constant vorticity lines are plotted at eight levels. Higher numbers on these lines indicate higher levels $(\bar{\omega}_{2,max} = 0.702)$.

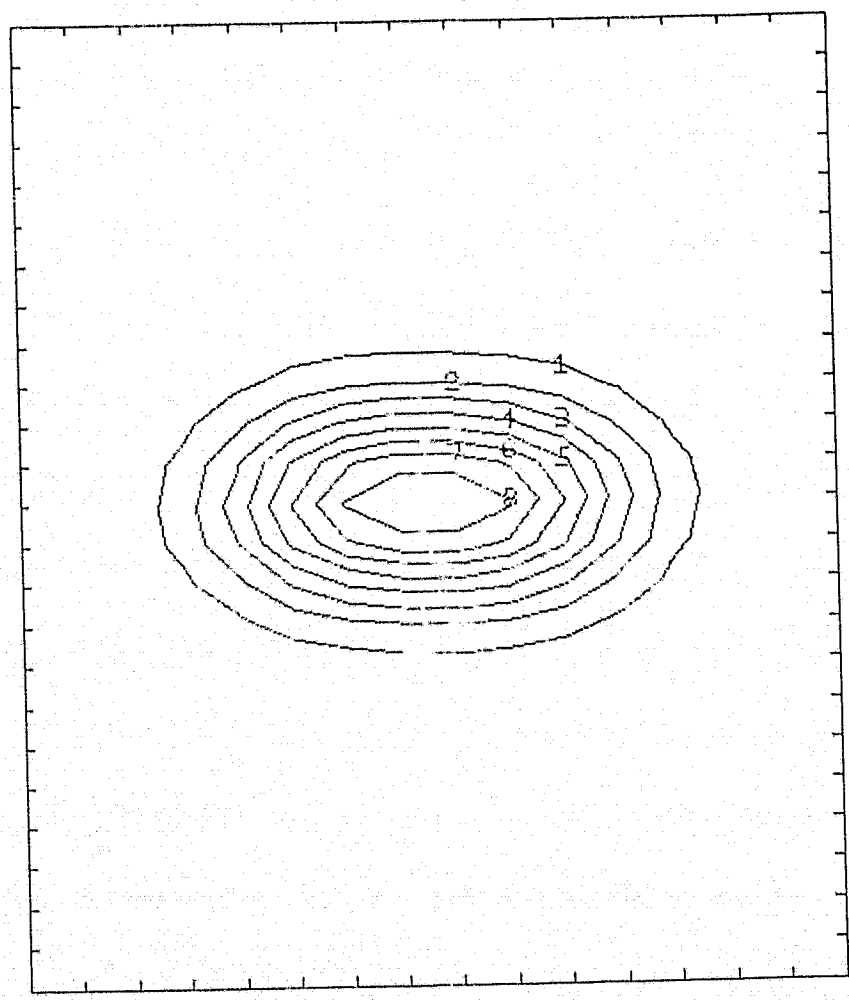

Fig. 5.6b. Contour plots of the spanwise vorticity $(\bar{\omega}_2)$ for $\beta = 5/16$, at time $T = 0$. Constant vorticity lines are plotted at eight levels. Higher numbers on these lines indicate higher levels $(\bar{\omega}_{2,max} = 0.564)$.

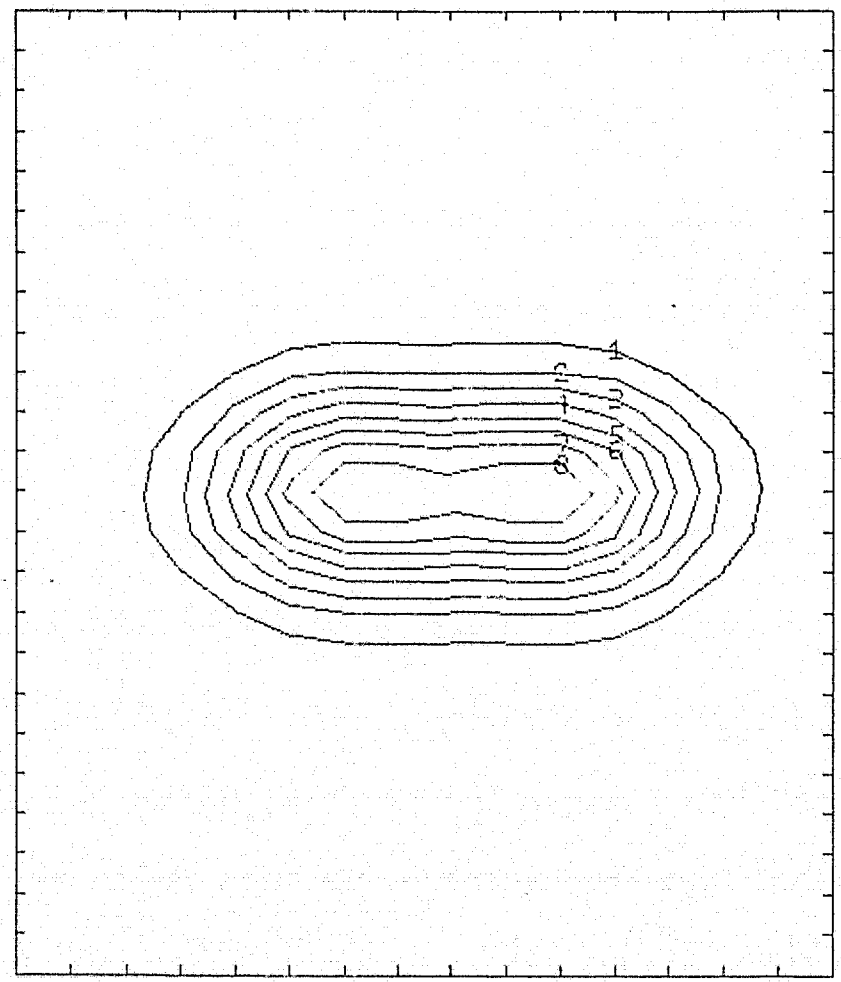

Fig. 5.6c. Contour plots of the spanwise vorticity $(\bar{\omega}_2)$ for $\beta = 4/16$, at time $T = 0$. Constant vorticity lines are plotted at eight levels. Higher numbers on these lines indicate higher levels $(\bar{\omega}_{2,max} = 0.444)$.

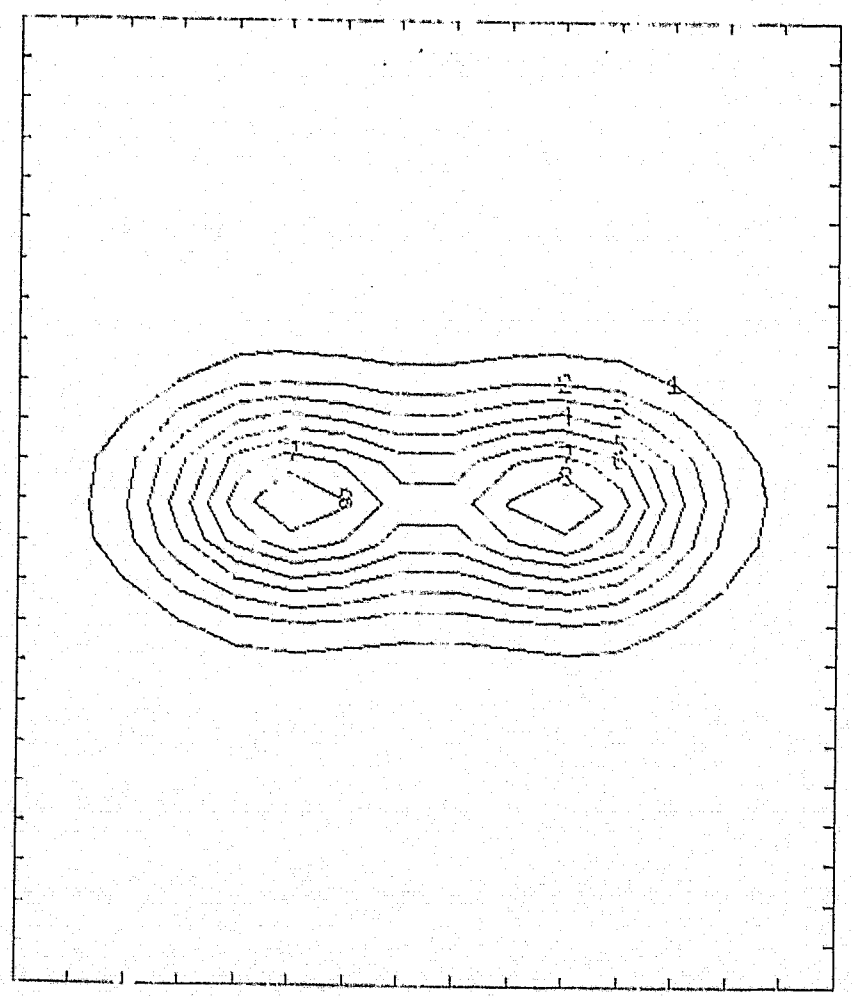

Fig. 5.6d. Contour plots of the spanwise vorticity $(\bar{\omega}_2)$ for $\beta = 3/16$, at time $T = 0$. Constant vorticity lines are plotted at eight levels. Higher numbers on these lines indicate higher vorticity levels $(\bar{\omega}_{2,max} = 0.421)$.

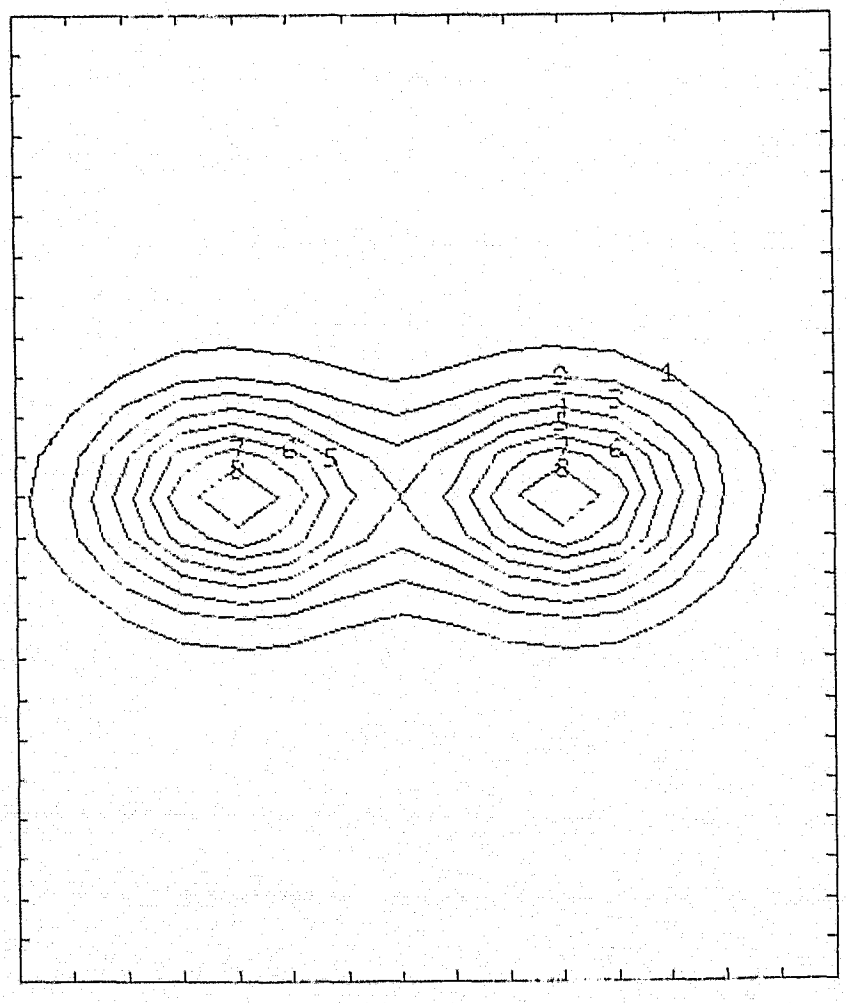

Fig. 5.6e. Contour plots of the spanwise vorticity $(\bar{\omega}_2)$ for $\beta = 2/16$, at time $T = 0$. Constant vorticity lines are plotted at eight levels. Higher numbers on these lines indicate higher levels $(\bar{\omega}_{2,max} = 0.416)$.

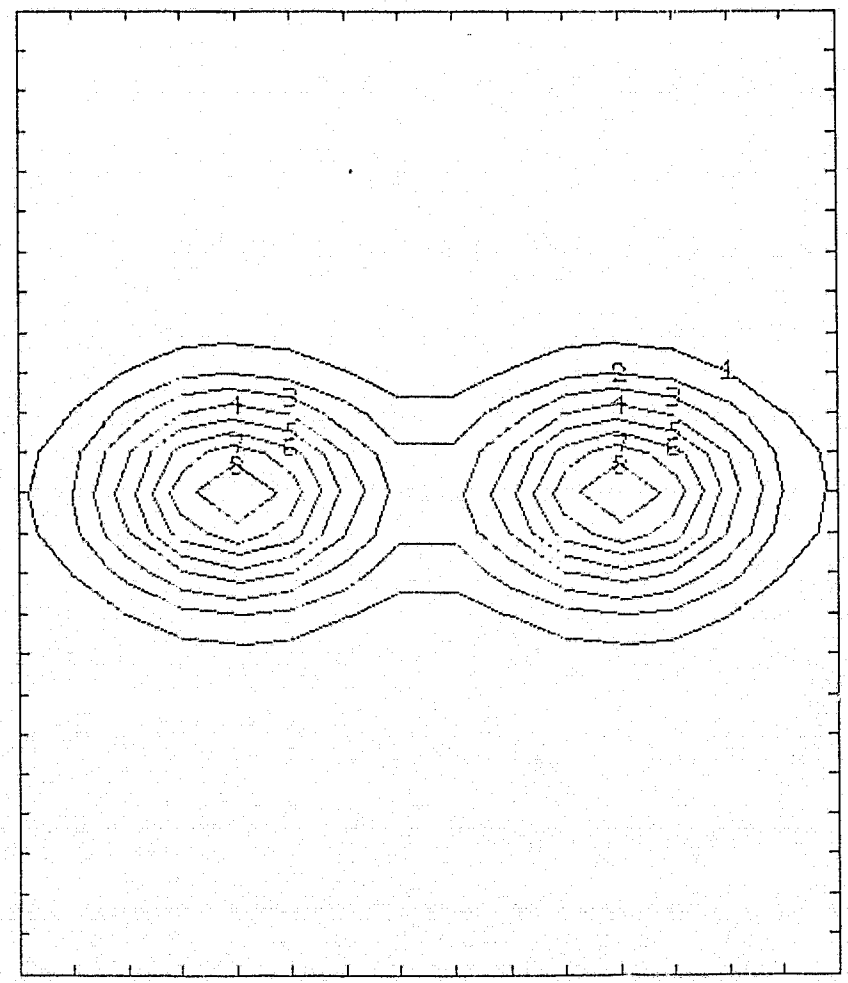

Fig. 5.6f. Contour plots of the spanwise vorticity $(\bar{\omega}_2)$ for $\beta = 1/16$, at time $T = 0$. Constant vorticity lines are plotted at eight levels. Higher numbers on these lines indicate higher levels $(\bar{\omega}_{2,max} = 0.415)$.

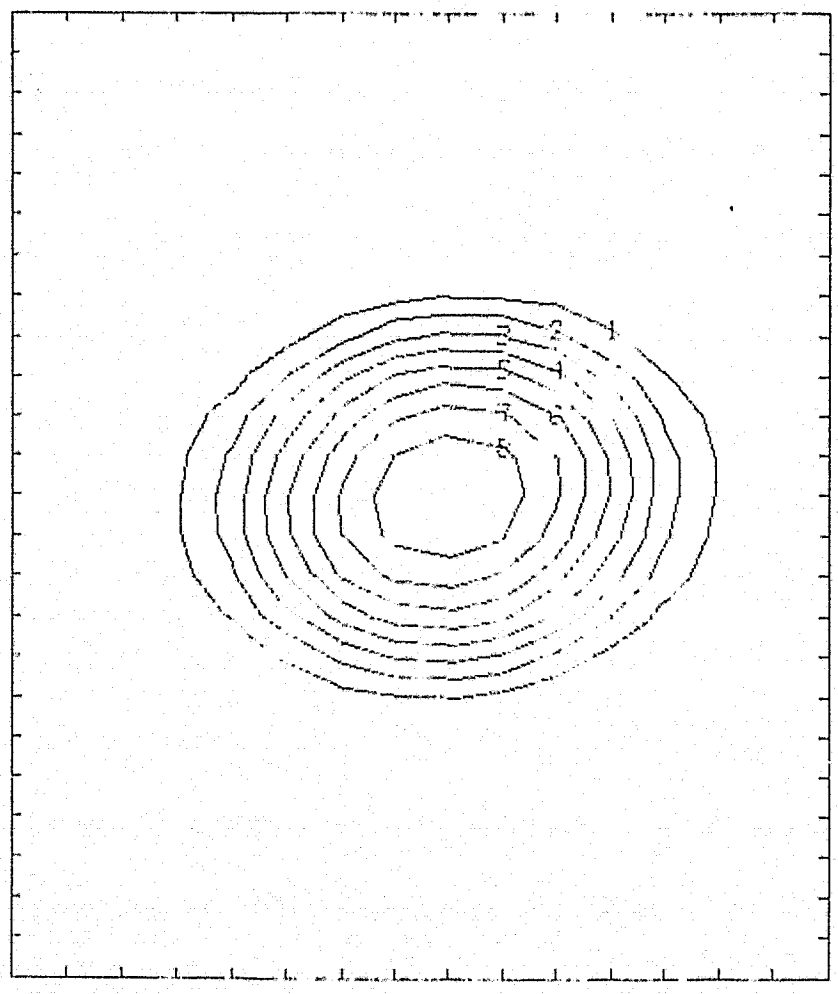

Fig. 5.7a. Contour plots of the spanwise vorticity ($\bar{\omega}_2$) for $\beta = 6/16$, at time $T = 16.78$. Constant vorticity lines are plotted at eight levels. Higher numbers on these lines indicate higher levels ($\bar{\omega}_{2,max} = 0.394$).

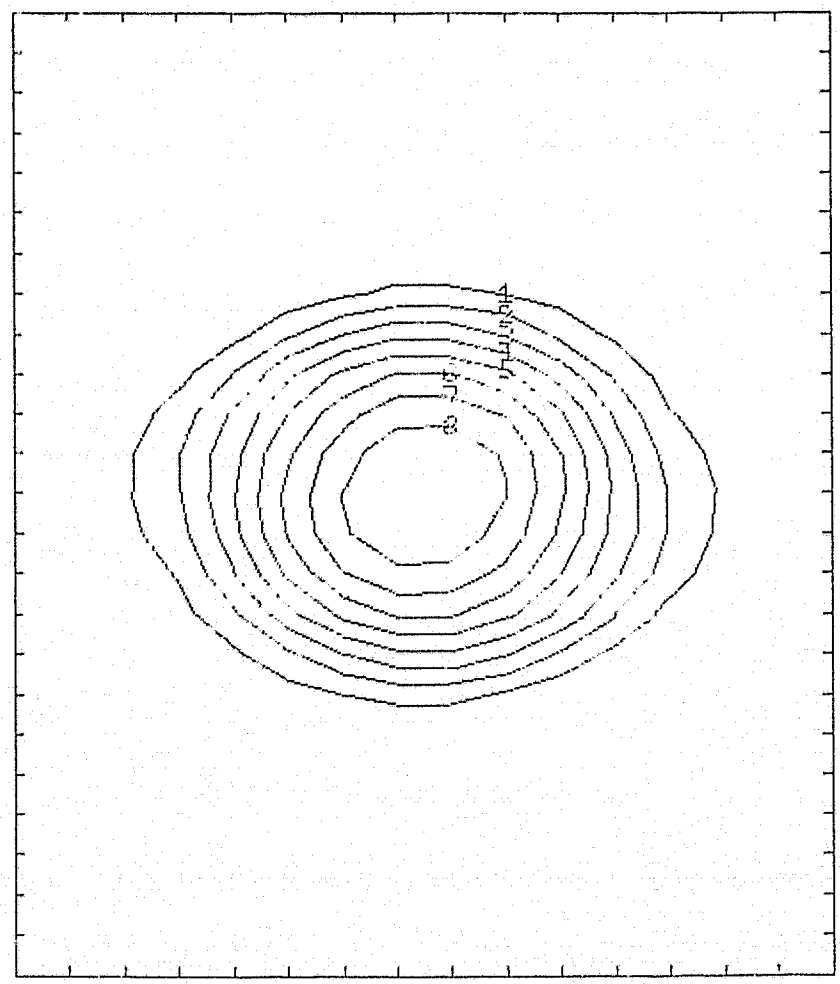

Fig. 5.7b. Contour plots of the spanwise vorticity $(\bar{\omega}_2)$ for $\beta = 5/16$, at time $T = 16.78$. Constant vorticity lines are plotted at eight levels. Higher numbers on these lines indicate higher levels $(\bar{\omega}_{2,max} = 0.358)$.

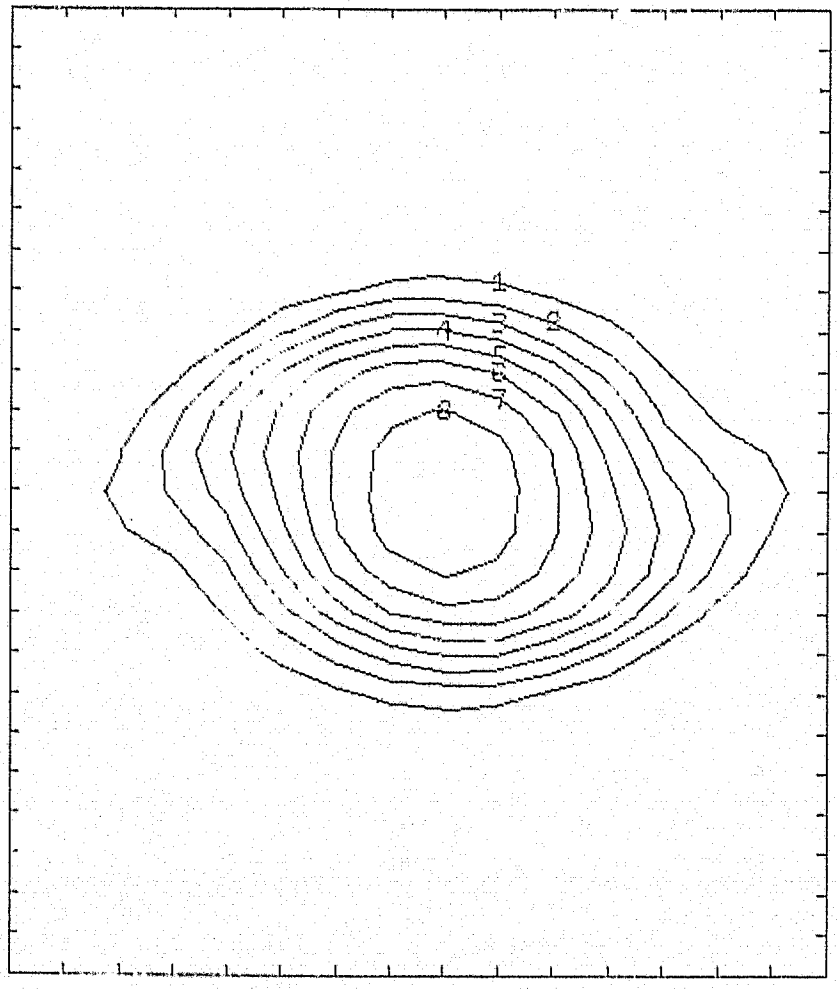

Fig. 5.7c. Contour plots of the spanwise vorticity $(\bar{\omega}_2)$ for $\beta = 4/16$, at time $T = 16.78$. Constant vorticity lines are plotted at eight levels. Higher numbers on these lines indicate higher vorticity levels $(\omega_{2,max} = 0.322)$.

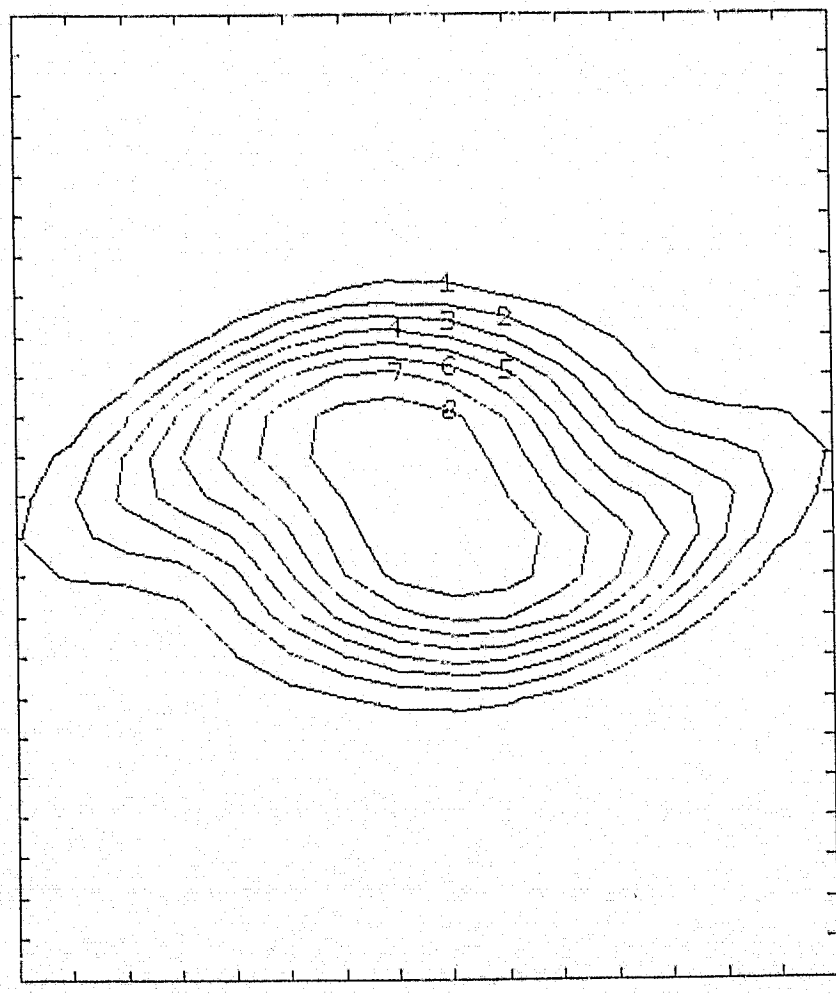

Fig. 5.7d. Contour plots of the spanwise vorticity $(\bar{\omega}_2)$ for $\beta = 3/16$, at time $T = 16.78$. Constant vorticity lines are plotted at eight levels. Higher numbers on these lines indicate higher levels $(\bar{\omega}_{2,max} = 0.276)$.

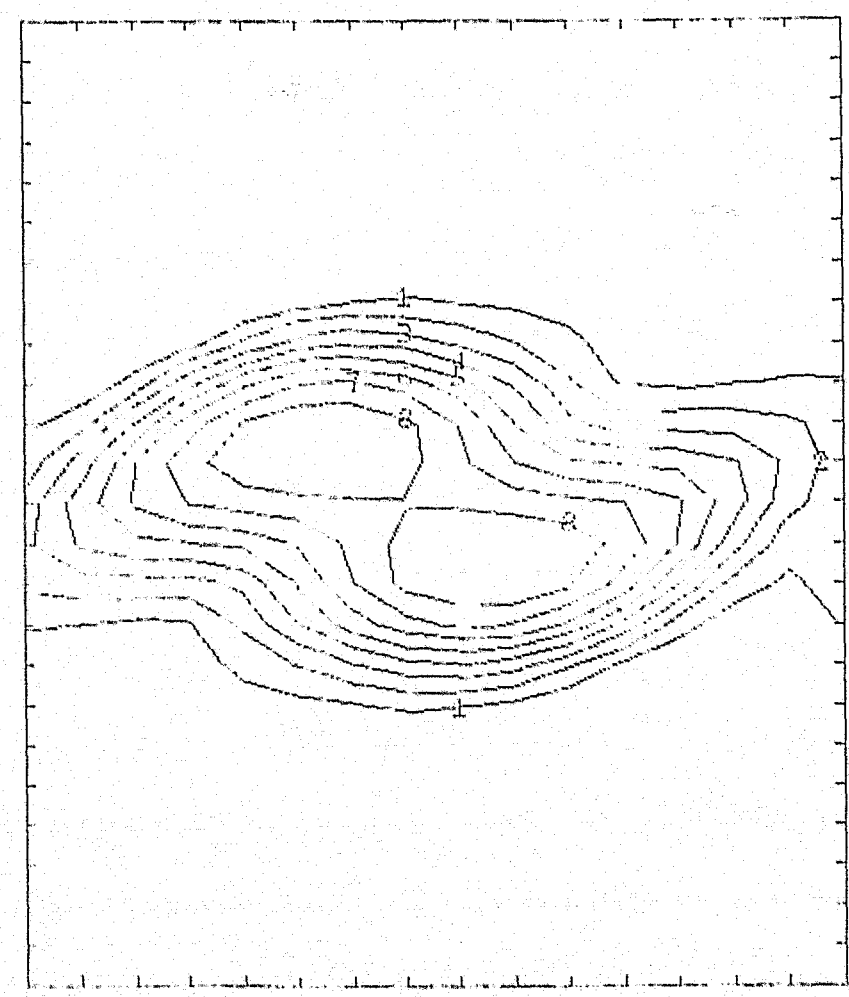

Fig. 5.7e. Contour plots of the spanwise vorticity $(\bar{\omega}_2)$ for $\beta = 2/16$, at time $T = 16.78$. Constant vorticity lines are plotted at eight levels. Higher numbers on these lines indicate higher levels $(\bar{\omega}_{2,max} = 0.248)$.

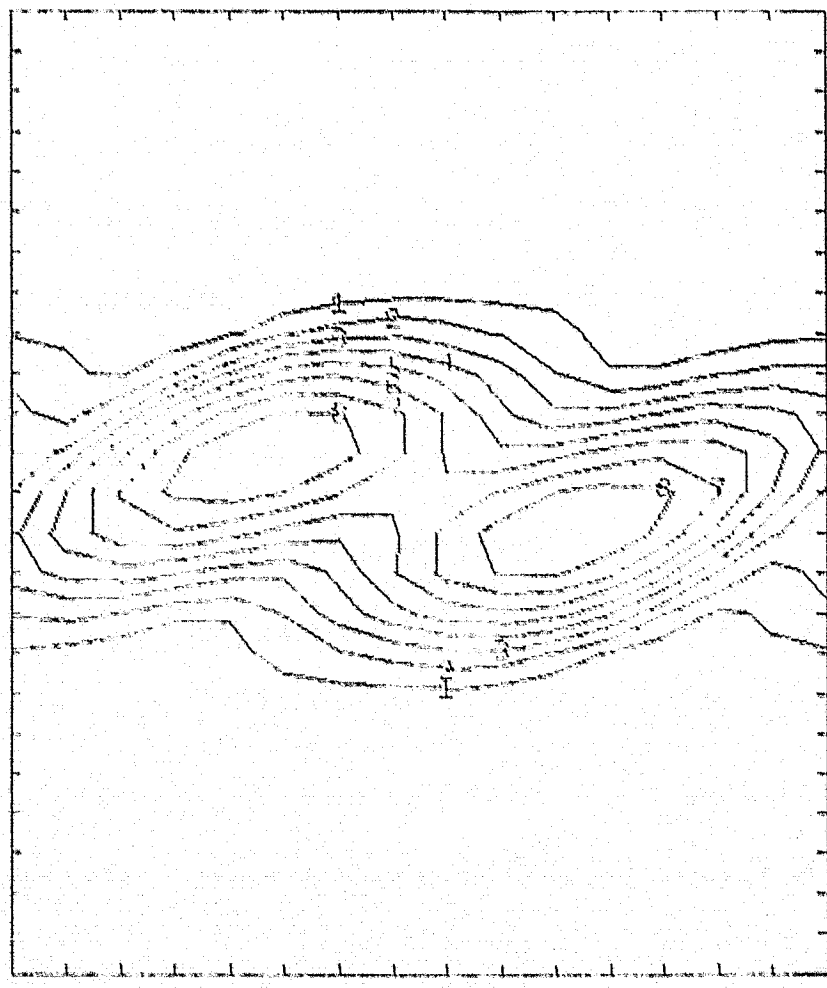

Fig. 5.7f. Contour plots of the spanwise vorticity ($\bar{\omega}_2$) for $\beta = 1/16$, at time $\mathcal{T} = 16.78$. Constant vorticity lines are plotted at eight levels. Higher numbers on these lines indicate higher levels ($\bar{\omega}_{2,max} = 0.245$).

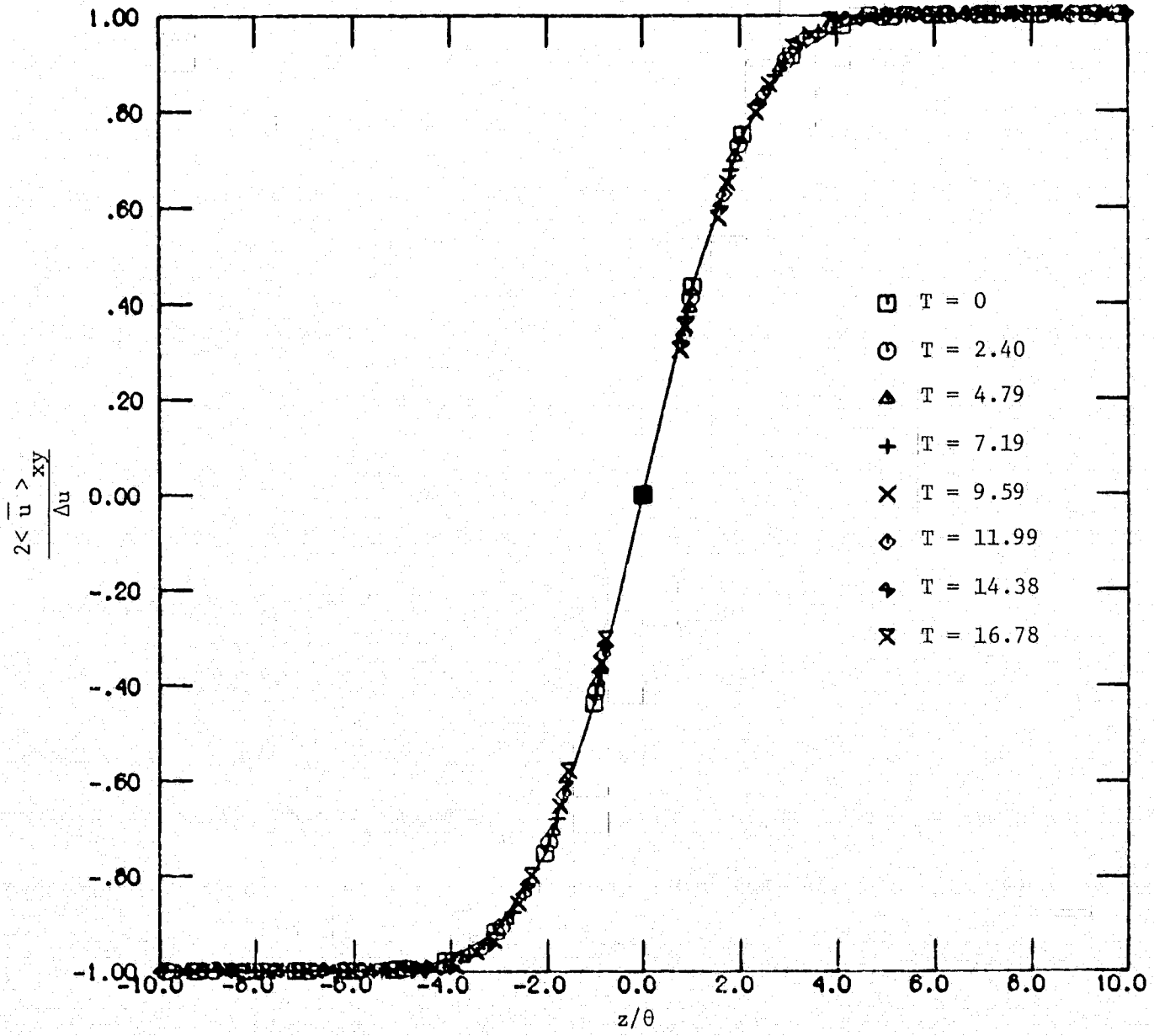

Fig. 5.8. Mean velocity profiles. Two-dimensional computations (β = 3/16).

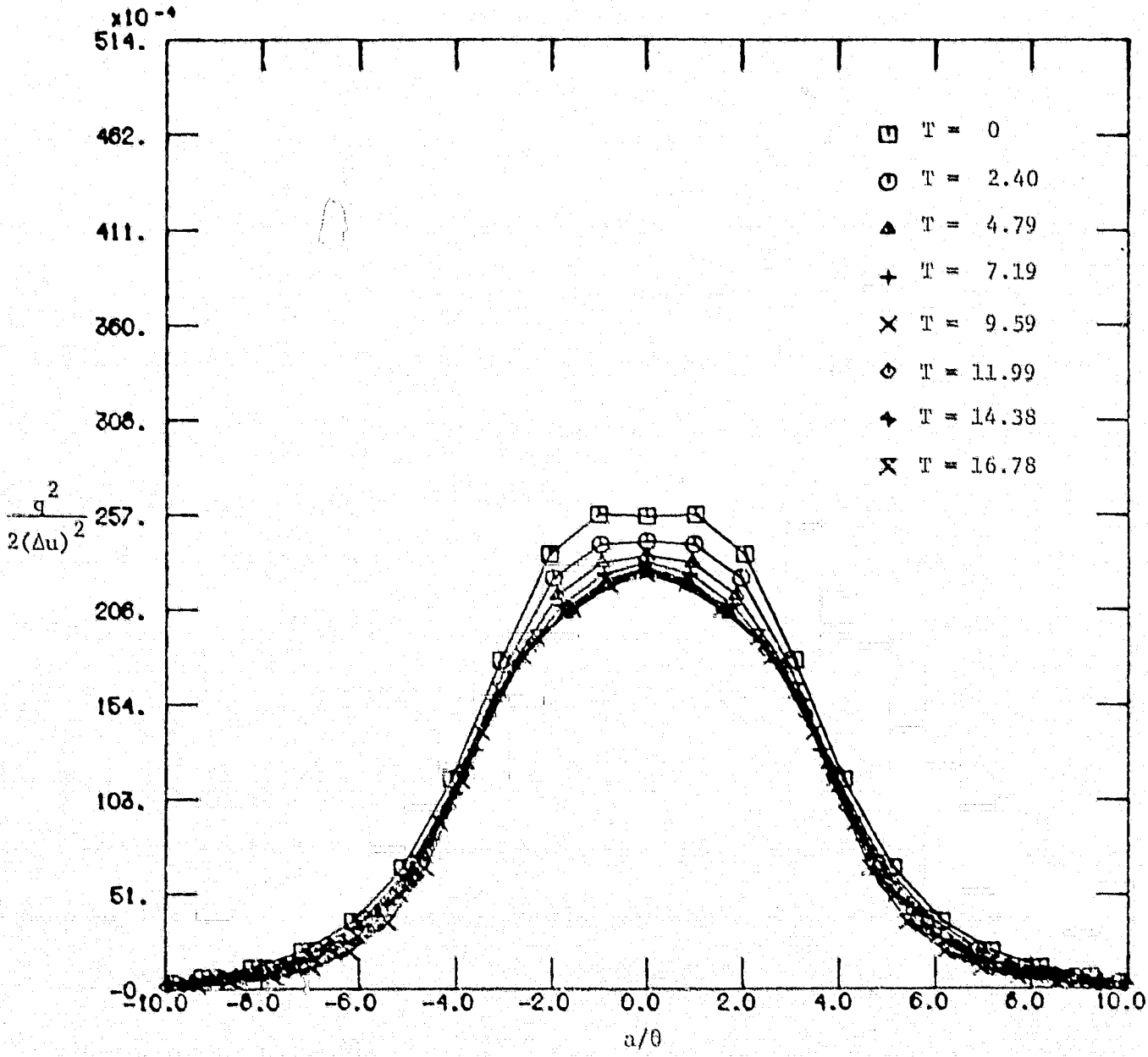

Fig. 5.9. Mean turbulence intensity profiles. Two-dimensional computations (β = 3/16).

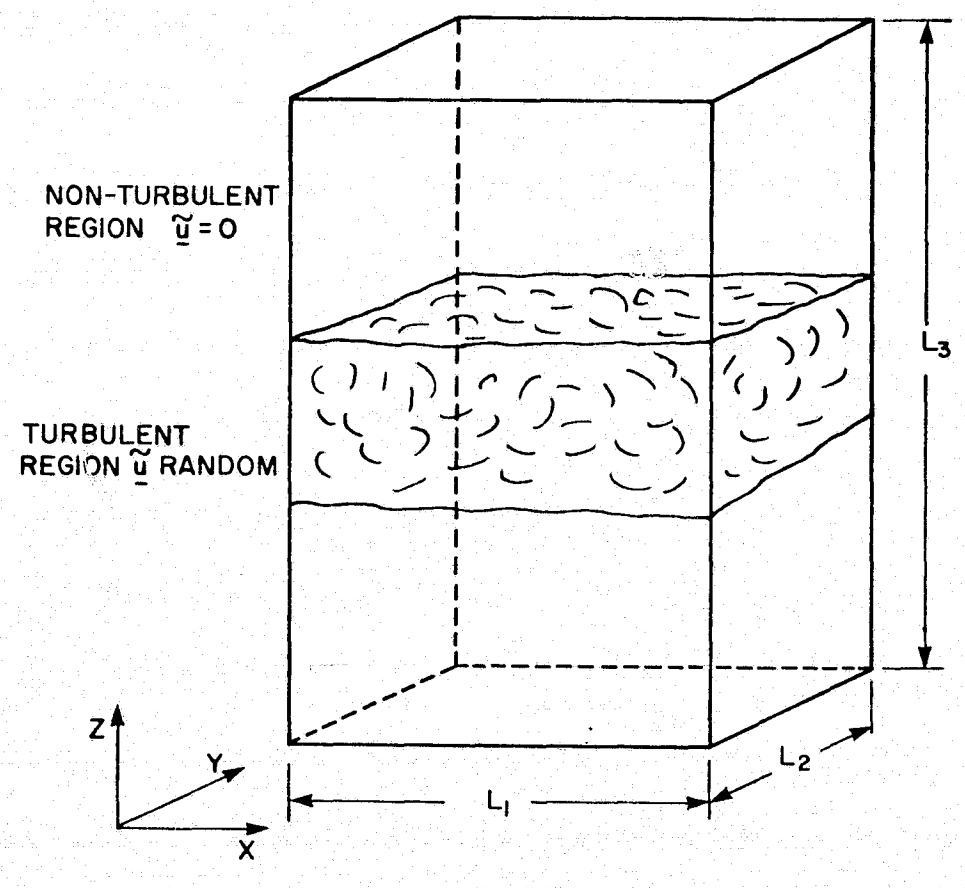

Fig. 6.1. Three-dimensional computation box. Random velocity setup and coordinate system.

Table 6.1

Three-Dimensional Computations of Turbulent Mixing Layers

Case	Amplitude of Random Field	Initial Conditions
a	$\frac{\lvert u_i \rvert_{max}}{\Delta u} = 0.01$	Random field + mean
b	$\frac{\lvert u_i \rvert_{max}}{\Delta u} = 0.30$	Random field + mean
c	$\frac{\lvert u_i \rvert_{max}}{\Delta u} = 0.30$	Random field + 2 spanwise vortices (β = 3/16)

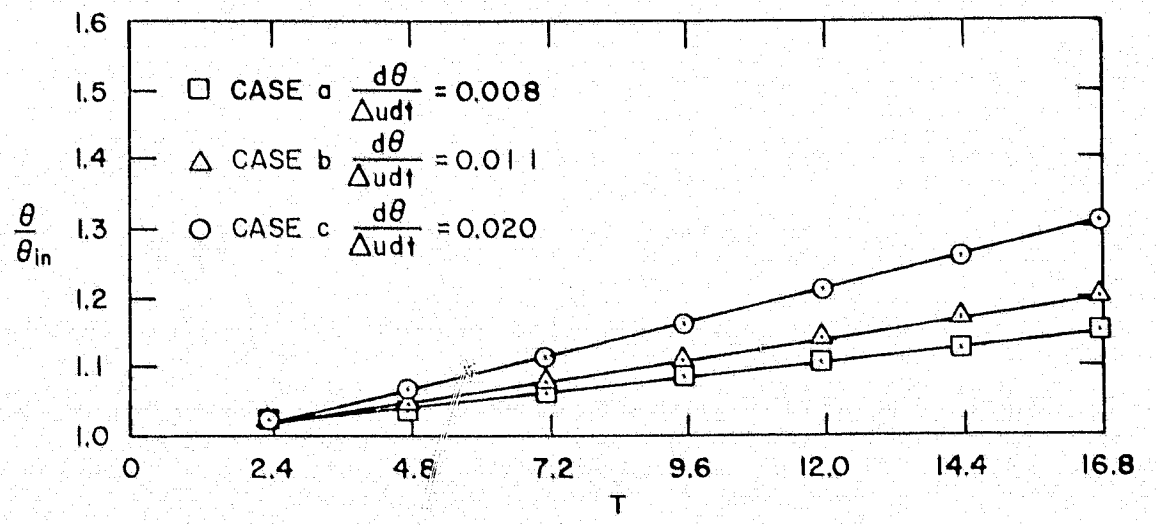

Fig. 6.2. Non-dimensional momentum thickness (θ/θ_{in}) as a function of time. Three-dimensional computations.

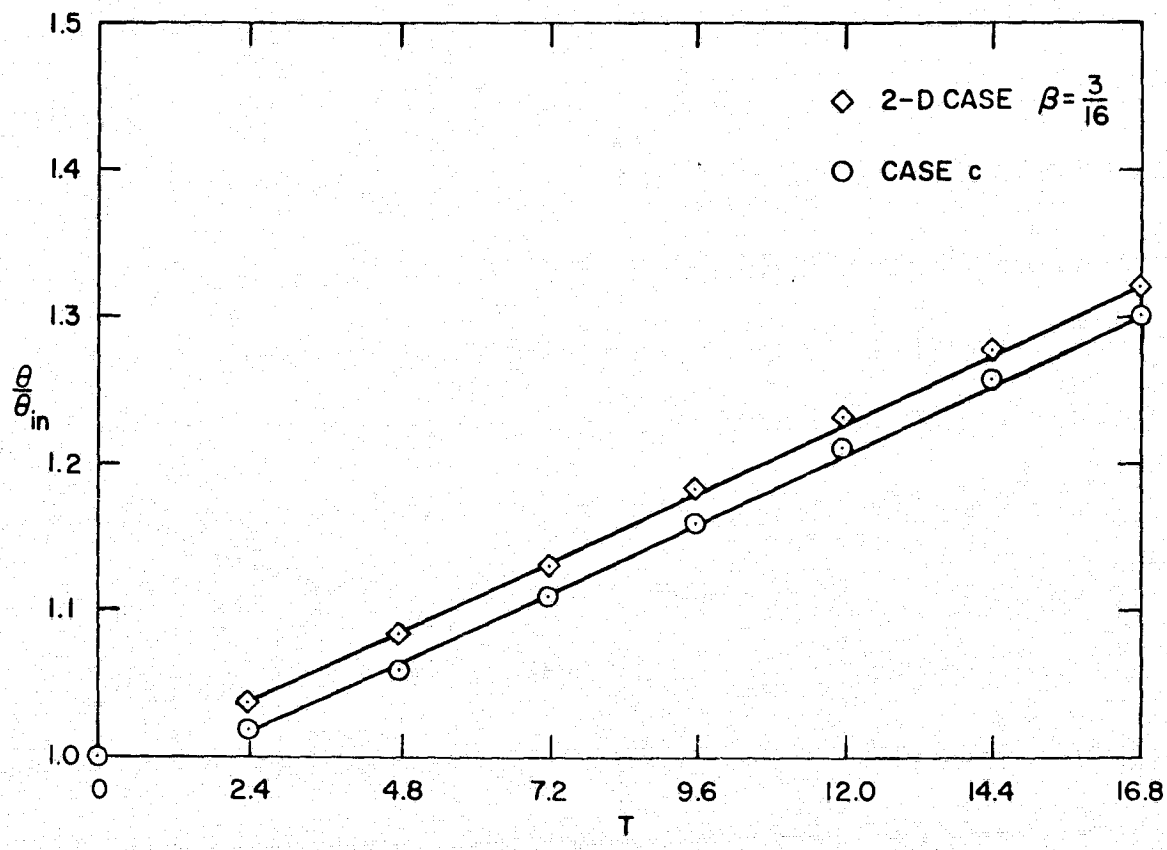

Fig. 6.3. Non-dimensional momentum thickness (θ/θ_{in}) as a function of time.

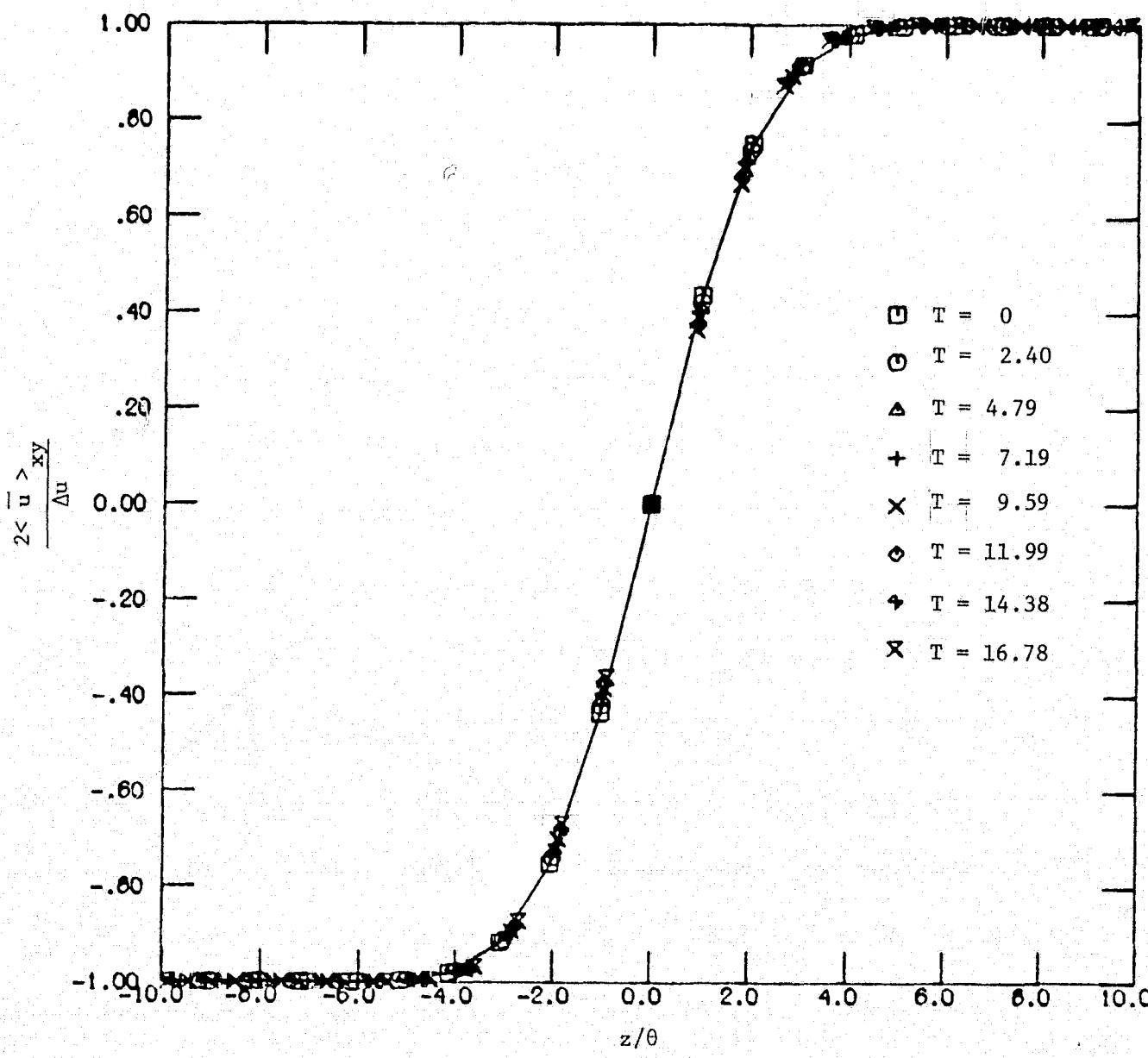

Fig. 6.4a. Mean velocity profiles. Three-dimensional computation (case a).

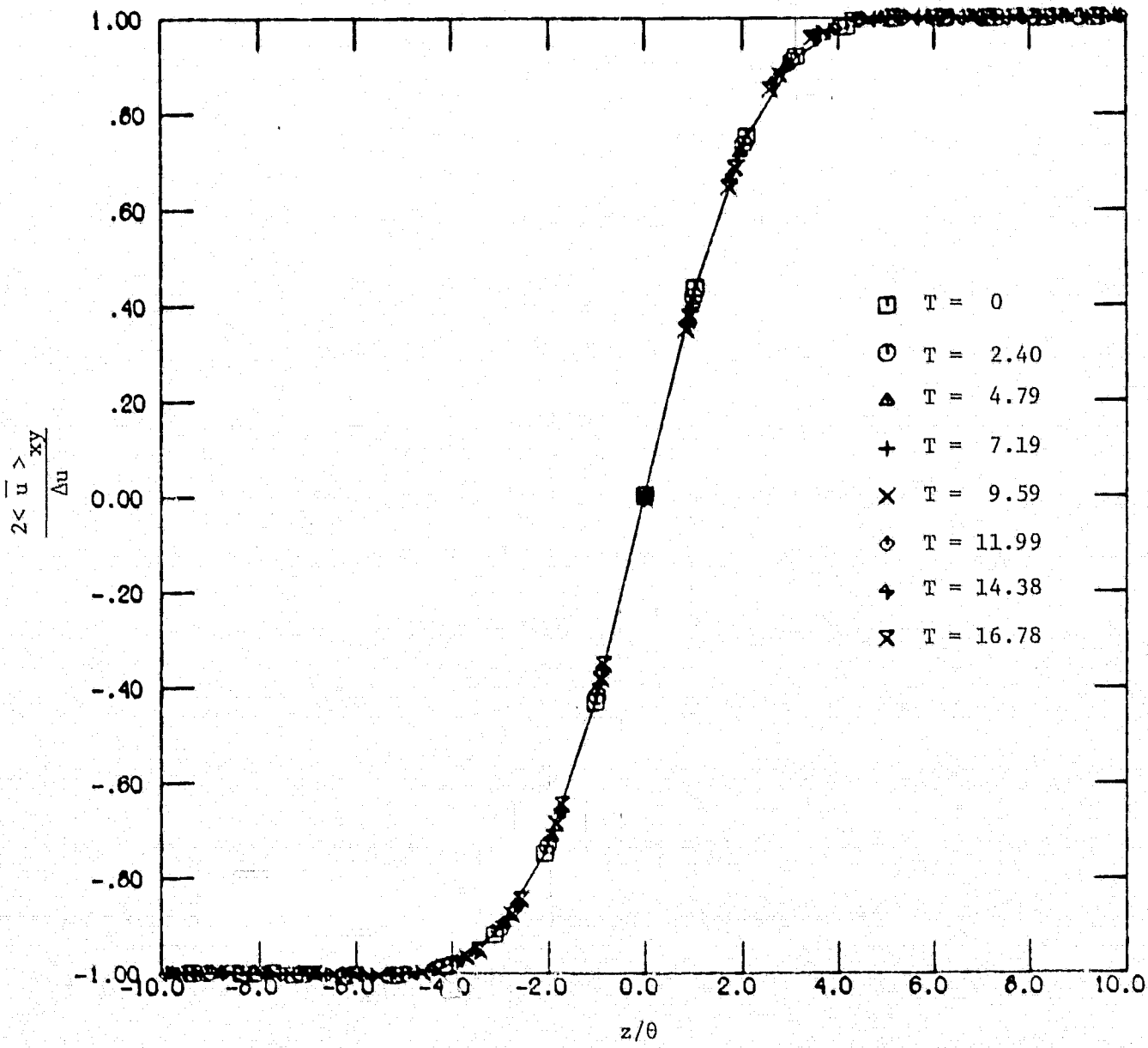

Fig. 6.4b. Mean velocity profiles. Three-dimensional computation (case b).

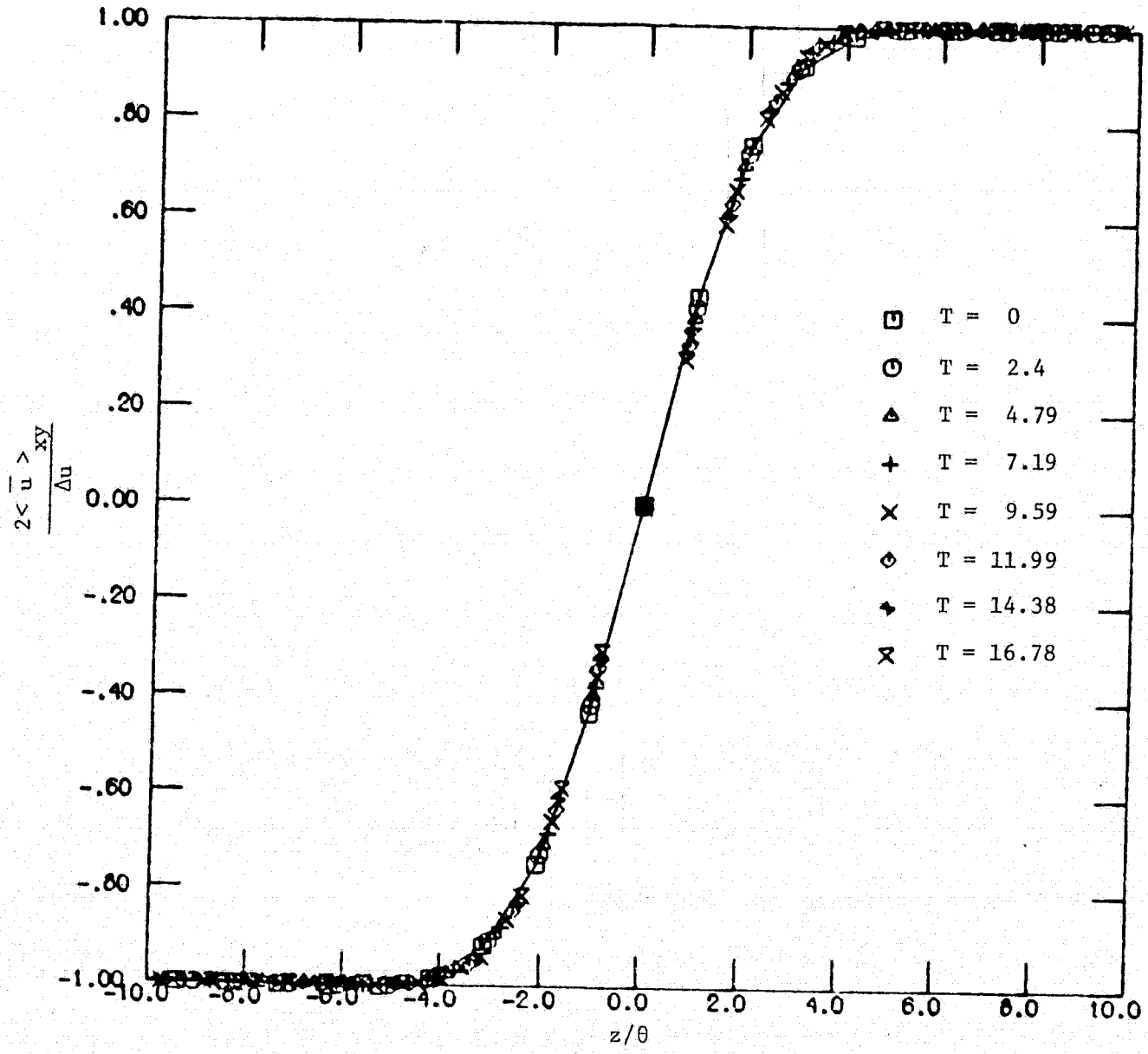

Fig. 6.4c. Mean velocity profiles. Three-dimensional computations (case c).

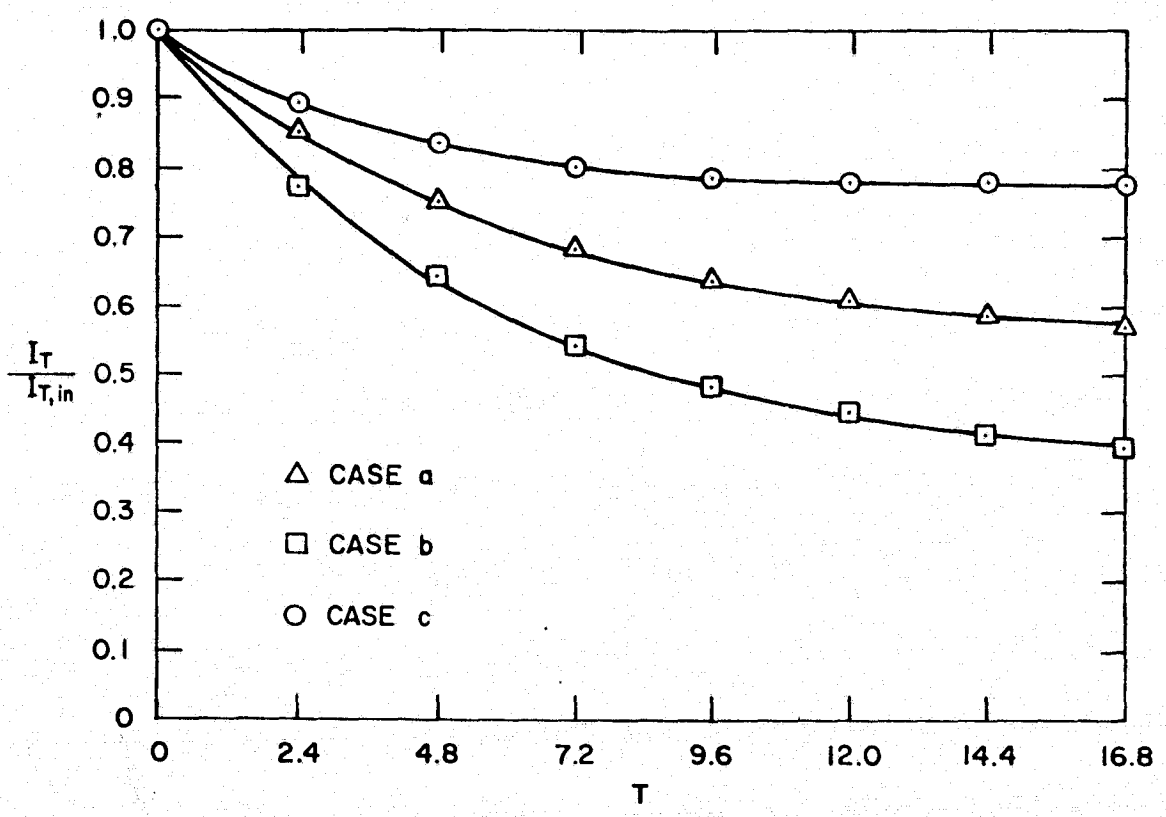

Fig. 6.5. Integral of the turbulence energy as a function of time.

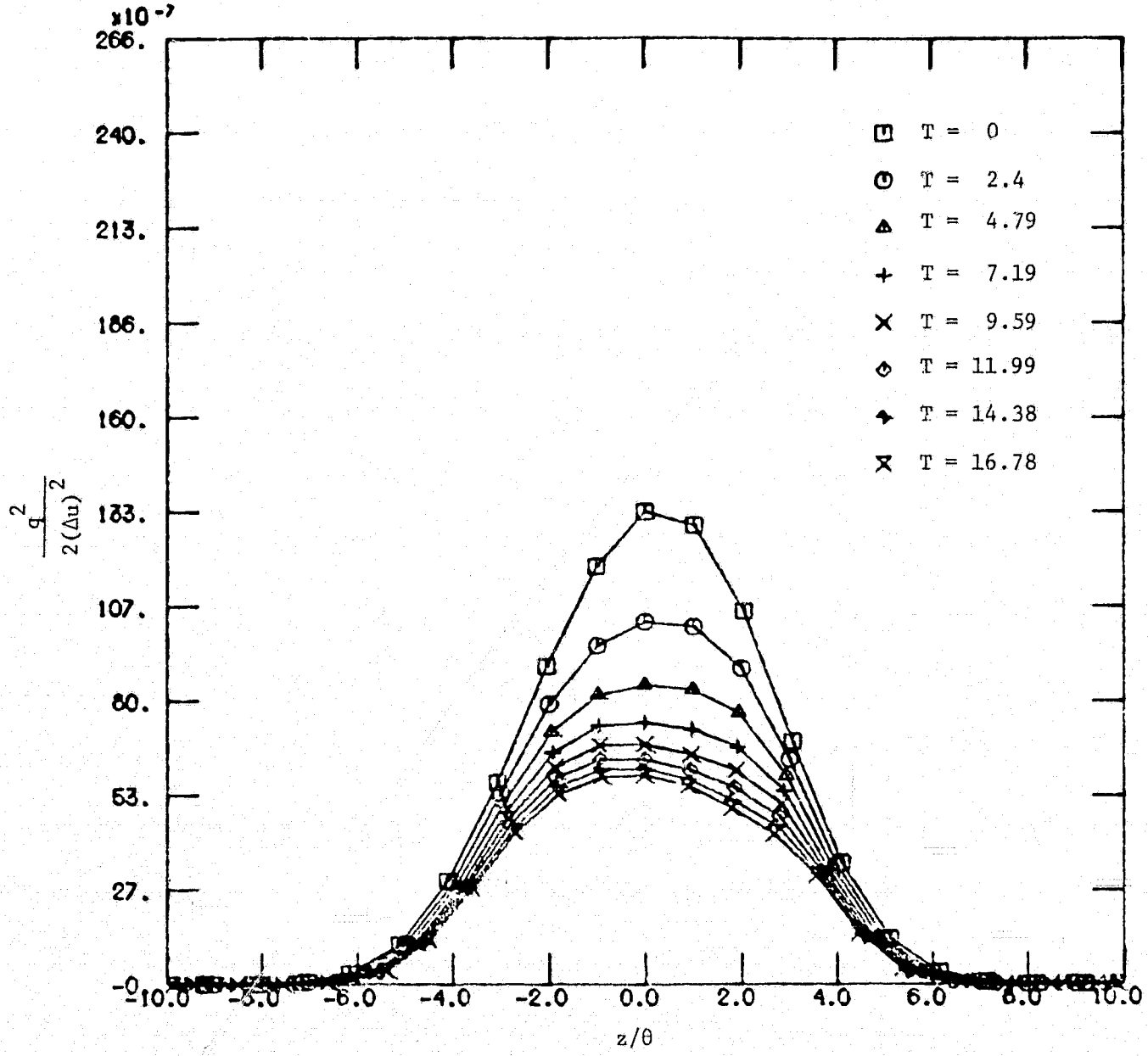

Fig. 6.6a. Mean turbulence intensity profiles. Three-dimensional computations (case a).

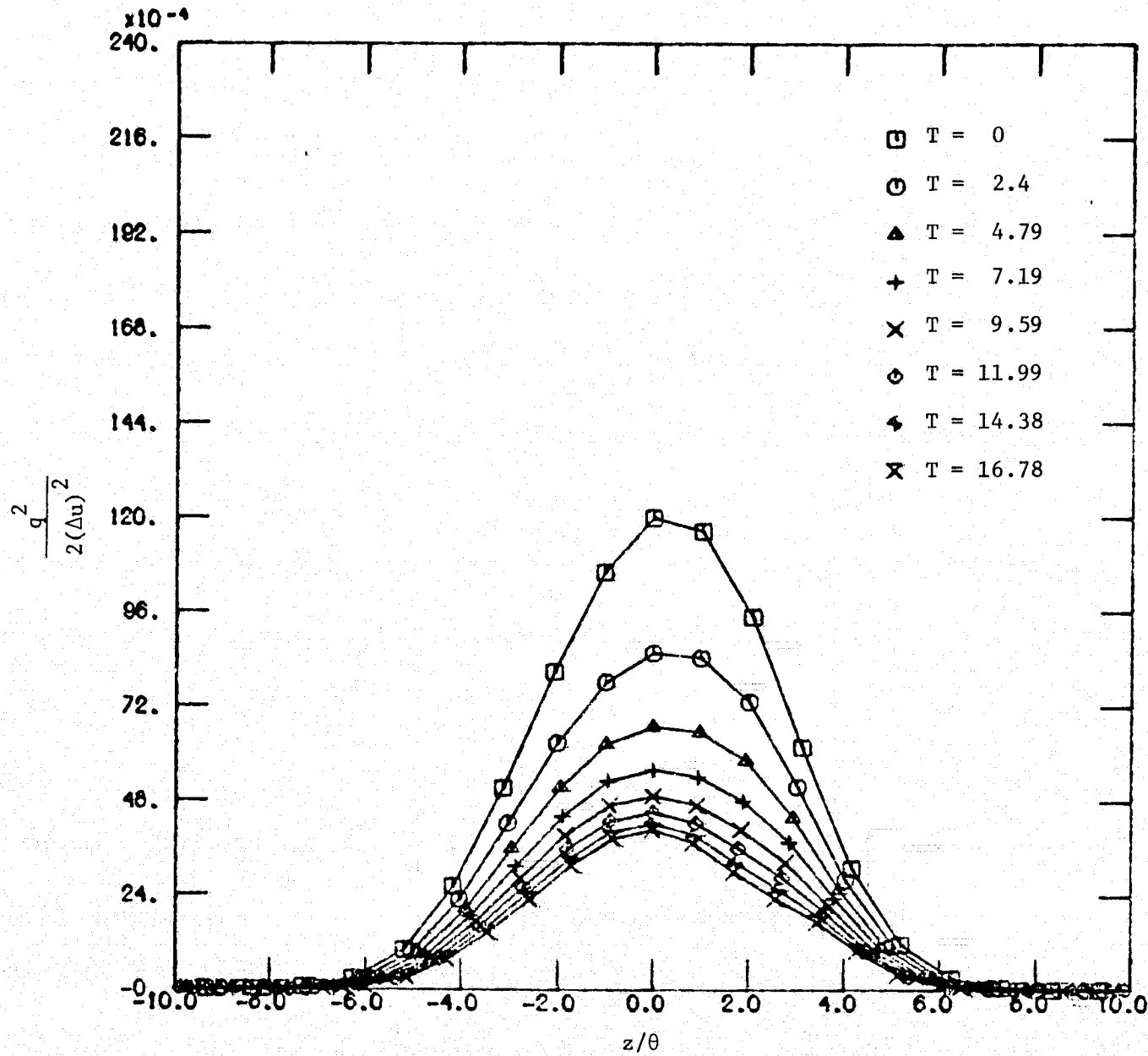

Fig. 6.6b. Mean turbulence intensity profiles. Three-dimensional computations (case b).

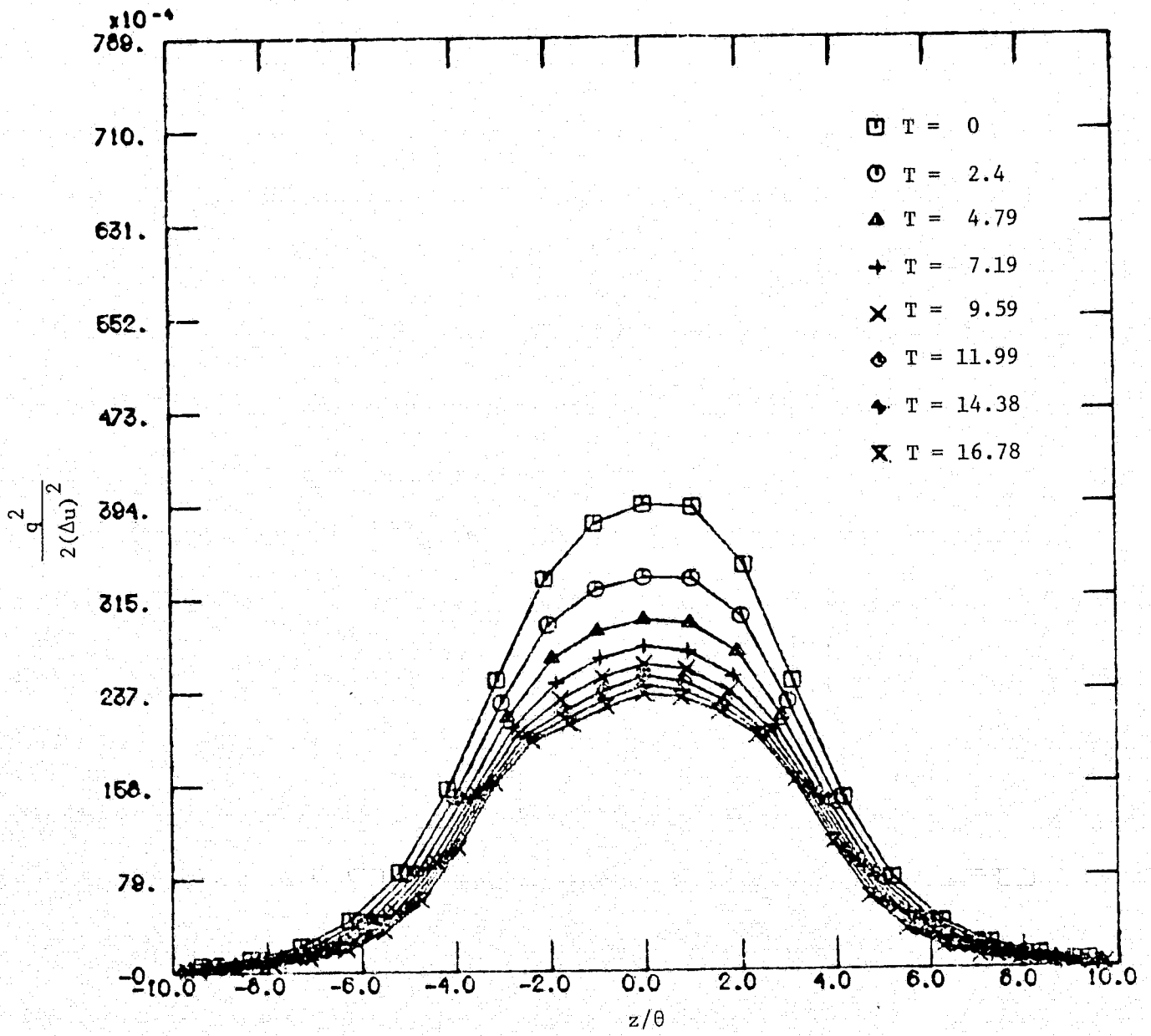

Fig. 6.6c. Mean turbulence intensity profiles. Three-dimensional computations (case c).

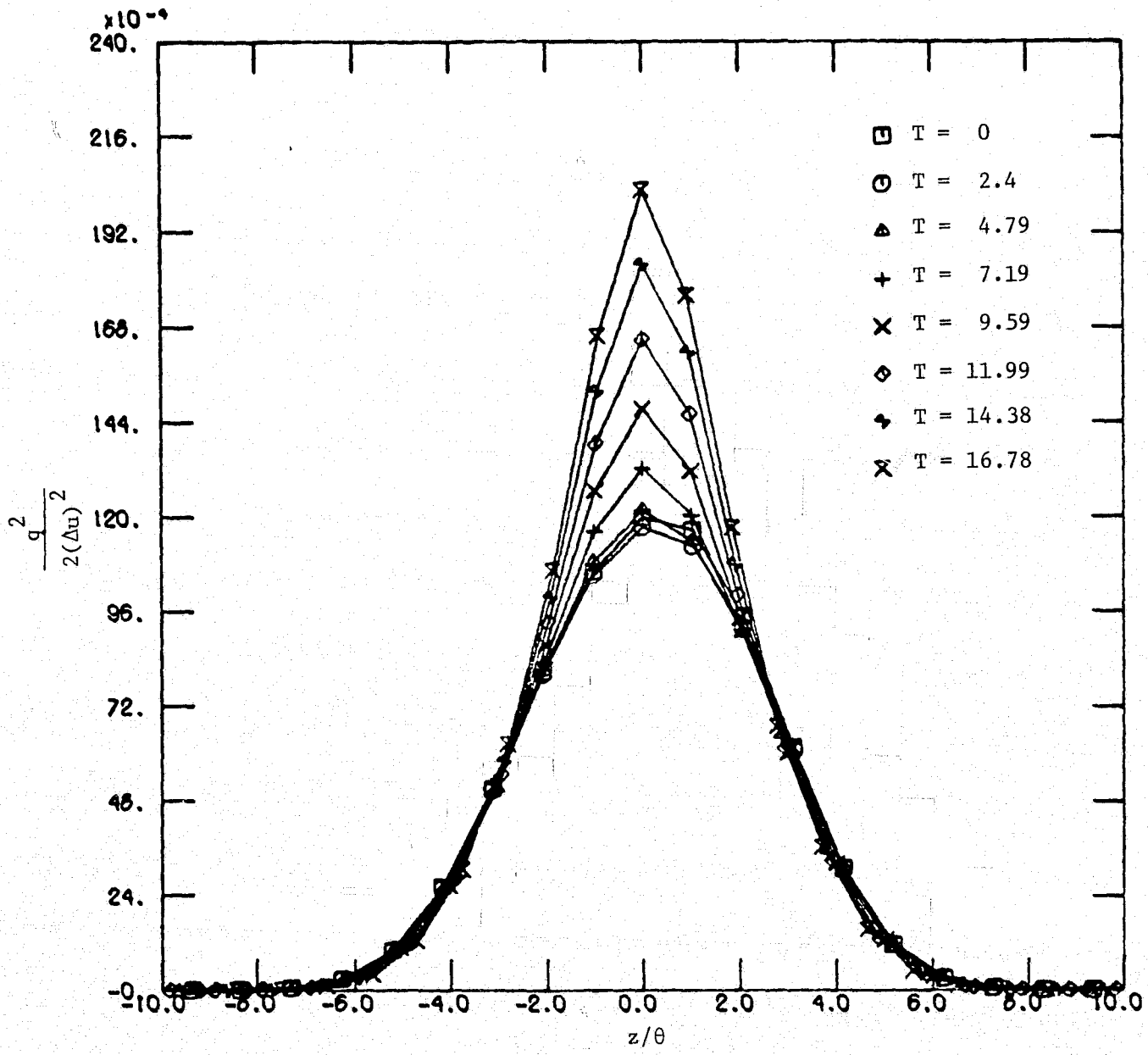

Fig. 6.7. Mean turbulence intensity profiles. Three-dimensional computation ($C_v = 0$).

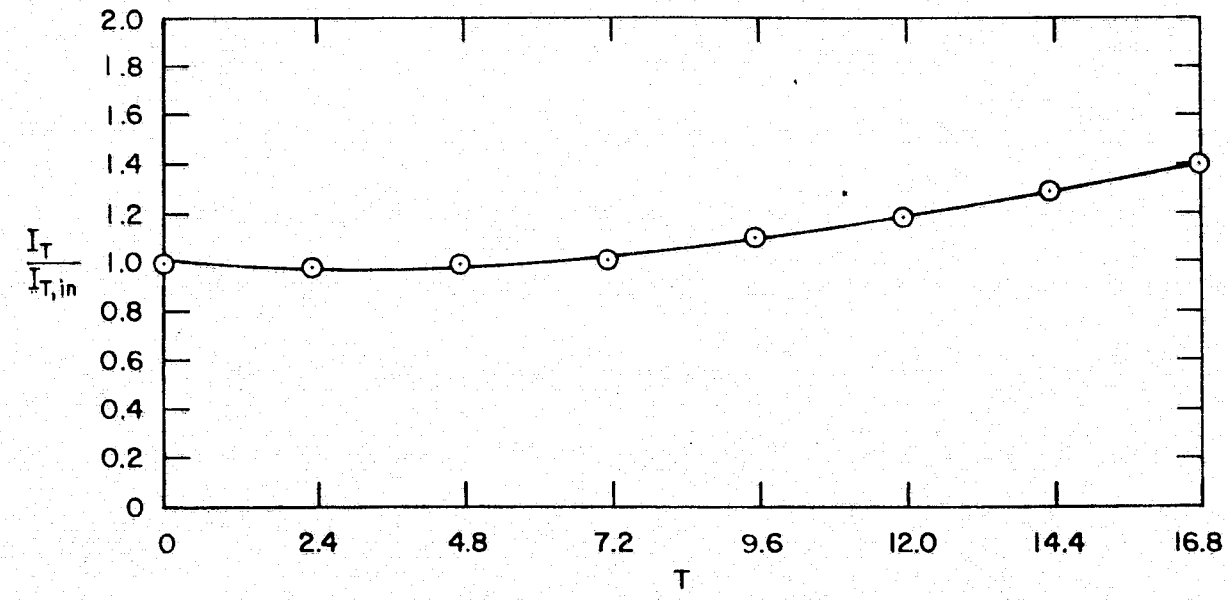

Fig. 6.8. Integral of the turbulence energy as a function of time. Three-dimensional computation ($C_v = 0$).

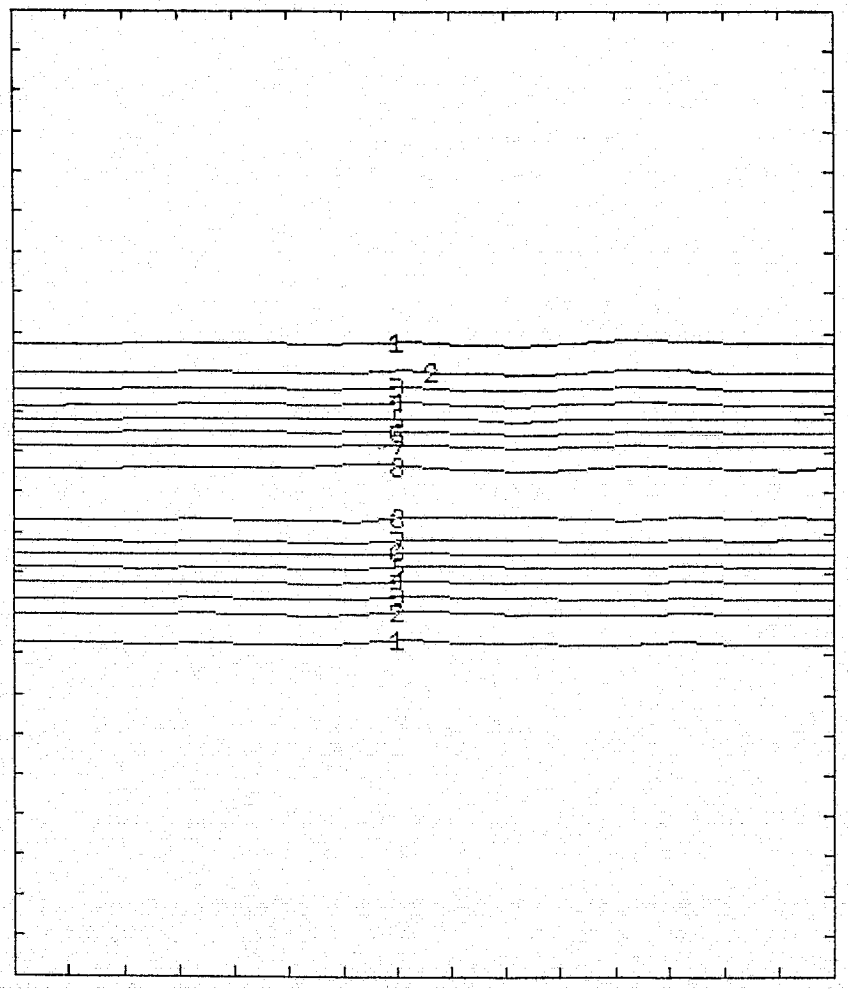

Fig. 6.9a. Contour plots of the spanwise vorticity $(\bar{\omega}_2)$ in an x-z plane, at time T = 0. Constant vorticity lines are plotted at eight levels. Higher numbers on these lines indicate higher vorticity levels ($\omega_{2,max} = 0.228$, case a).

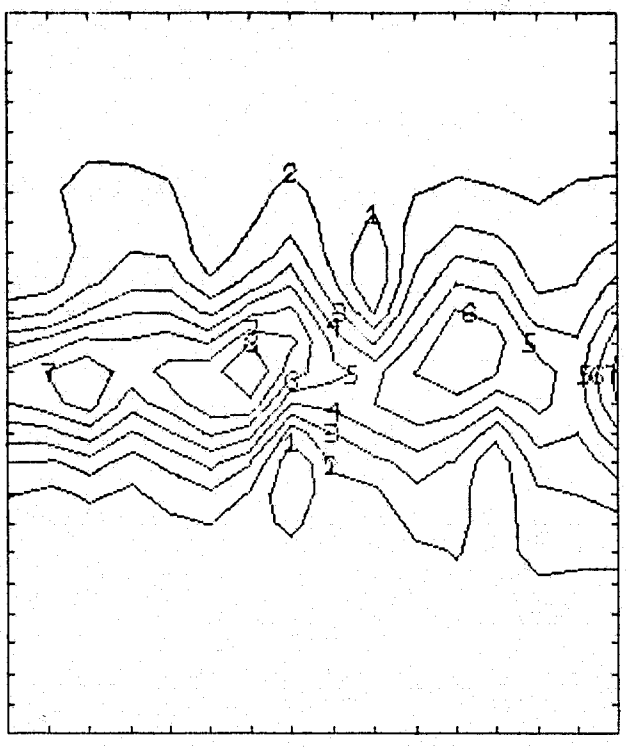

$\frac{y}{\theta_{in}} = 0$; $\bar{\omega}_{2,max} = 0.314$

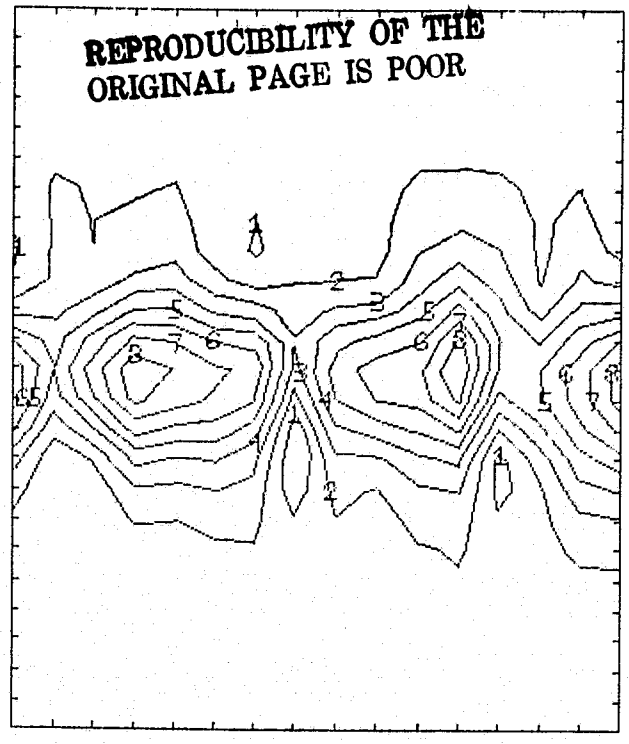

$\frac{y}{\theta_{in}} = 1.023$; $\bar{\omega}_{2,max} = 0.331$

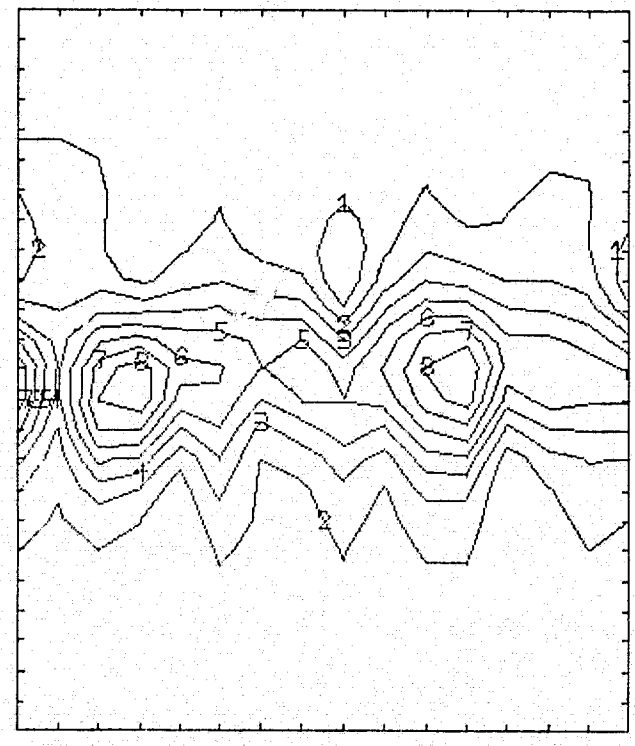

$\frac{y}{\theta_{in}} = 2.026$; $\bar{\omega}_{2,max} = 0.376$

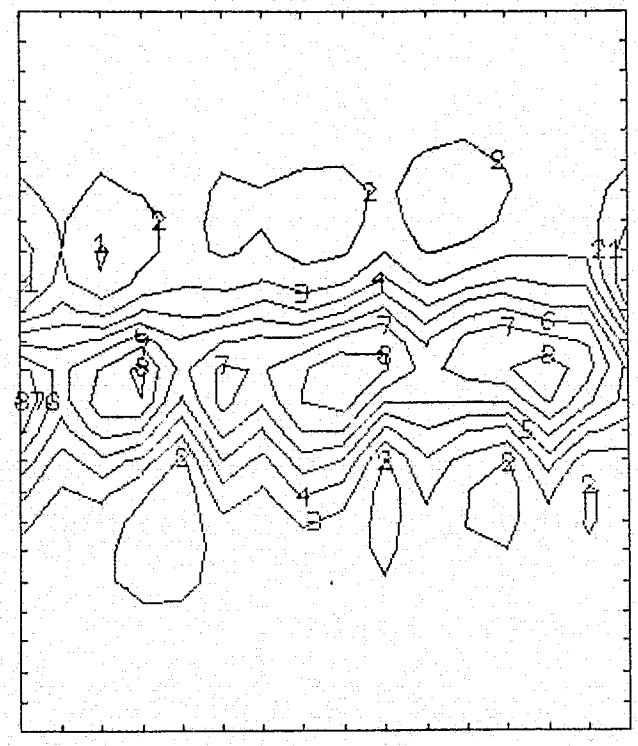

$\frac{y}{\theta_{in}} = 3.069$; $\bar{\omega}_{2,max} = 0.321$

Figs. 6.9b. Contour plots of the spanwise vorticity $(\bar{\omega}_2)$ for different x-z planes, at time T = 0. In each plane, constant vorticity lines are plotted at eight levels. Higher numbers on these lines indicate higher vorticity levels (case b).

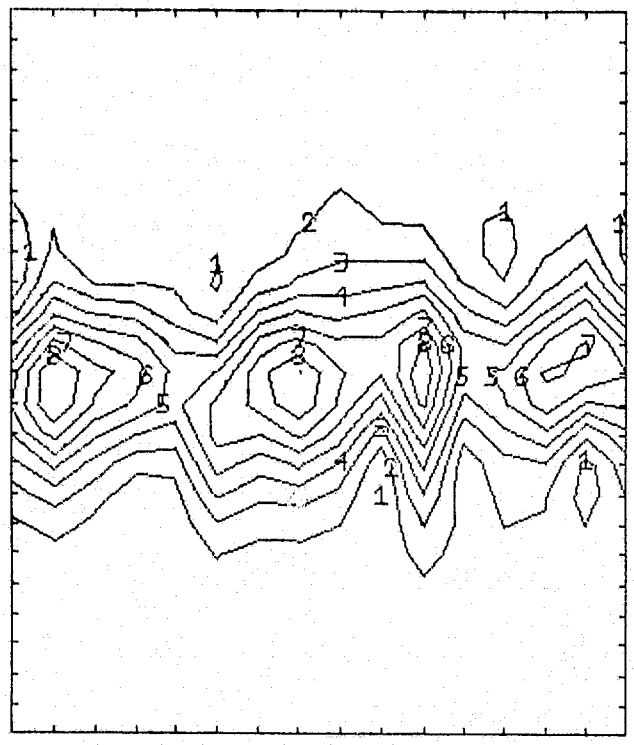

$\frac{y}{\theta_{in}} = 4.092$; $\bar{\omega}_{2,max} = 0.316$

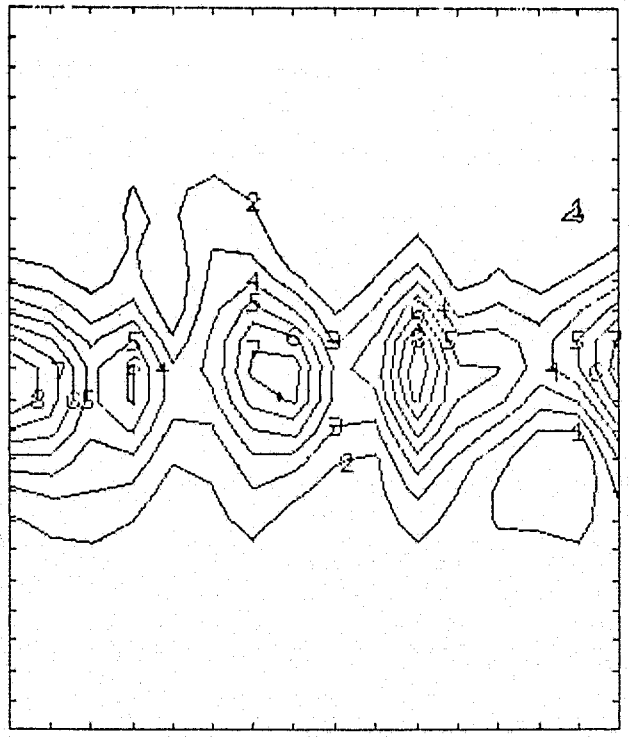

$\frac{y}{\theta_{in}} = 5.115$; $\bar{\omega}_{2,max} = 0.382$

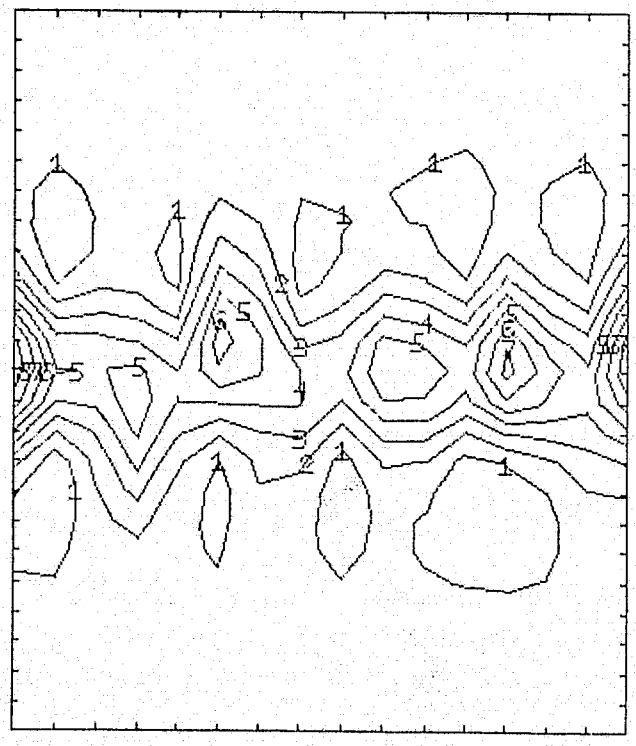

$\frac{y}{\theta_{in}} = 6.138$; $\bar{\omega}_{2,max} = 0.432$

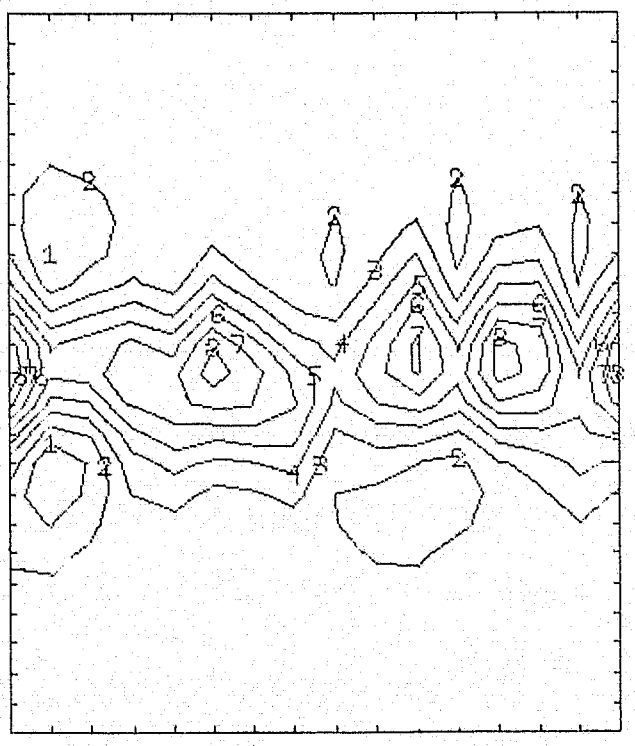

$\frac{y}{\theta_{in}} = 7.161$; $\bar{\omega}_{2,max} = 0.363$

Figs. 6.9b (continued)

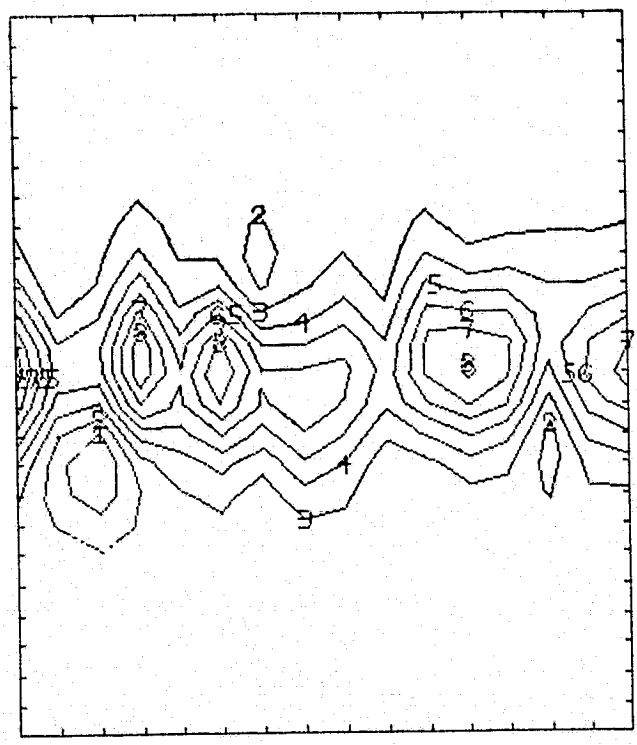

$\frac{y}{\theta_{in}} = 8.184$; $\bar{\omega}_{2,max} = 0.386$

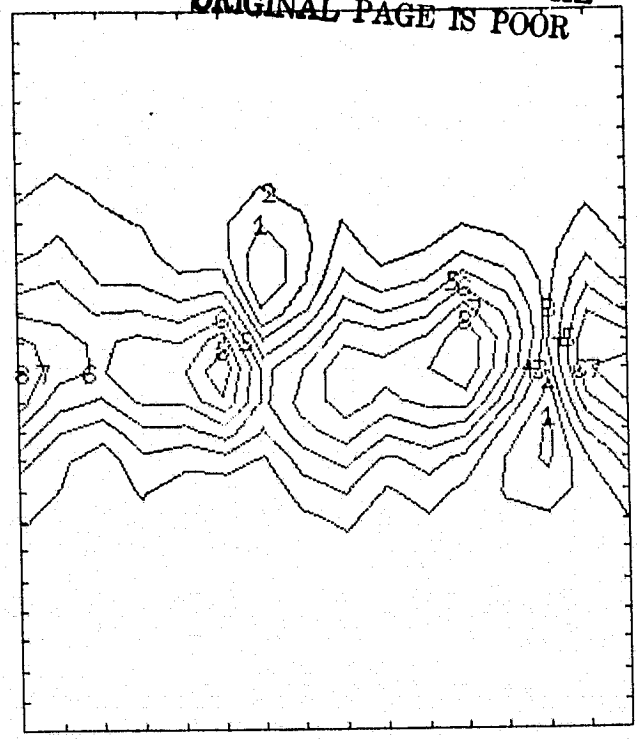

$\frac{y}{\theta_{in}} = 9.207$; $\bar{\omega}_{2,max} = 0.352$

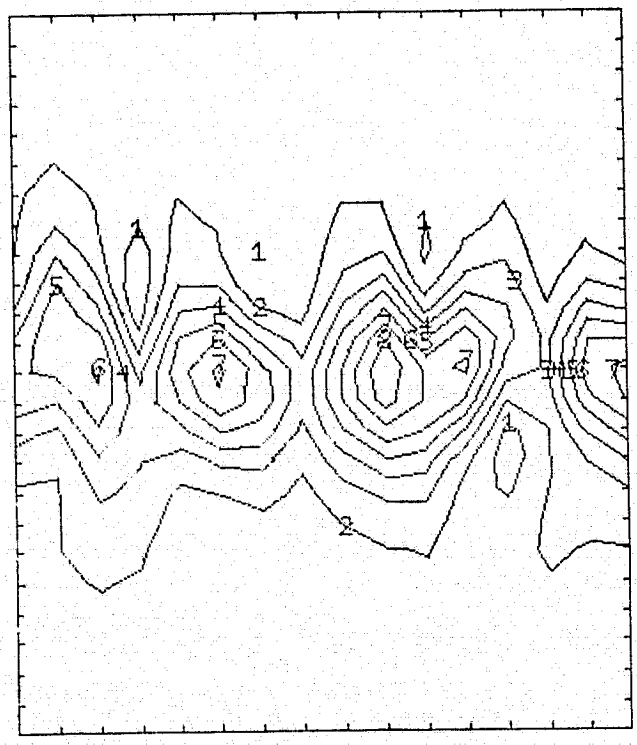

$\frac{y}{\theta_{in}} = 10.230$; $\bar{\omega}_{2,max} = 0.426$

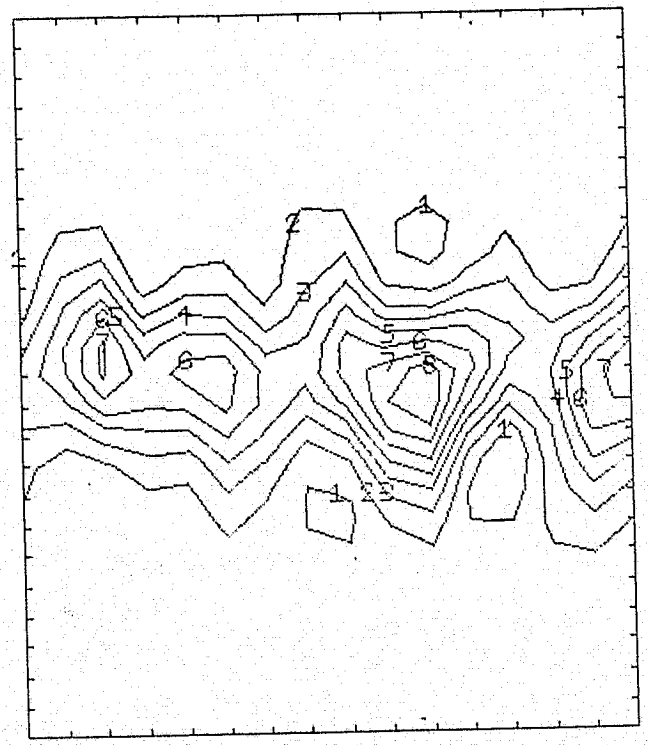

$\frac{y}{\theta_{in}} = 11.253$; $\bar{\omega}_{2,max} = 0.382$

Figs. 6.9b (continued)

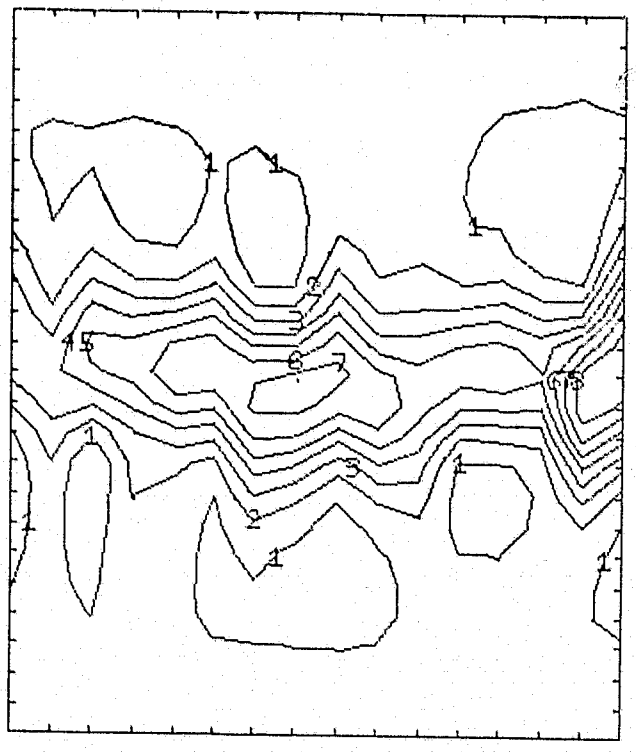

$\frac{y}{\theta_{in}} = 12.276$; $\overline{\omega}_{2,max} = 0.341$

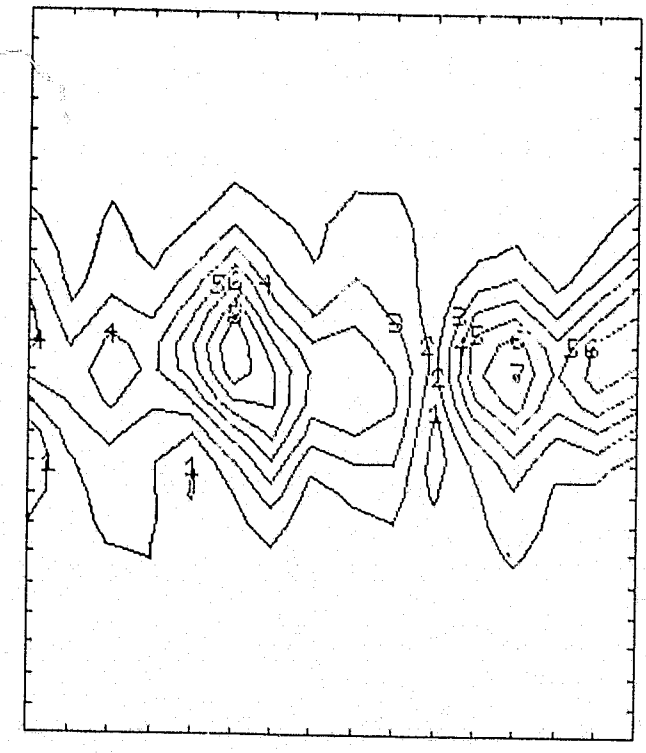

$\frac{y}{\theta_{in}} = 13.299$; $\overline{\omega}_{2,max} = 0.462$

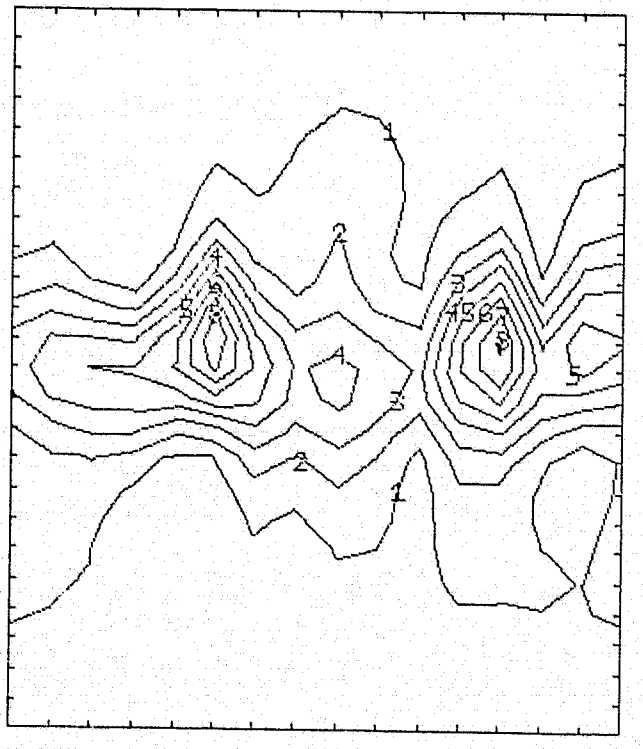

$\frac{y}{\theta_{in}} = 14.322$; $\overline{\omega}_{2,max} = 0.427$

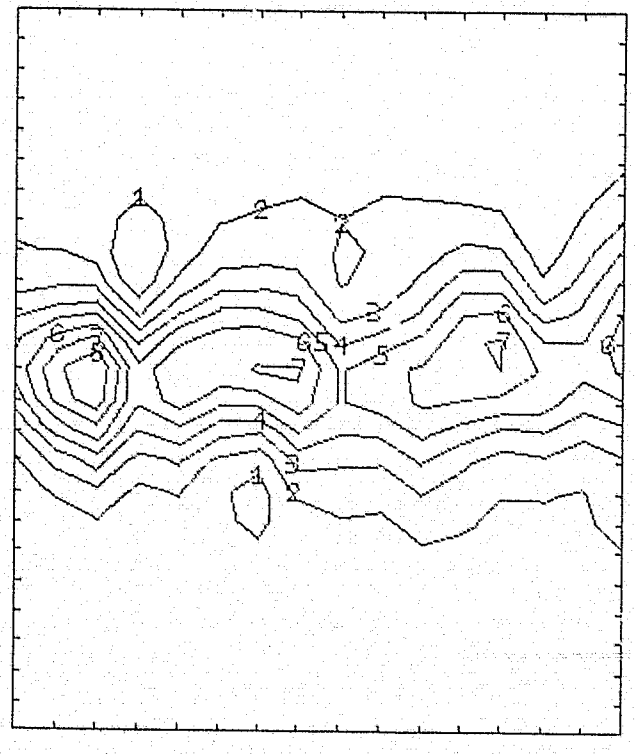

$\frac{y}{\theta_{in}} = 15.345$; $\overline{\omega}_{2,max} = 0.327$

Figs. 6.9b (continued)

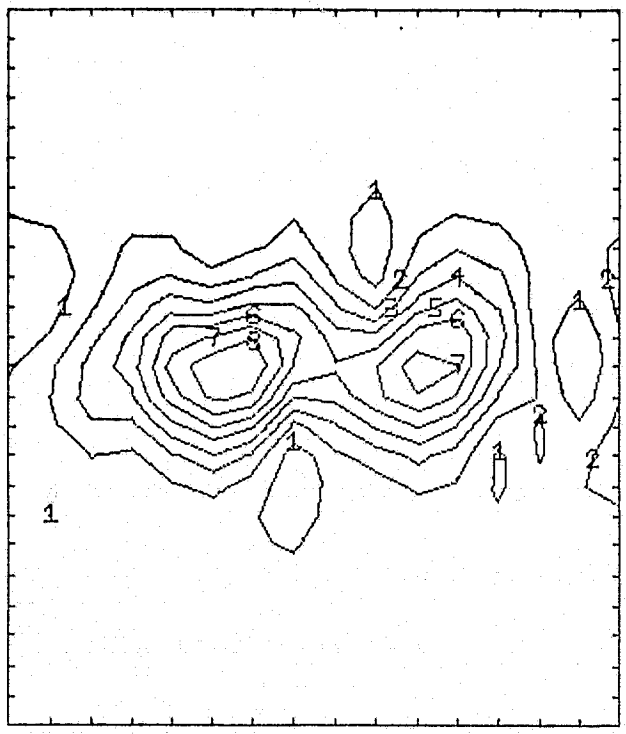

$\frac{y}{\theta_{in}} = 0$; $\bar{\omega}_{2,max} = 0.468$

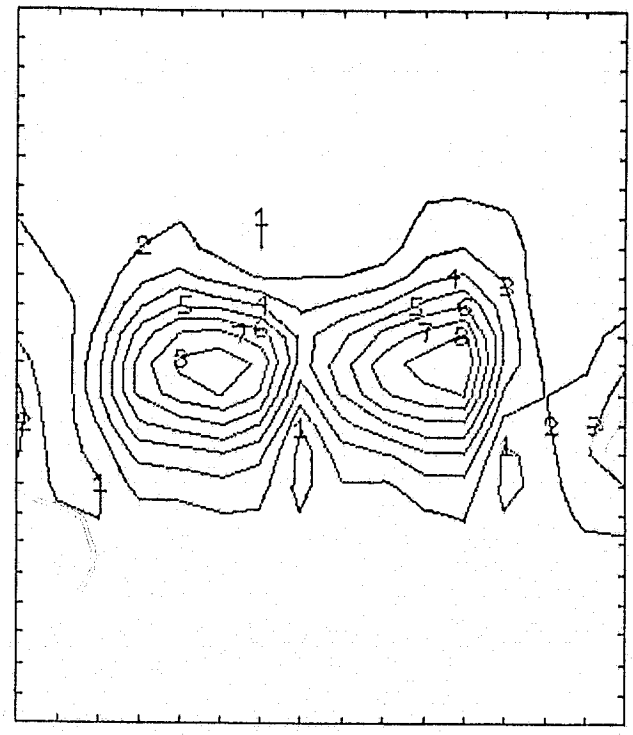

$\frac{y}{\theta_{in}} = 1.073$; $\bar{\omega}_{2,max} = 0.458$

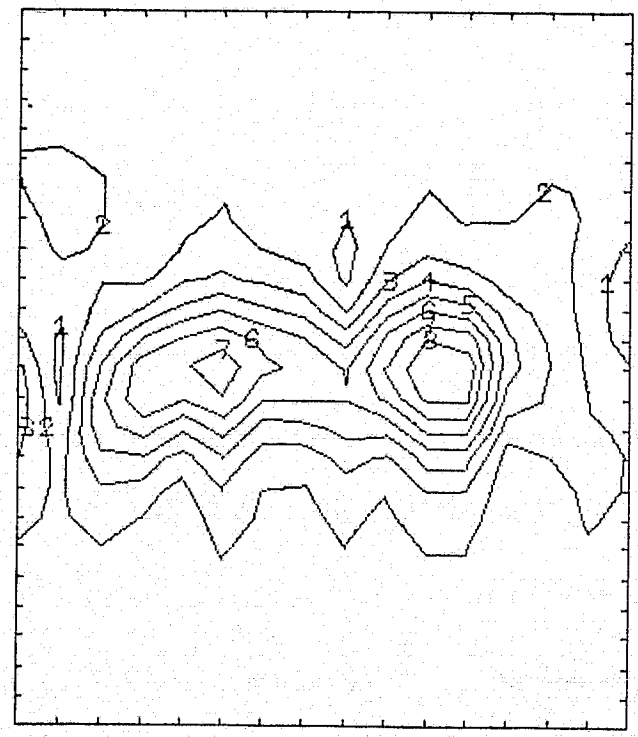

$\frac{y}{\theta_{in}} = 2.026$; $\bar{\omega}_{2,max} = 0.523$

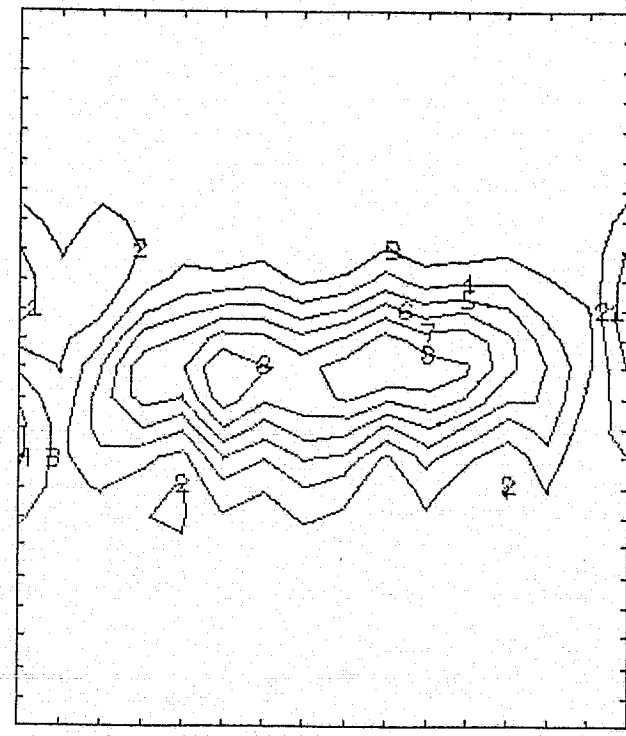

$\frac{y}{\theta_{in}} = 3.069$; $\bar{\omega}_{2,max} = 0.436$

Figs. 6.9c. Contour plots of the spanwise vorticity $(\bar{\omega}_2)$ for different x-z planes, at time T = 0. In each plane, constant vorticity lines are plotted at eight levels. Higher numbers on these lines indicate higher vorticity levels (case c).

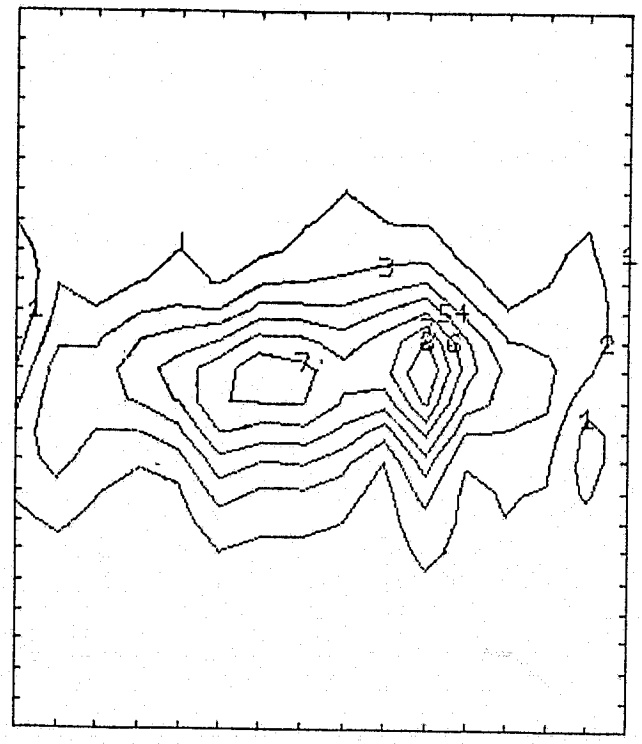

$\frac{y}{\theta_{in}} = 4.092$; $\overline{\omega}_{2,max} = 0.507$

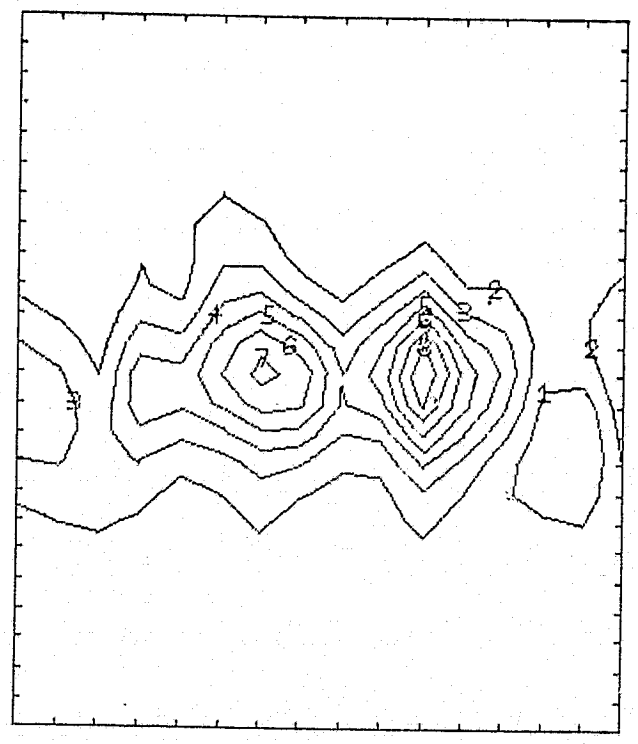

$\frac{y}{\theta_{in}} = 5.115$; $\overline{\omega}_{2,max} = 0.578$

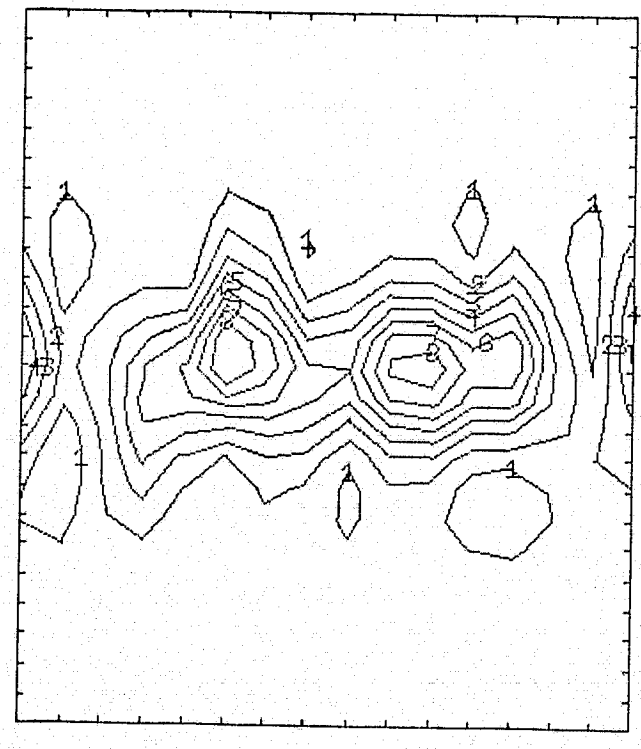

$\frac{y}{\theta_{in}} = 6.138$; $\overline{\omega}_{2,max} = 0.457$

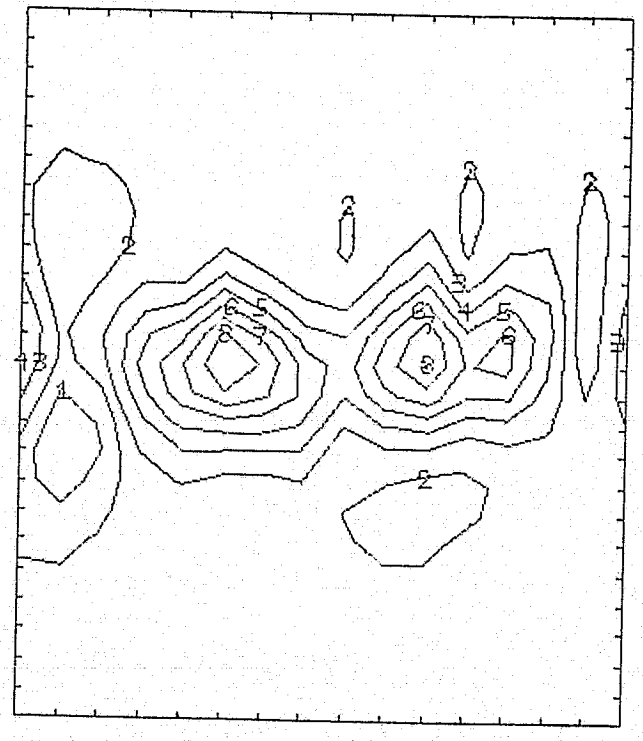

$\frac{y}{\theta_{in}} = 7.161$; $\overline{\omega}_{2,max} = 0.529$

Figs. 6.9c (continued)

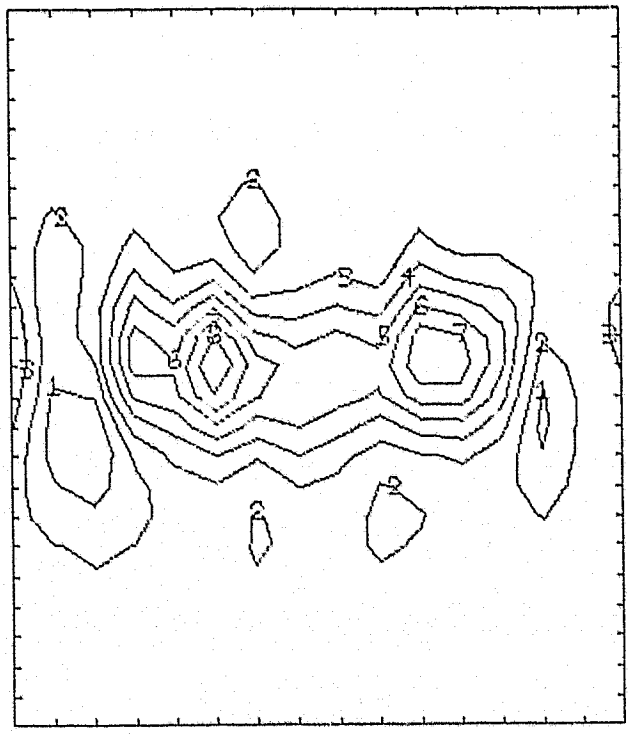

$\frac{y}{\theta_{in}} = 8.184$; $\overline{\omega}_{2,max} = 0.582$

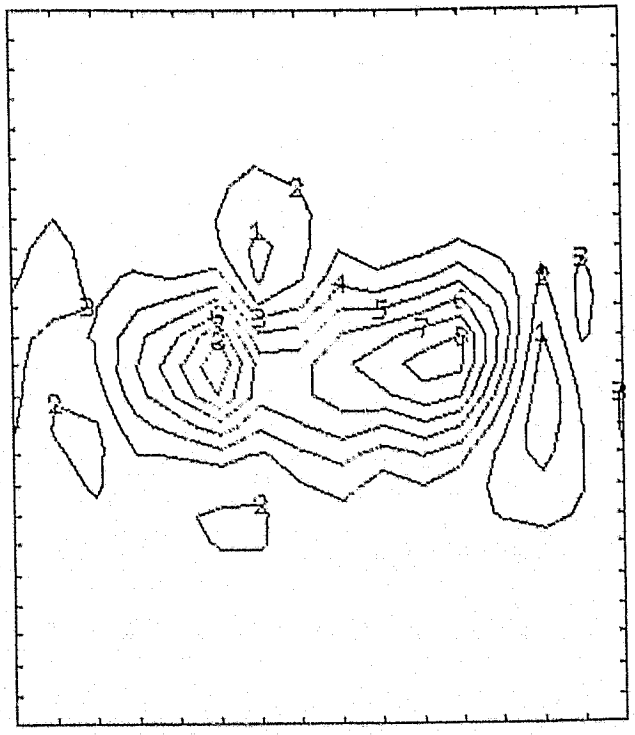

$\frac{y}{\theta_{in}} = 9.207$; $\overline{\omega}_{2,max} = 0.536$

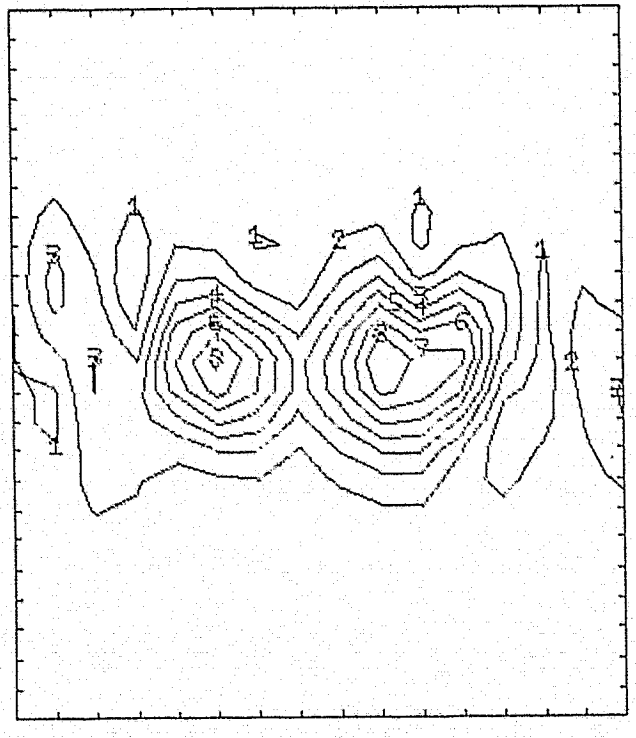

$\frac{y}{\theta_{in}} = 10.230$; $\overline{\omega}_{2,max} = 0.580$

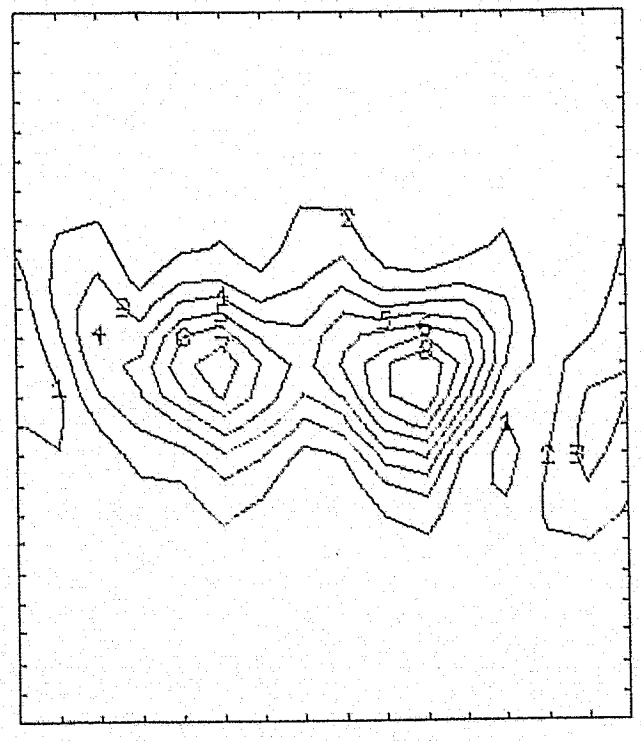

$\frac{y}{\theta_{in}} = 11.253$; $\overline{\omega}_{2,max} = 0.549$

Figs. 6.9c (continued)

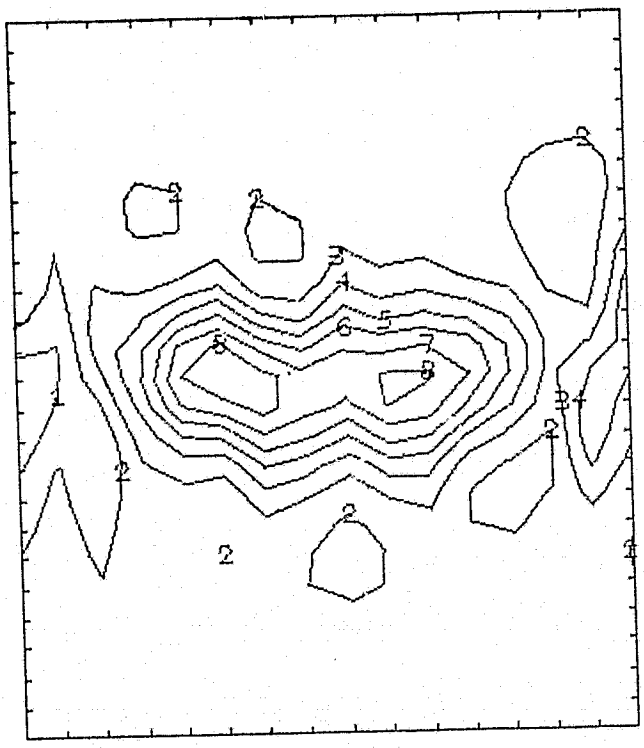

$\frac{y}{\theta_{in}} = 12.276$; $\overline{\omega}_{2,max} = 0.441$

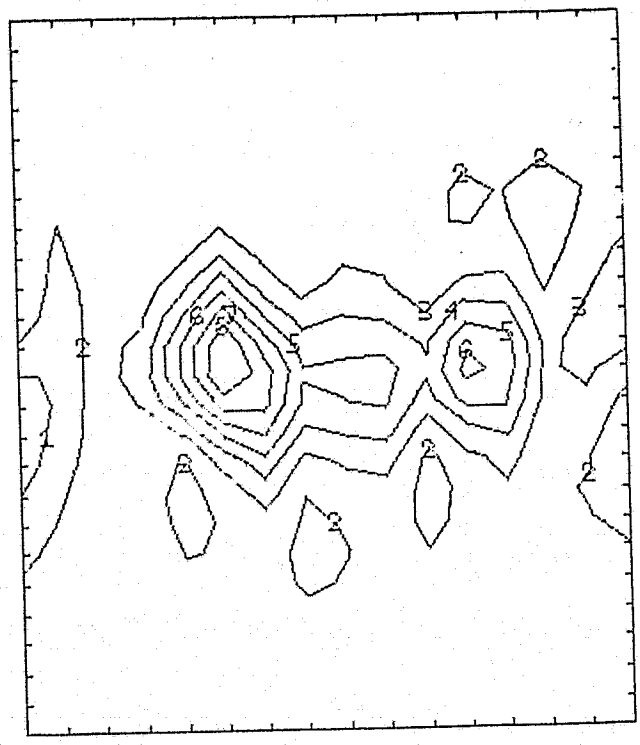

$\frac{y}{\theta_{in}} = 13.299$; $\overline{\omega}_{2,max} = 0.632$

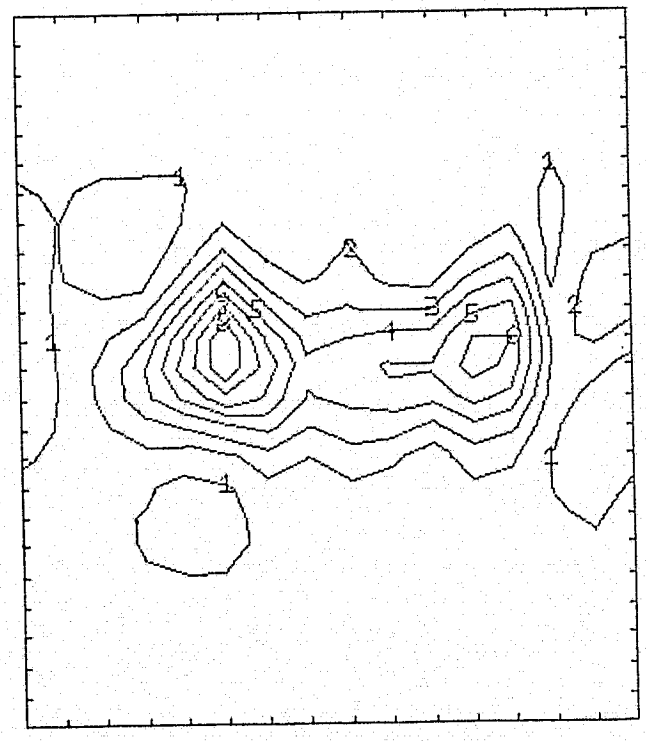

$\frac{y}{\theta_{in}} = 14.322$; $\overline{\omega}_{2,max} = 0.593$

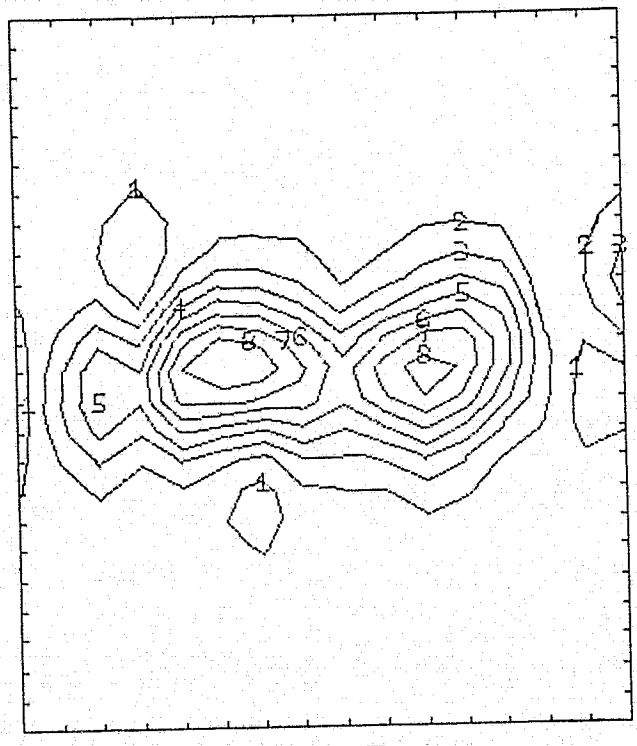

$\frac{y}{\theta_{in}} = 15.345$; $\overline{\omega}_{2,max} = 0.422$

Figs. 6.9c (continued)

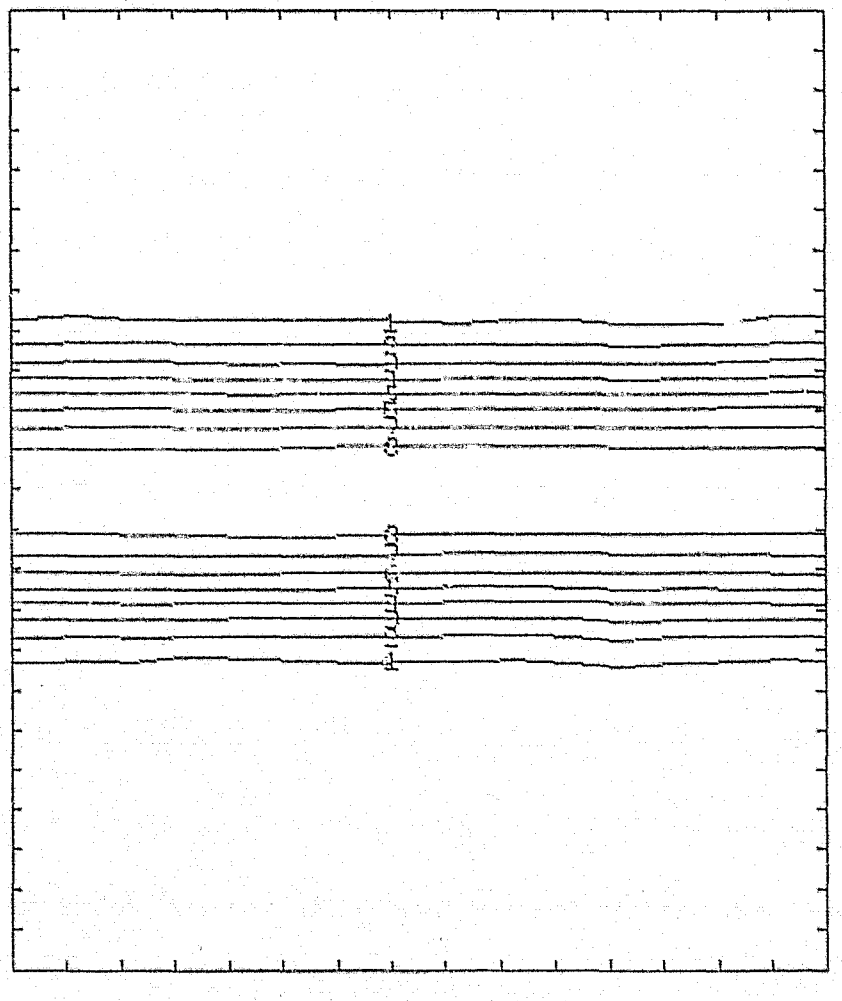

Fig. 6.10a. Contour plots of the spanwise vorticity $(\bar{\omega}_2)$ in an x-z plane, at time T = 16.78. Constant vorticity lines are plotted at eight levels. Higher numbers on these lines indicate higher vorticity levels ($\bar{\omega}_{2,max} = 0.185$, case a).

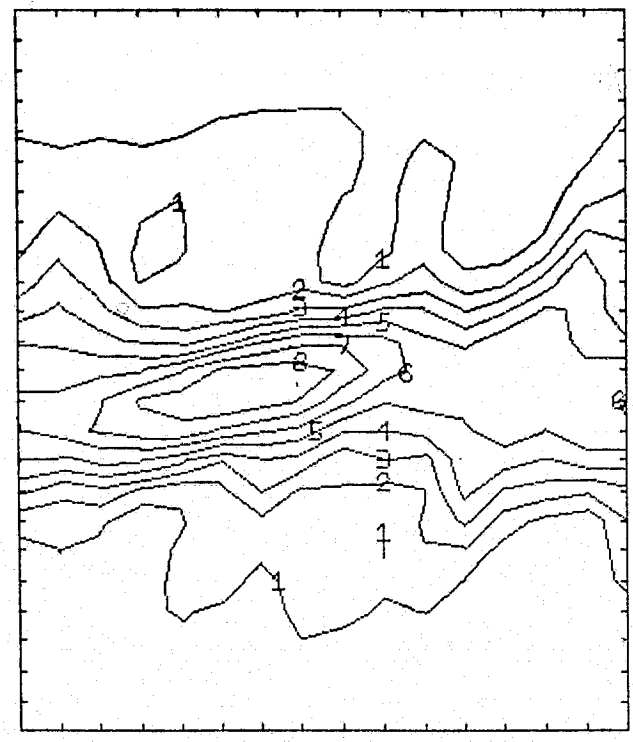

$\frac{y}{\theta_{in}} = 0$; $\bar{\omega}_{2,max} = 0.255$

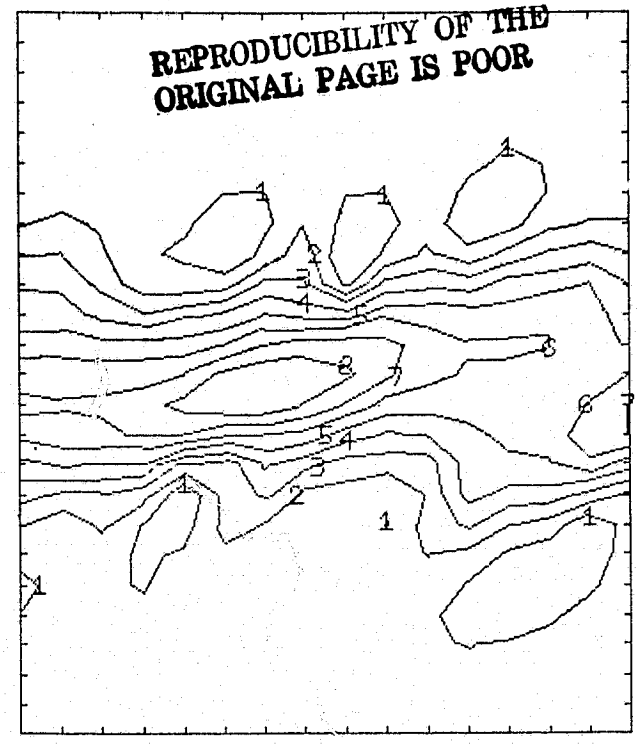

$\frac{y}{\theta_{in}} = 1.023$; $\bar{\omega}_{2,max} = 0.231$

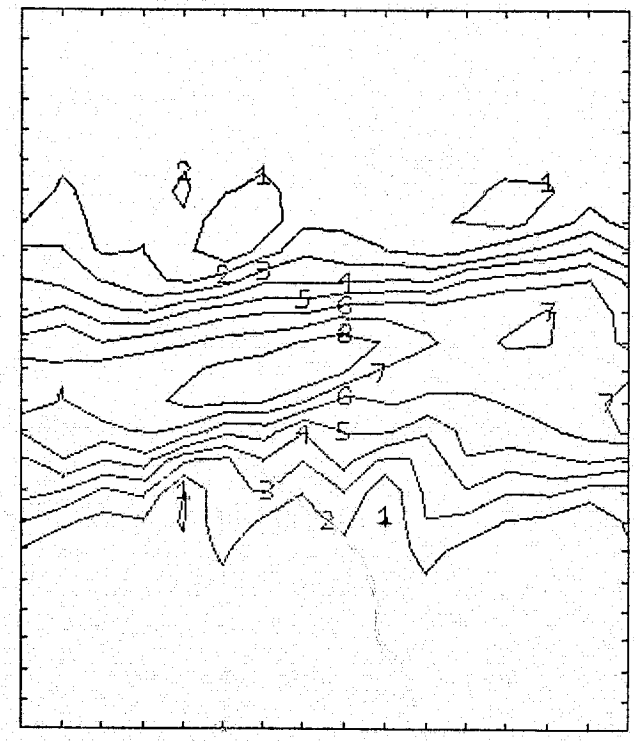

$\frac{y}{\theta_{in}} = 2.026$; $\bar{\omega}_{2,max} = 0.224$

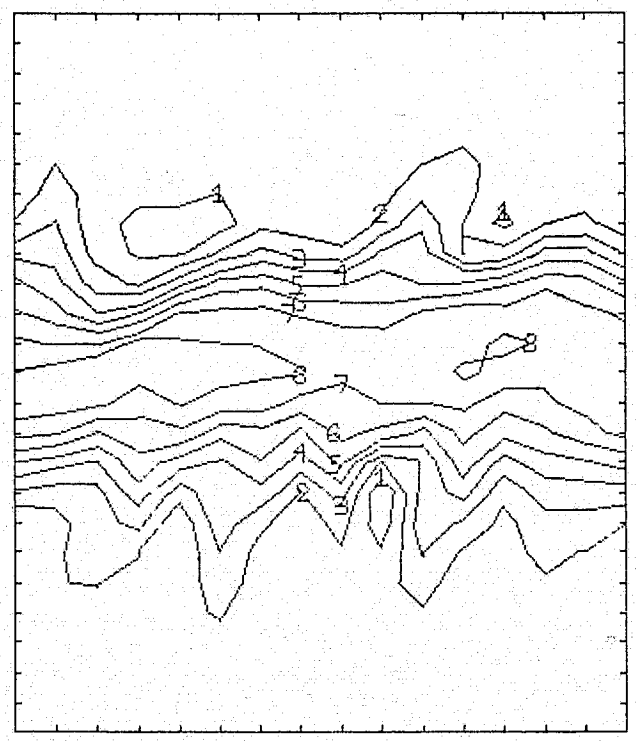

$\frac{y}{\theta_{in}} = 3.069$; $\bar{\omega}_{2,max} = 0.203$

Fig. 6.10b. Contour plots of the spanwise vorticity $(\bar{\omega}_2)$ for different x-z planes, at time T = 16.78. In each plane, constant vorticity lines are plotted at eight levels. Higher numbers on these lines indicate higher levels (case b).

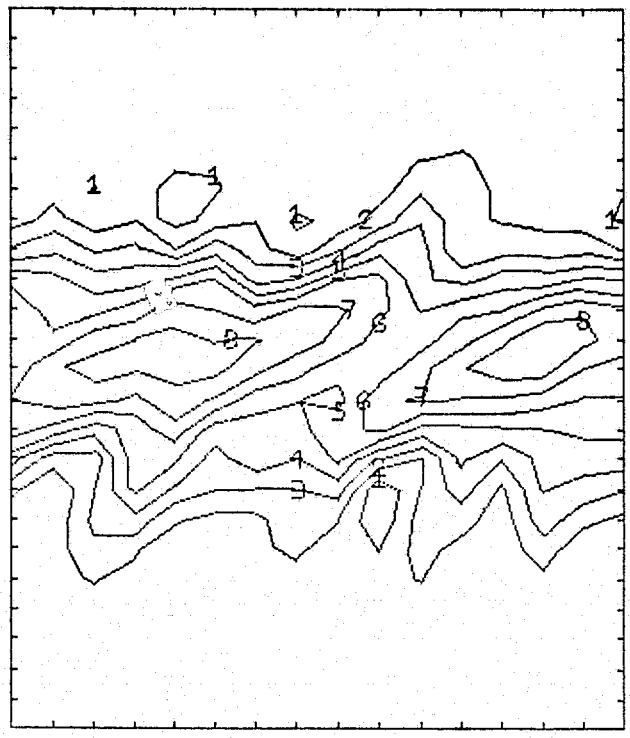

$\frac{y}{\theta_{in}} = 4.092$; $\overline{\omega}_{2,max} = 0.209$

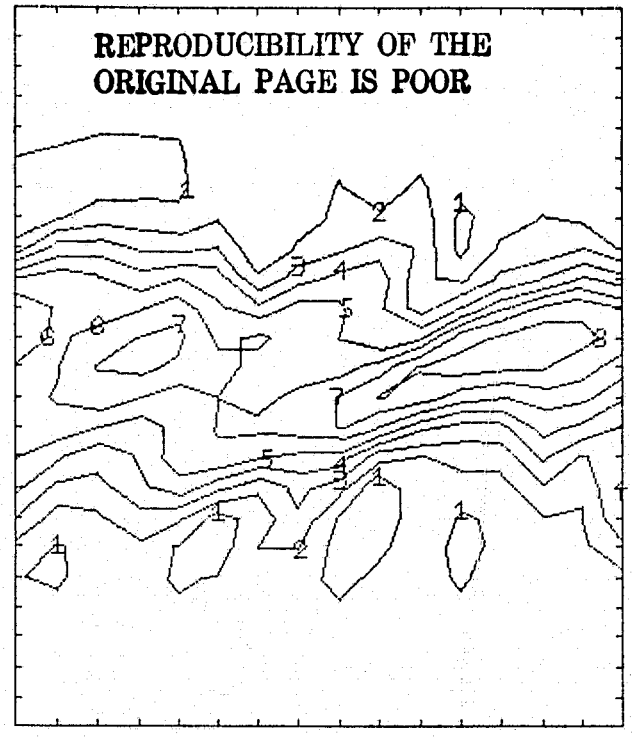

$\frac{y}{\theta_{in}} = 5.115$; $\overline{\omega}_{2,max} = 0.227$

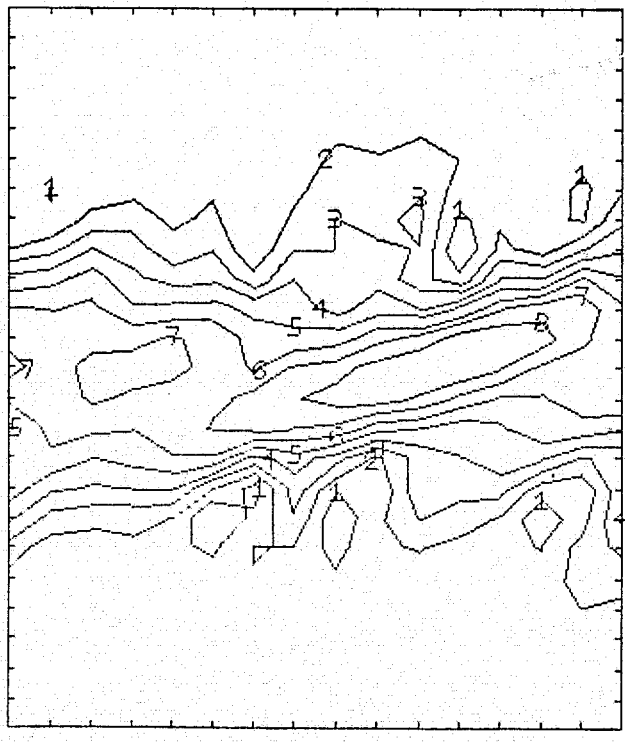

$\frac{y}{\theta_{in}} = 6.138$; $\overline{\omega}_{2,max} = 0.228$

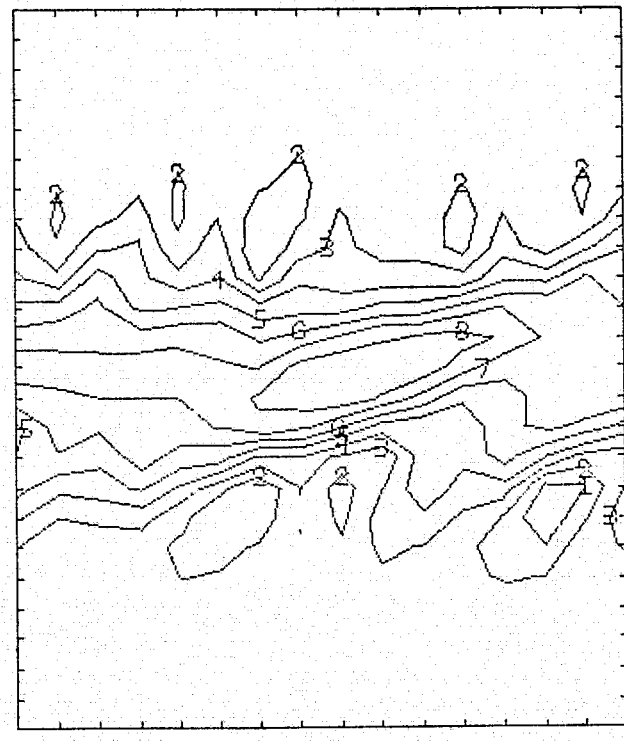

$\frac{y}{\theta_{in}} = 7.161$; $\overline{\omega}_{2,max} = 0.244$

Figs. 6.10b (continued)

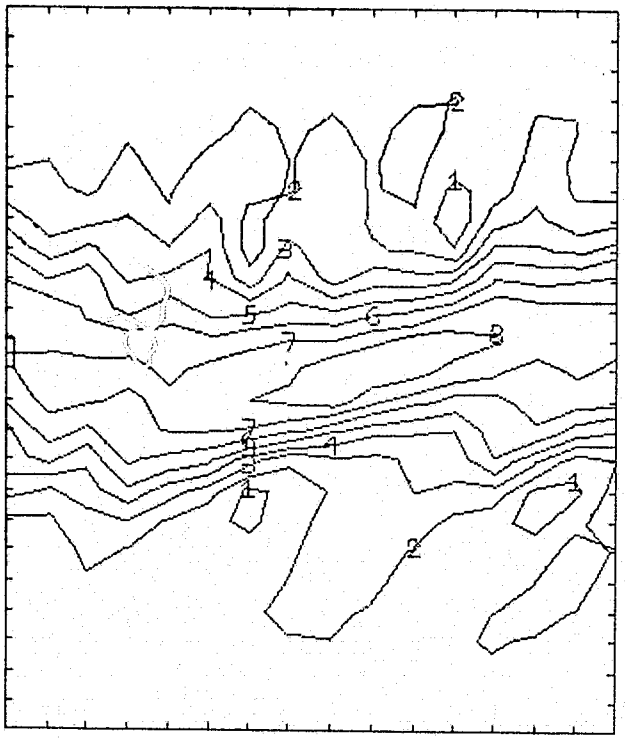

$\frac{y}{\theta_{in}} = 8.184$; $\overline{\omega}_{2,max} = 0.231$

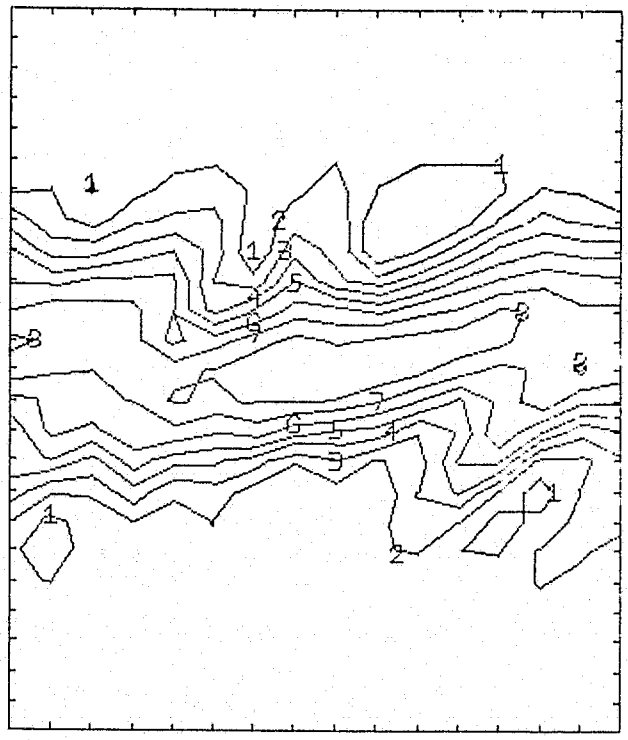

$\frac{y}{\theta_{in}} = 9.207$; $\overline{\omega}_{2,max} = 0.207$

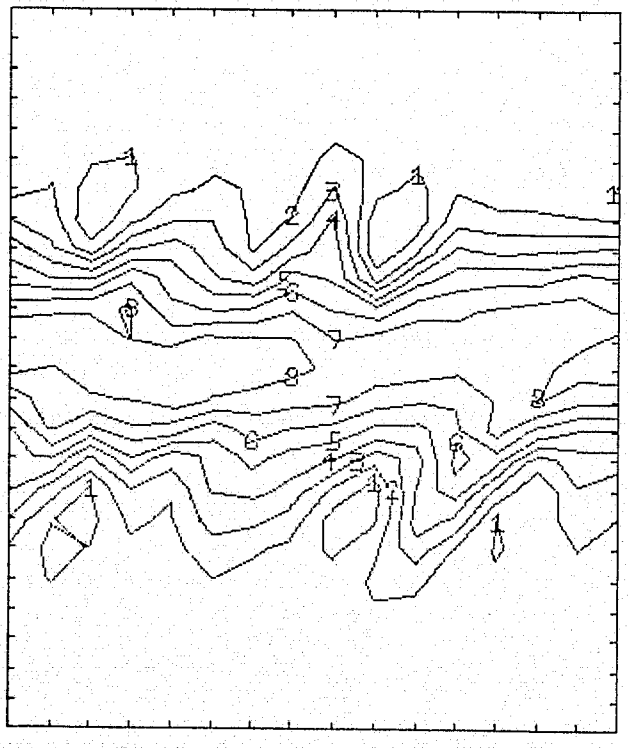

$\frac{y}{\theta_{in}} = 10.230$; $\overline{\omega}_{2,max} = 0.191$

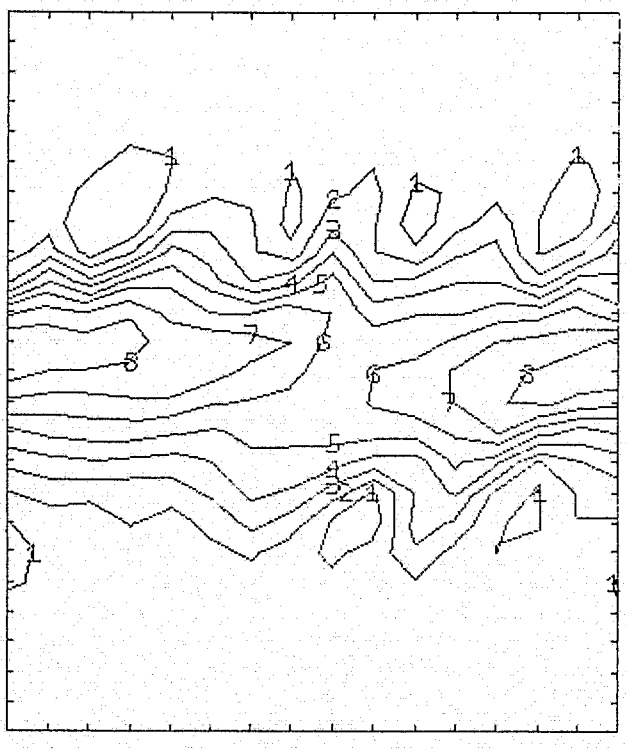

$\frac{y}{\theta_{in}} = 11.253$; $\overline{\omega}_{2,max} = 0.221$

Figs. 6.10b (continued)

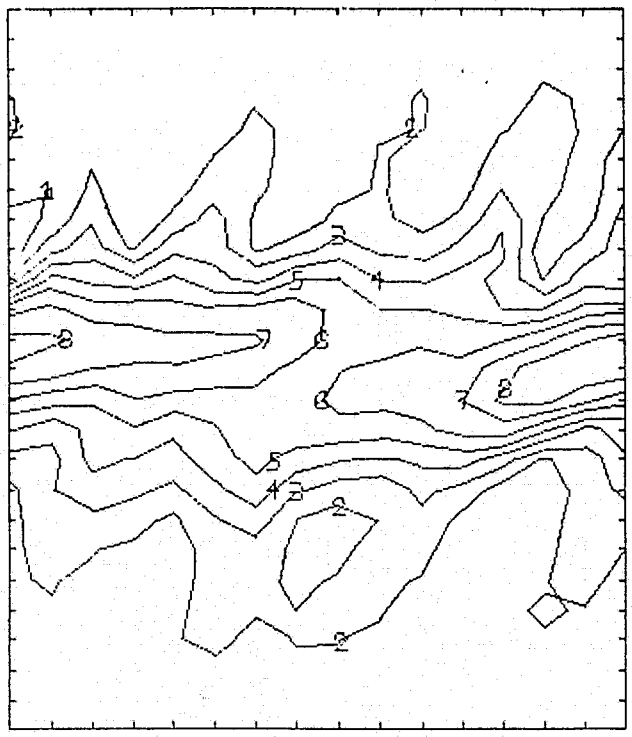

$\frac{y}{\theta_{in}} = 12.276$; $\overline{\omega}_{2,max} = 0.258$

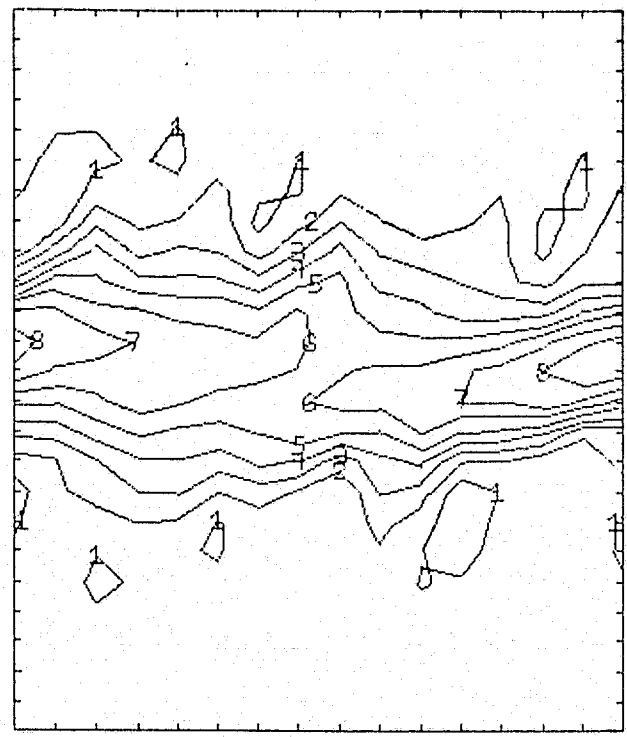

$\frac{y}{\theta_{in}} = 13.299$; $\overline{\omega}_{2,max} = 0.253$

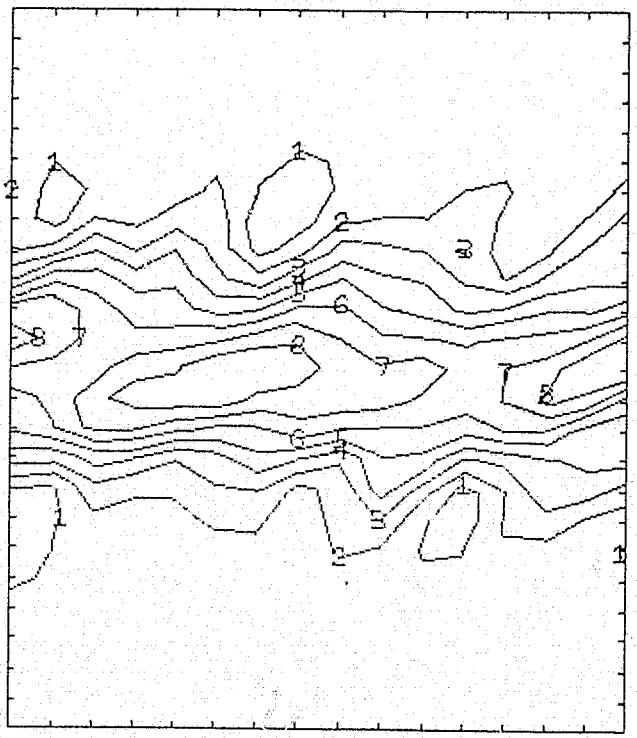

$\frac{y}{\theta_{in}} = 12.322$; $\overline{\omega}_{2,max} = 0.216$

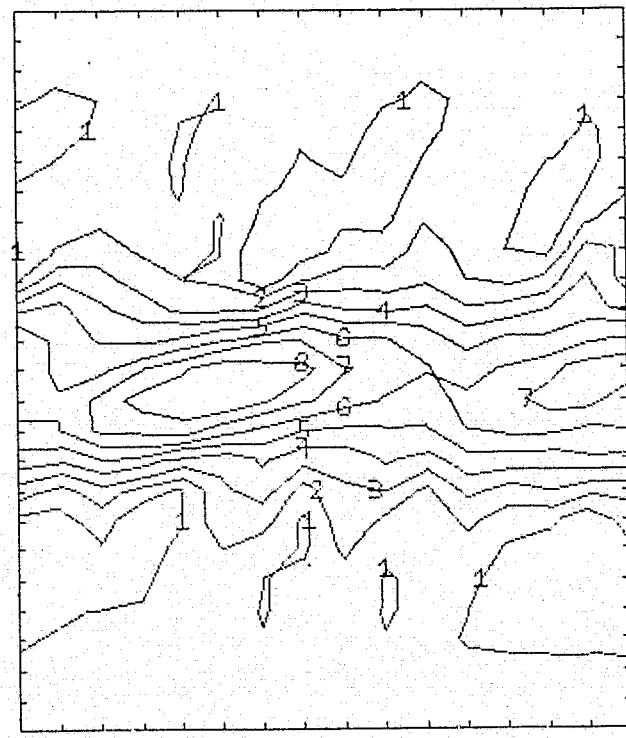

$\frac{y}{\theta_{in}} = 15.345$; $\overline{\omega}_{2,max} = 0.244$

Figs. 6.10b (continued)

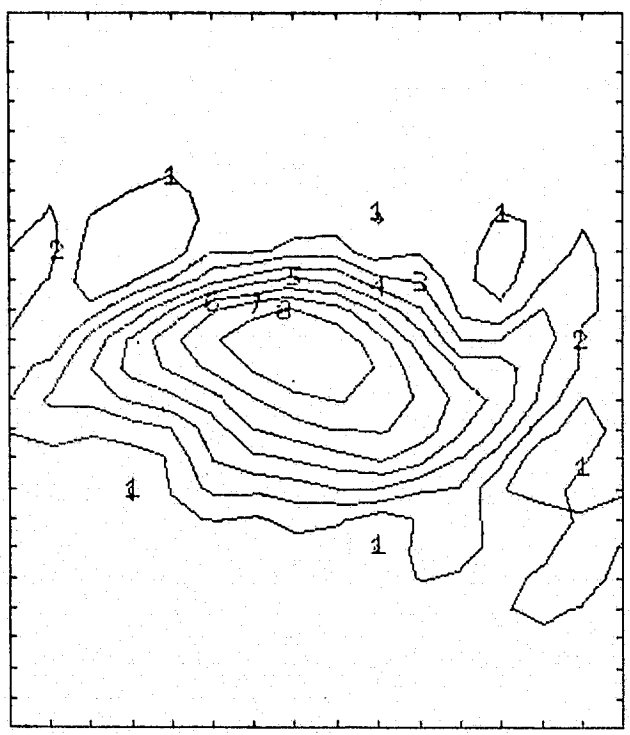

$\frac{y}{\theta_{in}} = 0$; $\bar{\omega}_{2,max} = 0.337$

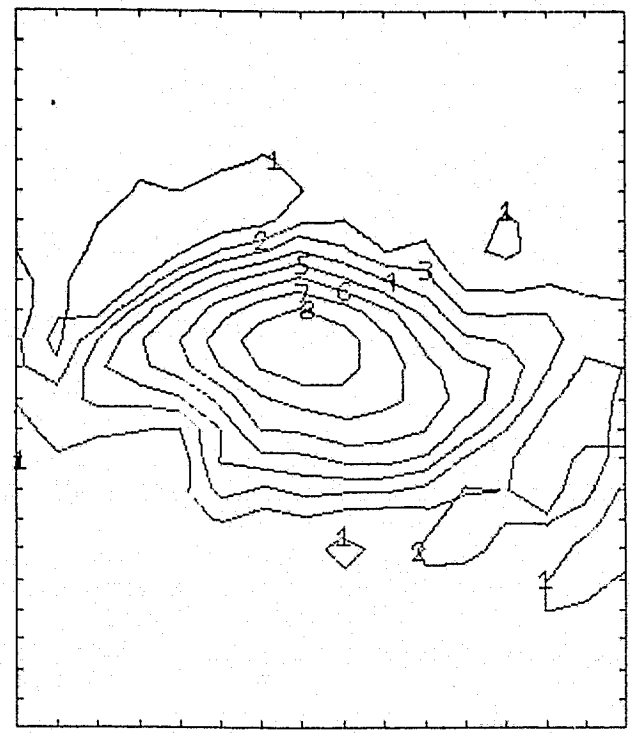

$\frac{y}{\theta_{in}} = 1.023$; $\bar{\omega}_{2,max} = 0.347$

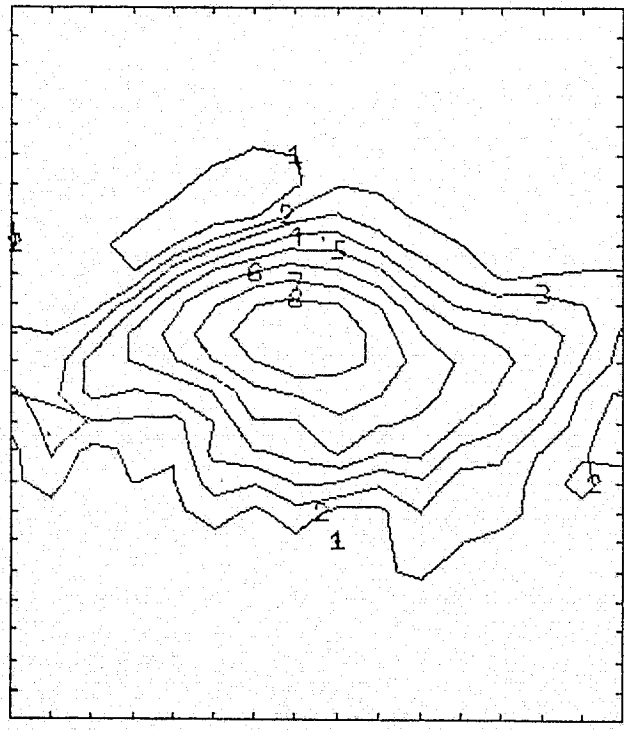

$\frac{y}{\theta_{in}} = 2.026$; $\bar{\omega}_{2,max} = 0.335$

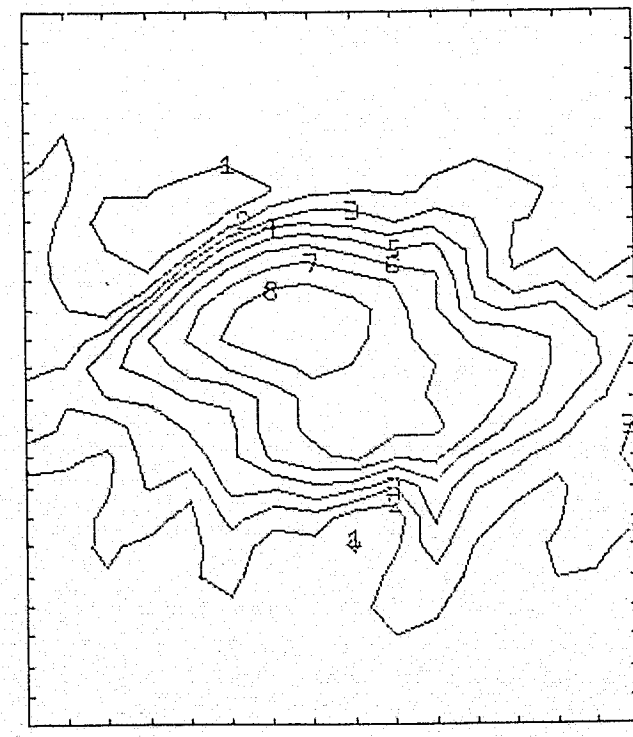

$\frac{y}{\theta_{in}} = 3.069$; $\bar{\omega}_{2,max} = 0.286$

Figs. 6.10c. Contour plots of the spanwise vorticity $(\bar{\omega}_2)$ for different x-z planes, at time T = 16.78. In each plane, constant vorticity lines are plotted at eight levels. Higher numbers on these lines indicate higher levels (case c).

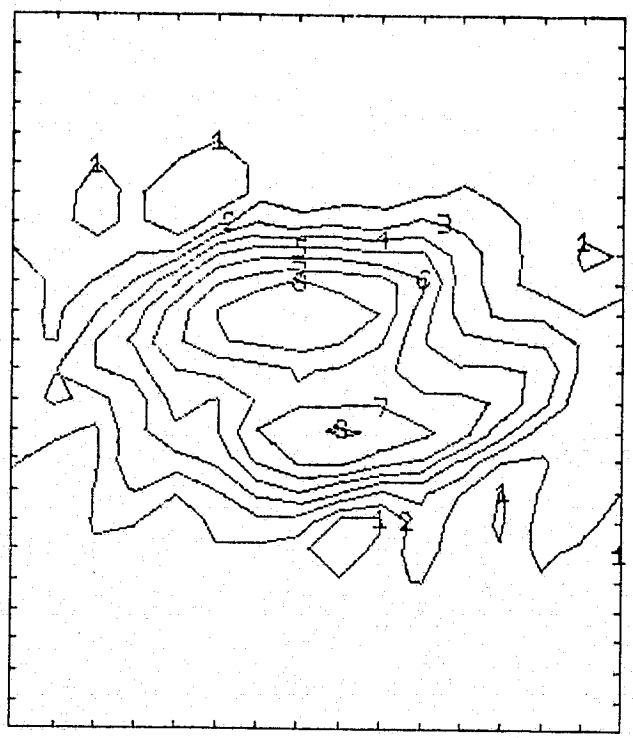

$\frac{y}{\theta_{in}} = 4.092$; $\overline{\omega}_{2,max} = 0.280$

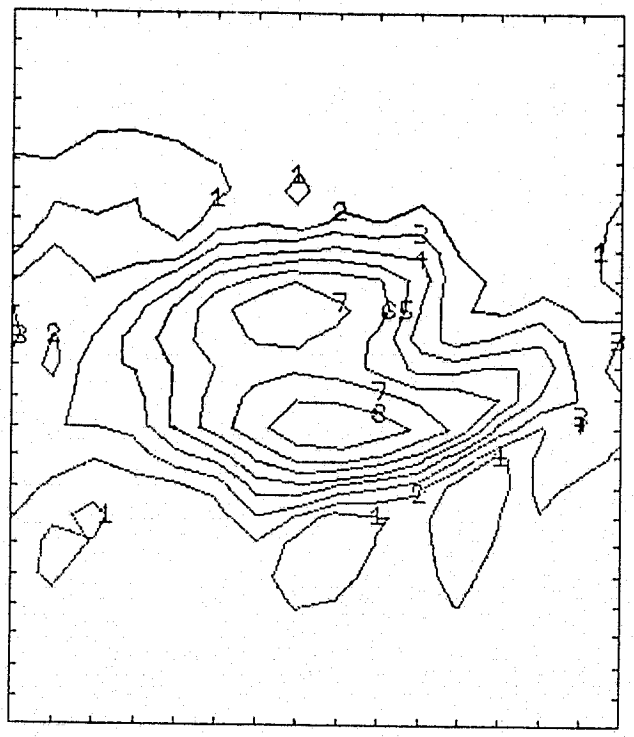

$\frac{y}{\theta_{in}} = 5.115$; $\overline{\omega}_{2,max} = 0.305$

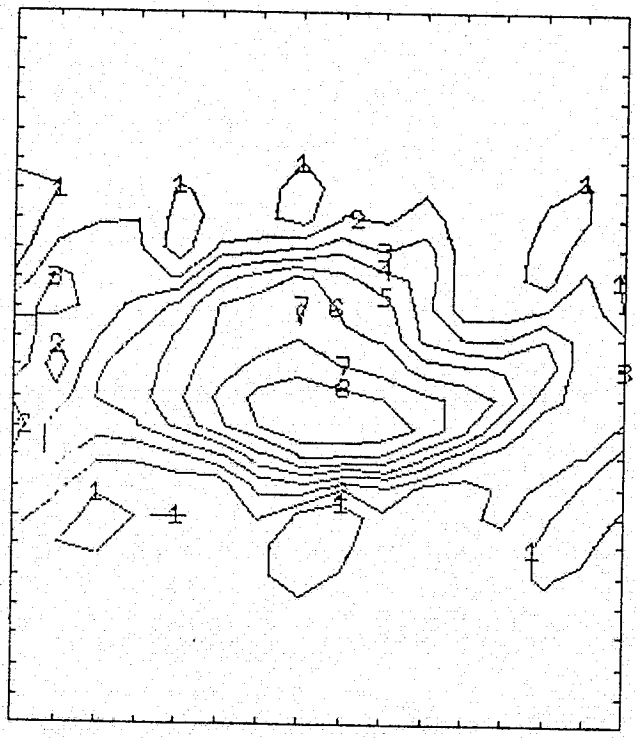

$\frac{y}{\theta_{in}} = 6.138$; $\overline{\omega}_{2,max} = 0.335$

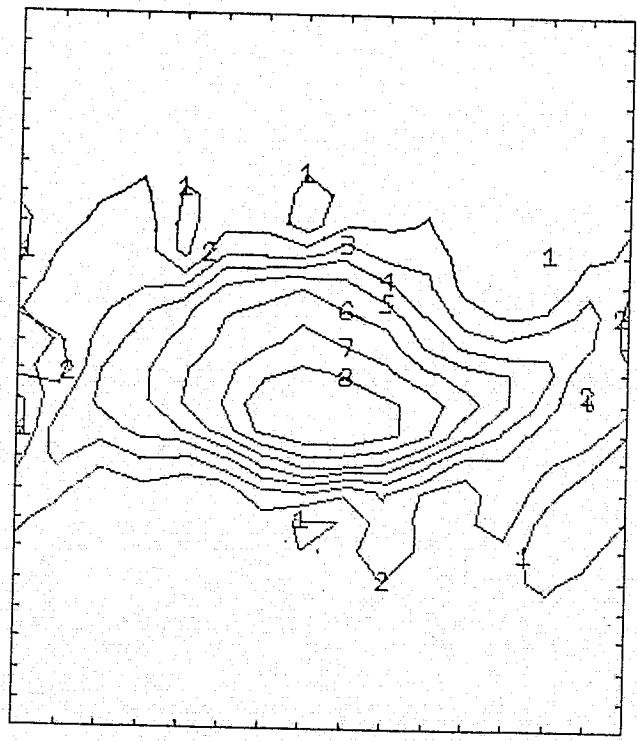

$\frac{y}{\theta_{in}} = 7.161$; $\overline{\omega}_{2,max} = 0.344$

Figs. 6.10c (continued)

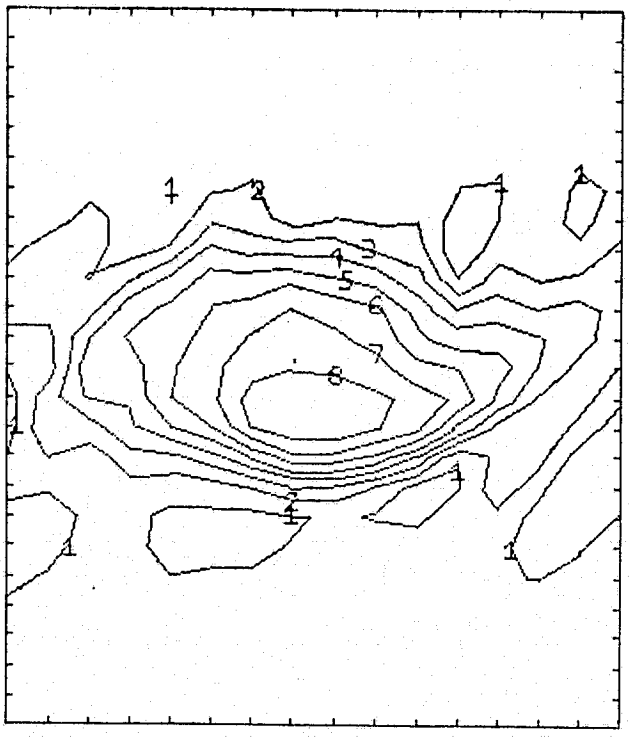

$\frac{y}{\theta_{in}} = 8.184$; $\overline{\omega}_{2,max} = 0.322$

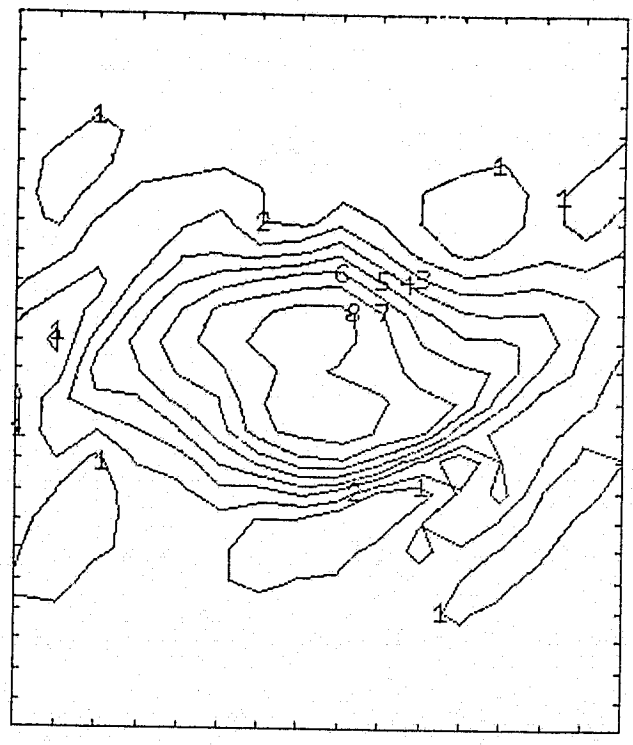

$\frac{y}{\theta_{in}} = 9.207$; $\overline{\omega}_{2,max} = 0.291$

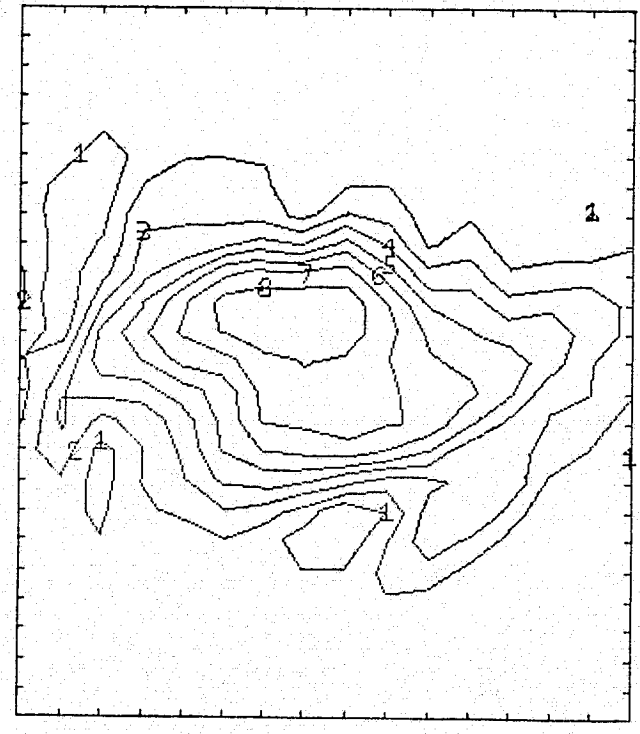

$\frac{y}{\theta_{in}} = 10.230$; $\overline{\omega}_{2,max} = 0.286$

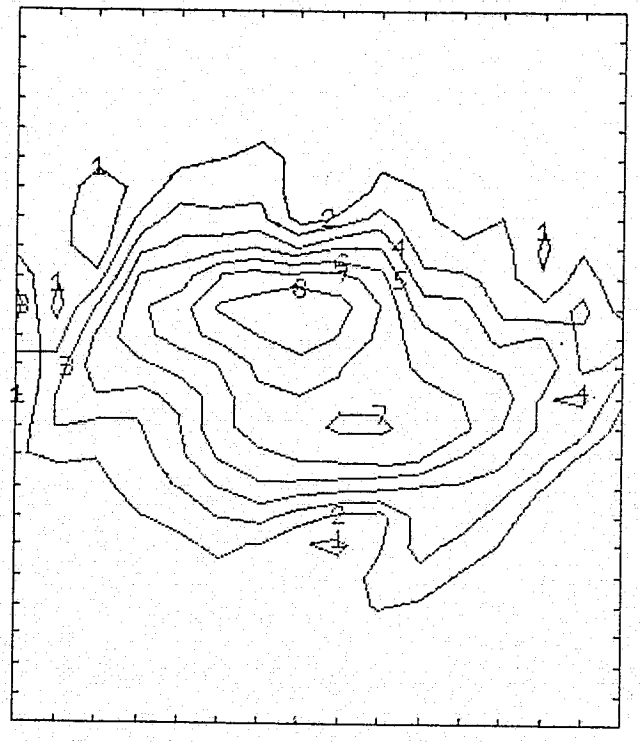

$\frac{y}{\theta_{in}} = 11.253$; $\overline{\omega}_{2,max} = 0.292$

Figs. 6.10c (continued)

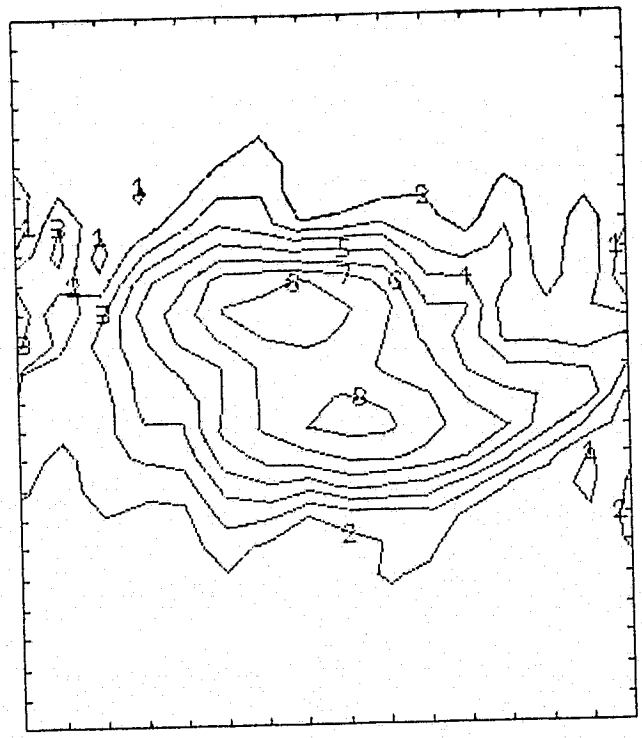

$\frac{y}{\theta_{in}} = 12.276$; $\bar{\omega}_{2,max} = 0.279$

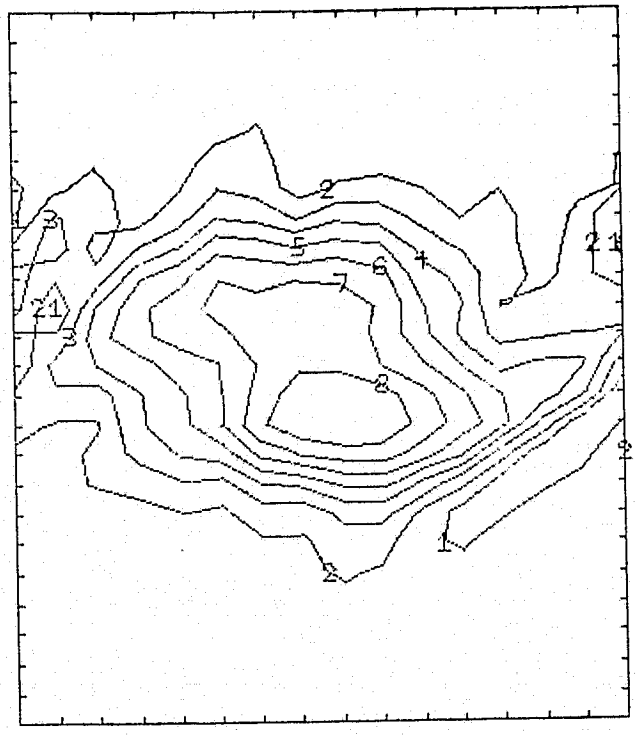

$\frac{y}{\theta_{in}} = 13.299$; $\bar{\omega}_{2,max} = 0.286$

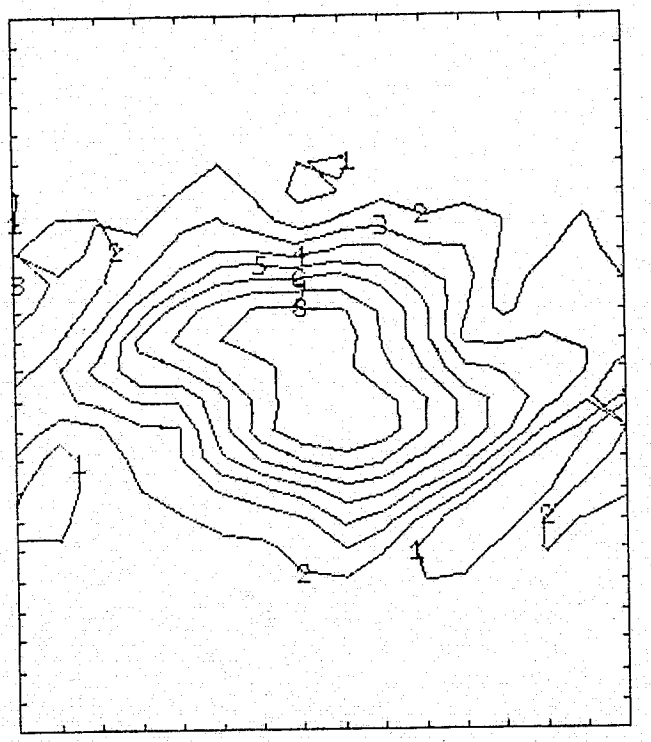

$\frac{y}{\theta_{in}} = 14.322$; $\bar{\omega}_{2,max} = 0.293$

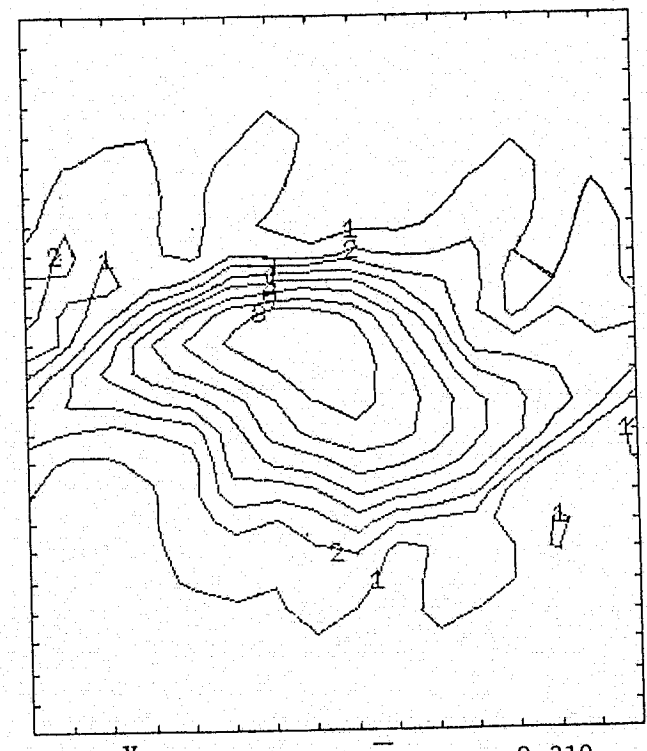

$\frac{y}{\theta_{in}} = 15.345$; $\bar{\omega}_{2,max} = 0.319$

Figs. 6.10c (continued)

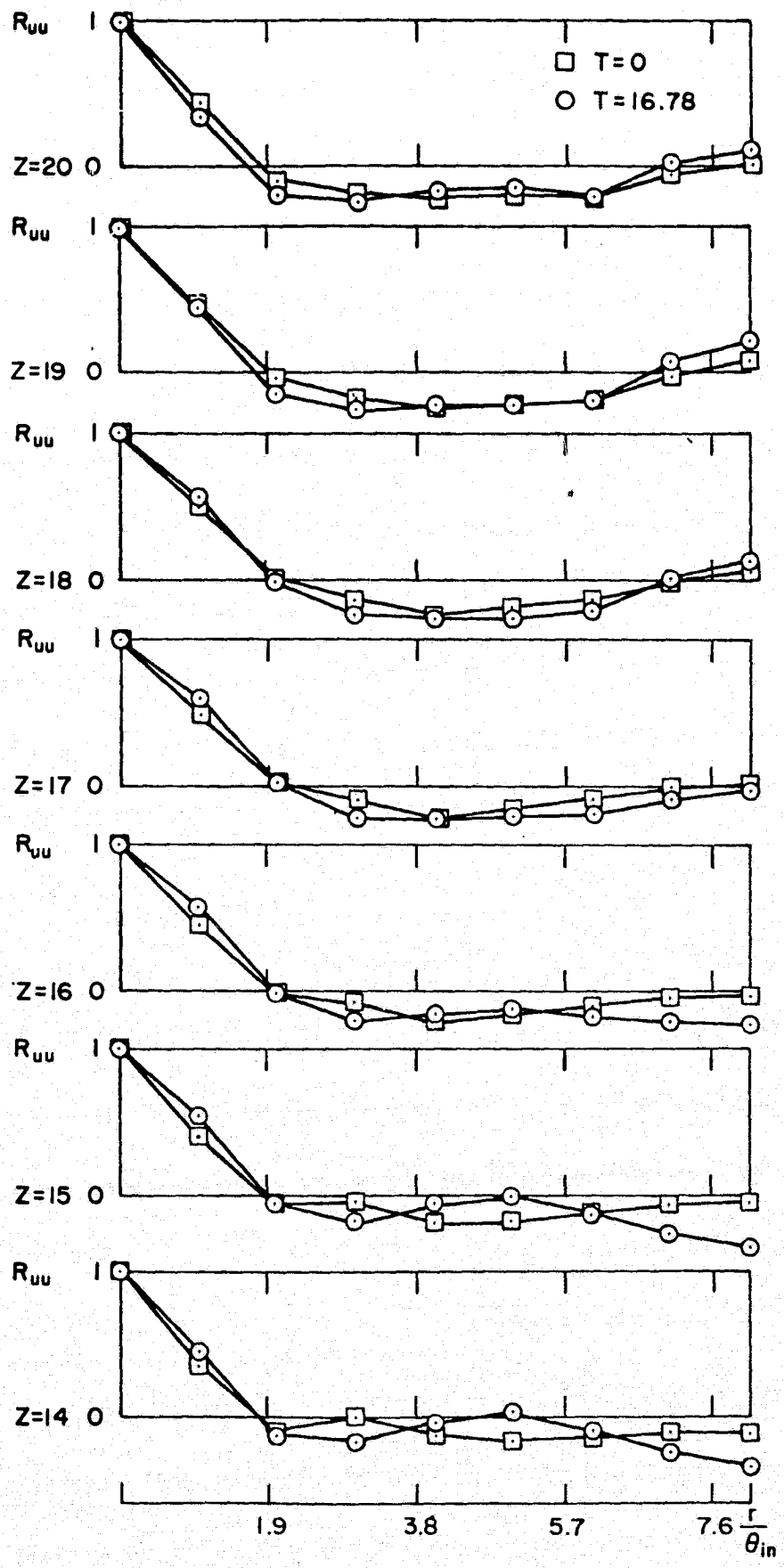

Fig. 6.11a. Two point correlations (z = 17 is the center plane of the mixing layer, $\Delta z/\theta_{in}$ = 1.023; case a).

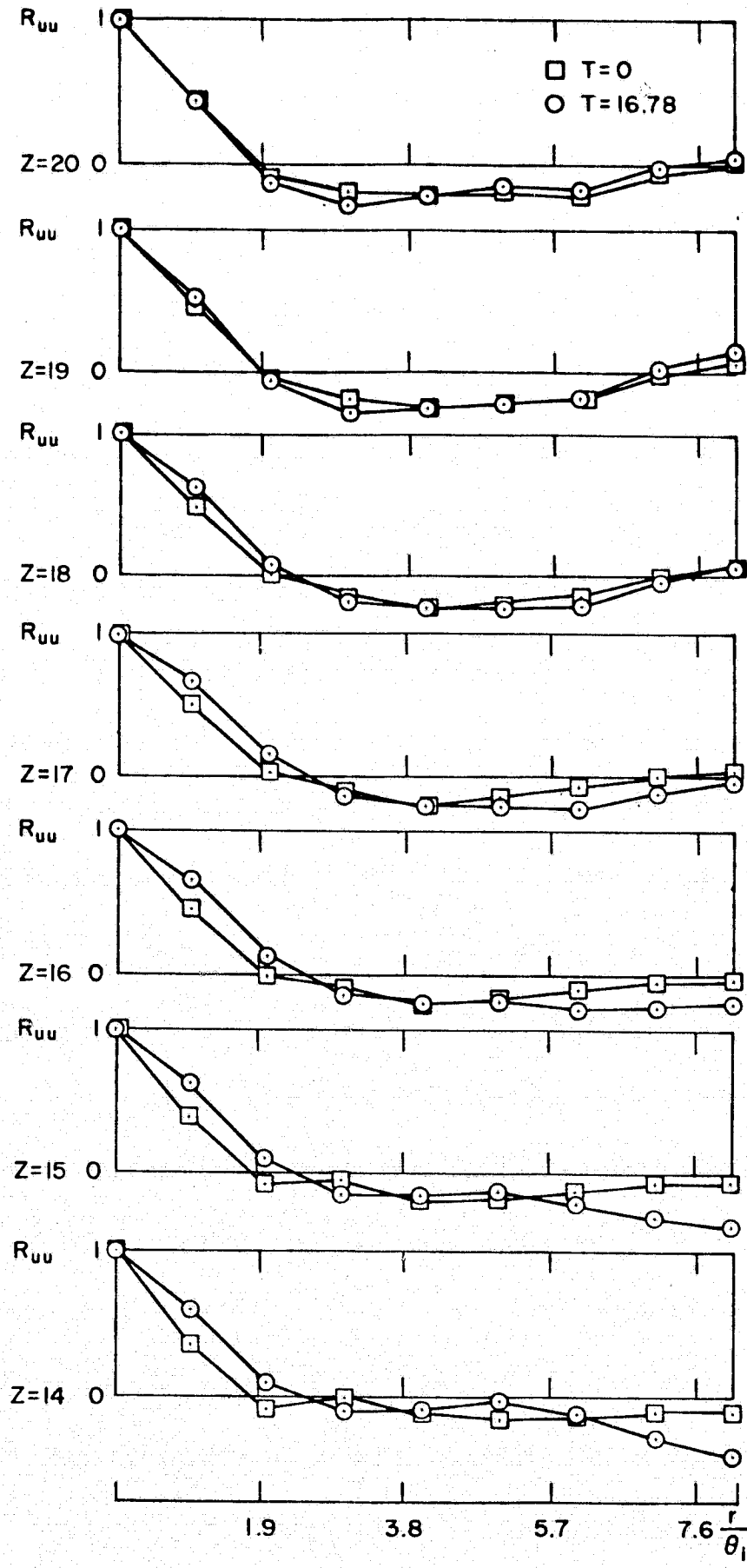

Fig. 6.11b. Two point correlations (z = 17 is the center plane of the mixing layer, $\Delta z/\theta_{in} = 1.023$; case b).

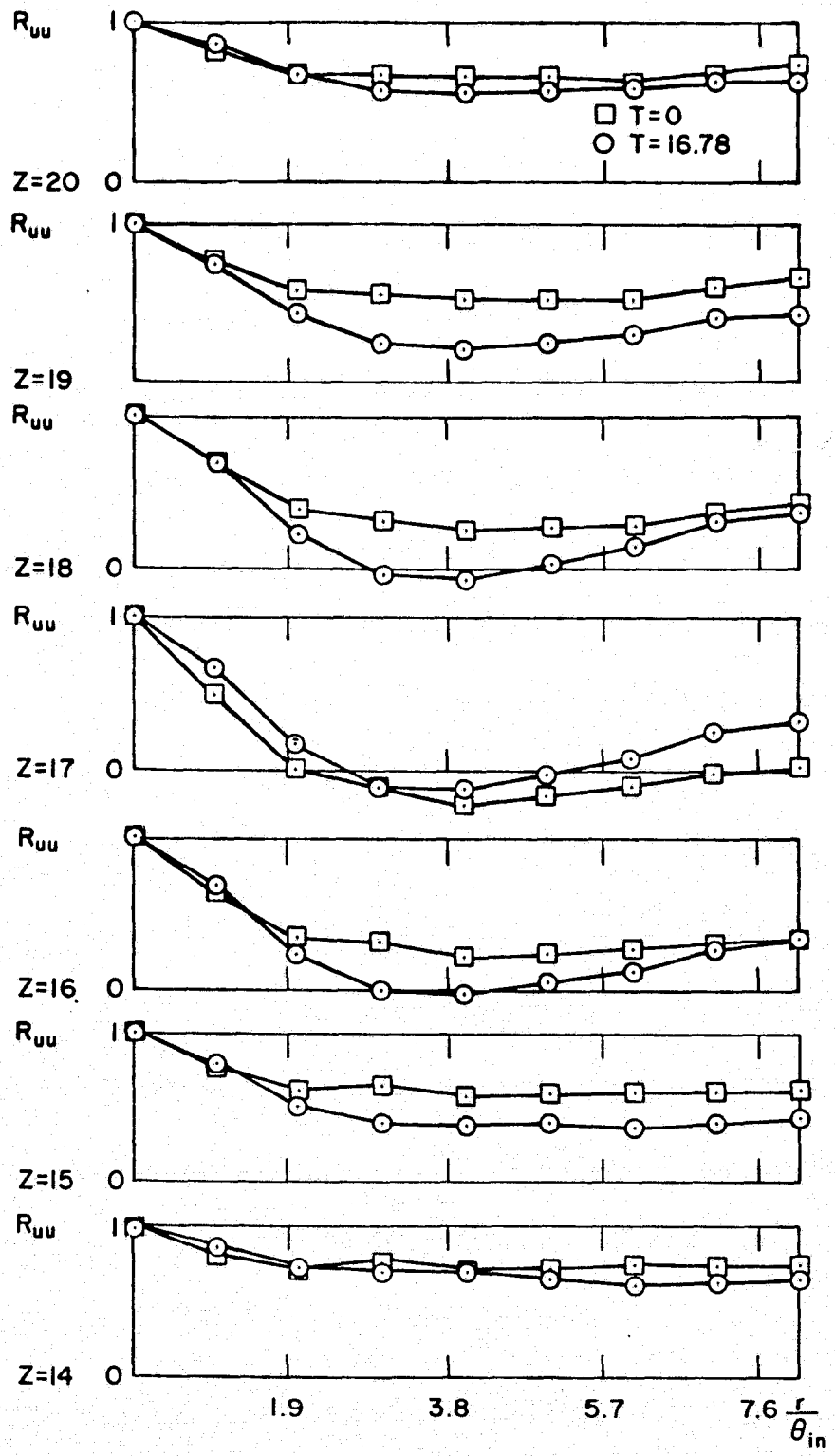

Fig. 6.11c. Two-point correlations ($z = 17$ is the center plane of the mixing layer, $\Delta z/\theta_{in} = 1.023$; case c).

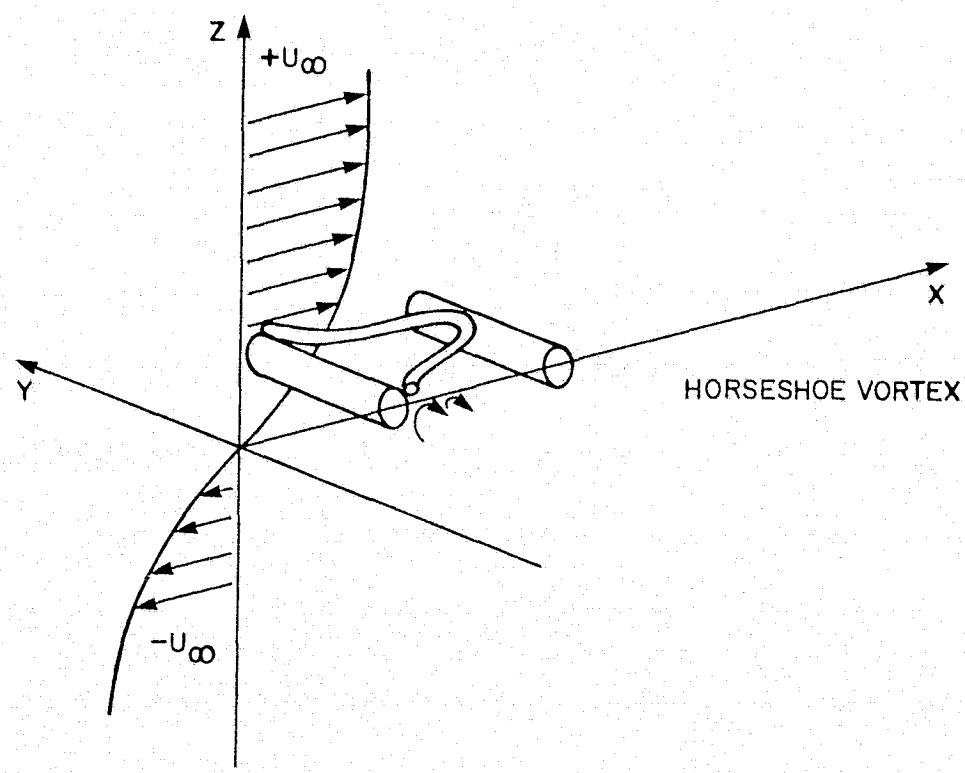

Fig. 7.1. Formation of streamwise cellular structures in a mixing layer.

Appendix A

SUBGRID SCALE MODELS FOR THE VORTICITY EQUATIONS

In Chapter 2 we propose to use the following models for W_{ij} (Eqn. (2.9)):

Model ω-1

$$W_{ij} = - \varepsilon_{ijk} \frac{\partial}{\partial x_\ell} (2\nu_T \bar{S}_{k\ell}) \tag{2.15}$$

Model ω-2

$$W_{ij} = - \frac{\partial}{\partial x_j} (\nu_T \bar{\omega}_i) + \frac{\partial}{\partial x_i} (\nu_T \bar{\omega}_j) \tag{2.16}$$

where

$$\nu_T = (C_v \Delta)^2 (\bar{\omega}_i \bar{\omega}_i)^{\frac{1}{2}} \tag{2.14}$$

$$\bar{S}_{ij} = \frac{1}{2} \left(\frac{\partial}{\partial x_j} \bar{u}_i + \frac{\partial}{\partial x_i} \bar{u}_j \right) \tag{2.12}$$

The models should satisfy the following necessary conditions:

1. they should be antisymmetric,
2. they should vanish in an irrotational region, and
3. they should be an energy sink.

Condition 1 is readily seen to be satisfied by these models. We note that in an irrotational region, $\bar{\omega}_i = 0$. Hence, $\nu_T = (C_v \Delta)^2 (\bar{\omega}_i \bar{\omega}_i)^{\frac{1}{2}} = 0$, and the model vanishes in an irrotational region; i.e., condition 2 is also satisfied.

In order to show the dissipative nature of the subgrid scale models ω-1 and ω-2, consider the following equation:

$$\frac{\partial \bar{\omega}_i}{\partial t} = - \frac{\partial}{\partial x_j} W_{ij} \tag{A.1}$$

where the nonlinear terms in Eqn. (2.28) have been dropped. Multiplying Eqn. (A.1) by ψ_i, and integrating over the flow volume, we get:

$$\int \psi_i \frac{\partial}{\partial t} \overline{\omega}_i \, dv = - \int \psi_i \frac{\partial}{\partial x_j} W_{ij} \, dv \qquad (A.2)$$

We want to show that Eqn. (A.2) reduces to

$$\frac{\partial}{\partial t} \int \frac{1}{2} \overline{u}_i \overline{u}_i \, dv = - \varepsilon \qquad (A.3)$$

where $\varepsilon \geq 0$.

Model ω-1

Substituting Eqn. (2.15) in Eqn. (A.2) for W_{ij}, integrating by parts, and using periodic boundary conditions, we obtain

$$\frac{\partial}{\partial t} \int \frac{1}{2} \overline{u}_i \overline{u}_i \, dv = - 2 \int \nu_T \overline{S}_{k\ell} \overline{S}_{k\ell} \, dv \qquad (A.4)$$

and we have for this case:

$$\varepsilon = 2 \int \nu_T \overline{S}_{k\ell} \overline{S}_{k\ell} \, dv \geq 0$$

since $\nu_T \geq 0$.

Model ω-2

In a similar way, substituting Eqn. (2.16) into Eqn. (A.2) for W_{ij}, we can show that

$$\frac{\partial}{\partial t} \int \frac{1}{2} u_i u_i \, dv = - \int \nu_T \overline{\omega}_i \overline{\omega}_i \, dv \qquad (A.5)$$

and we have for this case

$$\varepsilon = \int \nu_T \overline{\omega}_i \overline{\omega}_i \, dv \geq 0$$

Appendix B

Fast Discrete Sine Transform (FDST)

The discrete analogs to the expansion in Fourier sine series (Eqns. (3.14) and (3.15)) are

$$f(x) = \sum_{n=0}^{N-1} \hat{f}^s(n) \sin\left[\frac{n\pi x}{(N-1)h}\right] \tag{3.16}$$

$$\hat{f}^s(n) = \frac{2}{(N-1)} \sum_{j=0}^{N-1} f(x) \sin\left[\frac{n\pi x}{(N-1)h}\right] \tag{3.17}$$

where $n = 0,1,\ldots,N-1$,

$h = L/(N-1)$,

$x = jh, \quad j = 0,1,\ldots,N-1$,

N = number of mesh points,

L = length of the computational box.

Both the forward and inverse sine transforms involve identical sums. Eqn. (3.17) can be rewritten as:

$$\hat{f}^s(n) = -\frac{2}{(N-1)} \operatorname{Im}\left[\sum_{j=0}^{2(N-1)-1} F(x) \exp\left(\frac{-2\pi i n x}{2(N-1)h}\right)\right] \tag{B.1}$$

where

$F(x) = f(x) \quad j = 0,1,\ldots,N-1$,

$= 0 \quad j = N,N+1,\ldots,2(N-1)-1$

We note that the summation

$$\sum_{j=0}^{2(N-1)-1} F(x) \exp\left(\frac{-2\pi i n x}{2(N-1)h}\right) \tag{B.2}$$

is equivalent to (3.12) with $N_1 = 2(N-1)$, and an FFT routine can be used to evaluate this sum.

Fast Discrete Cosine Transform (FDCT)

The discrete analog to the expansion in Fourier cosine series (Eqns. (3.21) and (3.22)) are:

$$f(x) = \sum_{n=0}^{(N-1)} \hat{f}^c(n) \cos\left(\frac{n\pi x}{(N-1)h}\right) \tag{3.19}$$

$$\hat{f}^c(n) = \frac{2}{(N-1)} \sum_{j=0}^{(N-1)} f'(x) \cos\left(\frac{n\pi x}{(N-1)h}\right) \tag{3.20}$$

where

$$\hat{f}'^c(n) = \begin{cases} \frac{1}{2}\hat{f}^c(n) & n = 0,N-1 \\ \hat{f}^c(n) & n = 1,\ldots,N-2 \end{cases}$$

$$f'(x) = \begin{cases} \frac{1}{2}f(x) & j = 0,N-1 \\ f(x) & j = 1,\ldots,N-2 \end{cases}$$

where

$n = 0,\ldots,N-1$

$h = L/(N-1)$,

$x = jh \quad j = 0,\ldots,N-1$,

N = number of mesh points,

L = length of the computational box.

Both the forward and inverse transforms involve identical sums. Eqn. (3.19) can be rewritten as:

$$f(x) = \mathrm{Re}\left[\sum_{n=0}^{2(N-1)-1} F(n) \exp\left(\frac{-2\pi inx}{2(N-1)h}\right)\right] \tag{B.3}$$

where

$$F(n) = \begin{cases} \frac{1}{2}\hat{f}^c(n) & n = 0,N-1, \\ \hat{f}^c(n) & n = 1,\ldots,N-2, \\ 0 & n = N,\ldots,2(N-1)-1. \end{cases}$$

We note that the sum in (B.3) is identical to the sum(B.2), and an FFT routine can be used to evaluate it. In fact, the sine and cosine transforms can be done simultaneously, if it is necessary to have both.

Appendix C

Effect of a Sinusoidal Vorticity Perturbation on a Uniform Vortex Array

In Chapter 5 we have studied the effect of perturbing a uniform array of vortices by offsetting the spacing of the vortices ($\beta > 0$). In this appendix we study the effect of adding a sinusoidal vorticity perturbation to a uniform array of vortices ($\beta = 0$).

1. Initial Conditions

The initial conditions studied in this appendix were generated by starting with a uniform array of point vortices on the centerline of our computational box:

$$\omega_{2u} = C_1\left(\delta(x-L_1/4) + \delta(x-3L_1/4)\right)\delta(z-L_3/2) \qquad (C.1)$$

We then add a cosine vorticity distribution to (C.1):

$$\omega_2 = \omega_{2u} - C_2 \cos\left(\frac{2\pi x}{L}\right)\delta(z-L_3/2) \qquad (C.2)$$

Eqn. (C.2) is then filtered with a relatively wide Gaussian filter (Eqn. (5.19)) to yield the initial conditions. The initial velocity is then non-dimensionalized on Δu and the length scales on θ_{in}. The computational details, i.e., number of mesh points, mesh size, time steps, and boundary conditions, are the same as in Chapter 5. Only the initial conditions were changed.

2. Results

The momentum thickness (θ) is defined by Eqn. (5.4). Fig. C.1 shows θ/θ_{in} plotted vs. T for C_2/C_1 = 0.1/20, 1/20, 2/20, 4/20. We note that the growth rate of the layer is highly dependent on the strength of the perturbation. The growth rate more than doubles from 0.016 to 0.035 when the strength of the perturbation is doubled (C_2/C_1 from 2/20 to 4/20).

We note also that for high amplitude perturbations, $C_2/C_1 = 4/20$, the growth rate starts to level off for $T > 12.0$. This saturation is also observed experimentally by Oster et al. (1978); they have oscillated the initial conditions of a two-dimensional mixing layer.

Figures C.2 and C.3 show the non-dimensional mean velocity and turbulence intensity (as in Sections 5.7 and 5.8) plotted vs. z/θ for $C_2/C_1 = 2/20$. We note that the mean velocity profiles are self-similar. This is not surprising, since self-similarity of the mean velocity profiles is easily obtained (see Section 6.5). Turbulence intensity profiles (Fig. C.3) show that self-similarity is also more or less obtained for the present case.

These results are similar to those obtained in Chapter 5 by using a spacing perturbation. Apparently the perturbation can take any of a number of forms, and the characteristics of the shear layer will be nearly the same. Under experimental conditions, the nature of the perturbation is difficult to determine. What we do note is that reproduction of the experimentally observed growth rate does require large perturbations, which are apparently created by either the inflow or outflow conditions of the experiment.

Appendix D

INTERACTIONS BETWEEN STREAMWISE AND SPANWISE VORTICITY

In Chapter 6 we studied the effect of a random fluctuation on vortex pairing. In this appendix we study the interactions between a streamwise cellular vortex structure and spanwise vortex pairing.

1. Initial Conditions

The initial conditions studied in this appendix were generated by adding to a row of spanwise vortices ($\beta = 3/16$) a row of streamwise vortices of alternating signs:

$$\bar{\omega}_1 = C_2 \sin\left(\frac{2\pi y}{L_2}\right) \exp\left(-\frac{(z-L_3/2)^2}{6h_3^2}\right) \qquad (D.1)$$

The same computational setup described in Chapter 6 is used, i.e., the same boundary conditions, number of mesh points, mesh sizes, and time step.

Figure D.1 shows a contour map in the y-z plane of the streamwise vorticity. We note that $\bar{\omega}_1$ displays a cellular structure and that $\bar{\omega}_1$ does not initially have a streamwise variation. We ran two cases:

Case a:

$$\frac{|\omega_1|_{max}}{|\omega_2|_{max}} = 0.037$$

Case b:

$$\frac{|\omega_1|_{max}}{|\omega_2|_{max}} = 0.370$$

2. Results

We first look at the development of the momentum thickness, $\theta(t)$, defined by Eqn. (5.4), in time. The non-dimensional mean velocity (Section 5.7) and mean turbulence intensity (Section 5.8) are also considered. The interaction between the spanwise vortices and the streamwise vortices is studied using contour plots. Note that we have a three-dimensional box and that contour plots in different planes for different vorticity directions will be considered.

Figure D.2 shows θ/θ_{in} plotted vs. T. The momentum thickness growth rate, $d\theta/\Delta u dt = 0.020$, for Case (a) is the same as it was in the absence of the streamwise vortices. However, the momentum thickness growth rate, $d\theta/\Delta u dt = 0.040$, doubled for Case (b).

Figures D.3a and -b show $2< u >_{xy}/\Delta u$ plotted vs. z/θ for Cases (a) and (b), respectively, at $\Delta T = 2.4$ intervals. We note that both cases produce self-similar mean velocity profiles.

Figures D.4a and -b show $q^2/2(\Delta u)^2$ plotted vs. z/θ for Cases (a) and (b), respectively, at $\Delta T = 2.4$ intervals. The mean turbulence intensity results for Case (a) are similar to those we obtained when the streamwise vortices were not present. As in the 2-D case (with $\beta = 3/16$), the mean turbulence intensity decays slightly, then reaches a self-similar situation. For Case (b), in which we have strong streamwise vortices, Fig. D.4b shows that the turbulence intensity grows with time, and the profiles do not show self-similarity.

(a) Contour Plots in the x-z Planes

Figures D.5 show constant vorticity contours of the spanwise $(\bar{\omega}_2)$ vorticity at time T = 16.78. In both cases the spanwise vortices have paired. The shapes are similar, but the roller is slightly distorted for Case (b) as compared to Case (a) and to the 2-D results (see Fig. 5.7d). This indicates that the streamwise vortices did not affect the merging of the spanwise vortices, but the strong streamwise vortices (Case (b)) have affected the shape of the roller.

Figures D.6 show constant vorticity contours of the streamwise vorticity for Cases (a) and (b). These figures indicate that the streamwise vortices have been convected to the edges of the mixing layer by the spanwise vortices. There is also clear evidence of vortex stretching.

Figure D.7 shows the projection of the vorticity vector at T = 16.78, for Case (b). We can see clearly that the originally straight vortex lines have been convected and stretched by the spanwise vortices to assume an inverted S shape.

(b) Contour Plots in the y-z Planes

Figure D.8 shows constant vorticity contours of the spanwise vorticity for Case (b). The spanwise vortices have been convected and stretched by the strong counter-rotating streamwise vortices and exhibit spanwise waviness. This means that the contact area between the rotational fluid and the irrotational fluid has increased, which leads to an increase in the entrainment rate. This waviness also explains the increase in the turbulence intensity and high growth of the momentum thickness of the mixing layer. Note that the mean quantities are defined as horizontal planar averages and, with this definition, the wavy layer appears thicker and more turbulent than a strictly two-dimensional layer.

The above results indicate that the effect of the streamwise vorticity on the spanwise vorticity is almost independent of the effect of the spanwise vorticity on the streamwise vorticity. Indeed, a straight line of particles placed at the center of the layer in the streamwise direction would be convected to form an inverted S shape in the presence of the two-dimensional vortex pairing. A straight line of particles initially passing through the center of an array of counter-rotating vortices will be convected to assume a wavy shape.

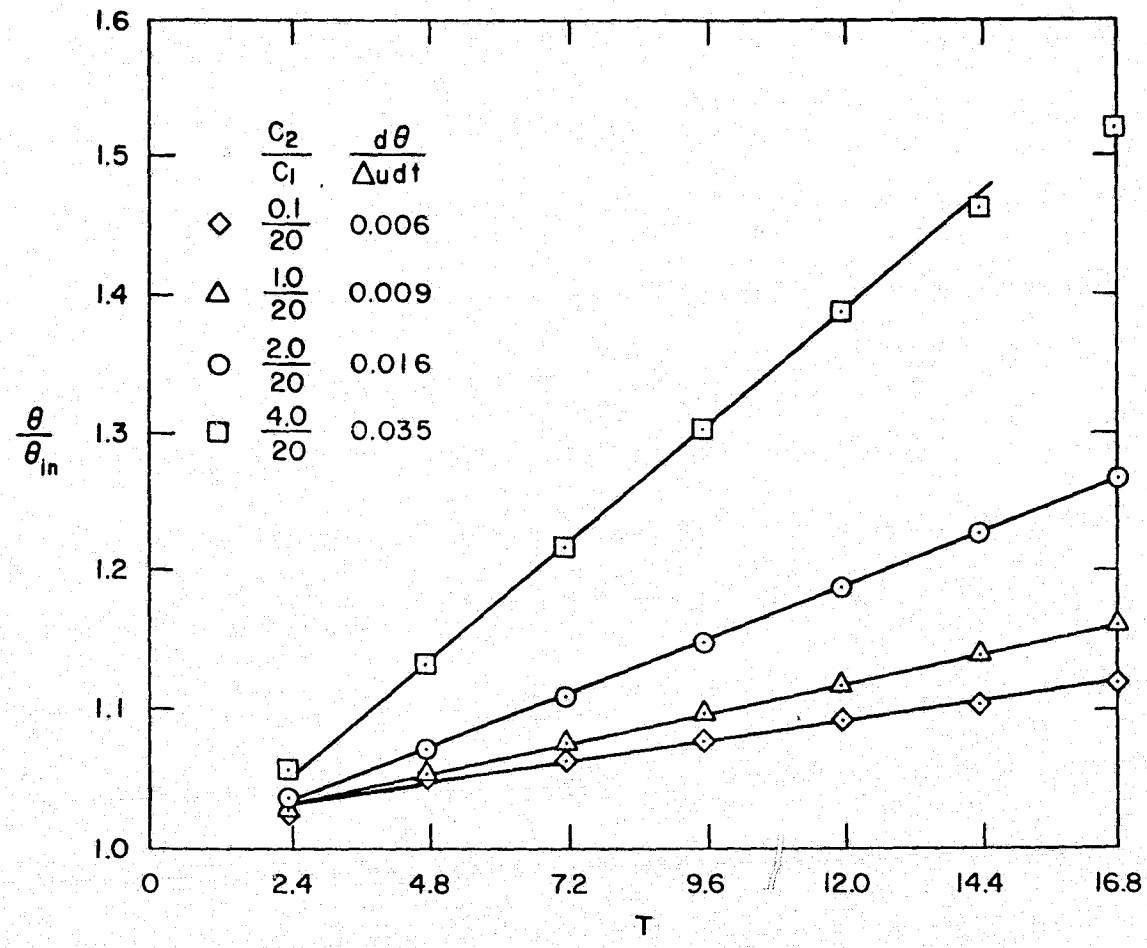

Fig. C.1. Non-dimensional momentum thickness (θ/θ_{in}) as a function of time for various C_2/C_1.

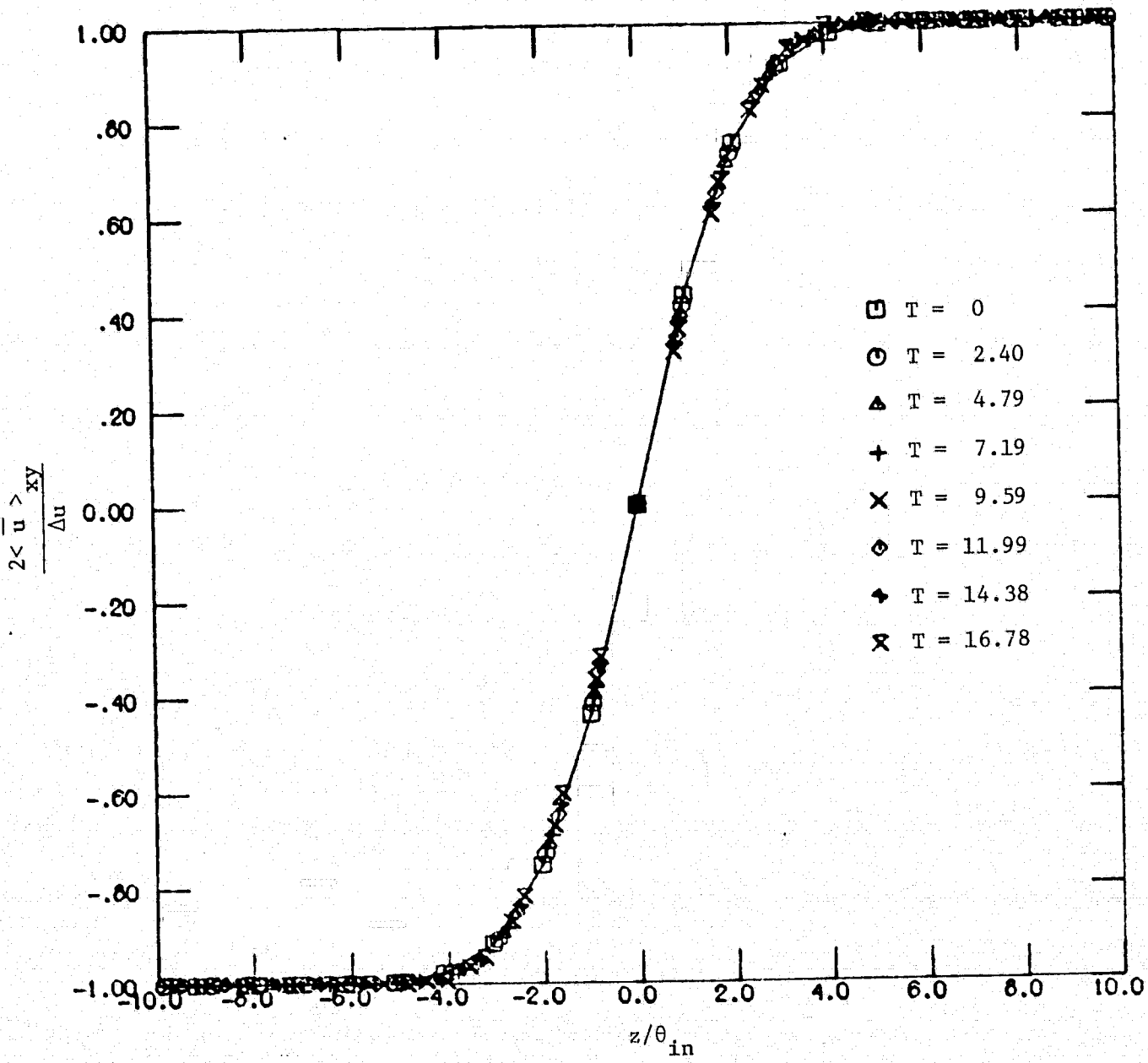

Fig. C.2. Mean velocity profiles ($C_2/C_1 = 0.1$)

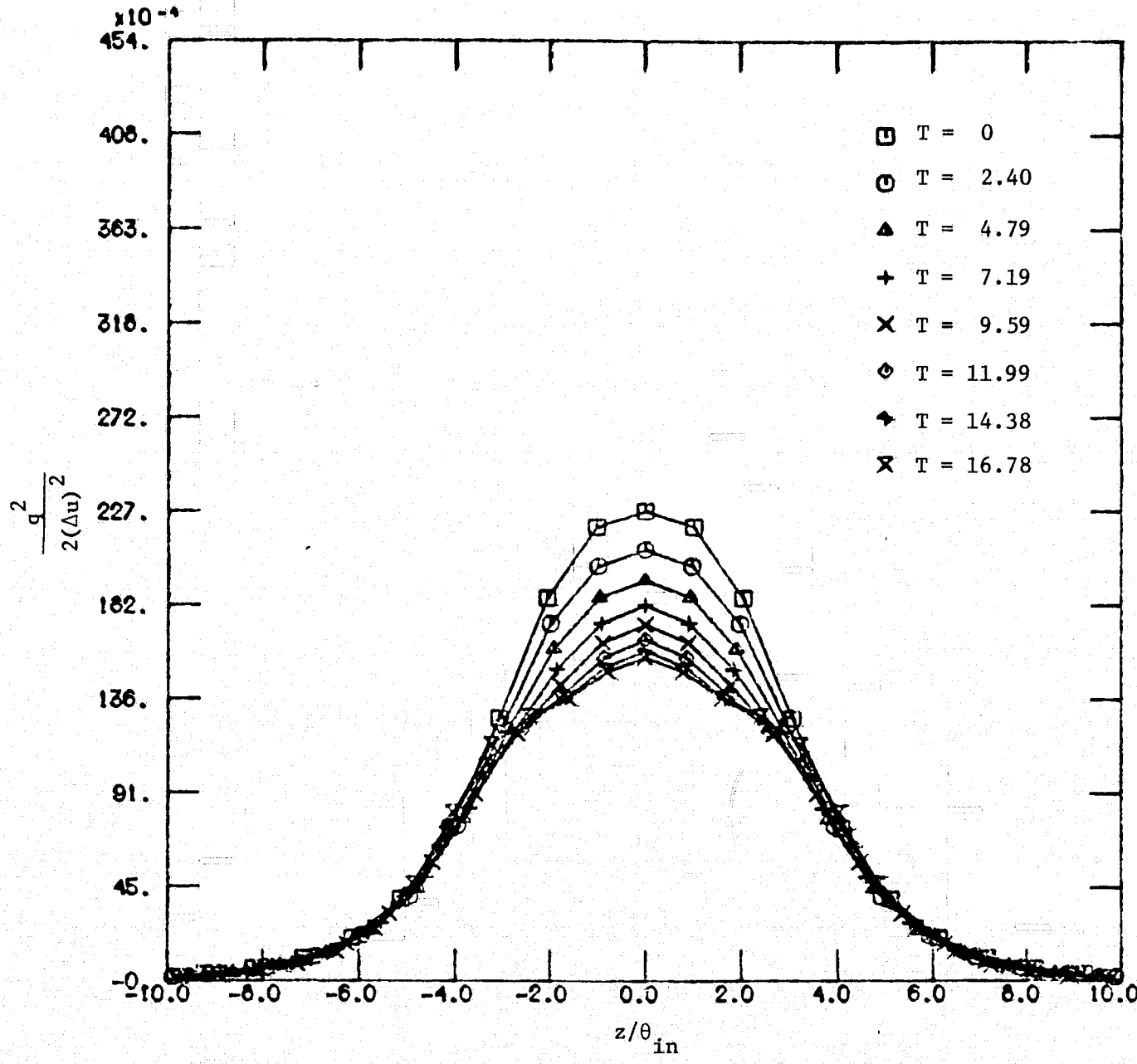

Fig. C.3. Mean turbulence intensity profiles (C_2/C_1 = 0.1).

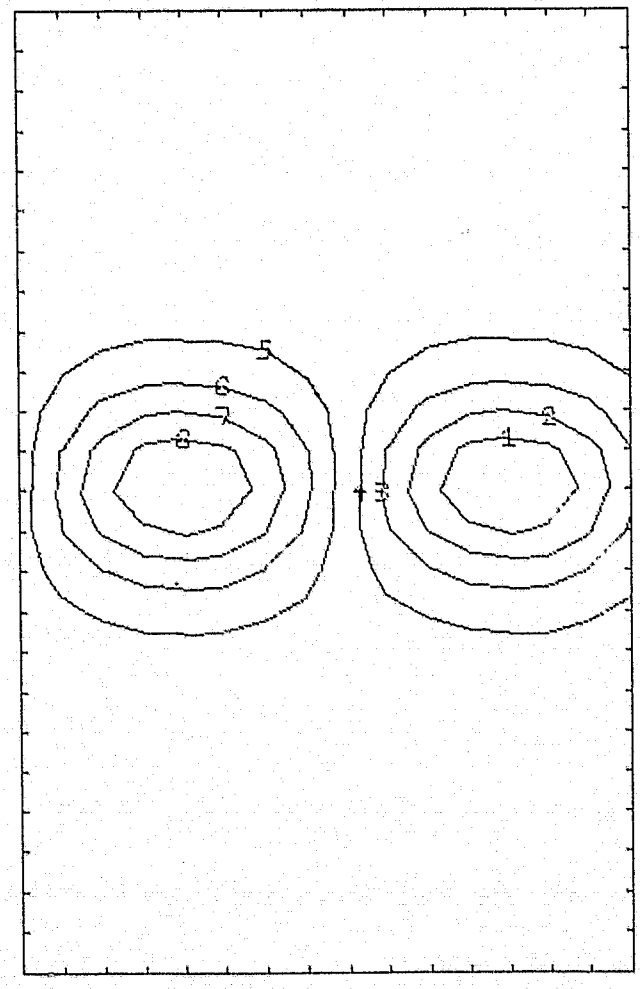

Fig. D.1. Contour plots of the streamwise vorticity $(\bar{\omega}_1)$ at time T = 0. Constant vorticity lines are plotted at eight levels. Higher numbers on these lines indicate higher vorticity levels.

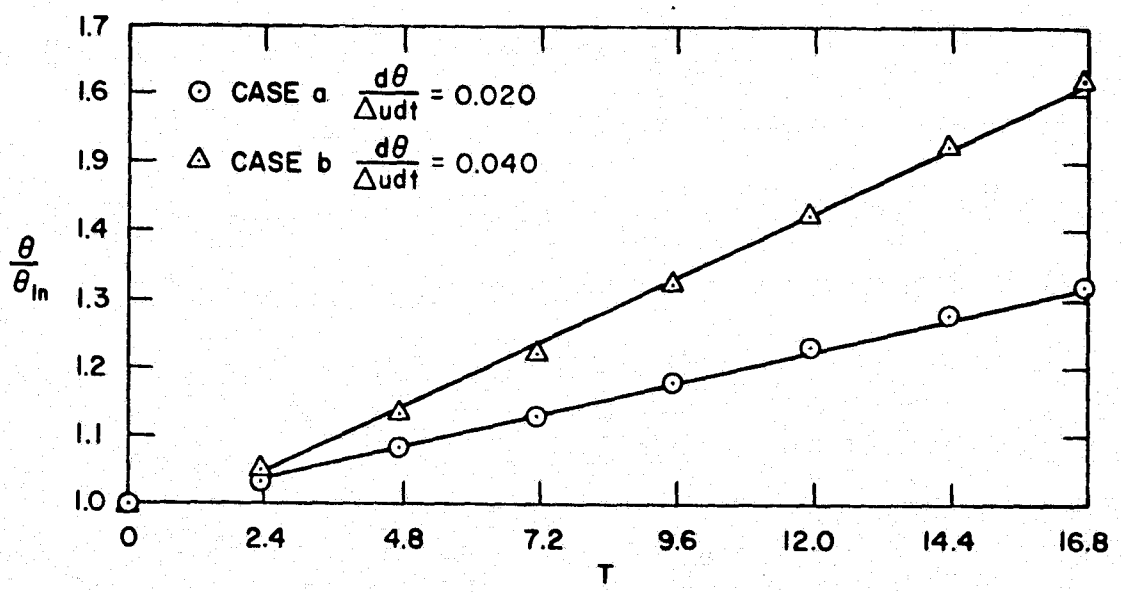

Fig. D.2. Non-dimensional momentum thickness (θ/θ_{in}) as a function of time.

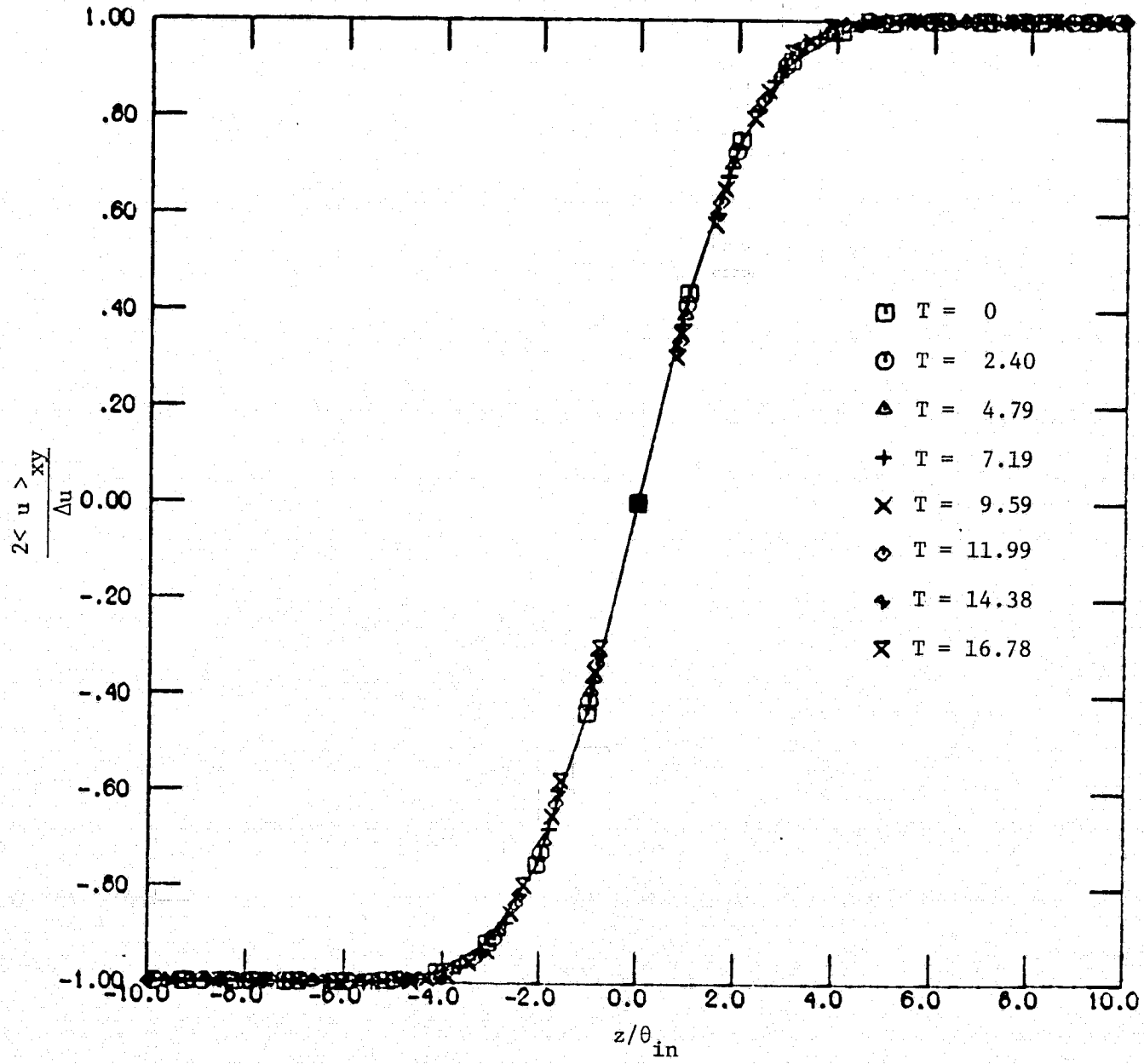

Fig. D.3a. Mean velocity profiles (case a)

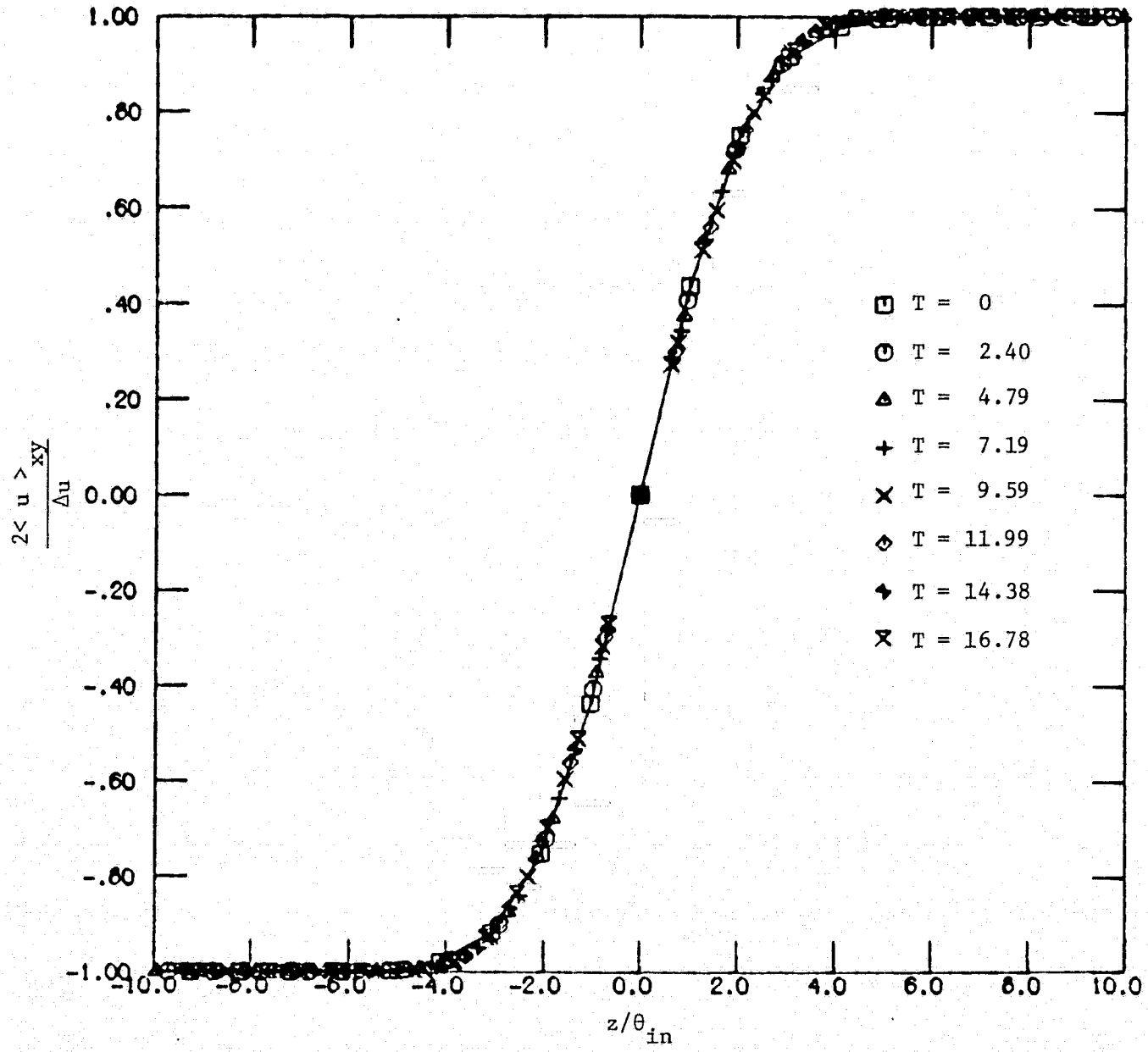

Fig. D.3b. Mean velocity profiles (case b)

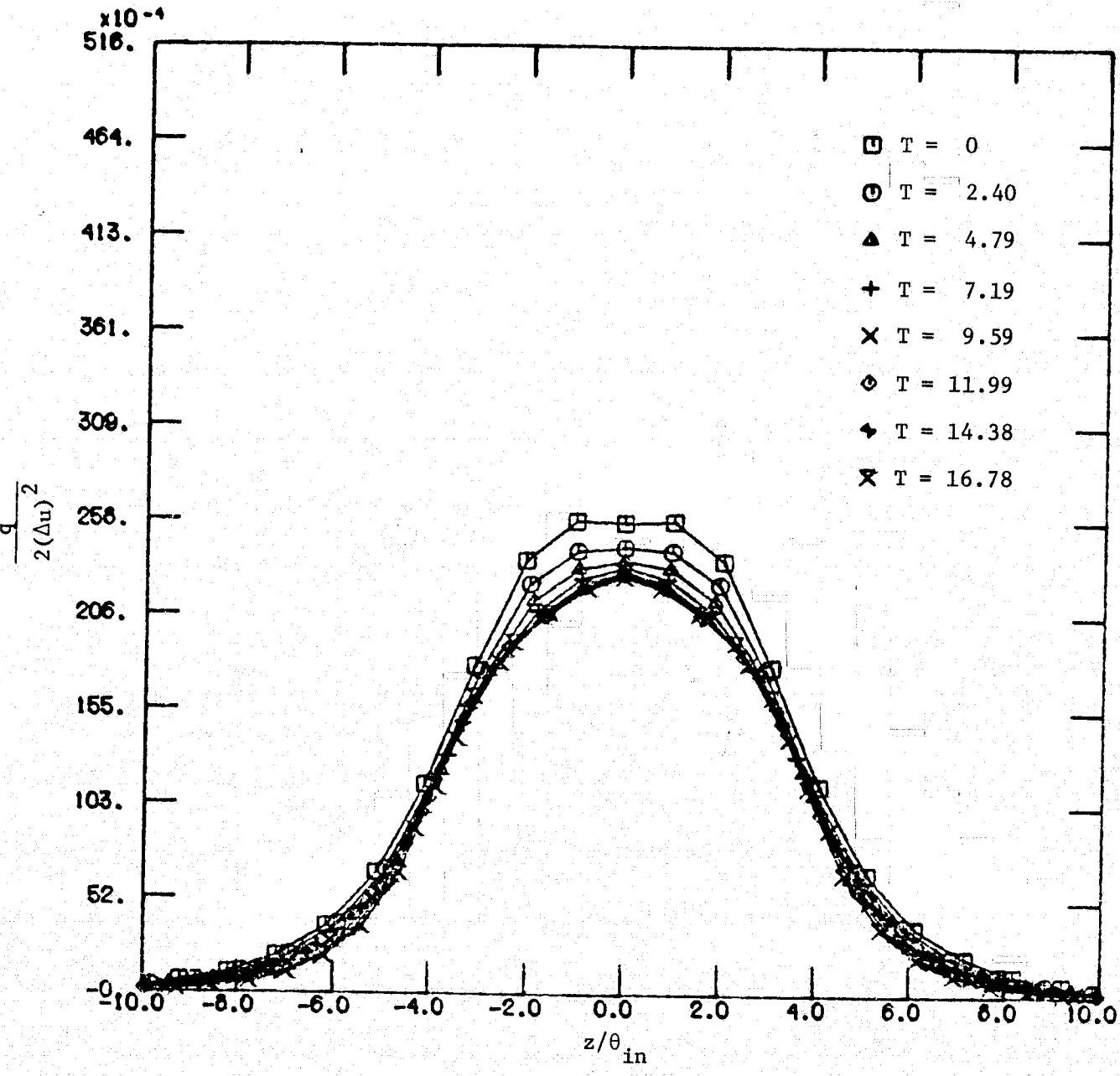

Fig. D.4a. Mean turbulence intensity profiles (case a).

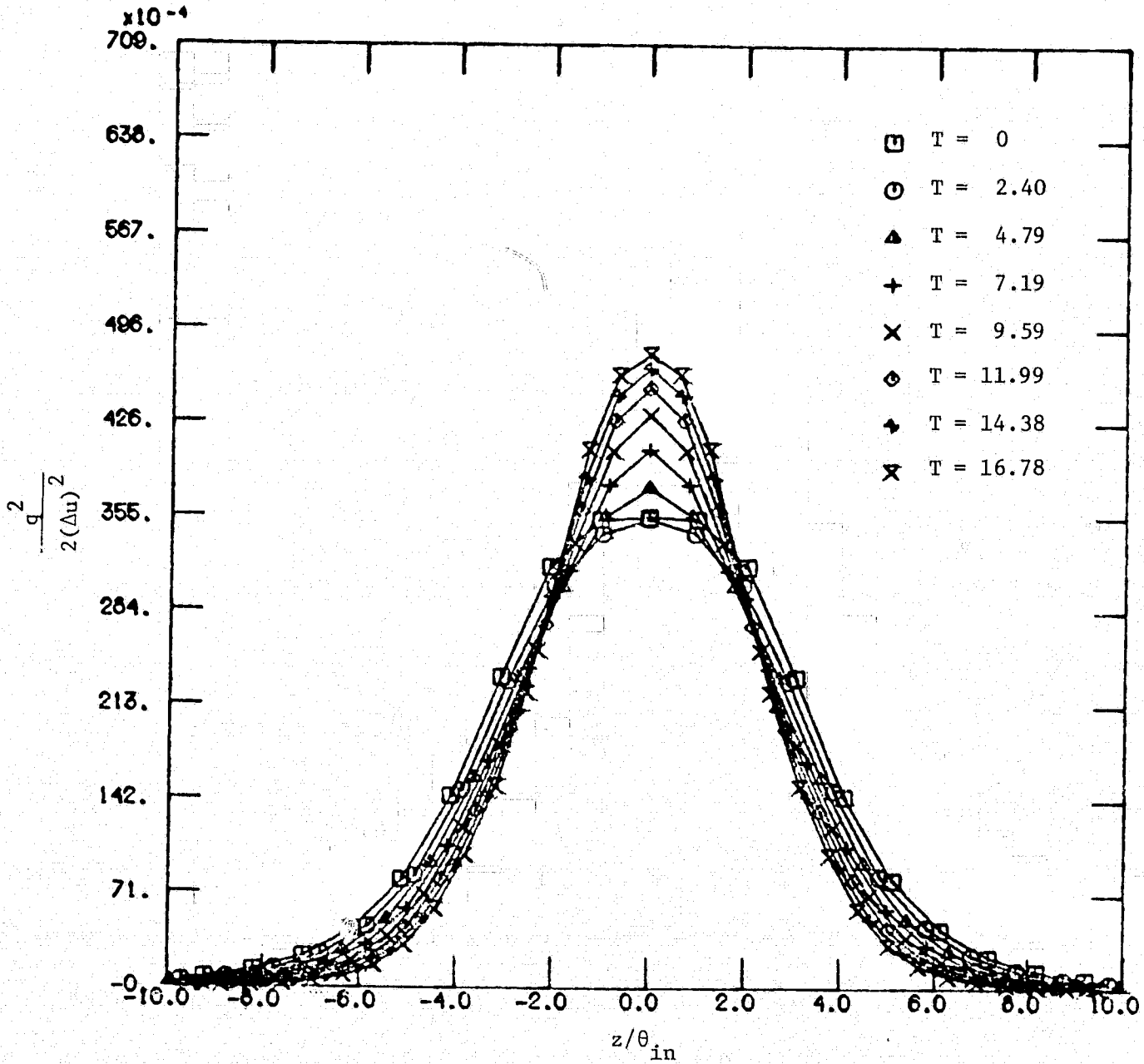

Fig. D.4b. Mean turbulence intensity profiles (case b).

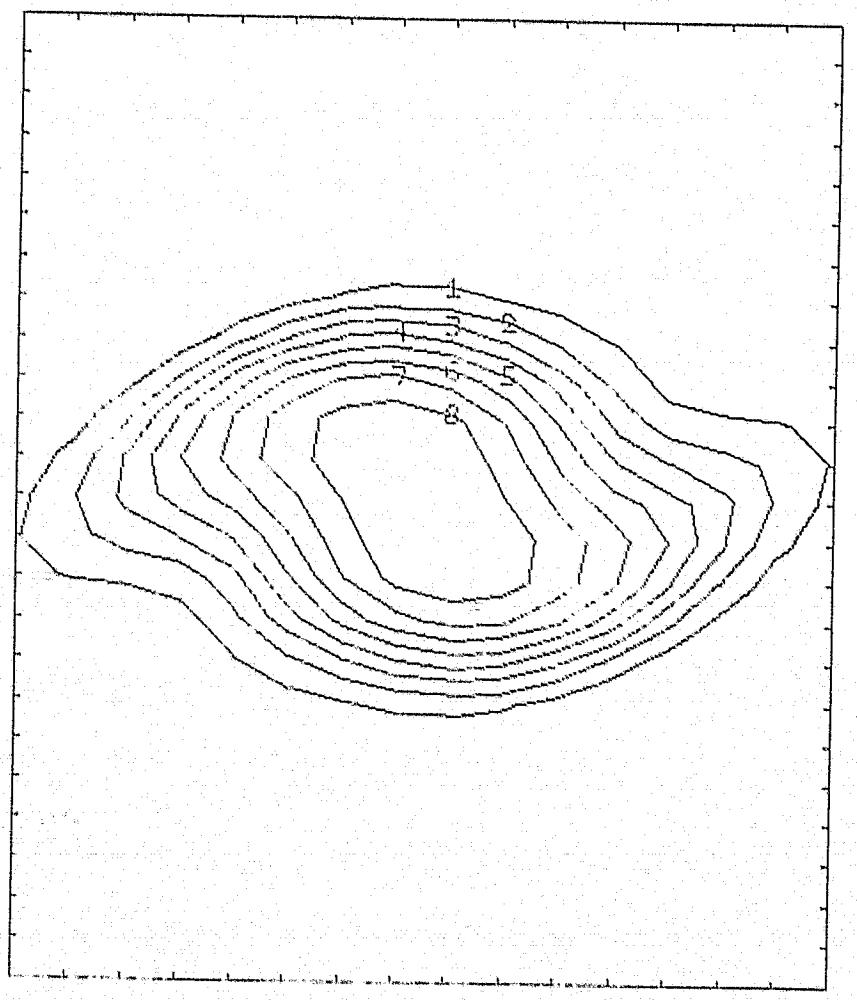

Fig. D.5a. Contour plots of the spanwise vorticity $(\bar{\omega}_2)$ in an x-z plane $(y/\theta_{in} = 4.09)$, at time $T = 16.78$. Constant vorticity lines are plotted at eight levels. Higher numbers on these lines indicate higher levels (case a).

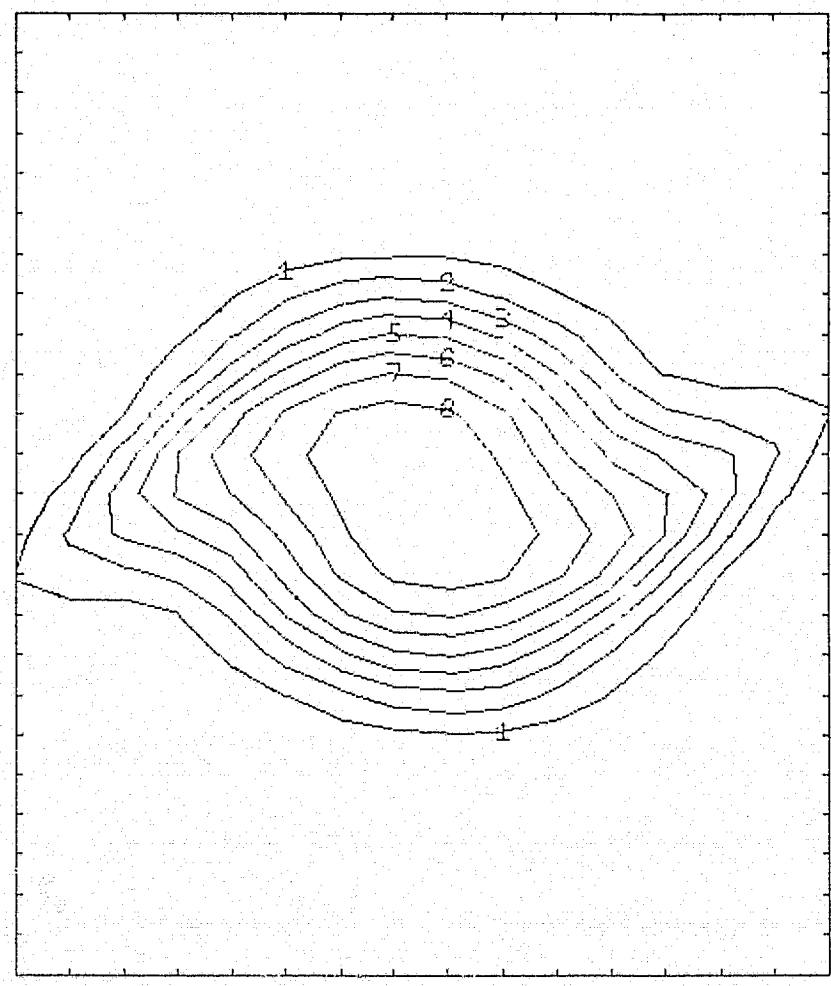

Fig. D.5b. Contour plots of the spanwise vorticity $(\bar{\omega}_2)$ in an x-z plane $(y/\theta_{in} = 4.09)$, at time T = 16.78. Constant vorticity lines are plotted at eight levels. Higher numbers on these lines indicate higher levels (case b).

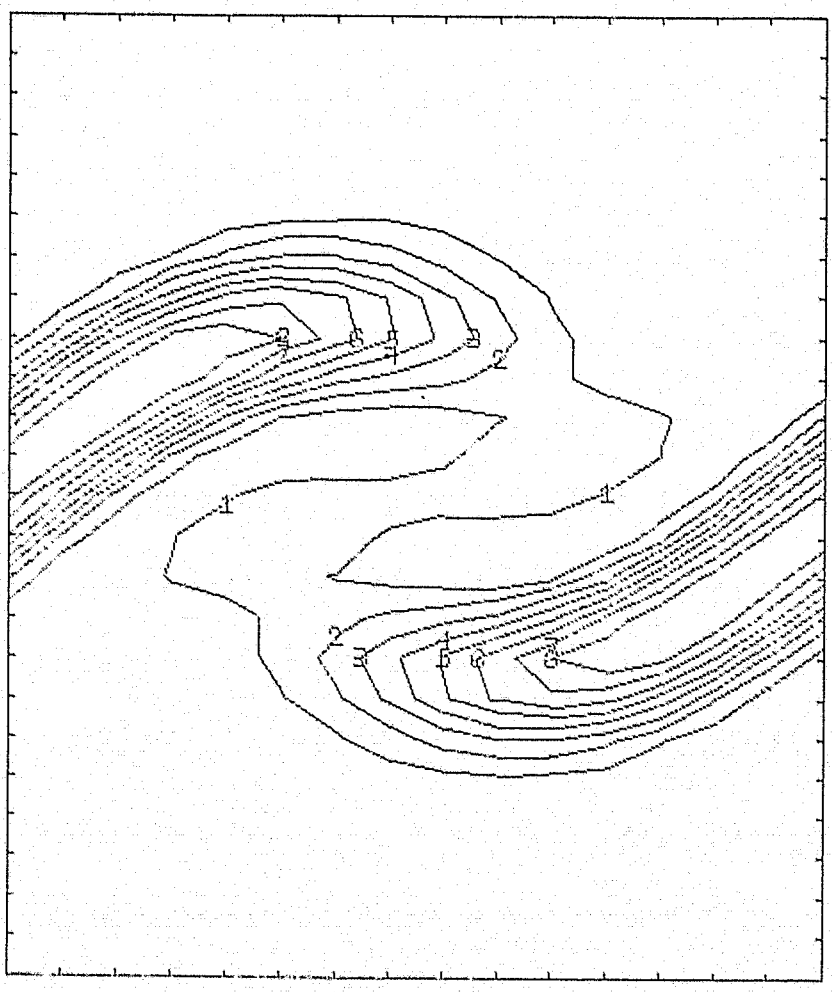

Fig. D.6a. Contour plots of the streamwise vorticity ($\bar{\omega}_1$) in an x-z plane ($y/\theta_{in} = 4.09$), at time T = 16.78. Constant vorticity lines are plotted at eight levels. Higher numbers on these lines indicate higher vorticity levels (case a).

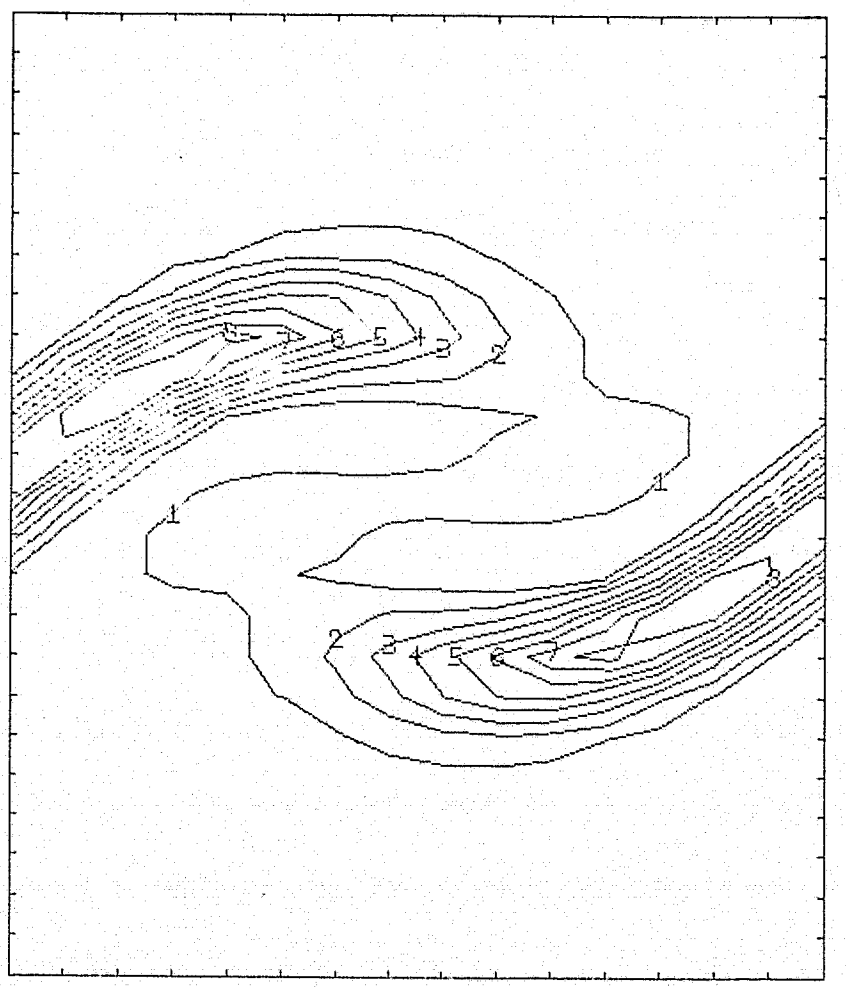

Fig. D.6b. Contour plots of the streamwise vorticity $(\bar{\omega}_1)$ in an x-z plane $(y/\theta_{in} = 4.09)$, at time T = 16.78. Constant vorticity lines are plotted at eight levels. Higher numbers on these lines indicate higher levels (case b).

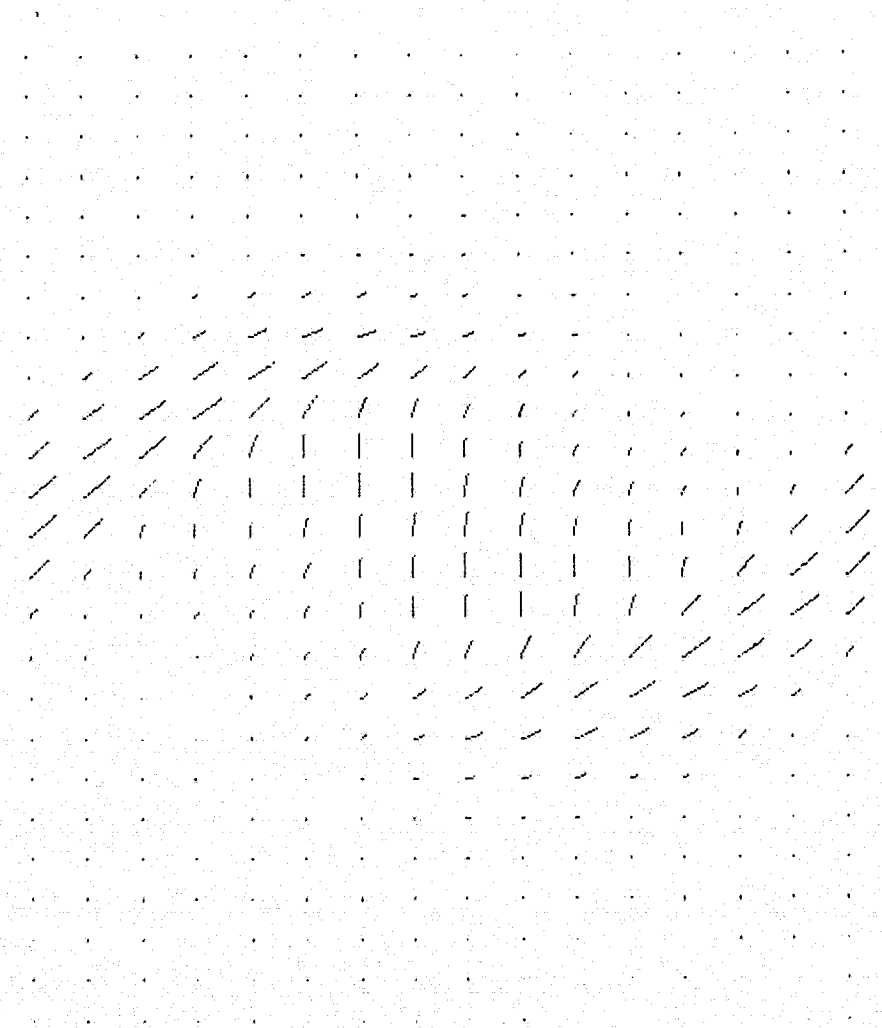

Fig. D.7. Projection of the vorticity vector in an x-z plane (y/θ_{in} = 4.09) at time T = 16.78.

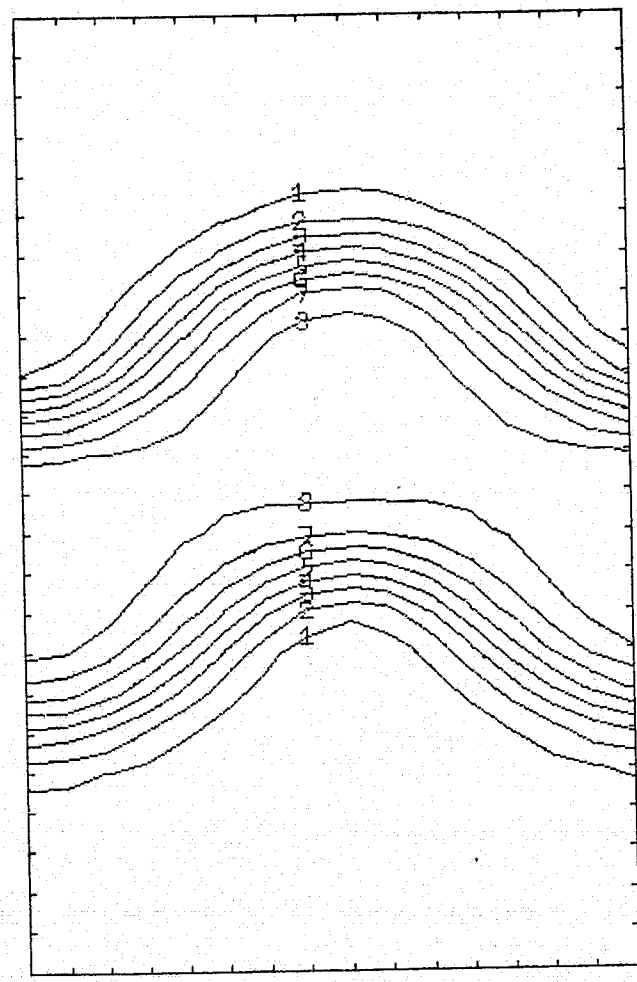

Fig. D.8. Contour plots of the spanwise vorticity $(\bar{\omega}_2)$ in a y-z plane $(x/\theta_{in} = 9.55)$, at time T = 16.78. Constant vorticity lines are plotted at eight levels. Higher numbers on these lines indicate higher vorticity levels $(\omega_{2,max} = 0.714$ case b).

```
C--------COMPUTER PROGRAM WRITTEN TO CALCULATE TURBULENT MIXING LAYERS
C
C
*COMDECK AVG
      COMMON/AVG/ AVG1,AVG2,AVG3,CCF
*COMDECK BLANK
      COMMON DUDX(16,16,33)
*COMDECK DATA7
      COMMON/DATA7/ FR(16,16),FI(16,16)
*COMDECK DATA9
      COMMON/DATA9/ IMAX,JMAX,LMAX
*COMDECK DAT21
      COMMON/DAT21/ XR(64),XI(64)
*COMDECK DEL
      COMMON/DEL/ DELTAX,DELTAY,DELTAZ
*COMDECK DIM
      COMMON/DIM/N1,N2,N3
*COMDECK FLT
      COMMON/FLT/ FILT1(16),FILT2(16),FILT3(33)
*COMDECK LARGE2
      COMMON/LARGE2/ U(16,16,33),V(16,16,33),W(16,16,33)
      LEVEL 2,U,V,W
*COMDECK LARGE3
      COMMON/LARGE3/ GU(16,16,33),GV(16,16,33),GW(16,16,33)
      LEVEL 2,GU,GV,GW
*COMDECK LARGE5
      COMMON/LARGE5/ O1(16,16,33),O2(16,16,33),O3(16,16,33)
      LEVEL 2,O1,O2,O3
*COMDECK MEANVOR
      COMMON/MEANVOR/ VOR(32,33)
*COMDECK PR
      COMMON/PR/ CCPW,CCPF,CCPD
*COMDECK WV
      COMMON/WV/ WAVEX(16),WAVEY(16),WAVEZ(33),WAVEXS(16),WAVEYS(16)
     1 ,WAVEZS(33)
*COMDECK XL
      COMMON/XL/ XPART(160),YPART(160),ZPART(160),NCHAR(160)
*DECK MAIN
      PROGRAM MAIN(INPUT,OUTPUT,TAPE8,TAPE9,TAPE10)
C*****************************************************************
C     MAIN CONTROLS THE COMPUTATION SEQUENCES.                   *
C     IN THIS ROUTINE WE ADVANCE IN TIME .                       *
C     THE EXTERNALS USED IN THIS ROUTINE ARE                     *
C     CFILTER                                                    *
C     CONVEC                                                     *
C     CURLO                                                      *
C     DATARED                                                    *
C     EDVIS                                                      *
C     INVERS                                                     *
C     MEANINI                                                    *
C     MOVLEV                                                     *
C     SFILTER                                                    *
C     SFILTER                                                    *
C     SGS                                                        *
C     STFILT                                                     *
C     STREAD                                                     *
C     STWV                                                       *
C*****************************************************************
      INTEGER TIME,TSTART,TEND
      COMMON/TIM/ TSTART,TEND
      COMMON/LARGE4/ RU(16,16,33),RV(16,16,33),RW(16,16,33)
      COMMON/NORM/ DELU,THETA
      LEVEL 2,RU,RV,RW
      COMMON/DATCNT/ IDATCNT
*CALL MEANVOR
*CALL XL
      COMMON/CONST/C100,C101,IJK,IJ,NHP1,HALF
*CALL DAT21
*CALL LARGE2
*CALL BLANK
```

```
*CALL LARGE5
*CALL DEL
*CALL DATA9
*CALL WV
*CALL DATA7
*CALL FLT
*CALL LARGE3
*CALL DIM
*CALL AVG
C       START THE READOUT OF INPUT
        CALL STREAD
C       SET THE COEFICIENT OF THE SUBGRID SCALE MODEL
        C=0.188
C       SET COF = 1 FOR THE FIRST TIME STEP
        COF=1.0
        IJ=N1*N2
        IJK=N1*N2*N3
        DO 1 L=1,LMAX
        DO 1 J=1,JMAX
        DO 1 I=1,IMAX
        U(I,J,L)=0.
        V(I,J,L)=0.
        W(I,J,L)=0.
        O1(I,J,L)=0.
        O2(I,J,L)=0.
        O3(I,J,L)=0.
    1   CONTINUE
C       SET THE WAVE NUMBERS
        CALL STWV
C*****SET THE INITIAL CONDITIONS
        CALL MEANINI
C       NON DIMENSIONALIZE THE TIME STEP ON DELU/THETA
        DT=0.03125*DELU/THETA
C       SET THE FILTER WIDTH = 2*MESH SIZE
        AVG1=2.0
        AVG2=2.0
        AVG3=2.0
        COEF2=(C*(AVG1*DELTAX*AVG2*DELTAY*AVG3*DELTAZ)**(1./3.))**2
        DO 123 L=1,LMAX
        DO 123 J=1,JMAX
        DO 123 I=1,IMAX
        RU(I,J,L)=0.
        RV(I,J,L)=0.
        RW(I,J,L)=0.
  123   CONTINUE
        ICOUNT=0
        TIME=0
C       WRITE ON TAPE 9 TO BE STORED ON DISC PACK
        PRINT 1100,TIME
        WRITE(9) TIME,O1,O2,O3,DT,DELTAX,DELTAY,DELTAZ,DELU,THETA
        IDATCNT=0
C       COMPUTE THE STATISTICS OF THE INITIAL CONDITIONS
        CALL DATARED
C       SET THE FOURIER TRANSFORM OF THE GAUSSIAN FILTER
        CALL STFILT
        IDUM=30
        DO 300 TIME=TSTART,TEND
C*****COMPUTE THE ADVECTIVE AND STRETCHING TERMS
        CALL CONVEC
        CALL SFILTER(GU,DUDX,N1,N2,N3)
        CALL SFILTER(GV,DUDX,N1,N2,N3)
        CALL CFILTER(GW,DUDX,N1,N2,N3)
C*****COMPUTE THE EDDY VISCOSITY
        CALL EDVIS(COEF2,DUDX,N1,N2,N3)
C*****COMPUTE THE SGS MODEL
        CALL SGS(U,V,W,N1,N2,N3)
C*****ADVANCE IN TIME
        DO 800 L=1,LMAX
        DO 800 J=1,JMAX
        DO 800 I=1,IMAX
```

```
      O1(I,J,L)=O1(I,J,L)+DT*(COF*GU(I,J,L)-0.5*RU(I,J,L))
      O2(I,J,L)=O2(I,J,L)+DT*(COF*GV(I,J,L)-0.5*RV(I,J,L))
      O3(I,J,L)=O3(I,J,L)+DT*(COF*GW(I,J,L)-0.5*RW(I,J,L))
  800 CONTINUE
C*****STORE THE PREVIOUS TIME STEP
      CALL MOVLEV(GU(1,1,1),RU(1,1,1),IJK)
      CALL MOVLEV(GV(1,1,1),RV(1,1,1),IJK)
      CALL MOVLEV(GW(1,1,1),RW(1,1,1),IJK)
C*****THE VORTICITY AT THE NEXT TIME STEP HAS BEEN COMPUTED
C*****FIND THE CORESPONDING VELOCITY FIELD
      CALL INVERS(O1,GU,DUDX,1,N1,N2,N3)
      CALL INVERS(O2,GV,DUDX,2,N1,N2,N3)
      CALL INVERS(O3,GW,DUDX,3,N1,N2,N3)
      CALL CURLO(GU,GV,GW,U,V,W,N1,N2,N3)
C     SET COF = 1.5 FOR SUBSEQUENT TIMES (ADAMS-BASHFORTH)
      COF=1.5
      ICOUNT=ICOUNT+1
      IICOUNT=ICOUNT-IDUM
      IF (IICOUNT .NE. 0) GO TO 300
      ICOUNT=0
      PRINT 1100,TIME
      WRITE(9) TIME,O1,O2,O3
      CALL DATARED
  300 CONTINUE
 1100 FORMAT(1H1,5X,* TIME STEP =*,I5)
 1000 FORMAT(1P8E15.7)
      STOP
      END
*DECK CFILTER
      SUBROUTINE CFILTER(HR,HI,N1,N2,N3)
C***********************************************************************
C     CFILTER COMPUTES THE FILTER OF THE HR VARIABLE BY EXPANDING IN
C     FOURIER SERIES IN THE X- AND Y- DIRECTIONS AND FOURIER COSINE
C     SERIES IN THE Z-DIRECTION
C     THIS ROUTINE USES AS EXTERNALS
C     FDCT
C     FFTX
C     FFTY
C     A CALL TO STFILT INITIATE THE VALUES OF FILT1,FILT2,AND FILT3
C***********************************************************************
      DIMENSION HR(N1,N2,N3),HI(N1,N2,N3)
*CALL DATA9
*CALL FLT
*CALL DATA7
*CALL DAT21
      LEVEL 2,HR
      CC=1.0/(IMAX*JMAX)
      IJ=N1*N2
      DO 10 J=1,JMAX
      DO 10 I=1,IMAX
      DO 20 L=1,LMAX
      XR(L)=HR(I,J,L)
   20 CONTINUE
      CALL FDCT(1.0)
      DO 30 L=1,LMAX
      HI(I,J,L)=XR(L)
   30 CONTINUE
   10 CONTINUE
      DO 40 L=1,LMAX
      CALL MOVLEV(HI(1,1,L),FR(1,1),IJ)
      CALL FFTX(1.0)
      CALL FFTY(1.0,1.0)
      DO 50 J=1,JMAX
      DO 50 I=1,IMAX
      FR(I,J)=FR(I,J)*FILT1(I)*FILT2(J)*FILT3(L)
      FI(I,J)=FI(I,J)*FILT1(I)*FILT2(J)*FILT3(L)
   50 CONTINUE
      CALL FFTX(-1.0)
      CALL FFTY(-1.0,CC)
      CALL MOVLEV(FR(1,1),HI(1,1,L),IJ)
```

```
   40 CONTINUE
      DO 60 J=1,JMAX
      DO 60 I=1,IMAX
      DO 70 L=1,LMAX

      DO 60 I=1,IMAX
      DO 70 L=1,LMAX
      XR(L)=HI(I,J,L)
   70 CONTINUE
      CALL FDCT(-1.0)
      DO 80 L=1,LMAX
      HR(I,J,L)=XR(L)
   80 CONTINUE
   60 CONTINUE
      RETURN
      END
*DECK CONVEC
      SUBROUTINE CONVEC
C*************************************************************************
C     THIS SUBROUTINE COMPUTES THE CONVECTIVE AND STRETCHING            *
C     TERMS AND STORES THEM IN GU,GV,GW                                 *
C     THIS ROUTINE USES AS EXTERNALS                                    *
C     COSPART                                                           *
C     PARTIAL                                                           *
C*************************************************************************
*CALL LARGE2
*CALL LARGE3
*CALL LARGE5
*CALL BLANK
*CALL DATA9
*CALL DIM
      IJK=N1*N2*N3
C*****TERM FOR THE X-DIRECTION
      DO 10 L=1,LMAX
      DO 10 J=1,JMAX
      DO 10 I=1,IMAX
      GU(I,J,L)=U(I,J,L)*O2(I,J,L)-V(I,J,L)*O1(I,J,L)
      GV(I,J,L)=U(I,J,L)*O3(I,J,L)-W(I,J,L)*O1(I,J,L)
   10 CONTINUE
      CALL PARTIAL(2,GU,N1,N2,N3)
      CALL MOVLEV(DUDX(1,1,1),GU(1,1,1),IJK)
      CALL COSPART(GV,N1,N2,N3)
      DO 20 L=1,LMAX
      DO 20 J=1,JMAX
      DO 20 I=1,IMAX
      GU(I,J,L)=GU(I,J,L)+DUDX(I,J,L)
   20 CONTINUE
C*****TERM FOR THE Y-DIRECTION
      DO 30 L=1,LMAX
      DO 30 J=1,JMAX
      DO 30 I=1,IMAX
      GV(I,J,L)=V(I,J,L)*O1(I,J,L)-U(I,J,L)*O2(I,J,L)
      GW(I,J,L)=V(I,J,L)*O3(I,J,L)-W(I,J,L)*O2(I,J,L)
   30 CONTINUE
      CALL PARTIAL(1,GV,N1,N2,N3)
      CALL MOVLEV(DUDX(1,1,1),GV(1,1,1),IJK)
      CALL COSPART(GW,N1,N2,N3)
      DO 40 L=1,LMAX
      DO 40 J=1,JMAX
      DO 40 I=1,IMAX
      GV(I,J,L)=GV(I,J,L)+DUDX(I,J,L)
   40 CONTINUE
C*****TERM FOR THE Z-DIRECTION
      DO 50 L=1,LMAX
      DO 50 J=1,JMAX
      DO 50 I=1,IMAX
      GW(I,J,L)=W(I,J,L)*O1(I,J,L)-U(I,J,L)*O3(I,J,L)
      U(I,J,L)=W(I,J,L)*O2(I,J,L)-V(I,J,L)*O3(I,J,L)
   50 CONTINUE
      CALL PARTIAL(1,GW,N1,N2,N3)
```

```
      CALL MOVLEV(DUDX(1,1,1),GW(1,1,1),IJK)
      CALL PARTIAL(2,U,N1,N2,N3)
      DO 60 L=1,LMAX
      DO 60 J=1,JMAX
      DO 60 I=1,IMAX
      GW(I,J,L)=GW(I,J,L)+DUDX(I,J,L)
   60 CONTINUE
      RETURN
      END
*DECK COSPART
      SUBROUTINE COSPART(U,N1,N2,N3)
C*****************************************************************
C     COSPART COMPUTES THE PARTIAL IN THE Z-DIRECTION OF U BY EXPANDING
C     IN FOURIER COSINE SERIES
C     THE EXTENALS USED IN THIS SUBROUTINE ARE
C     FDCT
C     FDST
C*****************************************************************
      DIMENSION U(N1,N2,N3)
*CALL BLANK
*CALL DAT21
*CALL WV
*CALL DATA9
      LEVEL 2,U
      DO 10 J=1,JMAX
      DO 10 I=1,IMAX
      DO 20 L=1,LMAX
      XR(L)=U(I,J,L)
   20 CONTINUE
      SIGN=1.0
      CALL FDCT(SIGN)
      DO 30 L=1,LMAX
      XR(L)=-XR(L)*WAVEZ(L)
   30 CONTINUE
      SIGN=-1.0
      CALL FDST(SIGN)
      DO 40 L=1,LMAX
      DUDX(I,J,L)=XR(L)
   40 CONTINUE
   10 CONTINUE
      RETURN
      END
*DECK CURLO
      SUBROUTINE CURLO(U,V,W,O1,O2,O3,N1,N2,N3)
      DIMENSION O1(N1,N2,N3),O2(N1,N2,N3),O3(N1,N2,N3)
      DIMENSION U(N1,N2,N3),V(N1,N2,N3),W(N1,N2,N3)
*CALL DATA9
*CALL BLANK
      LEVEL 2,U,V,W,O1,O2,O3
C*****************************************************************
C     THIS SUBROUTINE COMPUTES THE CURL OF THE VORTICITY FIELD        *
C     THE EXTERNALS USED IN THIS ROUTINE ARE
C     PARTIAL
C     SINPART
C*****************************************************************
C*****CURL IN THE X-DIRECTION
      IJK=N1*N2*N3
      CALL PARTIAL(2,W,N1,N2,N3)
      CALL MOVLEV(DUDX(1,1,1),O1(1,1,1),IJK)
      CALL SINPART(V,N1,N2,N3)
      DO 10 L=1,LMAX
      DO 10 J=1,JMAX
      DO 10 I=1,IMAX
      O1(I,J,L)=O1(I,J,L)- DUDX(I,J,L)
   10 CONTINUE
C*****CURL IN YHE Y-DIRECTION
      CALL SINPART(U,N1,N2,N3)
      CALL MOVLEV(DUDX(1,1,1),O2(1,1,1),IJK)
      CALL PARTIAL(1,W,N1,N2,N3)
      DO 20 L=1,LMAX
```

```
      DO 20 J=1,JMAX
      DO 20 I=1,IMAX
      02(I,J,L)=02(I,J,L)-DUDX(I,J,L)
   20 CONTINUE
C*****CURL IN THE Z-DIRECTION
      CALL PARTIAL(1,V,N1,N2,N3)
      CALL MOVLEV(DUDX(1,1,1),03(1,1,1),IJK)
      CALL PARTIAL(2,U,N1,N2,N3)
      DO 30 L=1,LMAX
      DO 30 J=1,JMAX
      DO 30 I=1,IMAX
      03(I,J,L)=03(I,J,L)-DUDX(I,J,L)
   30 CONTINUE
      RETURN
      END
*DECK CURLU
      SUBROUTINE CURLU(U,V,W,01,02,03,N1,N2,N3)
      DIMENSION 01(N1,N2,N3),02(N1,N2,N3),03(N1,N2,N3)
      DIMENSION U(N1,N2,N3),V(N1,N2,N3),W(N1,N2,N3)
*CALL DATA9
*CALL BLANK
      LEVEL 2,U,V,W,01,02,03
C*************************************************************************
C     THIS ROUTINE COMPUTES THE CURL OF THE VELOCITY FIELD              *
C     AND STORES IT IN 01,02,03,                                        *
C     THE EXYERNALS USED IN THIS SUBROUTINE ARE                         *
C     COSPART                                                           *
C     PARTIAL                                                           *
C*************************************************************************
C*****CURL IN THE X-DIRECTION
      IJK=N1*N2*N3
      CALL PARTIAL(2,W,N1,N2,N3)
      CALL MOVLEV(DUDX(1,1,1),01(1,1,1),IJK)
      CALL COSPART(V,N1,N2,N3)
      DO 10 L=1,LMAX
      DO 10 J=1,JMAX
      DO 10 I=1,IMAX
      01(I,J,L)=01(I,J,L)- DUDX(I,J,L)
   10 CONTINUE
C*****CURL IN YHE Y-DIRECTION
      CALL COSPART(U,N1,N2,N3)
      CALL MOVLEV(DUDX(1,1,1),02(1,1,1),IJK)
      CALL PARTIAL(1,W,N1,N2,N3)
      DO 20 L=1,LMAX
      DO 20 J=1,JMAX
      DO 20 I=1,IMAX
      02(I,J,L)=02(I,J,L)-DUDX(I,J,L)
   20 CONTINUE
C*****CURL IN THE Z-DIRECTION
      CALL PARTIAL(1,V,N1,N2,N3)
      CALL MOVLEV(DUDX(1,1,1),03(1,1,1),IJK)
      CALL PARTIAL(2,U,N1,N2,N3)
      DO 30 L=1,LMAX
      DO 30 J=1,JMAX
      DO 30 I=1,IMAX
      03(I,J,L)=03(I,J,L)-DUDX(I,J,L)
   30 CONTINUE
      RETURN
      END
*DECK DATARED
      SUBROUTINE DATARED
C*************************************************************************
C     THIS SUBROUTINE COMPUTES THE STATISTICS OF THE COMPUTATION
C     USUM = PLANAR AVERAGE OF THE STREAMWISE VELOCITY                  *
C     VSUM=PLANAR AVERAGE OF THE SPANWISE VELOCITY                      *
C     WSUM = PLANAR AVERAGE OF THE CROSSFLOW VELOCITY                   *
C     01SUM = PLANAR AVERAGE OF THE STREAMWISE VORTICITY                *
C     02SUM = PLANAR AVERAGE OF THE SPANWISE VORTICITY                  *
C     03SUM = PLANAR AVERAGE OF THE CROSSFLOW VORTICITY                 *
C     USQ = R.M.S STREAMWISE VELOCITY                                   *
```

```
C      VSQ = R.M.S. OF THE SPANWISE VELOCITY ETC...                          *
C      UVSTRES = PLANAR AVERAGE OF U@W@                                      *
C      PLOVALE = VOLUME AVERAGE OF THE TOTAL ENERGY                          *
C      ENERGY = INTEGRAL OF THE TURBULENCE ENERGY                            *
C*****************************************************************************
*CALL DEL
*CALL MEANVOR
*CALL PR
*CALL LARGE2
*CALL LARGE3
*CALL LARGE5
*CALL DAT21
*CALL DATA9
*CALL BLANK
*CALL DIM
      DIMENSION USM(33),VSM(33),US(33),VS(33),WS(33),O1S(33),O2S(33)
     1 ,O3S(33),ES(33),ENS(33),ZO(33)
      DIMENSION DUMSP(33)
      COMMON/DATCNT/ IDATCNT
      IDATCNT=IDATCNT+1
      LMAXM1=LMAX-1
      C3=1./LMAXM1
      CNORM3=1./(IMAX*JMAX)
      PRINT 1100
      UTOT=0.
      VTOT=0.
      WTOT=0.
      O1TOT=0.
      O2TOT=0.
      O3TOT=0.
      OVRALE=0.
      TOTENER=0.
      TOTENST=0.
      DO 100 L=1,LMAX
      USUM=0.
      VSUM=0.
      WSUM=0.
      O1SUM=0.
      O2SUM=0.
      O3SUM=0.
      USQ=0.
      VSQ=0.
      WSQ=0.
      O1SQ=0.
      O2SQ=0.
      O3SQ=0.
      ENERGY=0.
      ENSTROP=0.
      UVSTRES=0.
      PLOVALE=0.
      DO 110 J=1,JMAX
      DO 110 I=1,IMAX
      USUM=USUM+U(I,J,L)
      VSUM=VSUM+V(I,J,L)
      WSUM=WSUM+W(I,J,L)
      O1SUM=O1SUM+O1(I,J,L)
      O2SUM=O2SUM+O2(I,J,L)
      O3SUM=O3SUM+O3(I,J,L)
  110 CONTINUE
      USUM=USUM*CNORM3
      VSUM=VSUM*CNORM3
      WSUM=WSUM*CNORM3
      O1SUM=O1SUM*CNORM3
      O2SUM=O2SUM*CNORM3
      O3SUM=O3SUM*CNORM3
      GW(1,1,L)=USUM
      GW(2,1,L)=VSUM
      GW(3,1,L)=WSUM
      DO 160 J=1,JMAX
      DO 160 I=1,IMAX
```

```
      USQ=USQ+(U(I,J,L)-USUM)**2
      VSQ=VSQ+(V(I,J,L)-VSUM)**2
      WSQ=WSQ+(W(I,J,L)-WSUM)**2
      O1SQ=O1SQ+(O1(I,J,L)-O1SUM)**2
      O2SQ=O2SQ+(O2(I,J,L)-O2SUM)**2
      O3SQ=O3SQ+(O3(I,J,L)-O3SUM)**2
      UVSTRES=UVSTRES+(U(I,J,L)-USUM)*(W(I,J,L)-WSUM)
      PLOVALE=PLOVALE+(U(I,J,L)**2+V(I,J,L)**2+W(I,J,L)**2)
  160 CONTINUE
      USQ=USQ*CNORM3
      VSQ=VSQ*CNORM3
      WSQ=WSQ*CNORM3
      O1SQ=O1SQ*CNORM3
      O2SQ=O2SQ*CNORM3
      O3SQ=O3SQ*CNORM3
      ENERGY=(USQ+VSQ+WSQ)*0.5
      ENSTROP=(O1SQ+O2SQ+O3SQ)*0.5
      UVSTRES=UVSTRES*CNORM3
      USQ=SQRT(USQ)
      VSQ=SQRT(VSQ)
      WSQ=SQRT(WSQ)
      O1SQ=SQRT(O1SQ)
      O2SQ=SQRT(O2SQ)
      O3SQ=SQRT(O3SQ)
      US(L)=USQ
      VS(L)=VSQ
      WS(L)=WSQ
      O1S(L)=O1SQ
      O2S(L)=O2SQ
      O3S(L)=O3SQ
      USM(L)=USUM
      VSM(L)=VSUM
      ES(L)=ENERGY
      ENS(L)=ENSTROP
      GW(4,1,L)=O1SUM
      GW(5,1,L)=O2SUM
      GW(6,1,L)=O3SUM
      GV(1,1,L)=USQ
      GV(2,1,L)=WSQ
      XI(L)=UVSTRES
      CC=1.
      IF(L .EQ. 1) CC=0.5
      IF(L .EQ. LMAX) CC=0.5
      OVRALE=OVRALE+PLOVALE*CC*0.5
      UTOT=UTOT+USUM*CC
      VTOT=VTOT+VSUM*CC
      WTOT=WTOT+WSUM*CC
      O1TOT=O1TOT+O1SUM*CC
      O2TOT=O2TOT+O2SUM*CC
      O3TOT=O3TOT+O3SUM*CC
      TOTENER=TOTENER+ENERGY*CC
      TOTENST=TOTENST+ENSTROP*CC
  100 CONTINUE
      UTOT=UTOT*C3
      VTOT=VTOT*C3
      WTOT=WTOT*C3
      O1TOT=O1TOT*C3
      O2TOT=O2TOT*C3
      O3TOT=O3TOT*C3
      TOTENER=TOTENER*C3
      TOTENST=TOTENST*C3
      DELU=GW(1,1,LMAX)-GW(1,1,1)
      DELU=1./DELU
      THETA=(0.25-(GW(1,1,1)*DELU)**2)*0.5
      DO 170 L=2,LMAXM1
      THETA=THETA+(0.25-(GW(1,1,L)*DELU)**2)
  170 CONTINUE
      THETA=THETA+(0.25-(GW(1,1,LMAX)*DELU)**2)*0.5
      THETA=THETA*DELTAZ
      DO 300 L=1,LMAX
```

```
      ZO(L)=(L-((LMAX-1)/2+1))*DELTAZ/THETA
      USM(L)=USM(L)*DELU*2.0
      VSM(L)=VSM(L)*DELU
      GW(5,1,L)=GW(5,1,L)*DELU*THETA
      XI(L)=XI(L)*(DELU**2)
      US(L)=US(L)*DELU
      VS(L)=VS(L)*DELU
      WS(L)=WS(L)*DELU
      O3S(L)=O3S(L)*(DELU*THETA)
      O1S(L)=O1S(L)*(DELU*THETA)
      O2S(L)=O2S(L)*(DELU*THETA)
      ES(L)=ES(L)*DELU**2
      ENS(L)=ENS(L)*(DELU*THETA)**2
      PRINT 3000,USM(L),VSM(L),XI(L),GW(5,1,L),US(L),VS(L),WS(L),
     1 O1S(L),O2S(L),O3S(L),ES(L),ENS(L),ZO(L)
  300 CONTINUE
      WRITE(8) USM,VSM,XI,US,VS,WS,O1S,O2S,O3S,ES,ENS,ZO,THETA
      PRINT 1700,THETA
      PRINT 1200
      PRINT 1000,UTOT,VTOT,WTOT,O1TOT,O2TOT,O3TOT,TOTENER,TOTENST
      PRINT 2400,OVRALE
 2400 FORMAT(1X,* OVER ALL ENERGY IN COMPUTATION BOX =*,1PE15.7)
      DO 180 L=1,LMAX
      DO 180 I=1,IMAX
      GU(I,1,L)=0.
      GU(I,2,L)=0.
      GU(I,3,L)=0.
      GU(I,4,L)=0.
  180 CONTINUE
      C1OY=1./FLOAT(JMAX)
      DO 190 L=1,LMAX
      DO 190 J=1,JMAX
      DO 190 I=1,IMAX
      GU(I,1,L)=GU(I,1,L)+O2(I,J,L)*C1OY
      GU(I,2,L)=GU(I,2,L)+U(I,J,L)*C1OY
      GU(I,3,L)=GU(I,3,L)+W(I,J,L)*C1OY
  190 CONTINUE
      DO 230 L=1,LMAX
      DO 230 I=1,IMAX
      GU(I,2,L)=GU(I,2,L)-GW(1,1,L)
      GU(I,3,L)=GU(I,3,L)-GW(3,1,L)
  230 CONTINUE
      PRINT 2200
 2200 FORMAT(1H1,1X,* LINE AVERAGE OF VORTICITY*)
      PRINT 2300,(((GU(I,1,L),I= 1,16  ),L),L=1,LMAX)
      IF(CCPD .NE.1.) GO TO 240
      PRINT 2500
 2500 FORMAT(1H1,1X,* LINE AVERAGE OF U-COMPONENT *)
      PRINT 2300,(((GU(I,2,L),I= 1,16  ),L),L=1,LMAX)
      PRINT 2500
      PRINT 2300,(((GU(I,2,L),I=17,IMAX),L),L=1,LMAX)
      PRINT 2600
 2600 FORMAT(1H1,1X,* LINE AVERAGE OF W-COMPONENT *)
      PRINT 2300,(((GU(I,3,L),I= 1,16  ),L),L=1,LMAX)
      PRINT 2600
      PRINT 2300,(((GU(I,3,L),I=17,IMAX),L),L=1,LMAX)
 2300 FORMAT(1X,16F8.3,I3)
  240 CONTINUE
      PRINT 2000
      DO 250 L=14,20
      DO 260 I=1,IMAX
      XR(I)=GU(I,1,L)
      XI(I)=0.
  260 CONTINUE
      CALL FFT(XR,XI,IMAX,-1)
      IF(IDATCNT.EQ.1) DUMSP(L)=SQRT(XR(2)**2+XI(2)**2)
      IF(DUMSP(L).LT.0.0000001) GO TO 250
      DO 270 I=1,IMAX
      XR(I)=SQRT(XR(I)**2+XI(I)**2)/DUMSP(L)
  270 CONTINUE
```

```
      PRINT 1800,L,(XR(I),I=1,8)
  250 CONTINUE
 1800 FORMAT(1X,*WVO2*,I5,1P8E14.6)
 1000 FORMAT(1P8E15.7)
 1100 FORMAT(2X,*USUM*,6X,*VSUM*,5X,*UWSTR*,5X,*O2SUM*,7X,*USQ*,7X,*VSQ*
     1,7X,*WSQ*,6X,*O1SQ*,6X,*O2SQ*,6X,*O3SQ*,5X,*ENERGY*,4X,*ENSTROP*,3
     2X,*PLANE*)
 1200 FORMAT(///,1X,* UTOT IN X-Y    VTOT IN X-Y    WTOT IN X-Y   O1TOT
     1IN X-Y   O2TOT IN X-Y   O3TOT IN X-Y  *)
 1300 FORMAT(1X,* USUN IN Y-Z    VSUM IN Y-Z    WSUM IN Y-Z   O1SUM IN Y
     1-Z   O2SUM IN Y-Z   O3SUM IN Y-Z  *)
 1400 FORMAT(///,1X,* UTOT IN Y-Z    VTOT IN Y-Z    WTOT IN Y-Z   O1TOT
     1IN Y-Z   O2TOT IN Y-Z   O3TOT IN Y-Z  *)
 1500 FORMAT(1X,* USUN IN Z-X    VSUM IN Z-X    WSUM IN Z-X   O1SUM IN Z
     1-X   O2SUM IN Z-X   O3SUM IN Z-X  *)
 1600 FORMAT(///,1X,* UTOT IN Z-X    VTOT IN Z-X    WTOT IN Z-X   O1TOT
     1IN Z-X   O2TOT IN Z-X   O3TOT IN Z-X  *)
 1700 FORMAT(1X,* MOMENTUM THICKNESS *,1PE15.7)
 2000 FORMAT(1H1)
 3000 FORMAT(1P13E10.2)
C     TEST THE DIVERGENCE OF THE VELOCITY AND VORTICITY FIELDS
      CALL DIV
C     TEST THE SOLUTION OF THE POISSON EQUATIONS ,I.E. THAT              *
C     THE CURL OF OUR VELOCITY FIELD IS EQUAL TO THE VORTICITY FIELD
      CALL CURLU(U,V,W,GU,GV,GW,N1,N2,N3)
      ERRMAX1=0.
      ERRMAX2=0.
      ERRMAX3=0.
      DO 17 L=1,LMAX
      DO 17 J=1,JMAX
      DO 17 I=1,IMAX
      GU(I,J,L)=ABS(GU(I,J,L)-O1(I,J,L))
      GV(I,J,L)=ABS(GV(I,J,L)-O2(I,J,L))
      GW(I,J,L)=ABS(GW(I,J,L)-O3(I,J,L))
      IF (GU(I,J,L) .GT. ERRMAX1) ERRMAX1=GU(I,J,L)
      IF (GV(I,J,L) .GT. ERRMAX2) ERRMAX2=GV(I,J,L)
      IF (GW(I,J,L) .GT. ERRMAX3) ERRMAX3=GW(I,J,L)
   17 CONTINUE
      PRINT 1110,ERRMAX1,ERRMAX2,ERRMAX3
 1110 FORMAT(1X,* ERRMAX1 =*,E15.7,*ERRMAX2 =*,E15.7,* ERRMAX3 =*,E15.7)
      RETURN
      END
*DECK DIV
      SUBROUTINE DIV
C*********************************************************************
C     THIS ROUTINE TESTS THE DIVERGENCE OF THE VELOCITY FIELD          *
C     AND THE DIVERGENCE OF THE VORTICITY FIELD .                      *
C*********************************************************************
*CALL LARGE2
*CALL LARGE3
*CALL LARGE5
*CALL BLANK
*CALL DATA9
*CALL DIM
      IJK=N1*N2*N3
      CALL PARTIAL(1,U,N1,N2,N3)
      CALL MOVLEV(DUDX(1,1,1),GU(1,1,1),IJK)
      CALL PARTIAL(2,V,N1,N2,N3)
      CALL MOVLEV(DUDX(1,1,1),GV(1,1,1),IJK)
      CALL SINPART(W,N1,N2,N3)
      DIVMAX=0.
      DO 1 L=1,LMAX
      DO 1 J=1,JMAX
      DO 1 I=1,IMAX
      DUM=ABS(GU(I,J,L)+GV(I,J,L)+DUDX(I,J,L))
      IF (DUM .GT. DIVMAX) DIVMAX=DUM
    1 CONTINUE
      PRINT 1100,DIVMAX
      CALL PARTIAL(1,O1,N1,N2,N3)
      CALL MOVLEV(DUDX(1,1,1),GU(1,1,1),IJK)
```

```
      CALL PARTIAL(2,O2,N1,N2,N3)
      CALL MOVLEV(DUDX(1,1,1),GV(1,1,1),IJK)
      CALL COSPART(O3,N1,N2,N3)
      DIVMAX=0.
      DO 2 L=1,LMAX
      DO 2 J=1,JMAX
      DO 2 I=1,IMAX
      DUM=ABS(GU(I,J,L)+GV(I,J,L)+DUDX(I,J,L))
      IF (DUM .GT. DIVMAX) DIVMAX=DUM
    2 CONTINUE
      PRINT 1200,DIVMAX
 1100 FORMAT(1X,* MAXIMUM VELOCITY   DIVERGENCE =*,E15.7)
 1200 FORMAT(1X,* MAXIMUM VORTICITY  DIVERGENCE =*,E15.7)
      RETURN
      END
*DECK EDVIS
      SUBROUTINE EDVIS(COEF2,E,N1,N2,N3)
      DIMENSION E(N1,N2,N3)
C*****************************************************************
C     THIS SUBROUTINE COMPUTES THE EDDY VISCOSITY AND STORES IT IN E   *
C*****************************************************************
*CALL LARGE5
*CALL DATA9
      DO 3 L=1,LMAX
      DO 3 J=1,JMAX
      DO 3 I=1,IMAX
      E(I,J,L)=O1(I,J,L)**2+O2(I,J,L)**2+O3(I,J,L)**2
      E(I,J,L)=SQRT(E(I,J,L))*COEF2
    3 CONTINUE
      RETURN
      END
*DECK FDCT
      SUBROUTINE FDCT(SIGN)
C*****************************************************************
C     FDCT COMPUTES THE FAST DISCRETE COSINE TRANSFORM OF THE VARIABLE *
C     XR AND STORES IN XR                                              *
C*****************************************************************
*CALL DAT21
*CALL DATA9
      LM1=LMAX-1
      CC=2./FLOAT(LM1)
      LL=2*LM1
      XR(1)=XR(1)/2.
      XR(LMAX)=XR(LMAX)/2.
      LP1=LMAX+1
      DO 1 L=LP1,LL
      XR(L)=0.
    1 CONTINUE
      DO 3 L=1,LL
      XI(L)=0.
    3 CONTINUE
      ISN=-SIGN
      CALL FFT(XR,XI,LL,ISN)
      IF (SIGN .GT. 0.) GO TO 200
      DO 100 L=1,LMAX
      XR(L)=XR(L)*CC
  100 CONTINUE
  200 CONTINUE
      RETURN
      END
*DECK FDST
      SUBROUTINE FDST(SIGN)
C*****************************************************************
C     FDST COMPUTES THE FAST DISCRETE SINE TRANSFORM OF THE VARIABLE   *
C     XR AND STORES IT IN XR                                           *
C*****************************************************************
*CALL DAT21
*CALL DATA9
      LM1=LMAX-1
      CC=2./FLOAT(LM1)
```

```
      LL=2*LM1
      XR(1)=0.
      XR(LMAX)=0.
      LP1=LMAX+1
      DO 1 L=LP1,LL
      XR(L)=0.
    1 CONTINUE
      DO 3 L=1,LL
      XI(L)=0.
    3 CONTINUE
      ISN=-SIGN
      CALL FFT(XR,XI,LL,ISN)
      IF (SIGN .GT. 0.) GO TO 200
      DO 100 L=1,LMAX
      XI(L)=XI(L)*CC
  100 CONTINUE
  200 CONTINUE
      DO 2 L=1,LMAX
      XR(L)=-SIGN*XI(L)
    2 CONTINUE
      RETURN
      END
*DECK FFT
          IDENT  FFT  (A,B,N,ISN)                                          FFT2C  2
          ENTRY  FFT                                                       FFT2C  3
*  RADIX 2 COMPLEX FAST FOURIER TRANSFORM, COMPUTED IN PLACE.               FFT2C  4
*  SEE  ON COMPUTING THE FAST FOURIER TRANSFORM,  R. SINGLETON,             FFT2C  5
*    COMM. ACM, V.10, N.10, PP.647-654, OCT. 1967.                          FFT2C  6
*  ARRAY A CONTAINS THE REAL COMPONENT OF THE DATA AND RESULT,              FFT2C  7
*    ARRAY B CONTAINS THE IMAGINARY COMPONENT.                              FFT2C  8
*  N, THE NUMBER OF COMPLEX DATA VALUES,                                    FFT2C  9
*    MUST BE A POWER OF 2 AND GREATER THAN 1                                FFT2C 10
*  THE SIGN OF ISN IS THE SIGN OF THE EXPONENTIAL IN THE TRANSFORM.         FFT2C 11
*  THE MAGNITUDE OF ISN IS THE INCREMENT SIZE FOR INDEXING                  FFT2C 12
*    A AND B, AND IS ONE IN THE USUAL CASE.                                 FFT2C 13
*  DATA MAY ALTERNATIVELY BE STORED FORTRAN COMPLEX                         FFT2C 14
*    IN A SINGLE ARRAY, IN WHICH CASE THE MAGNITUDE                         FFT2C 15
*    OF ISN IS TWO AND ADDRESS B IS A(2), I.E.                              FFT2C 16
*        CALL FFT2(A,A(2),N,2)                                              FFT2C 17
*    INSTEAD OF                                                             FFT2C 18
*        CALL FFT2(A,B,N,1)                                                 FFT2C 19
*  PROGRAM CONTAINS SINE TABLE FOR MAXIMUM N OF 32768                       FFT2C 20
*  6400 TIME FOR N=1024, 220 M.SEC.                                         FFT2C 21
*  6400 TIME FOR N=2**M IS 21.5*N*M MICRO-SEC.                              FFT2C 22
*  6600 TIME FOR N=1024, 44 M.SEC.                                          FFT2C 23
*  6600 TIME FOR N=2**M IS 4.3*N*M MICRO-SEC.                               FFT2C 24
*  RMS ERROR FOR TRANSFORM-INVERSE IS LESS THAN 1.3E-13                     FFT2C 25
*    FOR N=32768 OR SMALLER.                                                FFT2C 26
*  FORTRAN 2.3 SUBROUTINE                                                   FFT2C 27
*  BY R. C. SINGLETON, STANFORD RESEARCH INSTITUTE, NOV. 1968               FFT2C 28
 L100     SX0    B3                NN                                      FFT2C 29
          SB4    B0                KK=0                                    FFT2C 30
          SB3    B3-B7             NN=NN-INC                               FFT2C 31
          AX0    1                 KSPAN=NN/2                              FFT2C 32
          SB5    B0                K2=0                                    FFT2C 33
          SB6    X0                                                        FFT2C 34
          SX1    B5                K2=K2                                   FFT2C 35
          EQ     B6,B7,FFT         IF(KSPAN .EQ. INC) RETURN               FFT2C 36
 L110     SB4    B3-B4             KK=NN-KK                                FFT2C 37
          SB5    B3-B5             K2=NN-K2                                FFT2C 38
          SA2    B1+B4             EXCHANGE A(KK),A(K2) AND B(KK),B(K2)    FFT2C 39
          SA3    B1+B5                                                     FFT2C 40
          SA4    B2+B4                                                     FFT2C 41
          NX7    X2                                                        FFT2C 42
          SA5    B2+B5                                                     FFT2C 43
          NX6    X3                                                        FFT2C 44
          SA7    A3                                                        FFT2C 45
          SA6    A2                                                        FFT2C 46
          NX7    X4                                                        FFT2C 47
          NX6    X5                                                        FFT2C 48
```

```
         SA7    A5                                                    FFT2C 49
         SA6    A4                 END OF EXCHANGE                    FFT2C 50
         LT     B6,B4,L110         IF(KSPAN .LT. KK) GO TO L110       FFT2C 51
L120     SB4    B4+B7              KK=KK+INC                          FFT2C 52
         SB5    B6+B5              K2=KSPAN+K2                        FFT2C 53
         SA2    B1+B4              EXCHANGE A(KK),A(K2) AND B(KK),B(K2) FFT2C 54
         SA3    B1+B5                                                 FFT2C 55
         SA4    B2+B4                                                 FFT2C 56
         NX7    X2                                                    FFT2C 57
         SA5    B2+B5                                                 FFT2C 58
         NX6    X3                                                    FFT2C 59
         SA7    A3                                                    FFT2C 60
         SA6    A2                                                    FFT2C 61
         NX7    X4                                                    FFT2C 62
         SX0    B6                 K=KSPAN                            FFT2C 63
         NX6    X5                                                    FFT2C 64
         SA7    A5                                                    FFT2C 65
         SA6    A4                 END OF EXCHANGE                    FFT2C 66
L130     AX0    1                  K=K/2                              FFT2C 67
         IX1    X1-X0              K2=K2-K                            FFT2C 68
         PL     X1,L130            IF(K2 .GE. 0) GO TO L130           FFT2C 69
         LX0    1                  K=K+K                              FFT2C 70
         SB4    B4+B7              KK=KK+INC                          FFT2C 71
         IX1    X1+X0              K2=K2+K                            FFT2C 72
         SB5    X1                 K2=K2                              FFT2C 73
         GE     B5,B4,L110         IF(K2 .GE. KK) GO TO L110          FFT2C 74
         LT     B4,B6,L120         IF(KK .LT. KSPAN) GO TO L120       FFT2C 75
FFT                                                                   FFT2C 76
      SB1    X1                                                       INSR1  1
      SA1    A1+1                                                     INSR1  2
      SB2    X1                                                       INSR1  3
      SA1    A1+1                                                     INSR1  4
      SB3    X1                                                       INSR1  5
      SA1    A1+1                                                     INSR1  6
      SB4    X1                                                       INSR1  7
       SA4    B4                 ISN                                FFT2C 77
       MX2    1                  MASK                               FFT2C 78
       SA5    L60                                                   FFT2C 79
       SA3    B3                 N                                  FFT2C 80
       LX2    57                                                    FFT2C 81
       PX7    X3                                                    FFT2C 82
       BX6    -X2*X5                                                FFT2C 83
       PL     X4,L10             IF(ISN .GE. 0) GO TO L10           FFT2C 84
       BX6    X2+X5                                                 FFT2C 85
       BX4    -X4                INC=-INC                           FFT2C 86
L10    LX3    32                                                    FFT2C 87
       SA6    A5                                                    FFT2C 88
       NX0    B5,X3                                                 FFT2C 89
       PX2    X4                                                    FFT2C 90
       SB7    X4                                                    FFT2C 91
       DX7    X2*X7                                                 FFT2C 92
       SA1    B5+S               S(M)                               FFT2C 93
       SB3    X7                 NN=INC*N                           FFT2C 94
       SB6    X7                 KSPAN=NN                           FFT2C 95
       EQ     L40                GO TO L40                          FFT2C 96
L20    SA3    CD                                                    FFT2C 97
       RX4    X2*X1              SD*CN                              FFT2C 98
       RX7    X2*X0              SD*SN                              FFT2C 99
       RX5    X3*X0              CD*SN                              FFT2C100
       RX6    X3*X1              CD*CN                              FFT2C101
       RX4    X4-X5                                                 FFT2C102
       RX6    X6+X7                                                 FFT2C103
       NX5    X4                                                    FFT2C104
       RX7    X1-X6                                                 FFT2C105
       RX0    X0+X5                                                 FFT2C106
       NX1    X7                                                    FFT2C107
L30    SB5    B6+B4              K2=KSPAN+KK                        FFT2C108
       SA2    B1+B4              A(KK)                              FFT2C109
       SA3    B1+B5              A(K2)                              FFT2C110
       SA4    B2+B4              B(KK)                              FFT2C111
```

```
          RX6     X2+X3                                                  FFT2C112
          SA5     B2+B5               B(K2)                              FFT2C113
          RX2     X2-X3               RE                                 FFT2C114
          SA6     A2                  A(KK)                              FFT2C115
          RX7     X4+X5                                                  FFT2C116
          RX3     X1*X2               CN*RE                              FFT2C117
          RX4     X4-X5               IM                                 FFT2C118
          SA7     A4                  B(KK)                              FFT2C119
          RX5     X0*X4               SN*IM                              FFT2C120
          RX2     X0*X2               SN*RE                              FFT2C121
          RX6     X3-X5                                                  FFT2C122
          RX4     X1*X4               CN*IM                              FFT2C123
          SA6     A3                  A(K2)                              FFT2C124
          RX7     X2+X4                                                  FFT2C125
          SB4     B6+B5               KK=KSPAN+K2                        FFT2C126
          SA7     A5                  B(K2)                              FFT2C127
          LT      B4,B3,L30           IF(KK .LT. NN) GO TO L30           FFT2C128
          SB5     B4-B3               K2=KK-NN                           FFT2C129
          BX1     -X1                 CN=-CN                             FFT2C130
          SB4     B6-B5               KK=KSPAN-K2                        FFT2C131
          LT      B5,B4,L30           IF(K2 .LT. KK) GO TO L30           FFT2C132
          SB4     B4+B7               KK=KK+INC                          FFT2C133
          SA2     SD                                                     FFT2C134
          LT      B4,B5,L20           IF(KK .LT. K2) GO TO L20           FFT2C135
L40       SB4     B0                  KK=0                               FFT2C136
          SX5     B6                                                     FFT2C137
          AX5     1                   KSPAN=KSPAN/2                      FFT2C138
          SB6     X5                                                     FFT2C139
L50       SB5     B6+B4               K2=KSPAN+KK                        FFT2C140
          SA2     B1+B4               A(KK)                              FFT2C141
          SA3     B1+B5               A(K2)                              FFT2C142
          SA4     B2+B4               B(KK)                              FFT2C143
          RX6     X2+X3                                                  FFT2C144
          SA5     B2+B5               B(K2)                              FFT2C145
          RX7     X2-X3                                                  FFT2C146
          SA6     A2                  A(KK)                              FFT2C147
          SA7     A3                  A(K2)                              FFT2C148
          RX6     X4+X5                                                  FFT2C149
          SB4     B6+B5               KK=KSPAN+K2                        FFT2C150
          RX7     X4-X5                                                  FFT2C151
          SA6     A4                  B(KK)                              FFT2C152
          SA7     A5                  B(K2)                              FFT2C153
          LT      B4,B3,L50           IF(KK .LT. NN) GO TO L50           FFT2C154
          EQ      B6,B7,L100          IF(KSPAN .EQ. INC) GO TO L100      FFT2C155
          SA1     A1                  S(M)                               FFT2C156
          SB4     B7                  KK=INC                             FFT2C157
          RX6     X1*X1                                                  FFT2C158
          SA1     A1+1                M=M+1, S(M)                        FFT2C159
          FX6     X6+X6                                                  FFT2C160
          SA3     ONE                                                    FFT2C161
          SA6     CD                  CD=2*S(M)**2                       FFT2C162
L60       BX0     X1                  SN=SD                              FFT2C163
          RX6     X3-X6               CN=1.0-CD                          FFT2C164
          BX7     X0                                                     FFT2C165
          NX1     X6                                                     FFT2C166
          SA7     SD                                                     FFT2C167
          EQ      L30                 GO TO L30                          FFT2C168
S         DATA    9.5873799095977346E-5                                  FFT2C169
          DATA    1.9174759731070331E-4                                  FFT2C170
          DATA    3.8349518757139559E-4                                  FFT2C171
          DATA    7.6699031874270453E-4                                  FFT2C172
          DATA    1.5339801862847656E-3                                  FFT2C173
          DATA    3.0679567629659763E-3                                  FFT2C174
          DATA    6.1358846491544754E-3                                  FFT2C175
          DATA    1.2271538285719926E-2                                  FFT2C176
          DATA    2.4541228522912288E-2                                  FFT2C177
          DATA    4.9067674327418014E-2                                  FFT2C178
          DATA    9.8017140329560602E-2                                  FFT2C179
          DATA    1.9509032201612827E-1                                  FFT2C180
          DATA    3.8268343236508977E-1                                  FFT2C181
```

```
          DATA    0.7071067811865475                                      FFT2C182
 ONE      DATA    1.0                                                     FFT2C183
 CD                                                                       FFT2C184
 SD                                                                       FFT2C185
      END
*DECK FFTX
      SUBROUTINE FFTX(SIGN)
C*************************************************************************
C FAST FOURIER TRANSFORM IN X-DIRECTION
C*************************************************************************
*CALL DATA9
*CALL DATA7
*CALL DAT21
      ISN=-SIGN
      IF (SIGN .LT. 0.) GO TO 3
      DO 1 J=1,JMAX
      DO 1 I=1,IMAX
      FI(I,J)=0.
    1 CONTINUE
    3 CONTINUE
      DO 100 J=1,JMAX
      DO 110 I=1,IMAX
      XR(I)=FR(I,J)
      XI(I)=FI(I,J)
  110 CONTINUE
      CALL FFT(XR,XI,IMAX,ISN)
      DO 120 I=1,IMAX
      FR(I,J)=XR(I)
      FI(I,J)=XI(I)
  120 CONTINUE
  100 CONTINUE
      RETURN
      END
*DECK FFTY
      SUBROUTINE FFTY(SIGN,COEF3)
C*************************************************************************
C FAST FOURIER TRANSFORM IN Y-DIRECTION                                  *
C*************************************************************************
*CALL DATA9
*CALL DATA7
*CALL DAT21
      ISN=-SIGN
      DO 100 I=1,IMAX
      DO 110 J=1,JMAX
      XR(J)=FR(I,J)
      XI(J)=FI(I,J)
  110 CONTINUE
      CALL FFT(XR,XI,JMAX,ISN)
      IF (SIGN .LT. 0.) GO TO 200
      DO 120 J=1,JMAX
      FR(I,J)=XR(J)
      FI(I,J)=XI(J)
  120 CONTINUE
      GO TO 100
  200 DO 130 J=1,JMAX
      FR(I,J)=XR(J)*COEF3
      FI(I,J)=XI(J)*COEF3
  130 CONTINUE
  100 CONTINUE
      RETURN
      END
*DECK FIX
      SUBROUTINE FIX(IM1,I,IP1,IMAX)
      IM1=I-1
      IP1=I+1
      IF(I .EQ. 1) IM1=IMAX
      IF(I .EQ. IMAX) IP1=1
      RETURN
      END
*DECK INICON
```

```
      SUBROUTINE INICON(C,COF,DT,UR,VR,WR,UI,VI,WI,L1,L2,L3)
      REAL NDIV,N12,NSQR
      DIMENSION UR(L1,L2,L3),VR(L1,L2,L3),WR(L1,L2,L3)
      DIMENSION UI(L1,L2,L3),VI(L1,L2,L3),WI(L1,L2,L3)
C*****************************************************************
C THIS SUBROUTINE INITIATES THE PROGRAM. FOR STARTING PROBLEM, THE INI-*
C TIAL FIELD IS GENERATED.  FOR CONTINUATION PROBLEM, THE DATA STORED  *
C ON TAPE AT THE END OF THE PREVIOUS RUN ARE READ IN.                  *
C*****************************************************************
C-----NSTART=1  STARTING FROM TIME STEP=0
C-----NSTART=2 CONTINUED FROM PREVIOUS RUN
C-----IMAX=MAXIMUM MESH NUMBER IN X-DIRECTION
C-----JMAX=MAXIMUM MESH NUMBER IN Y-DIRECTION
C-----LMAX=MAXIMUM MESH NUMBER IN Z-DIRECTION
C-----TSTART=STARTING TIME STEP
C-----TEND=ENDING TIME STEP
C-----DELTA= MESH SIZE
C-----DT=TIME STEP
C-----C=MODEL CONSTANT
C-----NAVG=DELTA(AVERAGING)/DELTA(MESH)
C-----ANISO= R IN EQUATION (5.16B)
C-----GAMMA=STRAIN RATE
      REAL NAVG
      COMMON/LARGE1/EN(1024),EN1(1024),WN(2048)
      LEVEL 2,UR,VR,WR,UI,VI,WI
      LEVEL 2,EN,EN1,WN
*CALL DATA7
      READ 4, DELTA,DT,C, NAVG,ANISO,UTM,GAMMA
      IMAX=16
      JMAX=16
      LMAX=16
      IJK=IMAX*JMAX*LMAX
      IJ=IMAX*JMAX
      IMM1=IMAX-1
      IMP1=IMAX+1
      NMESH=IMAX
      TDIV=1.0/(IMAX*JMAX*LMAX)
      NHALF=NMESH/2
      NHP1=NHALF+1
      HALF=FLOAT(NHALF)
      NM1=NMESH-1
      RISO=3./(3.+ANISO)
      TEMP=ANISO/3.
      RANISO=SQRT(TEMP)
      CC=1.
      TFAC=IMAX*JMAX*LMAX
      FAC=SQRT(TFAC)
      COEF10=3.1415926535898/NHALF
      COEF11=COEF10
      COEF12=3.1415926535898*2.
      CONST=COEF10/ DELTA
      COEF15=COEF12*FAC
      PI1=COEF10
      PI2=PI1*2.
      COF=1.0
      NCONT=1
      DO 2 M=1,25
      Y9=RGEN(X9)
    2 CONTINUE
C-----ENERGY SPECTRUM DATA
C-----  0.1 INTERVAL UP TO 1.0   THEN .5 INTERVALL UP TO 6.0
C-----EN IS THE ENERGY SPECTRUM FOR THE ISOTROPIC PART.  EN1 IS FOR THE
C ANISOTROPIC PART.
      PRINT 1960
      WN(1)=0.1
      DO 1900 M=2,10
 1900 WN(M)=0.1+WN(M-1)
      DO 1950 M=11,24
 1950 WN(M)=0.5+WN(M-1)
 1960 FORMAT(/5X,*WAVE NUMBER*,/)
```

```
      PRINT 4, (WN(M),M=1,24)
      PRINT 2000
 2000 FORMAT(/5X,*UNFILTERED SPECTRUM*,/)
      DO 3 M=1,24,8
      M7=M+7
      READ 4, (EN(MM),MM=M,M7)
      PRINT 702,(EN(MM),MM=M,M7)
    3 CONTINUE
      DO 503 M=1,24,8
      M7=M+7
      READ 4, (EN1(MM),MM=M,M7)
      PRINT 702,(EN1(MM),MM=M,M7)
  503 CONTINUE
    4 FORMAT (8E10.4)
      DELAVG=(DELTA*NAVG)**2/12.0
      PAI=3.1415926535898
      DO    2100 M=1,24
      EXPF=EXP(-DELAVG*WN(M)*WN(M))
      EN(M)=EN(M)*EXPF
 2100 EN1(M)=EN1(M)*EXPF
      PRINT 2200
 2200 FORMAT(/5X,*FILTERED SPECTRUM*,/)
      PRINT 702,(EN(M),M=1,24)
      PRINT 702,(EN1(M),M=1,24)
      DO 5 L=1,LMAX
      DO 5 J=1,JMAX
      DO 5 I=1,IMAX
      UR(I,J,L)=0.
      VR(I,J,L)=0.
      WR(I,J,L)=0.
      UI(I,J,L)=0.
      VI(I,J,L)=0.
      WI(I,J,L)=0.
    5 CONTINUE
      DO 40 L=1,NHALF
      LL=L
      N3=L-1
      N3S=N3**2
      DO 30 J=1,NM1
      JINDEX=J/NHALF
      JJ=J+NHP1-JINDEX*JMAX
      N2=J-NHALF
      N2S=N2**2
      DO 20 I=1,NM1
      IINDEX=I/NHALF
      II=I+NHP1-IINDEX*IMAX
      N1=I-NHALF
      N1S=N1**2
      NSQR=N1S+N2S+N3S
      IF (NSQR .LT. 0.1) GO TO 20
      WAVN=SQRT(NSQR)
      NDIV=1./WAVN
      N12=N1S+N2S
      IF (N12 .LT. 0.1) NCONT=2
      IF (IABS(N1) .EQ. NHALF .AND.IABS(N2) .EQ. NHALF) NCONT=2
C-----GET FOURIER AMPLITUDE OF THE INITIAL FIELD AD DESCRIBED IN SEC 4.4
      X=CONST*WAVN
      NREG=X+1.
      GO TO (310,315,315,315,315,315,315) NREG
  310 M=X/0.1
      YM=X-0.1*M
      M1=M+1
      ED=EN(M1)-EN(M)
      ENERGY=EN(M)+ED*YM*10.
      EDA=EN1(M1)-EN1(M)
      EANISO=EN1(M)+EDA*YM*10.
      GO TO 320
  315 M=(X-1.)*2.
      YM=X-1.-0.5*M
      M=M+10
```

```
      M1=M+1
      ED=EN(M1)-EN(M)
      ENERGY=EN(M)+ED*YM*2.
      EDA=EN1(M1)-EN1(M)
      EANISO=EN1(M)+EDA*YM*2.
  320 QS=ENERGY*RISO/(COEF15*X**2)
      QN=SQRT(QS)
      QSA=EANISO*RISO/(COEF15*X**2)
      QNA=SQRT(QSA)
C-----CHANGE WAVE NUMBER VECTOR TO SATISFY NUMERICSL DIV FREE
C-----R1,R2 AND R3 ARE THE MODIFIED WAVE NUMBER
      IF(NCONT.EQ.2)GO TO 340
      ARG1=PI1*N1
      ARG2=PI2*N1
      R1=ARG1/DELTA
      ARG1=PI1*N2
      ARG2=PI2*N2
      R2=ARG1/DELTA
      ARG1=PI1*N3
      ARG2=PI2*N3
      R3=ARG1/DELTA
      R1S=R1**2
      R2S=R2**2
      R3S=R3**2
      R12S=R1S+R2S
      RSQ=R12S+R3S
      IF(NCONT.EQ.2) GO TO 340
      R12=SQRT(R12S)
      R12DIV=1./R12

      R12=SQRT(R12S)
      R12DIV=1./R12
      RDIV=1./SQRT(RSQ)
C ----GET A & B  VECTOR
C     FIRST CHOOSE RANDOM PHI
  340 CONTINUE
      YY=RGEN(XX)
      PHI=YY*COEF12
      CPHI=COS(PHI)
      SPHI=SIN(PHI)
      IF(NCONT.EQ.2)GO TO 11
      A1=(-R2*CPHI+R1*R3*RDIV*SPHI)*R12DIV
      A2=(R1*CPHI+R2*R3*RDIV*SPHI)*R12DIV
      A3=-R12*RDIV*SPHI
C     CALL RANDOM PHI
      Y2=RGEN(X2)
      PHI=Y2*COEF12
      CPHI=COS(PHI)
      SPHI=SIN(PHI)
      B1=(-R2*CPHI+R1*R3*RDIV*SPHI)*R12DIV
      B2=(R1*CPHI+R2*R3*RDIV*SPHI)*R12DIV
      B3=-R12*RDIV*SPHI
      GO TO 12
   11 CONTINUE
      INDEX=(YY+0.25)*4
      PHI=0.7853982*(2*INDEX-1)
      A1=SIN(PHI)
      A2=COS(PHI)
      A3=0.
      Y1=RGEN(X1)
      INDEX=(Y1+0.25)*4
      PHI=0.7853982*(2*INDEX-1)
      B1=SIN(PHI)
      B2=COS(PHI)
      B3=0.
      NCONT=1
   12 CONTINUE
C     DETERMINE A AND B IN EQUATION (4.6)
C     RANDOM THETA
      Y3=RGEN(X3)
```

```
      THETA=Y3*COEF12
      CA=COS(THETA)
      CB=SIN(THETA)
      UR(II,JJ,LL)=QN*CA*A1
      VR(II,JJ,LL)=QN*CA*A2
      WR(II,JJ,LL)=QN*CA*A3
      UI(II,JJ,LL)=QN*CB*B1
      VI(II,JJ,LL)=QN*CB*B2
      WI(II,JJ,LL)=QN*CB*B3
      IF (N3 .NE. 0) GO TO 20
      WSIGN=ABS(A3)/A3
      VSIGN=ABS(B3)/B3
      WRAN=QNA*CA*RANISO
      WIAN=QNA*CB*RANISO
      WR(II,JJ,LL)=WR(II,JJ,LL)+WRAN*WSIGN
      WI(II,JJ,LL)=WI(II,JJ,LL)+WIAN*VSIGN
   20 CONTINUE
   30 CONTINUE
   40 CONTINUE
C     NOW THE UPPER HALF OF THE K-SPACE HAS BEEN DETERMINED
C     GET THE TRANSFORMED VELOCITY AT THE CONJUGATE POINTS
C-----CONJUGATE FORM
C     N3=1 TO 7, N1 & N2=-7 TO 7
C     N3=L-1     -N3=LM
C     N2=J-1     -N2=JM
      IMP2=IMAX+2
      DO 41 L=2,NHALF
      LM=L+IMP2-2*L
      DO 41 J=1,JMAX
      M=(J+IMM1)/IMP1
      JM=J+(IMP2-2*J)*M
      DO 41 I=1,IMAX
      M=(I+IMM1)/IMP1
      IM=I+(IMP2-2*I)*M
      UR(IM,JM,LM)= UR(I,J,L)
      VR(IM,JM,LM)= VR(I,J,L)
      WR(IM,JM,LM)= WR(I,J,L)
      UI(IM,JM,LM)=-UI(I,J,L)
      VI(IM,JM,LM)=-VI(I,J,L)
      WI(IM,JM,LM)=-WI(I,J,L)
   41 CONTINUE
C     N3=0, N1=1 TO 7, N2=-7 TO 7
      DO 42 I=2,NHALF
      IM=I+(IMP2-2*I)
      DO 42 J=1,JMAX
      M=(J+IMM1)/IMP1
      JM=J+(IMP2-2*J)*M
      IF(J.EQ.NHP1) GO TO 42
      UR(IM,JM,1 )= UR(I,J,1)
      VR(IM,JM,1 )= VR(I,J,1)
      WR(IM,JM,1 )= WR(I,J,1)
      UI(IM,JM,1 )=-UI(I,J,1)
      VI(IM,JM,1 )=-VI(I,J,1)
      WI(IM,JM,1 )=-WI(I,J,1)
   42 CONTINUE
C     N1=N3=0
      DO 43 J=2,NHALF
      JM=J+(IMP2-2*J)
      UR(1,JM,1)= UR(1,J,1)
      VR(1,JM,1)= VR(1,J,1)
      WR(1,JM,1)= WR(1,J,1)
      UI(1,JM,1)=-UI(1,J,1)
      VI(1,JM,1)=-VI(1,J,1)
      WI(1,JM,1)=-WI(1,J,1)
   43 CONTINUE
C     X AND Y TRANSFORM
      SIGN=-1.
      DO 50 L=1,LMAX
      CALL MOVLEV(UR(1,1,L),FR(1,1),IJ)
      CALL MOVLEV(UI(1,1,L),FI(1,1),IJ)
```

```
      CALL FFTX(SIGN)
      CALL FFTY(SIGN,CC)
      CALL MOVLEV(FR(1,1),UR(1,1,L),IJ)
      CALL MOVLEV(FI(1,1),UI(1,1,L),IJ)
      CALL MOVLEV(VR(1,1,L),FR(1,1),IJ)
      CALL MOVLEV(VI(1,1,L),FI(1,1),IJ)
      CALL FFTX(SIGN)
      CALL FFTY(SIGN,CC)
      CALL MOVLEV(FR(1,1),VR(1,1,L),IJ)
      CALL MOVLEV(FI(1,1),VI(1,1,L),IJ)
      CALL MOVLEV(WR(1,1,L),FR(1,1),IJ)
      CALL MOVLEV(WI(1,1,L),FI(1,1),IJ)
      CALL FFTX(SIGN)
      CALL FFTY(SIGN,CC)
      CALL MOVLEV(FR(1,1),WR(1,1,L),IJ)
      CALL MOVLEV(FI(1,1),WI(1,1,L),IJ)
   50 CONTINUE
C     Z TRANSFORM
      DO 51 I=1,IMAX
      DO 52 L=1,LMAX
      DO 52 J=1,JMAX
      FR(J,L)=UR(I,J,L)
      FI(J,L)=UI(I,J,L)
   52 CONTINUE
      CALL FFTY(SIGN,1.0)
      DO 53 L=1,LMAX
      DO 53 J=1,JMAX
      UR(I,J,L)=FR(J,L)
   53 CONTINUE
   51 CONTINUE
      DO 54 I=1,IMAX
      DO 55 L=1,LMAX
      DO 55 J=1,JMAX
      FR(J,L)=VR(I,J,L)
      FI(J,L)=VI(I,J,L)
   55 CONTINUE
      CALL FFTY(SIGN,1.0)
      DO 56 L=1,LMAX
      DO 56 J=1,JMAX
      VR(I,J,L)=FR(J,L)
   56 CONTINUE
   54 CONTINUE
      DO 57 I=1,IMAX
      DO 58 L=1,LMAX
      DO 58 J=1,JMAX
      FR(J,L)=WR(I,J,L)
      FI(J,L)=WI(I,J,L)
   58 CONTINUE
      CALL FFTY(SIGN,1.0)
      DO 59 L=1,LMAX
      DO 59 J=1,JMAX
      WR(I,J,L)=FR(J,L)
   59 CONTINUE
   57 CONTINUE
C-----THE INITIAL FIELD HAS BEEN GENERATED.  THE FOLLOWING IS TO PRINT
C     OUT  INFORMATION ON THE GENERATED FIELD
C     VELOCITIES ARE STORED IN UR. VR AND WR
C-----TURBULENT ENERGY CHECK
      TKU=0.
      TKV=0.
      TKW=0.
      DO 95 L=1, LMAX
      DO 95 J=1, JMAX
      DO 95 I=1, IMAX
      TKU=TKU+UR(I,J,L)**2
      TKV=TKV+VR(I,J,L)**2
      TKW=TKW+WR(I,J,L)**2
   95 CONTINUE
      TKU=TKU*TDIV
      TKV=TKV*TDIV
```

```
      TKW=TKW*TDIV
      TKSUM=TKU+TKV+TKW
      TKUR=TKU/TKSUM
      TKVR=TKV/TKSUM
      TKWR=TKW/TKSUM
      PRINT 707
      PRINT 706
      PRINT 700,DT,DELTA,C,NAVG,ANISO,UTM,GAMMA
      PRINT 702, TKU,TKV,TKW, TKSUM
      PRINT 702,TKUR,TKVR,TKWR
      PRINT 706
      PRINT 601.
      UTOT=0.
      VTOT=0.
      WTOT=0.
      DO 120 L=1,LMAX
      PRINT 710,L
      USUM=0.
      VSUM=0.
      WSUM=0.
      DO 116 J=1,JMAX
      DO 116 I=1,IMAX
      USUM=USUM+UR(I,J,L)
      VSUM=VSUM+VR(I,J,L)
      WSUM=WSUM+WR(I,J,L)
  116 CONTINUE
      PRINT 702,(UR(I,10,L),I=1,NHALF)
      PRINT 702,(VR(I,10,L),I=1,NHALF)
      PRINT 702,(WR(I,10,L),I=1,NHALF)
      PRINT 702, USUM,VSUM,WSUM
      UTOT=UTOT+USUM
      VTOT=VTOT+VSUM
      WTOT=WTOT+WSUM
  120 CONTINUE
      PRINT 702,UTOT,VTOT,WTOT
  700 FORMAT(1X  ,*INITIAL CONDITION.  DT=*1PE10.4,*  DELTA=*1PE10.4,
     1 *   C=*,0PF7.4,3X,*AVERAGING GRID=*,F4.1, *  DELTA*,/,18X,
     2*ANISO=*,E12.5,3X,*UTM=*,E12.5,3X,*GAMMA=*,E12.5)
  702 FORMAT(1P8E15.7)
  705 FORMAT(1X,  *CONTINUED AT TIME STEP=*,I4,/,/)
  706 FORMAT(1H0,130H**********************************************************
     -**********************************************************
     -**********    )
  707 FORMAT (1H1)
  710 FORMAT(1X,*PLANE=*,I3)
  711 FORMAT(1X,* INITIAL CONDITION*,/1X,*DT=*1PE10.4,*  DELTA=*1PE10.4
     - ,*  C=*,F7.4, *  U0=*1PE10.4,/)
  601 FORMAT(1X,*UM,VM,WM*)
      RETURN
      END
*DECK INIFILT
      SUBROUTINE INIFILT(U,N1,N2,N3)
      DIMENSION U(N1,N2,N3)
C*****************************************************************
C     THIS SUBROUTINE IS USED TO FILTER THE INITIAL FIELD WITH A WIDE
C     FILTER ONLY IN THE Z-DIRECTION.
C*****************************************************************
*CALL FLT
*CALL DAT21
*CALL DATA7
*CALL DATA9
      LEVEL 2,U
      LMAXM1=LMAX-1
      DO 5 L=1,LMAX
      XR(L)=EXP(-FLOAT(L-1)**2/8.0)
    5 CONTINUE
      AREA=0.5*XR(1)
      DO 6 L=2,LMAXM1
      AREA=AREA+XR(L)
    6 CONTINUE
```

```
      AREA=AREA+0.5*XR(LMAX)
      DO 7 L=1,LMAX
      XR(L)=XR(L)/AREA
    7 CONTINUE
      CALL FDCT(1.0)
      DO 8 L=1,LMAX
      FILT3(L)=XR(L)
    8 CONTINUE
      DO 1 J=1,JMAX
      DO 1 I=1,IMAX
      DO 2 L=1,LMAX
      XR(L)=U(I,J,L)
    2 CONTINUE
      CALL FDCT(1.0)
      DO 3 L=1,LMAX
      XR(L)=XR(L)*FILT3(L)
    3 CONTINUE
      CALL FDCT(-1.0)
      DO 4 L=1,LMAX
      U(I,J,L)=XR(L)
    4 CONTINUE
    1 CONTINUE
      RETURN
      END
*DECK INVERS
      SUBROUTINE INVERS(G,PM,HM,IC,N1,N2,N3)
C*****************************************************************
C     INVERS IS A POISSON SOLVER. IC = 3 IT EXPANDS THE VARIABLE G     *
C     IN COSINE SERIES IN THE Z-DIRECTION OTHERWISE IT EXPANDS G       *
C     IN SINE SERIES IN THE Z-DIRECTION. IN THE OTHER TWO DIRECTIONS   *
C     FOURIER SERIES ARE USED TO EXPAND G                              *
C*****************************************************************
      DIMENSION G(N1,N2,N3),PM(N1,N2,N3),HM(N1,N2,N3)
*CALL DATA9
*CALL DAT21
*CALL DATA7
*CALL WV
      LEVEL 2,G,PM
      IJ=N1*N2
      CC=1./(IMAX*JMAX)
C*****TRANSFER G TO HM
      DO 10 J=1,JMAX
      DO 10 I=1,IMAX
      DO 20 L=1,LMAX
      XR(L)=-G(I,J,L)
   20 CONTINUE
      IF (IC .EQ. 3) GO TO 100
      CALL FDST(1.0)
      GO TO 200
  100 CALL FDCT(1.0)
  200 DO 30 L=1,LMAX
      HM(I,J,L)=XR(L)
   30 CONTINUE
   10 CONTINUE
      DO 40 L=1,LMAX
      CALL MOVLEV(HM(1,1,L),FR(1,1),IJ)
      CALL FFTX(1.0)
      CALL FFTY(1.0,1.0)
      DO 50 J=1,JMAX
      DO 50 I=1,IMAX
      WAV=WAVEXS(I)+WAVEYS(J)+WAVEZS(L)
      IF (ABS(WAV) .LT. 0.00001) GO TO 500
      WAV=1./WAV
      FR(I,J)=FR(I,J)*WAV
      FI(I,J)=FI(I,J)*WAV
      GO TO 50
  500 FR(I,J)=0.
      FI(I,J)=0.
   50 CONTINUE
      CALL FFTY(-1.0,CC)
```

```
      CALL FFTX(-1.0)
      CALL MOVLEV(FR(1,1),HM(1,1,L),IJ)
   40 CONTINUE
      DO 60 J=1,JMAX
      DO 60 I=1,IMAX
      DO 70 L=1,LMAX
      XR(L)=HM(I,J,L)
   70 CONTINUE
      IF (IC .EQ. 3) GO TO 300
      CALL FDST(-1.0)
      GO TO 400
  300 CALL FDCT(-1.0)
  400 DO 80 L=1,LMAX
      PM(I,J,L)=XR(L)
   80 CONTINUE
   60 CONTINUE
      RETURN
      END
*DECK MEANINI
      SUBROUTINE MEANINI
      COMMON/NORM/ DELU,THETA
*CALL DEL
C
      COMMON/LARGE4/O1D(16,16,33),O2D(16,16,33),O3D(16,16,33)
      LEVEL 2,O1D,O2D,O3D
*CALL BLANK
*CALL DIM
*CALL LARGE2
*CALL LARGE3
*CALL LARGE5
*CALL DATA9
C*********************************************************************
C     THIS ROUTINE CREATS THE MEAN INITIAL FIELD . INITIAL SPICKS     *
C     ARE STORED IN GU THEN FILTERED TO THE CREAT THE GAUSIAN CORE  . *
C*********************************************************************
      DO 500 L=1,LMAX
      DO 500 J=1,JMAX
      DO 500 I=1,IMAX
      GU(I,J,L)=0.
  500 CONTINUE
      DO 501 J=1,JMAX
      GU( 6,J,17)=20.
      GU(11,J,17)=20.
  501 CONTINUE
      PRINT 1110
 1110 FORMAT(1H1,5X,* INITIAL VORTEX AT PLANE 1*)
      PRINT 1115,(((GU(I,1,L),I=1,IMAX),L),L=1,LMAX)
 1115 FORMAT(1X,16F8.2,I3)
      CALL STFILT
      CALL SFILTER(GU,DUDX,N1,N2,N3)
      PRINT 1113
 1113 FORMAT(1H1,5X,*FILTERED VORTEX AT PLANE 1*)
      PRINT 1115,(((GU(I,1,L),I= 1,16  ),L),L=1,LMAX)
      DO 508 L=1,LMAX
      DUDX(1,1,L)=0.0
      DO 508 J=1,JMAX
      DO 508 I=1,IMAX
      DUDX(1,1,L)=DUDX(1,1,L)+GU(I,J,L)/(IMAX*JMAX)
  508 CONTINUE
      DO 509 L=1,LMAX
      DO 509 J=1,JMAX
      DO 509 I=1,IMAX
      GU(I,J,L)=DUDX(1,1,L)
  509 CONTINUE
      DO 502 L=1,LMAX
      DO 502 J=1,JMAX
      DO 502 I=1,IMAX
      O2(I,J,L)=O2(I,J,L)+GU(I,J,L)
  502 CONTINUE
      CALL INVERS(O1,GU,DUDX,1,N1,N2,N3)
```

```
      CALL INVERS(02,GV,DUDX,2,N1,N2,N3)
      CALL INVERS(03,GW,DUDX,3,N1,N2,N3)
      CALL CURLO(GU,GV,GW,U,V,W,N1,N2,N3)
C     COMPUTE THE MEAN INITIAL VELOCITY FIELD AND NORMILIZE THE EQUATION
C     WITH DELTA U(DELU) FOR THE VELOCITY SCALE AND THETA THE MOMENTUM
C     THICKNESS FOR THE LENGTH SCALES.
      CDUM=1./(IMAX*JMAX)
      DO 506 L=1,LMAX
      DUDX(1,1,L)=0.
      DO 506 J=1,JMAX
      DO 506 I=1,IMAX
      DUDX(1,1,L)=DUDX(1,1,L)+U(I,J,L)*CDUM
  506 CONTINUE
      DELU=DUDX(1,1,LMAX)-DUDX(1,1,1)
      THETA=(0.25-(DUDX(1,1,1)/DELU)**2)*0.5
      LMAXM1=LMAX-1
      DO 504 L=2,LMAXM1
      THETA=THETA+(0.25-(DUDX(1,1,L)/DELU)**2)
  504 CONTINUE
      THETA=THETA+(0.25-(DUDX(1,1,LMAX)/DELU)**2)*0.5
      THETA=THETA*DELTAZ
      DELTAX=DELTAX/THETA
      DELTAY=DELTAY/THETA
      DELTAZ=DELTAZ/THETA
      CALL STWV
      DO 505 L=1,LMAX
      DO 505 J=1,JMAX
      DO 505 I=1,IMAX
      U(I,J,L)=U(I,J,L)/DELU
      V(I,J,L)=V(I,J,L)/DELU
      W(I,J,L)=W(I,J,L)/DELU
  505 CONTINUE
      CALL CURLU(U,V,W,01,02,03,N1,N2,N3)
      PRINT 708
  708 FORMAT(1H0,130H**********************************************************
     1**********************************************************************
     2************    )
      DT=0.03125*DELU/THETA
      PRINT 1116,DELU,THETA,DT
 1116 FORMAT(1X,1H*,* DELU=*,E15.7,10X,* THETA=*,E15.7,10X,* DT=*,E15.7,
     &46X,1H*)
      PRINT 1117,DELTAX,DELTAY,DELTAZ
 1117 FORMAT(1X,1H*,* DELTAX=*,E15.7,10X,* DELTAY=*,E15.7,10X,* DELTAZ=*
     &,E15.7,35X,1H*)
      PRINT 708
      CALL RNDINIC
      UDUM=0.
      DO 507 L=1,LMAX
      DO 507 J=1,JMAX
      DO 507 I=1,IMAX
      IF(ABS(U(I,J,L)).GT.UDUM) UDUM=ABS(U(I,J,L))
      IF(ABS(V(I,J,L)).GT.UDUM) UDUM=ABS(V(I,J,L))
      IF(ABS(W(I,J,L)).GT.UDUM) UDUM=ABS(W(I,J,L))
  507 CONTINUE
      CUDUM=0.30/UDUM
      DO 510 L=1,LMAX
      DO 510 J=1,JMAX
      DO 510 I=1,IMAX
      U(I,J,L)=U(I,J,L)*CUDUM
      V(I,J,L)=V(I,J,L)*CUDUM
      W(I,J,L)=W(I,J,L)*CUDUM
  510 CONTINUE
      CALL CURLU(U,V,W,01D,02D,03D,N1,N2,N3)
      DO 512 L=1,LMAX
      DO 512 J=1,JMAX
      DO 512 I=1,IMAX
      01(I,J,L)=01(I,J,L)+01D(I,J,L)
      02(I,J,L)=02(I,J,L)+02D(I,J,L)
      03(I,J,L)=03(I,J,L)+03D(I,J,L)
  512 CONTINUE
```

```
      CALL INVERS(O1,GU,DUDX,1,N1,N2,N3)
      CALL INVERS(O2,GV,DUDX,2,N1,N2,N3)
      CALL INVERS(O3,GW,DUDX,3,N1,N2,N3)
      CALL CURLO(GU,GV,GW,U,V,W,N1,N2,N3)
      DO 513 L=1,LMAX
      DO 513 J=1,JMAX
      DO 513 I=1,IMAX
      O1D(I,J,L)=0.
      O2D(I,J,L)=0.
      O3D(I,J,L)=0.
  513 CONTINUE
      DUMM1=0.
      DUMM2=0.
      DO 3333 I=1,IMAX
      DO 3333 J=1,JMAX
      DO 3333 L=1,LMAX
      IF(O1(I,J,L).GT.DUMM1) DUMM1=O1(I,J,L)
      IF(O2(I,J,L).GT.DUMM2) DUMM2=O2(I,J,L)
 3333 CONTINUE
      PRINT 3334,DUMM1,DUMM2
 3334 FORMAT(1X,* DUMM1= *,E15.7,2X,* DUMM2= *,E15.7)
      RETURN
      END
*DECK PARPLOT
      SUBROUTINE PARPLOT
C*********************************************************************
C     THIS ROUTINE PLOTS THE PARTICLES TRACKS .                      *
C     XMIN IS FIXED TO BE ZERO                                       *
C     ZMIN IS FIXED TO BE ZERO                                       *
C     XMAX IS FLOATING AND DEPENDS ON NUMBER OF MESHES USED AND DELTAX *
C     ZMAX IS FLOATING AND DEPENDS ON NUMBER OF MESHES USED AND DELTAZ *
C     SCX IS THE SCALING FACTOR TO ADJUST TO A PAGE LENGHT OF 8 INCHES *
C     SCZ IS THE SCALING FACTOR TO ADJUST TO A PAGE LENGHT OF 8 INCHES *
C*********************************************************************
*CALL DATA9
*CALL DEL
*CALL XL
      DATA LB/1HX/
      DATA NL/1HZ/
      XMIN=0.
      XMAX=(IMAX-1)*DELTAX
      ZMIN=0.
      ZMAX=(LMAX-1)*DELTAZ
      PPXMAX=13.0
      PPZMAX=10.
      SCX=PPXMAX/XMAX
      SCZ=PPZMAX/ZMAX
      CALL LINAXS(0.,0.,PPXMAX,PPZMAX,.1,-1,10,1,XMIN,XMAX,3,4,LB)
      CALL LINAXS(0.,0.,PPXMAX,PPZMAX,.1,+1,10,1,ZMIN,ZMAX,3,4,NL)
      DO 1 N=1,140
      X=XPART(N)*SCX
      Z=ZPART(N)*SCZ
      NC=NCHAR(N)
      CALL SYMBOL(X,Z,0.1,0,0.,-NC)
    1 CONTINUE
      CALL PLOT(0.,0.,6)
      RETURN
      END
*DECK PARTRAC
      SUBROUTINE PARTRAC(NPART,DT)
C*********************************************************************
C     THIS SUBROUTINE COMPUTES THE PARTICLES TRACK OF A TWO DIM MEAN.  *
C     IT USES LINEAR INTERPOLATION TO COMPUTR THE VELOCITIES BETWEEN   *
C     THE MESHES. TIME ADVANCING IS A FIRST ORDER EULER METHOD.        *
C*********************************************************************
*CALL LARGE2
*CALL DATA9
*CALL DEL
*CALL LARGE3
*CALL XL
```

```
      RLX=(IMAX-1)*DELTAX
      RLY=(JMAX-1)*DELTAY
      RLZ=(LMAX-1)*DELTAZ
      DO 1 M=1,NPART
      IX=XPART(M)/DELTAX+1
      IY=YPART(M)/DELTAY+1
      LZ=ZPART(M)/DELTAZ+1
      IXP1=IX+1
      IYP1=IY+1
      LZP1=LZ+1
      IF(IX.EQ.IMAX) IXP1=1
      IF(IY .EQ. JMAX) IYP1=1
      IF(LZ.EQ.LMAX) LZP1=LZ
      CCX=(XPART(M)-(IX-1)*DELTAX)/DELTAX
      CCY=(YPART(M)-(IY-1)*DELTAY)/DELTAY
      CCZ=(ZPART(M)-(LZ-1)*DELTAZ)/DELTAZ
      U1PART=U(IX,IY   ,LZ   )+(U(IXP1,IY   ,LZ   )-U(IX,IY   ,LZ   ))*CCX
      V1PART=V(IX,IY   ,LZ   )+(V(IXP1,IY   ,LZ   )-V(IX,IY   ,LZ   ))*CCX
      W1PART=W(IX,IY   ,LZ   )+(W(IXP1,IY   ,LZ   )-W(IX,IY   ,LZ   ))*CCX
      U2PART=U(IX,IY   ,LZP1)+(U(IXP1,IY   ,LZP1)-U(IX,IY   ,LZP1))*CCX
      V2PART=V(IX,IY   ,LZP1)+(V(IXP1,IY   ,LZP1)-V(IX,IY   ,LZP1))*CCX
      W2PART=W(IX,IY   ,LZP1)+(W(IXP1,IY   ,LZP1)-W(IX,IY   ,LZP1))*CCX
      U1PART=U1PART+(U2PART-U1PART)*CCZ

      W2PART=W(IX,IY   ,LZP1)+(W(IXP1,IY   ,LZP1)-W(IX,IY   ,LZP1))*CCX
      U1PART=U1PART+(U2PART-U1PART)*CCZ
      V1PART=V1PART+(V2PART-V1PART)*CCZ
      W1PART=W1PART+(W2PART-W1PART)*CCZ
      U2PART=U(IX,IYP1,LZ   )+(U(IXP1,IYP1,LZ   )-U(IX,IYP1,LZ   ))*CCX
      V2PART=V(IX,IYP1,LZ   )+(V(IXP1,IYP1,LZ   )-V(IX,IYP1,LZ   ))*CCX
      W2PART=W(IX,IYP1,LZ   )+(W(IXP1,IYP1,LZ   )-W(IX,IYP1,LZ   ))*CCX
      U3PART=U(IX,IYP1,LZP1)+(U(IXP1,IYP1,LZP1)-U(IX,IYP1,LZP1))*CCX
      V3PART=V(IX,IYP1,LZP1)+(V(IXP1,IYP1,LZP1)-V(IX,IYP1,LZP1))*CCX
      W3PART=W(IX,IYP1,LZP1)+(W(IXP1,IYP1,LZP1)-W(IX,IYP1,LZP1))*CCX
      U2PART=U2PART+(U3PART-U2PART)*CCZ
      V2PART=V2PART+(V3PART-V2PART)*CCZ
      W2PART=W2PART+(W3PART-W2PART)*CCZ
      U1PART=U1PART+(U2PART-U1PART)*CCY
      V1PART=V1PART+(V2PART-V1PART)*CCY
      W1PART=W1PART+(W2PART-W1PART)*CCY
      XPART(M)=XPART(M)+DT*U1PART
      YPART(M)=YPART(M)+DT*V1PART
      ZPART(M)=ZPART(M)+DT*W1PART
      IF(XPART(M).GT.RLX) GO TO 10
      GO TO 20
   10 XPART(M)=XPART(M)-RLX
   20 IF(XPART(M).LT.0.) GO TO 30
      GO TO 40
   30 XPART(M)=XPART(M)+RLX
   40 IF(YPART(M).GT.RLY) GO TO 70
      GO TO 80
   70 YPART(M)=YPART(M)-RLY
   80 IF(YPART(M).LT.0.) GO TO 90
      GO TO 100
   90 YPART(M)=YPART(M)+RLY
  100 IF(ZPART(M).GT.RLZ) GO TO 50
      GO TO 60
   50 ZPART(M)=RLZ
   60 IF(ZPART(M).LT.0.) ZPART(M)=0.
    1 CONTINUE
      RETURN
      END
*DECK PARTIAL
      SUBROUTINE PARTIAL(M,U,N1,N2,N3)
      DIMENSION U(N1,N2,N3)
*CALL DATA9
*CALL BLANK
*CALL WV
*CALL DATA7
      LEVEL 2,U
```

```
      IJ=N1*N2
      IF (M .EQ. 2) GO TO 30
C*****DERIVATIVE IN THE X-DIRECTION**************************************
      DO 10 L=1,LMAX
      CALL MOVLEV(U(1,1,L),FR(1,1),IJ)
      CALL FFTX(1.0)
      DO 15 J=1,JMAX
      DO 15 I=1,IMAX
      DUM=FI(I,J)
      FI(I,J)=WAVEX(I)*FR(I,J)
      FR(I,J)=-WAVEX(I)*DUM
   15 CONTINUE
      CALL FFTX(-1.0)
      CALL MOVLEV(FR(1,1),DUDX(1,1,L),IJ)
   10 CONTINUE
      GO TO 300
C*****DERIVATIVE IN THE Y- DIRECTION     ******************************
   30 CONTINUE
      DO 35 L=1,LMAX
      CALL MOVLEV(U(1,1,L),FR(1,1),IJ)
      DO 32 J=1,JMAX
      DO 32 I=1,IMAX
      FI(I,J)=0.0
   32 CONTINUE
      CALL FFTY(1.0,1.0)
      DO 40 J=1,JMAX
      DO 40 I=1,IMAX
      DUM=FI(I,J)
      FI(I,J)=WAVEY(J)*FR(I,J)
      FR(I,J)=-WAVEY(J)*DUM
   40 CONTINUE
      CALL FFTY(-1.0,1.0)
      CALL MOVLEV(FR(1,1),DUDX(1,1,L),IJ)
   35 CONTINUE
  300 CONTINUE
      RETURN
      END
*DECK RGEN
      IDENT  RGEN - PSEUDO RANDOM NUMBER GENERATOR
***   FUNCTION RGEN(D)
*           CALLED AS A FUNCTION WITH 1 ARGUMENT (WHICH IS IGNORED)
*           RETURNS IN X6 A RANDOM NUMBER GENERATED BY MULTIPLYING
*           1 OF 5 INTEGER CONSTANTS BY THE CORRESPONDING GENERATOR
*           SEE BKY USERS HANDBOOK FOR REFERENCES
      SST
**     RGENCOM - USED TO STORE THE GENERATORS AND POINTER
*
      USE    /RGENCOM/
GEN   DATA   1048015011D THE 5 GENERATORS
      DATA   2236846573D
      DATA   4216793093D
      DATA   7792106907D
      DATA   9630191977D
PTR   DATA 1             POINTER TO CURRENT GENERATOR
      USE    *
      ENTRY  RGEN
      IF     -DEF,FTN,1
      ENTRY  RGEN$
      COMMENT RANDOM NUMBER GENERATOR (#MODLEVEL#)
NAME  VFD    42/4LRGEN,18/RGEN
      IF     DEF,FTN
      ELSE   2
RGEN  PS                 ENTRY  /  EXIT
RGEN$ EQU    RGEN        SINCE ARG IS IGNORED
      SA1    PTR         GET POINTER
      SA3    RGEN        GET ENTRY POINT
      SB1    1
      SX7    4
      SA4    X1+GEN-1    GET GENERATOR
      SA5    X1+CON-1    GET CONSTANT
```

```
          MX2     60-35
          AX3     30
          IX0     X7-X1          4 - PTR
          SB7     X3             B7 = RETURN ADDRESS
          DX6     X4*X5          GEN * CON
          PL      X0,RGEN1       UNLESS PTR =5
          MX1     0              IF PTR WAS  5
RGEN1     BSS     0
          SA3     EXP
          SX7     B1+X1          INCREMENT PTR
          SA7     PTR            STORE NEW POINTER
          BX7     -X2*X6         MASK LOW 35 BITS
          BX5     X7+X3          PUT IN EXPONENT
          SA7     A4             STORE NEW GENERATOR
          NX6     X5
          JP      B7             JUMP DIRECTLY  BACK
CON       DATA    131075D        CONSTANTS TO MULTIPLY BY
          DATA    163843D
          DATA    196611D
          DATA    229379D
          DATA    262147D
EXP       DATA    1734B548
          END
*DECK RNDINIC
      SUBROUTINE RNDINIC
C*****************************************************************************
C     THIS SUBROUTINE CREATS THE INITIAL RANDOM FIELD BY CALL INICON    *
C     INICON WAS INITIALY WRITTEN BY KWAK,D. AND IS USED HERE AS A MEAN*
C     TO CREAT A RANDOM INITIAL FIELD.THE ROUTINE WAS WRITTEN FOR EQUAL*
C     MESH,AND HENCE THE COMPLICATIONS IN THIS ROUTINE TO TRANSFER THE *
C     FIELD TO THE MIDDLE OF THE BOX    .                              *
C*****************************************************************************
*CALL BLANK
*CALL LARGE2
*CALL LARGE3
      COMMON/LARGE4/01(16,16,33),02(16,16,33),03(16,16,33)
      LEVEL 2,01,02,03
*CALL DATA9
*CALL DIM
      COMMON/DUM1/ UM(16,16,16),VM(16,16,16),WM(16,16,16)
      COMMON/DUM2/ GUI(16,16,16),GVI(16,16,16),GWI(16,16,16)
      LEVEL 2,UM,VM,WM,GUI,GVI,GWI
      CALL INICON(C,COF,DT,UM,VM,WM,GUI,GVI,GWI,16,16,16)
      IMAX=N1
      JMAX=N2
      LMAX=N3
      DO 1 L=1,16
      DO 1 J=1,JMAX
      DO 1 I=1,IMAX
      L1=25-L
      L2=17-L
      U(I,J,L1)=UM(I,J,L2)
      V(I,J,L1)=VM(I,J,L2)
      W(I,J,L1)=WM(I,J,L2)
    1 CONTINUE
      DO 2 L=1,13
      DO 2 J=1,JMAX
      DO 2 I=1,IMAX
      U(I,J,L)=0.
      V(I,J,L)=0.
      W(I,J,L)=0.
    2 CONTINUE
      DO 3 L=21,LMAX
      DO 3 J=1,JMAX
      DO 3 I=1,IMAX
      U(I,J,L)=0.
      V(I,J,L)=0.
      W(I,J,L)=0.
    3 CONTINUE
      CALL INIFILT(U,N1,N2,N3)
```

```
      CALL INIFILT(V,N1,N2,N3)
      CALL INIFILT(W,N1,N2,N3)
      CALL CURLO(U,V,W,O1,O2,O3,N1,N2,N3)
      DO 16 L=1,LMAX
      DO 16 J=1,JMAX
      DO 16 I=1,IMAX
      U(I,J,L)=O1(I,J,L)
      V(I,J,L)=O2(I,J,L)
      W(I,J,L)=O3(I,J,L)
   16 CONTINUE
      CALL CURLU(U,V,W,O1,O2,O3,N1,N2,N3)
      CALL INVERS(O1,GU,DUDX,1,N1,N2,N3)
      CALL INVERS(O2,GV,DUDX,2,N1,N2,N3)
      CALL INVERS(O3,GW,DUDX,3,N1,N2,N3)
      CALL CURLO(GU,GV,GW,U,V,W,N1,N2,N3)
      RETURN
      END
*DECK SINPART
      SUBROUTINE SINPART(U,N1,N2,N3)
C*****************************************************************
C     THIS ROUTINE COMPUTES THE PARTIAL DERIVATIVE OF U IN THE Z-  *
C     DIRECTION BY EXPANDING IN FOURIER SINE SERIES.               *
C     THE PARTIAL IS STORED IN DUDX.                               *
C*****************************************************************
      DIMENSION U(N1,N2,N3)
*CALL BLANK
*CALL WV
*CALL DAT21
*CALL DATA9
      LEVEL 2,U
      DO 10 J=1,JMAX
      DO 10 I=1,IMAX
      DO 20 L=1,LMAX
      XR(L)=U(I,J,L)
   20 CONTINUE
      SIGN=1.0
      CALL FDST(SIGN)
      DO 30 L=1,LMAX
      XR(L)=XR(L)*WAVEZ(L)
   30 CONTINUE
      SIGN=-1.0
      CALL FDCT(SIGN)
      DO 40 L=1,LMAX
      DUDX(I,J,L)=XR(L)
   40 CONTINUE
   10 CONTINUE
      RETURN
      END
*DECK SFILTER
      SUBROUTINE SFILTER(HR,HI,N1,N2,N3)
C*****************************************************************
C     SFILTER FILTERS HR BY EXPANDING IT IN A FOURIER SINE SERIES IN  *
C     THE Z/DIRECTION AND FOURIER SERIES IN THE OTHER TWO DIRECTIONS.  *
C*****************************************************************
      DIMENSION HR(N1,N2,N3),HI(N1,N2,N3)
*CALL FLT
*CALL DATA9
*CALL DATA7
*CALL DAT21
      LEVEL 2,HR
      CC=1.0/(IMAX*JMAX)
      IJ=N1*N2
      DO 10 J=1,JMAX
      DO 10 I=1,IMAX
      DO 20 L=1,LMAX
      XR(L)=HR(I,J,L)
   20 CONTINUE
      CALL FDST(1.0)
      DO 30 L=1,LMAX
      HI(I,J,L)=XR(L)
```

```
   30 CONTINUE
   10 CONTINUE
      DO 40 L=1,LMAX
      CALL MOVLEV(HI(1,1,L),FR(1,1),IJ)
      CALL FFTX(1.0)
      CALL FFTY(1.0,1.0)
      DO 50 J=1,JMAX
      DO 50 I=1,IMAX
      FR(I,J)=FR(I,J)*FILT1(I)*FILT2(J)*FILT3(L)
      FI(I,J)=FI(I,J)*FILT1(I)*FILT2(J)*FILT3(L)
   50 CONTINUE
      CALL FFTX(-1.0)
      CALL FFTY(-1.0,CC)
      CALL MOVLEV(FR(1,1),HI(1,1,L),IJ)
   40 CONTINUE
      DO 60 J=1,JMAX
      DO 60 I=1,IMAX
      DO 70 L=1,LMAX
      XR(L)=HI(I,J,L)
   70 CONTINUE
      CALL FDST(-1.0)
      DO 80 L=1,LMAX
      HR(I,J,L)=XR(L)
   80 CONTINUE
   60 CONTINUE
      RETURN
      END
*DECK SGS
      SUBROUTINE SGS(U,V,E,N1,N2,N3)
      DIMENSION U(N1,N2,N3),V(N1,N2,N3),E(N1,N2,N3)
*CALL DEL
*CALL LARGE3
*CALL LARGE5
*CALL BLANK
*CALL DATA9
      LEVEL 2,U,V,E
C*****************************************************************************
C     THE SGS MODEL IS COMPUTED IN THIS ROUTINE BY SECOND ORDER DIFF          *
C     AND STORED IN GU,GV,GW                                                  *
C*****************************************************************************
      CSGSX=1./(2.*DELTAX)
      CSGSY=1./(2.*DELTAY)
      CSGSZ=1./(2.*DELTAZ)
      IJK=N1*N2*N3
      CALL MOVLEV(DUDX(1,1,1),E(1,1,1),IJK)
      DO 210 L=1,LMAX
      LM1=L-1
      LP1=L+1
      IF (L .EQ. 1) LM1=LP1
      IF (L .EQ. LMAX) LP1=LM1
      DO 210 J=1,JMAX
      CALL FIX(JM1,J,JP1,JMAX)
      DO 210 I=1,IMAX
      CALL FIX(IM1,I,IP1,IMAX)
      U(I,J,L)=(E(I,JP1,L)*O1(I,JP1,L)-E(I,JM1,L)*O1(I,JM1,L))*CSGSY
     1 -(E(IP1,J,L)*O2(IP1,J,L)-E(IM1,J,L)*O2(IM1,J,L))*CSGSX
      V(I,J,L)=(E(I,J,LP1)*O1(I,J,LP1)-E(I,J,LM1)*O1(I,J,LM1))*CSGSZ
     1 -(E(IP1,J,L)*O3(IP1,J,L)-E(IM1,J,L)*O3(IM1,J,L))*CSGSX
  210 CONTINUE
      CALL PARTIAL(2,U,N1,N2,N3)
      CALL MOVLEV(DUDX(1,1,1),U(1,1,1),IJK)
      CALL COSPART(V,N1,N2,N3)
      DO 220 L=1,LMAX
      DO 220 J=1,JMAX
      DO 220 I=1,IMAX
      GU(I,J,L)=GU(I,J,L)+U(I,J,L)+DUDX(I,J,L)
  220 CONTINUE
      DO 230 L=1,LMAX
      LM1=L-1
      LP1=L+1
```

```
      IF (L .EQ. 1) LM1=LP1
      IF (L .EQ. LMAX) LP1=LM1
      DO 230 J=1,JMAX
      CALL FIX(JM1,J,JP1,JMAX)
      DO 230 I=1,IMAX
      CALL FIX(IM1,I,IP1,IMAX)
      U(I,J,L)=(E(IP1,J,L)*O2(IP1,J,L)-E(IM1,J,L)*O2(IM1,J,L))*CSGSX
     1 -(E(I,JP1,L)*O1(I,JP1,L)-E(I,JM1,L)*O1(I,JM1,L))*CSGSY
      V(I,J,L)=(E(I,J,LP1)*O2(I,J,LP1)-E(I,J,LM1)*O2(I,J,LM1))*CSGSZ
     1 -(E(I,JP1,L)*O3(I,JP1,L)-E(I,JM1,L)*O3(I,JM1,L))*CSGSY
  230 CONTINUE
      CALL PARTIAL(1,U,N1,N2,N3)
      CALL MOVLEV(DUDX(1,1,1),U(1,1,1),IJK)
      CALL COSPART(V,N1,N2,N3)
      DO 240 L=1,LMAX
      DO 240 J=1,JMAX
      DO 240 I=1,IMAX
      GV(I,J,L)=GV(I,J,L)+U(I,J,L)+DUDX(I,J,L)
  240 CONTINUE
      DO 250 L=1,LMAX
      LM1=L-1
      LP1=L+1
      IF (L .EQ. 1) LM1=LP1
      IF (L .EQ. LMAX) LP1=LM1
      DO 250 J=1,JMAX
      CALL FIX(JM1,J,JP1,JMAX)
      DO 250 I=1,IMAX
      CALL FIX(IM1,I,IP1,IMAX)
      U(I,J,L)=(E(IP1,J,L)*O3(IP1,J,L)-E(IM1,J,L)*O3(IM1,J,L))*CSGSX
     1 -(E(I,J,LP1)*O1(I,J,LP1)-E(I,J,LM1)*O1(I,J,LM1))*CSGSZ
      V(I,J,L)=(E(I,JP1,L)*O3(I,JP1,L)-E(I,JM1,L)*O3(I,JM1,L))*CSGSY
     1 -(E(I,J,LP1)*O2(I,J,LP1)-E(I,J,LM1)*O2(I,J,LM1))*CSGSZ
  250 CONTINUE
      CALL PARTIAL(1,U,N1,N2,N3)
      CALL MOVLEV(DUDX(1,1,1),U(1,1,1),IJK)
      CALL PARTIAL(2,V,N1,N2,N3)
      DO 260 L=1,LMAX
      DO 260 J=1,JMAX
      DO 260 I=1,IMAX
      GW(I,J,L)=GW(I,J,L)+U(I,J,L)+DUDX(I,J,L)
  260 CONTINUE
      RETURN
      END
*DECK STFILT
      SUBROUTINE STFILT
C*****************************************************************************
C     THIS SUBROUTINE INITIALIZE THE TRANSFORM OF THE FILTER IN EACH
C     DIRECTION. THE TRANSFORM IS STORED IN FILT1,FILT2,FILT3,FOR USE
C     IN SUBROUTINE FILTER.
C*****************************************************************************
*CALL AVG
*CALL FLT
*CALL DATA7
*CALL DAT21
*CALL DATA9
*CALL PR
      NHP1X=IMAX/2+1
      NHP1Y=JMAX/2+1
      NHP2X=NHP1X+1
      NHP2Y=NHP1Y+1
      LMAXM1=LMAX-1
      IF(CCF .NE. 0.) GO TO 400
C*****FIX THE TRANSFORM OF THE FILTER IN THE X-DIRECTION
      DO 100 J=1,JMAX
      DO 100 I=1,NHP1X
      FR(I,J)=EXP(-6.*(FLOAT(I-1)/AVG1)**2)
  100 CONTINUE
      DO 110 J=1,JMAX
      DO 110 I=NHP2X,IMAX
      II=IMAX-I+2
```

```
      FR(I,J)=FR(II,J)
  110 CONTINUE
      AREA=0.0
      DO 120 I=1,IMAX
      AREA=AREA+FR(I,1)
  120 CONTINUE
      DO 130 J=1,JMAX
      DO 130 I=1,IMAX
      FR(I,J)=FR(I,J)/AREA
      FI(I,J)=0.0
  130 CONTINUE
      CALL FFTX(1.0)
      DO 140 I=1,IMAX
      FILT1(I)=FR(I,1)
  140 CONTINUE
C*****FIX THE TRANSFORM OF THE FILTER IN THE Y-DIRECTION
      DO 200 J=1,NHP1Y
      DO 200 I=1,IMAX
      FR(I,J)=EXP(-6.*(FLOAT(J-1)/AVG2)**2)
  200 CONTINUE
      DO 210 J=NHP2Y,JMAX
      DO 210 I=1,IMAX
      JJ=JMAX-J+2
      FR(I,J)=FR(I,JJ)
  210 CONTINUE
      AREA=0.0
      DO 220 J=1,JMAX
      AREA=AREA+FR(1,J)
  220 CONTINUE
      DO 230 J=1,JMAX
      DO 230 I=1,IMAX
      FR(I,J)=FR(I,J)/AREA
      FI(I,J)=0.0
  230 CONTINUE
      CALL FFTY(1.0,1.0)
      DO 240 J=1,JMAX
      FILT2(J)=FR(1,J)
  240 CONTINUE
C*****FIX THE TRANSFORM OF THE FILTER IN THE Z-DIRECTION
      DO 300 L=1,LMAX
      XR(L)=EXP(-6.*(FLOAT(L-1)/AVG3)**2)
  300 CONTINUE
      AREA=0.5*XR(1)
      DO 310 L=2,LMAXM1
      AREA=AREA+XR(L)
  310 CONTINUE
      AREA=AREA+0.5*XR(LMAX)
      DO 320 L=1,LMAX
      XR(L)=XR(L)/AREA
  320 CONTINUE
      CALL FDCT(1.0)
      DO 330 L=1,LMAX
      FILT3(L)=XR(L)
  330 CONTINUE
      FILT1(NHP1X)=0.
      FILT2(NHP1Y)=0.
      FILT3(LMAX)=0.
      GO TO 410
  400 IF(CCF .NE. 1.0) GO TO 410
      MC=(LMAX-1)*2/3
      DO 7 L=1,LMAX
      FILT3(L)=0.
    7 CONTINUE
      DO 8 L=1,MC
      FILT3(L)=1.0
    8 CONTINUE
      MC=JMAX/3+1
      DO 9 J=1,JMAX
      FILT2(J)=0.
    9 CONTINUE
```

```
      DO 10 J=1,MC
      FILT2(J)=1.0
      JJ=JMAX-J+1
      FILT2(JJ)=1.0
   10 CONTINUE
      MC=JMAX-MC+1
      FILT2(MC)=0.
      MC=IMAX/3+1
      DO 11 I=1,IMAX
      FILT1(I)=0.
   11 CONTINUE
      DO 12 I=1,MC
      FILT1(I)=1.0
      II=IMAX+1-I
      FILT1(II)=1.0
   12 CONTINUE
      MC=IMAX-MC+1
      FILT1(MC)=0.
  410 PRINT 1119,CCF
 1119 FORMAT(1H0,* CCF=*,1PE15.7)
      IF(CCPF .NE. 1.0) GO TO 340
      PRINT 1116,(FILT1(I),I=1,IMAX)
      PRINT 1117,(FILT2(J),J=1,JMAX)
      PRINT 1118,(FILT3(L),L=1,LMAX)
 1116 FORMAT(1X,* FILT1 =*,1PE15.7)
 1117 FORMAT(1X,* FILT2 =*,1PE15.7)
 1118 FORMAT(1X,* FILT3 =*,1PE15.7)
  340 CONTINUE
      RETURN
      END
*DECK STPART
      SUBROUTINE STPART(NPART)
*CALL LARGE5
*CALL XL
*CALL DATA9
*CALL DEL
      YPART(1)=0.
      YPART(17)=0.
      XPART(1)=(6-1)*DELTAX
      XPART(17)=(11-1)*DELTAX
      ZPART(1)=(17.-1.)*DELTAZ
      ZPART(17)=(17.-1.)*DELTAZ
      NCHAR(1)=1
      NCHAR(17)=2
      YPART(33)=0.
      YPART(49)=0.
      YPART(65)=0.
      YPART(81)=0.
      YPART(97)=0.
      YPART(113)=0.
      YPART(129)=0.
      YPART(145)=0.
      XPART(33)=XPART(1)+0.5*DELTAX
      XPART(49)=XPART(1)-0.5*DELTAX
      XPART(65)=XPART(1)
      XPART(81)=XPART(1)
      ZPART(33)=ZPART(1)
      ZPART(49)=ZPART(1)
      ZPART(65)=ZPART(1)+0.5*DELTAZ
      ZPART(81)=ZPART(1)-0.5*DELTAZ
      XPART(97)=XPART(17)+0.5*DELTAX
      ZPART(97)=ZPART(17)
      XPART(113)=XPART(17)-0.5*DELTAX
      ZPART(113)=ZPART(17)
      XPART(129)=XPART(17)
      ZPART(129)=ZPART(17)+0.5*DELTAZ
      XPART(145)=XPART(17)
      ZPART(145)=ZPART(17)-0.5*DELTAZ
      NCHAR( 33)=3
      NCHAR( 49)=4
```

```
      NCHAR( 65)=5
      NCHAR( 81)=6
      NCHAR( 97)=7
      NCHAR(113)=8
      NCHAR(129)=9
      NCHAR(145)=10
      NPART=160
      DELX=0.
      DELZ=0.
      N=0
      DO 1 M=1,10
      N=N+1
      DO 2 J=2,JMAX
      N=N+1
      NCHAR(N)=M
      IX=XPART(N-1)/DELTAX+1
      LZ=ZPART(N-1)/DELTAZ+1
      IXP1=IX+1
      LZP1=LZ+1
      CCX=(XPART(N-1)-(IX-1)*DELTAX)/DELTAX
      CCZ=(ZPART(N-1)-(LZ-1)*DELTAZ)/DELTAZ
      O1P1=O1(IX,J,LZ)+(O1(IXP1,J,LZ)-O1(IX,J,LZ))*CCX
      O2P1=O2(IX,J,LZ)+(O2(IXP1,J,LZ)-O2(IX,J,LZ))*CCX
      O3P1=O3(IX,J,LZ)+(O3(IXP1,J,LZ)-O3(IX,J,LZ))*CCX
      O1P2=O1(IX,J,LZP1)+(O1(IXP1,J,LZP1)-O1(IX,J,LZP1))*CCX
      O2P2=O2(IX,J,LZP1)+(O2(IXP1,J,LZP1)-O2(IX,J,LZP1))*CCX
      O3P2=O3(IX,J,LZP1)+(O3(IXP1,J,LZP1)-O3(IX,J,LZP1))*CCX
      O1P1=O1P1+(O1P1-O1P2)*CCZ
      O2P1=O2P1+(O2P1-O2P2)*CCZ
      O3P1=O3P1+(O3P1-O3P2)*CCZ
      DELX=O1P1*DELTAY/O2P1
      DELZ=O3P1*DELTAY/O2P1
      XPART(N)=XPART(N-1)+DELX
      YPART(N)=YPART(N-1)+DELTAY
      ZPART(N)=ZPART(N-1)+DELZ
    2 CONTINUE
    1 CONTINUE
      RETURN
      END
*DECK STREAD
      SUBROUTINE STREAD
C*****************************************************************************
C     THIS SUBROUTINE READ THE INPUT PARAMETERS                               *
C     IMAX=NUMBER OF GRID POINTS IN THE X-DIRECTION                           *
C     JMAX=NUMBER OF GRID POINTS IN THE Y-DIRECTION                           *
C     LMAX=NUMBER OF GRID POINTS IN THE Z-DIRECTION                           *
C     AVG2=FILTERING WIDTH IN THE Y-DIRECTION                                 *
C     AVG3=FILTERING WIDTH IN THE Z-DIRECTION                                 *
C     AVG1=FILTERING WIDTH IN THE X-DIRECTION                                 *
C     DELTAX= MESH SIZE IN THE X-DIRECTION                                    *
C     DELTAY= MESH SIZE IN THE Y-DIRECTION                                    *
C     DELTAZ= MESH SIZE IN THE Z-DIRECTION                                    *
C     N1= ARRAY SIZE IN THE X-DIRECTION                                       *
C     N2= ARRAY SIZE IN THE Y-DIRECTION                                       *
C     N3= ARRAY SIZE IN THE Z-DIRECTION                                       *
C     CCPW= 1 IF PRINT OUT OF WAVE IS WANTED,OTHERWIZE NO PRINT OUT           *
C     CCPF= 1 IF PRINT OUT OF FILT IS WANTED,OTHERWIZE NO PRINT OUT           *
C     CCPD= 1 IF PRINT OUT OF LINE AVERAGE OF U-COMPONENT ,                   *
C        LINE AVERAGE OF W-COMPONENT AND ENSEMBLE AVERAGE PERTURBATIONS*
C        IS REQUIRED ,OTHERWIZE NO PRINT OUT .                                *
C*****************************************************************************
      INTEGER TSTART,TEND
*CALL DATA9
      COMMON/TIM/ TSTART,TEND
*CALL DEL
*CALL DIM
*CALL AVG
*CALL PR
      READ 703,IMAX,JMAX,LMAX,TSTART,TEND
      READ 704,DELTAX,DELTAY,DELTAZ
```

```
      READ 704,AVG1,AVG2,AVG3,CCF
      READ 703,N1,N2,N3
      READ 704,CCPW,CCPF,CCPD
      PRINT 708
      PRINT 705,IMAX,JMAX,LMAX,TSTART,TEND
      PRINT 706,DELTAX,DELTAY,DELTAZ
      PRINT 707,AVG1,AVG2,AVG3
      PRINT 709,N1,N2,N3
      PRINT 708
  703 FORMAT(10I5)
  704 FORMAT(4E10.4)
  705 FORMAT(1X,* IMAX=*,I5,5X,* JMAX=*,I5,5X,* LMAX=*,I5,5X,* TSART=*I5
     + ,5X,* TEND=*,I5,52X,1H*)
  706 FORMAT(1X,* DELTAX=*,1PE10.4,5X,* DELTAY=*,1 E10.4,5X,* DELTAZ=*,1
     +PE10.4,64X,1H*)
  707 FORMAT(1X,*  AVG1X=*,1PE10.4,5X,*   AVG2=*,1 E10.4,5X,*   AVG3=*,1
     +PE10.4,64X,1H*)
  708 FORMAT(1H0,130H**********************************************************
     1**********************************************************
     2************    )
  709 FORMAT(1X,*   N1=*,I5,5X,*   N2=*,I5,5X,*   N3=*,I5,5X,70X,1H*)
      RETURN
      END
*DECK STWV
      SUBROUTINE STWV
C*************************************************************************
C     STWV SETS THE WAVE NUMBERS FOR A GIVEN MESH SIZE DELTA AND       *
C     NUMBER OF MESH POINTS NMAX . THIS ROUTINE MUST BE CALLED         *
C     TO INITIALIZE THE WAVE NUMBERS FOR THE PARTIAL ROUTINES AND      *
C     INVERS ROUTINE .                                                 *
C*************************************************************************
C*************************************************************************
*CALL WV
*CALL DATA9
*CALL DEL
*CALL PR
      PAI=3.1415926535898
      CX=2.0*PAI/(FLOAT(IMAX)*DELTAX)
      CY=2.0*PAI/(FLOAT(JMAX)*DELTAY)
      CZ=PAI/(FLOAT(LMAX-1)*DELTAZ)
      C2X=CX/FLOAT(IMAX)
      C2Y=CY/FLOAT(JMAX)
      NHP1X=IMAX/2+1
      NHP1Y=JMAX/2+1
      DO 100 L=1,LMAX
      WAVEZ(L)=CZ*FLOAT(L-1)
      WAVEZS(L)=-WAVEZ(L)**2
  100 CONTINUE
      DO 101 J=1,JMAX
      MM=J/NHP1Y
      M=MM*JMAX+1
      WAVEY(J)=C2Y*FLOAT(J-M)
      WAVEYS(J)=-(CY*FLOAT(J-M))**2
  101 CONTINUE
      DO 102 I=1,IMAX
      MM=I/NHP1X
      M=MM*IMAX+1
      WAVEX(I)=C2X*FLOAT(I-M)
      WAVEXS(I)=-(CX*FLOAT(I-M))**2
  102 CONTINUE
      WAVEX(NHP1X)=0.
      WAVEY(NHP1Y)=0.
      WAVEXS(NHP1X)=0.
      WAVEYS(NHP1Y)=0.
      WAVEZ(LMAX)=0.
      WAVEZS(LMAX)=0.
      IF(CCPW .NE. 1) GO TO 104
      PRINT 1000,(WAVEX(I),WAVEXS(I),I=1,IMAX)
      PRINT 1001,(WAVEY(J),WAVEYS(J),J=1,JMAX)
      PRINT 1002,(WAVEZ(L),WAVEZS(L),L=1,LMAX)
```

```
 104 CONTINUE
1000 FORMAT(1X,* WAVEX =*,1PE15.7,5X,* WAVEXS =*,1PE15.7)
1001 FORMAT(1X,* WAVEY =*,1PE15.7,5X,* WAVEYS =*,1PE15.7)
1002 FORMAT(1X,* WAVEZ =*,1PE15.7,5X,* WAVEZS =*,1PE15.7)
     RETURN
     END
```